POLITECNICO DI MILANO

Department of Electronics, Information and Bioengineering

PhD in Data Analytics and Decision Sciences

Healthy smart cities – development of healthcare-focused urban analytics models and decision making tools to reduce heat waves impact on public health

Doctoral dissertation of:
Julia Nawaro

Supervisor:
Prof. Enrico Gianluca Caiani

Tutor:
Prof. Simone Vantini

The Chair of the Doctoral Program:
Prof. Piercesare Secchi

2024 – XXXVII Cycle

The research activities underlying this thesis were made possible thanks to the financial support received under the European project PON FSE REACT-EU, and the resources allocated by Ministerial Decree No. 1061 of August 10, 2021, for active and accredited doctoral programs in the framework of the XXXVII cycle.

Acknowledgements

I am deeply grateful to my PhD supervisor, Prof. Enrico G. Caiani, for his unwavering guidance, encouragement, and insightful feedback throughout my research journey. His mentorship has been instrumental in shaping both this dissertation and my growth as a researcher.

I would also like to express my sincere thanks to Dr. Lorenzo Gianquintieri, whose collaboration and contributions greatly enriched this research. His support and expertise have been invaluable throughout this project.

I would like to express my gratitude to *Agenzia Regionale Emergenza Urgenza* (AREU) for providing the ambulance dispatch data, without which this dissertation would not have been possible. I am particularly thankful to Dr. Maurizio Migliari, Andrea Pagliosa, Dr. Giuseppe M. Sechi, and Dr. Giuseppe Stirparo for their invaluable support and contributions throughout the research process.

I extend my deepest appreciation to Prof. Cristina Santos and Prof. Steve MacFeely for their invaluable role as reviewers. Their thorough assessment, insightful comments, and constructive suggestions have significantly enhanced the quality of this dissertation and broadened its impact.

Abstract

This thesis presents a comprehensive investigation into healthcare-focused urban analytics and decision-making tools designed to mitigate the public health impacts of heat, specifically within the context of transitioning toward healthier smart cities. Using Italy and the city of Milan as case studies, the research adopts a holistic approach to explore the key determinants of heat-health risks, such as population vulnerability, environmental hazards, and residents' exposure. The methodologies developed in this thesis are characterized by their flexibility, offering both academic contributions and practical applications for addressing the increasing public health challenges posed by rising temperatures.

The research is framed within the broader context of global efforts to combat climate change, particularly reflecting the guidance of leading international organizations such as the World Health Organization, Intergovernmental Panel on Climate Change, United Nations, and World Meteorological Organization. This work aims at contributing to three specific Sustainable Development Goals (SDGs): 1) it promotes SDG3 ("Ensure healthy lives and promote well-being for all at all ages") by emphasizing cardiovascular health, one of the leading causes of death globally; 2) by integrating socio-urban features at the neighbourhood and municipal level with health determinants, it supports SDG11 ("Make cities and human settlements inclusive, safe, resilient, and sustainable"); 3) the research directly addresses SDG13 ("Take urgent action to combat climate change and its impacts") through its focus on the health impacts of heat events. These interconnections highlight the importance of comprehensive strategies that target health, urban sustainability, and climate resilience.

The thesis begins by proposing a novel municipality-level SDG3 index for Italy, addressing disparities in data availability and spatial granularity while identifying significant regional variations in public health performance. The SDG3 index for 7,900 municipalities is calculated by mapping 29 Italian indicators to 28 official SDG3 indicators, covering 11 of the 13 SDG3 targets. The final SDG3 index is defined as the arithmetic mean of the scores for all considered targets, with each target score calculated as the average of the normalized scores (ranging from 0 to 1) of its indicators. The values of the index for Italy range between 0.595 in Terragnolo (Trentino-Alto Adige/Südtirol region) and 0.810 in Girasole (Sardinia region), with median equal to 0.697. Despite the limitations in data quality and temporal accuracy, the SDG3 index provides a valuable tool for local policymakers to compare municipalities and tailor public health interventions. By highlighting geographic disparities, in particular the gap between three main macro-areas of Italy (northern, central and southern parts), this index serves as a step toward more nuanced assessments of population health vulnerability.

A systematic review of the literature on heat effects on cardiovascular health reveals substantial heterogeneity in the definitions of heat used across studies (with a total of 21 combinations of indicator, method, and comparison threshold found in 54 articles), posing challenges for comparability and meta-analyses. Despite this variability, percentile-based thresholds, rather than absolute temperature values, emerged as the most commonly used approach in heat-related health studies, accounting for 46 out of 57 (80.7%) definitions (multiple definitions were tested in some articles). To address this inconsistency, the thesis proposes a guideline for standardizing heat definitions in health research by integrating well-established statistical techniques, such as the distributed lag non-linear model and Poisson

regression. This guideline contributes to the advancement of the field by enhancing the consistency of studies on temperature hazards and public health. However, the exclusion of restricted-access articles and grey literature, along with the limitation of the publication period to five years (2018–2022) in the systematic review, may introduce selection bias, potentially overlooking emerging international trends in defining heat.

Using Milan as a case study, the research further investigates the impact of heat on cardiovascular ambulance dispatches. By applying the proposed heat definition guideline to ambulance dispatches data from May to September in the years 2017-2022, the analysis identifies the 95th percentile of annual mean daily apparent temperature distribution as the proper heat threshold for Milan, accounting for key temporal factors that could significantly alter ambulance dispatches distribution, i.e., day of week, day of year, and long-term trend. The corresponding relative risk is assessed at 1.11, with 95% confidence interval (CI) equal to 1.09-1.14 The findings also reveal that certain emergencies, such as those fatal and which occur on the street, are particularly susceptible to the effect of extreme temperature, with associated relative risk at 1.56 (95% CI [1.36-1.80]) and 1.25 (95% CI [1.16-1.34]), respectively. These insights could have practical implications for emergency medical services, enabling better resource allocation and preparedness during extreme weather conditions.

The thesis also explores the socio-urban characteristics that influence cardiovascular vulnerability to heat, using machine learning techniques, such as k-means clustering and hierarchical density-based spatial clustering of applications with noise, and spatial regression models. For each district of an urban environment, cardiovascular vulnerability to heat is defined as percentage of emergencies which happened during heat in relation to all the emergencies, and in Milan it reached the median of 15.05%, with 25th-75th percentile equal to 13.99%-16.08%. Regression analysis identifies key socio-urban variables, including mean summer temperature, the density of drinking water fountains, the percentages of elderly, female, and graduate residents, that significantly affect cardiovascular vulnerability during heat. The research produces a socio-urban vulnerability index, which is combined with medical data to create a vulnerability map, offering valuable tools for urban planners and policymakers to target interventions in most high-risk areas, found as encompassing 18 of 86 Milan's districts, where more than 300,000 people reside. Also, 20 districts, with a population of nearly 280,000 residents, are identified as resilient to heat in the context of cardiovascular health.

The final phase of the research involves the use of artificial intelligence to forecast daily cardiovascular emergencies, with a focus on meteorological parameters, i.e., mean daily apparent temperature on the emergency day, on the previous day and two days earlier. By testing three machine learning algorithms (eXtreme Gradient Boosting - XGBoost, CatBoost, Long Short-Term Memory neural network - LSTM), the research demonstrates the potential of artificial intelligence to predict the volume of next-day cardiovascular emergencies with strong accuracy (mean absolute error equal to 10 cardiovascular emergencies, making it close to the absolute random component of the corresponding time-series), confirming its better performance compared to simpler, i.e., non-machine learning, frameworks. The application of explainable artificial intelligence, derived from Shapley values, enhances transparency in the model's decision-making process, revealing that while temperature has minimal influence on the predictions on most days, its impact sharply increases above approximately 25 °C. In particular, the relationship between temperature and the forecasted number of emergencies

during heat days is well captured by a linear model (R^2=0.79). These findings underscore the importance of incorporating meteorological features into predictive models to improve the accuracy of forecasts and the efficiency of EMS responses in extreme weather.

This thesis offers significant contributions to the development of smart, resilient cities that proactively safeguard public health in the face of climate change, providing tangible insights to the emergency medical services, urban planners and local policymakers, as well as methodological solutions advancing the state-of-the-art. However, it also acknowledges several limitations, including data temporal misalignment, the use of relative indices, and the exclusion of certain urban areas. Further application of the proposed framework is needed to differentiate between findings that are generalizable and those that are specific to particular geographical contexts, such as Milan. Future research should focus on improving data integration, enhancing spatio-temporal resolution, and expanding interdisciplinary collaboration.

Table of Contents

Acknowledgements *5*

Abstract *7*

Acronyms and Abbreviations *14*

Chapter 1. Introduction *16*

1.1. Study background and research gaps **17**
1.1.1. Climate change and human health 17
Natural and anthropogenic climate changes 17
Global warming 18
Impact of elevated temperature on human health 21
1.1.2. Urbanization and healthy smart cities 22
Historical context of urban settlements 22
Urbanization and public health 24
Heat-resilient smart cities 25

1.2. Research questions and methodology overview **27**
1.2.1 Research objectives and research questions 27
1.2.2. Methodology overview 28

1.3. Thesis outline **32**

Chapter 2. Development of SDG3 index for Italian municipalities and geospatial analysis of the results *33*

2.1. Introduction **34**

2.2. Materials and methods **35**
2.2.1. Study area 35
2.2.2. SDG3 data sources 38
2.2.3. SDG3 index computation 43
2.2.4. Statistical analysis and visualization 45

2.3. Results **47**
2.3.1. Mapping between SDG3 official indicators and Italian indicators 47
2.3.2. SDG3 index for Italian municipalities 50
2.3.3. SDG3 index and cardiovascular mortality in Milan, Italy 56

2.4. Discussion **59**
2.4.1. Comparison of the Italian results with literature 61
2.4.2. Municipal SDG3 as an urban health index 63
2.4.3. Limitations and conclusions 64

Chapter 3. Heatwave definition and its impact on adverse cardiovascular events: a systematic review and a framework proposal *67*

3.1. Introduction **68**

3.2. Methods: systematic review of the literature **69**

3.3. Results **70**
3.3.1. Definition of heat 71
3.3.2. Study characteristics 74
3.3.3. Quantification of heat impact on cardiovascular health 77

3.4. Discussion **82**
3.4.1. Applied definitions of heat 83
3.4.2. Impact of heat on cardiovascular health 84
3.4.3. Limitations and conclusions 86

3.5. Framework proposal for percentile threshold selection for heat definition **86**

Chapter 4. Influence of passive heat stress on cardiovascular emergencies in Milan, Italy *90*

4.1. Introduction **91**

4.2. Materials and methods **92**
4.2.1. Study area 92
4.2.2. Emergency medical services data: ambulance dispatches 94
4.2.3. Meteorological data 95
4.2.4. Statistical methods 97
Percentile threshold for defining heat 97
Characteristics of meteorological, air pollution and ambulance data 98

4.3. Results and discussion **99**
4.3.1. Selecting temperature threshold for defining heat 100
4.3.2. Meteorological characteristics and air pollution in the city of Milan 103
4.3.3. Ambulance dispatches for cardiovascular problems in the city of Milan 107

4.4. Limitations and conclusion **113**

Chapter 5. Socio-urban characteristics and cardiovascular vulnerability to heat: a geospatial perspective *115*

5.1. Introduction **116**

5.2. Materials and methods **117**
5.2.1. Cardiovascular vulnerability to heat 118
5.2.2. Socio-urban characteristics 119
5.2.3. Statistical methods 120
K-means clustering of socio-urban characteristics 120
Regression analysis 121
Socio-urban vulnerability to heat 122
Hierarchical density-based spatial clustering of applications with noise of ambulance dispatches 123

5.3. Results **124**
5.3.1. Socio-urban characteristics and cardiovascular vulnerability to heat 124
5.3.2. Socio-urban vulnerability to heat 131
5.3.3. Mapping of low and highly vulnerable districts 134

5.4. Discussion **137**
5.4.1. Novelties of the proposed framework 137
5.4.2. Influence of socio-urban characteristics for the whole city of Milan 138
5.4.3. Influence of socio-urban characteristics for particular clusters of Milan 140
5.4.4. Highly and low vulnerable districts of Milan 141
5.4.5. Limitations and conclusions 142

Chapter 6. Impact of meteorological variables on daily cardiovascular emergencies forecast: an explainable artificial intelligence approach *145*

6.1. Introduction **146**

6.2. Materials and methods **147**
6.2.1. Statistical processing and time series analysis 147
6.2.2. Feature selection for predictive models 148
6.2.3. Predictive modelling 149
6.2.4. Explainable artificial intelligence 150

6.3. Results **151**
6.3.1. Characteristics of apparent temperature and cardiovascular emergencies 151
6.3.2. Feature selection for predictive modelling 155
6.3.3. Predictive modelling 158
6.3.3. Explainable artificial intelligence 162

6.4. Discussion **165**

6.4.1. Time series forecasting 166
6.4.2. Heat and cardiovascular health in urban environment 168
6.4.3. Limitations and conclusions 169

Chapter 7. Conclusions and further research 171

7.1. Is it possible to construct a national municipality-level SDG3 index and how do Italian municipalities differ from each other? 173

7.2. What are currently applied definitions of heat in CV health context, do they influence the results, and how to standardize them? 174

7.3. How to quantify the impact of heat on CV events on a certain area by analysing the geolocalized data relevant to CV ambulance dispatches? 174

7.4. What are the socio-urban characteristics that could influence CV health in presence of heat? 175

7.5. How can artificial intelligence be used to forecast CV emergencies in a big city considering meteorological parameters? 176

7.6. Final remarks, limitations and future developments 177

Bibliography and Sitography 180

List of Figures 208

List of Tables 211

Appendix 213

Acronyms and Abbreviations

AI – artificial intelligence
AIC – Akaike information criterion
AREU – Regional Agency for Emergency and Urgency (in Italian: *Agenzia Regionale Emergenza Urgenza*)
ARPA – Regional Agency for Environmental Protection (in Italian: *Agenzia regionale per la protezione dell'ambiente*)
AT – apparent temperature
CI – confidence interval
CO_2 – carbon dioxide
COVID-19 – Coronavirus disease 2019
CV – cardiovascular
CV_VtoH – cardiovascular vulnerability to heat
DBSCAN – density-based spatial clustering of applications with noise
DLNM – distributed lag non-linear model
EMS – emergency medical services
gMI – global Moran's Index
GWR – geographically weighted regression
HDBSCAN -– hierarchical density-based spatial clustering of applications with noise
HH – high-high local indicators of spatial autocorrelation type
HL – high-low local indicators of spatial autocorrelation type
IDR – incidence density ratio
IPCC – Intergovernmental Panel on Climate Change
IQ – intelligence quotient
ISO – International Organization for Standardization
Istat – Italian National Institute of Statistics
k-NN – k-nearest neighbours
LH – low-high local indicators of spatial autocorrelation type
LISA – local indicators of spatial autocorrelation type
LL – low-low local indicators of spatial autocorrelation type
lMI – local Moran's Index
LST – land surface temperature
LSTM – long short-term memory
MAE – mean absolute error
MAPE – mean absolute percentage error
MAUP – modifiable areal unit problem
ML – machine learning
MMT – minimum mortality temperature
Moran's I – Moran's Index
NIL – Nuclei of Local Identity
NO_2 – nitrogen dioxide
O_3 – ozone

OLS – ordinary least squares
OR – odds ratio
PM10 – particulate matters of less than 10 µm in diameter
PM2.5 – particulate matters of less than 2.5 µm in diameter
r – Pearson correlation coefficient
RQ – research question
RR – relative risk
SDEM – spatial Durbin error model
SDGs – Sustainable Development Goals
SDSN – Sustainable Development Solutions Network
SEM – spatial error model
SHAP – Shapley additive explanations
SLX – spatially lagged X model
SO_2 – sulfur dioxide
SU_VtoH – socio-urban vulnerability to heat
SVM – support vector machines
UHI – urban heat island
UN – United Nations
VIF – variance inflation factor
WHO – World Health Organization
WMO – World Meteorological Organization
XAI – explainable artificial intelligence
XGBoost – extreme gradient boosting
ρ – Spearman correlation coefficient

Chapter 1. Introduction

1.1. Study background and research gaps

1.1.1. Climate change and human health

Natural and anthropogenic climate changes

The Earth's climate system is a dynamic interplay of various factors, relevant to atmosphere, hydrosphere, cryosphere, lithosphere, and biosphere, which govern global weather patterns over geological timescales (WMO, 2024). While weather can be defined as “the state of the atmosphere and ocean at a given moment in time, i.e., it is what you get”, climate “includes all quantities defined by averaging over time scales of many weather events, i.e., it is what you expect” (Neelin, 2010).

The foundations of modern climatology trace back to ancient Greece, where conceptual models linking climate with the inclination of the sun, grounded in the spherical shape of Earth, emerged (Edwards, 2011). These early ideas persevered and significantly influenced subsequent advancements in the field during the Scientific Revolution of the 16th and 17th centuries, facilitated by experimental methods and technological breakthroughs such as the discoveries of barometer and thermometer (Heymann, 2010). The 19th century witnessed the systematic development of scientific climatology and meteorology, with notable emphasis on localized measurements, and Alexander von Humboldt as a pioneering figure in scientific climatology during this period (Heymann, 2010).

At the beginning of the 20th century, the first comprehensive map delineating Earth's climate classes was created by Wladimir Köppen (Heymann, 2010). This classification system, which categorized climates into descriptors such as "tropical" and "polar," remains influential to this day (Heymann, 2010). Subsequently, the 20th century saw a growing interest in the physical climate system and its impacts on vital sectors such as vegetation, agriculture, and human health. However, despite notable scientific advancements regarding phenomena like ice ages and carbon dioxide (CO_2) concentrations, they received relatively limited attention from contemporaneous climatologists (Heymann, 2010). In the 1930s, the International Meteorological Organization, the first worldwide climate-related institution founded in 1873, superseded by the World Meteorological Organization in the 1950s, acknowledged the dynamic spatial and temporal nature of climate by defining it as “the average state of the atmosphere above specific locations within a specific period of time”, with the “specific period of time” recommended to be set at 30 years (Heymann, 2010).

Throughout the second half of the 20th century and particularly over the past two decades, there has been a considerable increase in cross-sector collaboration and technological advancements, leading to a more cohesive understanding of climate dynamics and enhanced modeling capabilities based on mathematical simulations (Edwards, 2011). This collaborative endeavor has facilitated the generation of more nuanced and realistic predictions of climatic changes, encompassing both natural variability and anthropogenic influences. Consequently, these refined climate projections have contributed to increased international attention to the matter of climate and its impacts on the health and sustainability of ecosystems, biodiversity, and human populations.

Centuries of studies on Earth climate contributed to the current knowledge of its historical variability and underlying processes. One crucial factor influencing long-term

climate variability are Earth movement changes, known as Milankovitch cycles (Buis, 2020). These cycles involve periodic variations in Earth's orbit, axial tilt, and precession, which collectively influence the distribution of solar radiation reaching the planet's surface. In particular, changes in Earth's tilt and orbital eccentricity can affect the intensity and seasonality of sunlight received at different latitudes, leading to shifts in climate patterns over thousands of years. As a result of these changes in orbital parameters, but also in greenhouse gas concentrations and volcanic activity, the planet has experienced cycles of glacial and interglacial periods, characterized by alternating intervals of extensive ice cover and warmer conditions (Paillard, 2001).

Another important aspect of Earth's climate system is the albedo effect (Stephens et al., 2015), which describes how different surfaces reflect sunlight. Surfaces covered by ice and snow have a high albedo, meaning they reflect a significant portion of incoming solar radiation back into space. This reflection of sunlight helps to cool the planet and to maintain lower temperatures in regions with extensive ice cover, such as polar regions. However, when temperatures rise and ice melts, darker surfaces such as land and ocean absorb more sunlight, leading to further warming - a feedback loop that amplifies the initial warming trend.

All the changes in Earth's weather patterns over millions of years were driven by natural processes and they can be defined as “climate variability” (Neelin, 2010). Specifically, currently observed natural phenomena include for example El Niño, North Atlantic Oscillation and Indian Ocean Dipole which affect sea surface temperatures and atmospheric pressure. However, recent human activity, altering the composition of the atmosphere, reshaped the climate changes, with all the consequent phenomena such as unprecedented rates of global warming, ozone hole, or acid rain referred to as “anthropogenic climate change” (Neelin, 2010).

Global warming

Trace gases represent a very small fraction of Earth’s atmospheric mass and include, among others, CO_2, methane (CH_4), and nitrous oxide (N_2O), all of which have shown a continuous increase in their concentrations since the beginning of measurements (between the 1950s and 1980s) to the present (Neelin, 2010). These gases, along with water vapour (H_2O), ozone (O_3) and chlorofluorocarbons (CFCs), constitute the greenhouse gases. When sunlight enters the Earth's atmosphere, some of it is absorbed by the Earth's surface, warming it. The Earth's surface then emits infrared radiation back into the atmosphere. The greenhouse effect is a natural process in which greenhouse gases trap this infrared radiation (i.e., heat), leading to an increase in the temperature of the planet's surface and lower atmosphere (Mitchell, 1989).

Theoretical premises regarding the importance of CO_2 in absorbing infrared radiation were hypothesized as early as 1827 by Joseph Fourier (Neelin, 2010). Subsequent interest in this topic primarily emerged in the 20th century, notably with the works of Swedish Nobel Prize winner Svante Arrhenius and British engineer Guy Callendar. Despite employing different methodologies, both Arrhenius and Callendar postulated a rise in global temperatures due to increasing CO_2 levels and the resultant greenhouse effect (Heymann, 2010). The popularization of the concept of anthropogenic global warming accelerated in the late 1950s, thanks to the scientific contributions of Roger Revelle and Charles David Keeling (Neelin, 2010). In 1958,

Keeling initiated the monitoring of CO_2 concentrations at the Mauna Loa Observatory in Hawaii. This pioneering effort led to the creation of the Keeling Curve, which graphically illustrates the continuous increase in CO_2 levels over time. Subsequent measurements have confirmed this trend on a global scale, extending to other trace gases as well (Neelin, 2010).

Human activities, such as the burning of fossil fuels for energy, industrial processes, deforestation, and agricultural practices, have significantly increased atmospheric concentrations of greenhouse gases since the Industrial Revolution (Neelin, 2010). This has resulted in an unprecedently strong and fast heating tendency, exacerbating the greenhouse effect and contributing to global warming (Mitchellm, 1989). Since the late 19th century, when widespread temperature monitoring began, the planet has experienced a notable rise in average surface temperatures, with each of the last four decades surpassing the previous ones in terms of warmth, with higher increase in temperatures over the land than the ocean (IPCC, 2023). This trend is particularly pronounced in recent decades, with the 21st century witnessing some of the warmest years on record. In particular, the global surface temperature during the initial two decades of this century showed an increase of 0.99 °C compared to the period from 1850 to 1900 (IPCC, 2023), with the rise of 1.09 °C in global surface temperatures specifically for the years 2011–2020 relative to the same baseline period of 1850–1900 (IPCC, 2023). Regarding the specific anthropogenic dimension of the phenomenon of global warming, as graphically summarized in Figure 1.1, it is estimated that the range of human-induced global surface temperature rise from 1850–1900 to 2010–2019 is between 0.8°C and 1.3°C, with the best estimate of 1.07 °C (IPCC, 2023).

Figure 1.1. Change in annual average global surface temperature as observed and simulated using human and natural, and only natural factors between 1850 and 2020. Shaded area represents 90% confidence interval for simulated values.

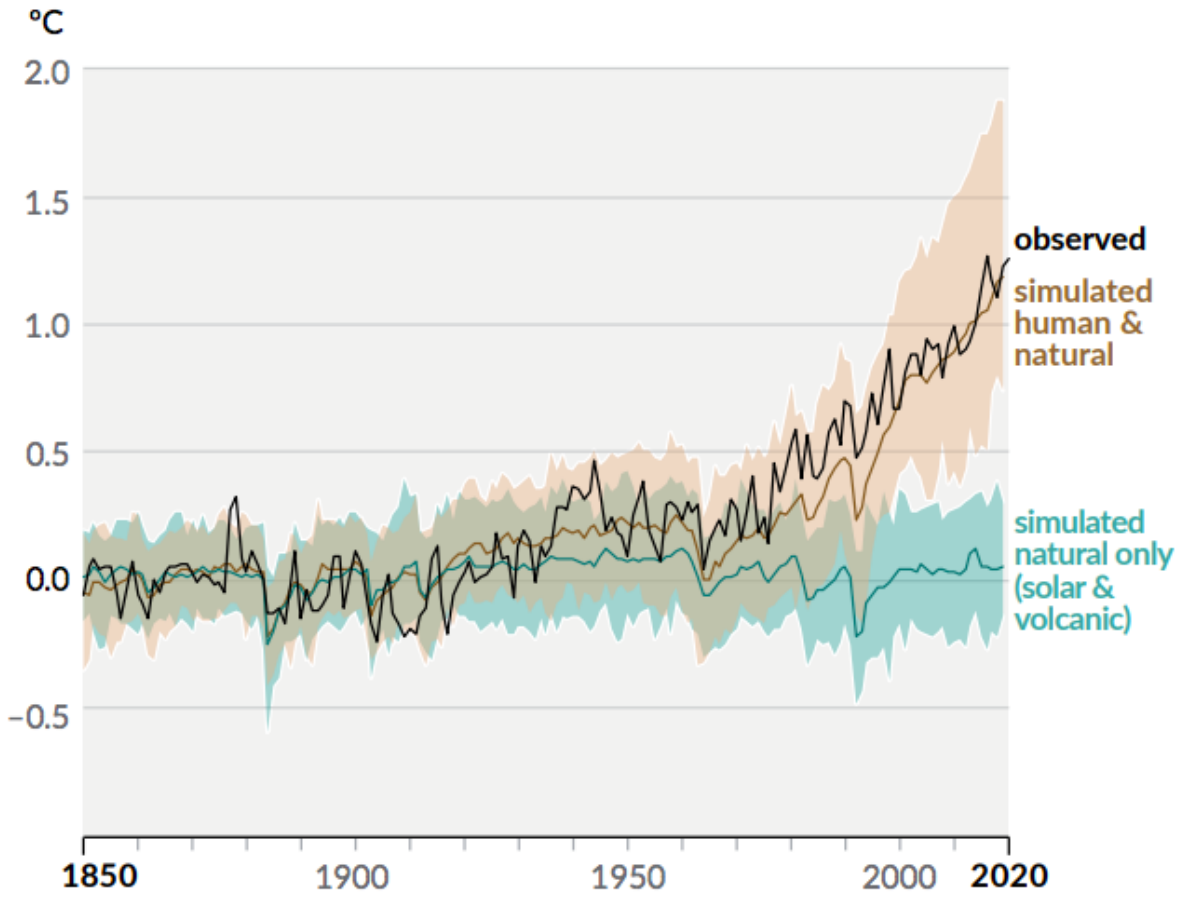

Source: IPCC (2023). Summary for Policymakers. In: *Climate Change 2023: Synthesis Report.*Contribution of Working Groups I, II and III to the Sixth Assessment Report of the Intergovernmental Panel on Climate Change [Core Writing Team, H. Lee and J. Romero (eds.)]. IPCC, Geneva, Switzerland, p. 6.

As highlighted in preceding paragraphs, the spatial dimension of global warming is another aspect to consider in understanding its impacts. International organizations provide maps depicting temperature anomalies, offering valuable insights into regions that are particularly susceptible to the effects of global warming, thereby aiding in targeted mitigation and adaptation efforts. Figure 1.2 is an example of surface air temperature anomaly in 2023, the warmest year on record, which noted an increase of 0.6 °C in average temperature compared to the 1991-2020 and of 1.48 °C compared to the second half of 19th century (Copernicus, 2024). Despite notable local disparities, two expansive regions characterized by heightened vulnerability emerge: the western part of Eurasia and North America. The presence of local variability in temperature anomaly within these regions underscores the imperative for regional investigations into the origins and impacts of global warming. By leveraging temperature anomaly maps provided by international organizations, scientist, policymakers and stakeholders can better identify and prioritize areas in need of targeted interventions to mitigate and adapt to the impacts of global warming.

Figure 1.2. Global surface air temperature anomaly in 2023 with respect to 1991-2020 average

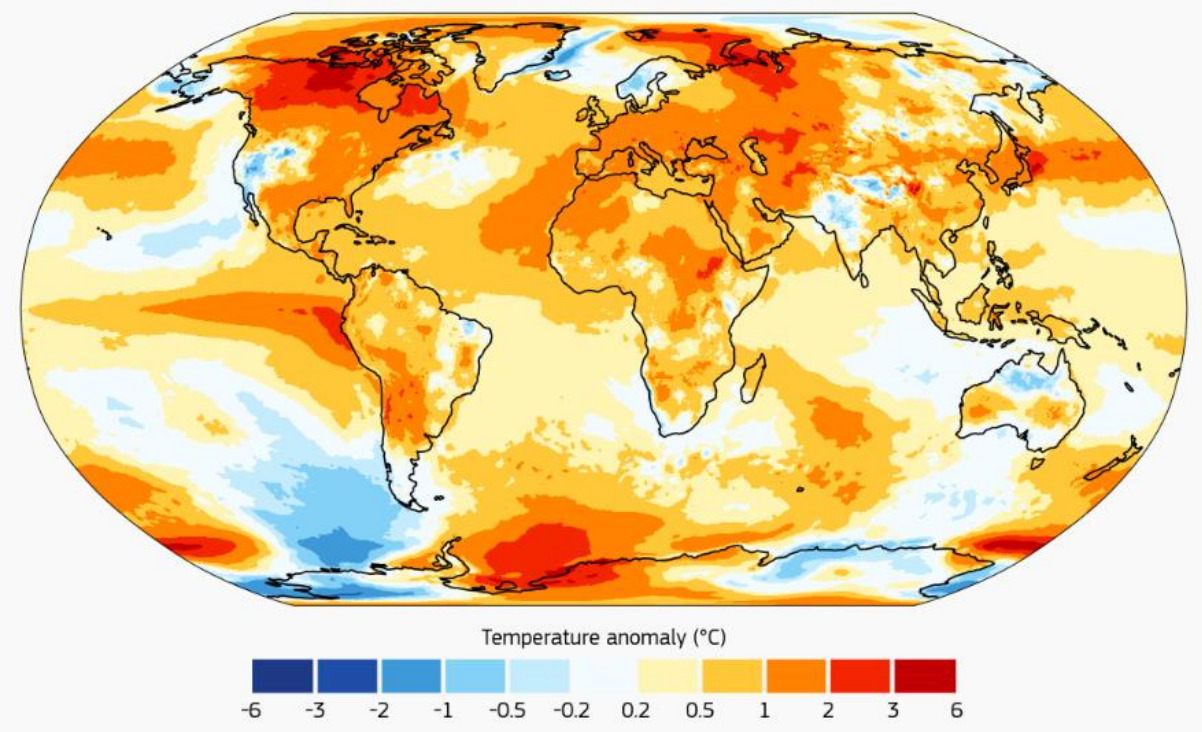

Source: Copernicus (2024). *Global Climate Highlights 2023*. Retrieved from https://climate.copernicus.eu/global-climate-highlights-2023 on 29/04/2024.

Impact of elevated temperature on human health

The implications of the warming trend are far-reaching, encompassing alterations in weather patterns, shifts in precipitation regimes, rising sea levels, and disruptions to ecosystems and biodiversity, thus affecting virtually every aspect of the natural and human environment (Smith et al., 2009). In particular, shifts in temperature and precipitation patterns alter growing seasons and reduce crop yields, threatening food security, ecosystems face extinction due to habitat destruction and changing environmental conditions, diminishing biodiversity and disrupting ecological relationships, and water scarcity intensifies as changing precipitation patterns and melting glaciers affect freshwater availability, leading to increased competition for water resources (Smith et al., 2009).

All of the above impacts affect human health either directly or indirectly, with possible consequences including the exacerbation of pre-existing chronic conditions (e.g., cardiovascular (CV) or respiratory), outbreak and spread of infectious diseases, worsening of mental health or direct injuries and even death (Kim et al., 2014). Specifically, according to the World Health Organization (WHO), 489,000 people died each year as a result of heatwaves between 2000 and 2019, with more than one in three deaths occurring in Europe (WHO, 2024a). Accordingly, climate change impacts on human health have attracted the attention of scholars, with almost a hundred systematic reviews analysing this topic published since 2007, of which most published since 2014 (Rocque et al. 2021).

In particular, CV diseases are the leading cause of death worldwide, with ischemic heart disease and stroke accounting for 27% of global deaths in 2019, particularly affecting

middle- and high-income countries (WHO, 2024b). Moreover, medical evidence suggests that the human CV system is susceptible to the effects of elevated temperatures (Crandall and Wilson, 2015; Crandall and Gonzalez-Alonso, 2010; González-Alonso, 2012). High temperatures can exacerbate chronic CV conditions such as hypertension, leading to an increase in CV emergencies and hospitalizations during heat waves (Kenny et al., 2010; Maria Bruno et al., 2017). The physiological stress imposed by heat can also trigger acute cardiovascular events, including myocardial infarction and stroke, thereby further straining healthcare systems (Bhaskaran et al., 2009; Ranta et al., 2024). The physiological mechanisms underlying these effects are complex and disease-specific, involving factors such as central hypovolemia, increased cardiac output, heart rate, and systemic vascular conductance (Crandall and Wilson, 2015). Empirical research consistently showed a significant increase in CV mortality associated with high temperatures (Singh et al., 2024; Liu et al., 2022; Moghadamnia et al., 2017; Basu, 2009; Basu and Samet, 2002). However, the relationship between heatwaves and CV morbidity, as indicated by hospital admissions, emergency department visits, or ambulance calls, remains inconsistent and varies among specific populations, e.g., the elderly and urban residents, disproportionately bearing the burden of heat-related CV health impacts (Liu et al., 2022; Song et al., 2017; Turner et al., 2012). Moreover, the economic costs of heat-related CV illnesses and deaths are substantial, reducing labour productivity, and exacerbating socioeconomic inequalities (Huang et al., 2023; Chiabai et al., 2018; Roldán et al., 2015).

Although numerous studies have analysed the impact of elevated temperatures on CV emergencies, significant research gaps remain. One major gap is the absence of a universal definition of passive heat stress relevant to outdoor conditions. Various studies use different temperature indicators and thresholds to define “heat” or “heatwave,” impeding a comprehensive analysis of trends, which is crucial in the context of ongoing climate change and projected temperature rises. Additionally, previous research has often focused solely on patient-level medical data, neglecting environmental population-level factors such as climate, weather, pollution, behaviour, habits, and socioeconomic status. Nonetheless, these factors are important determinants of human health (Marmot et al., 2012; Huijts et al., 2017; Donkin et al., 2018), with the external environment accounting for 9.8% of health outcomes, nearly as much as healthcare (11.4%), with the most significant determinants including socioeconomic conditions (19.1%), genetics (22.1%), and behavioural factors (37.6%) (Rochat and Marty, 2018).

1.1.2. Urbanization and healthy smart cities

Historical context of urban settlements

While the history of urban settlements dates back to ancient civilizations, when the development of agriculture played a crucial role in enabling permanent communities, the Industrial Revolution, beginning in the late 18th century, marked a significant transformation in their spread (Williamson, 1988). Technological innovations in manufacturing, transportation, and communication led to unprecedented urban growth, particularly in Europe and North America. As a matter of fact, this period saw the development of key urban infrastructures, including railways, sewage systems, and electricity networks, which facilitated

further urban expansion. The concentration of factories and the growth of the working-class population led to significant changes in the urban landscape, including the development of distinct industrial districts and worker housing (Hopkins, 1986). However, the rapid urbanization of that era also brought important social challenges, including overcrowding, poor sanitary conditions, and the spread of infectious diseases (Neiderud, 2015).

In the latter half of the 20th century, the transition from industrial to service-based economies further transformed urban landscapes. The decline of manufacturing in many Western cities led to deindustrialization and the rise of the post-industrial city, characterized by a focus on finance, technology, and creative industries (Gospodini, 2006). This period also witnessed significant urban sprawl, driven by the expansion of suburban areas, partly due to the proliferation of automobiles and the development of extensive road networks (Gospodini, 2006). However, this urban sprawl brought further challenges of increased traffic congestion, environmental degradation, and social disparities.

Urbanization has accelerated even more in the 21st century. According to the United Nations Human Settlements Programme (2022), the proportion of the global population residing in cities doubled from 1950 to 2020. This significant demographic shift reflects the widespread migration of people from rural to urban areas, driven by the pursuit of better economic opportunities, improved living standards, and access to services. The growth of urban populations has been particularly pronounced in developing regions, with Africa and Asia experiencing rapid urbanization rates. In contrast, regions such as Europe and North America have relatively more stabilized urban populations, with slower recent growth rates due to already high levels of urbanization (United Nations Human Settlements Programme, 2022). As of 2023, it was estimated that approximately 57% of the world's population (i.e., approximately 4.6 billion people; Figure 1.3) resides in urban areas (World Bank, 2024), and this percentage is expected to increase in the upcoming decades, specifically to estimated 70% by 2050 (United Nations Human Settlements Programme, 2022).

Currently, Europe is one of the most urbanized regions in the world, with approximately 76% of European Union population living in urban areas in 2023 (Figure 1.3), noting an increase of 17 percentage points compared to 59% in 1960 (World Bank, 2024). This high level of urbanization reflects a long history of urban development and the concentration of economic activities in European cities, which, nevertheless, are characterized by a high degree of diversity in terms of size, economic structure, and historical background. Major cities serve as global financial and cultural hubs, while smaller urban areas and towns often play important regional roles. Despite their economic strengths, European cities face several challenges, including aging population and infrastructure, within- and between-city socio-economic disparities relevant to unemployment, income inequality, and housing affordability, as well as environmental sustainability, represented by carbon emissions, air quality, urban heat island phenomenon (UHI, characterized by more elevated temperatures within the city compared to its rural surroundings) and green spaces (Ehrlich and Overman, 2020; Clifton et al., 2016; Nikolov and Botseva, 2018).

Figure 1.3. World's and European Union's urban population as percentage of total population in 1960-2023 (World Bank, 2024)

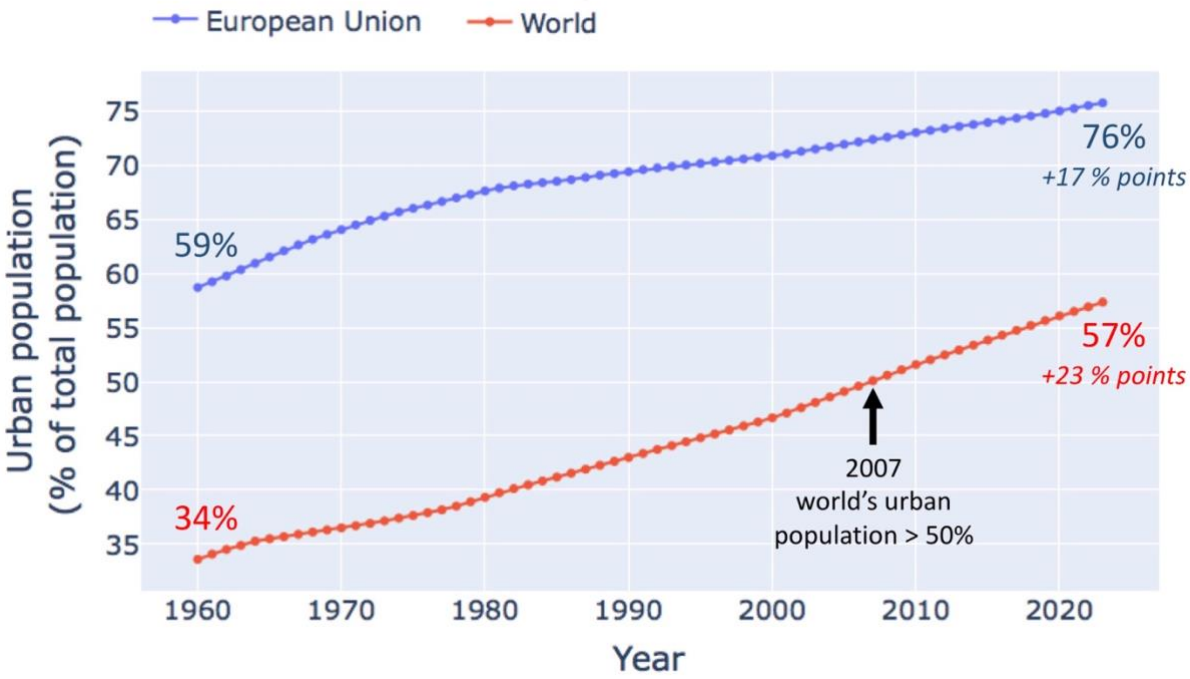

Urbanization and public health

The effects of urbanization have sparked considerable debate among researchers due to its multifaceted influence on various aspects of society, including economic growth, environmental sustainability and public health, presenting both opportunities and challenges (Zhang et al., 2023). Specifically, three main areas of urbanization's positive impact on public health can be distinguished (Zhang et al., 2023; Ye et al., 2022; Vlahov and Galea, 2002; Leon, 2008; Phillips, 1993):

- Access to healthcare: Urban environments typically offer superior access to healthcare services compared to rural areas. Proximity to hospitals, clinics, and specialized medical services facilitates improves health outcomes of residents and enhances better management of chronic patients, as the concentration of advanced medical technologies and medical professionals in cities enables more rapid and accurate diagnosis and treatment.

- Health promotion: Urbanization promotes health by enhancing public infrastructure like sanitation and clean water, and by offering recreational facilities that encourage physical activity. In addition, social support systems and community engagement opportunities in cities contribute to improved well-being.

- Wealth: Urbanization can also indirectly affect public health by increased education and income, which have previously been found to positively influence human health.

On the other hand, urban environment can worsen health, mainly due to the three following factors (Zhang et al., 2023; Ye et al., 2022; Vlahov and Galea, 2002; Leon, 2008; Phillips, 1993):

- Urban lifestyle: Factors such as sedentary behaviour, unhealthy diets, and high stress levels associated with urban living increase the risk of non-communicable illnesses, such as CV diseases, diabetes, and obesity.

- Socio-economic conditions: Life in fast-paced urban environments, along with issues such as social isolation, light and noise pollution, and high living costs, can contribute to mental health problems such as depression and anxiety.

- Environmental factors: Urbanization is closely linked with increased air pollution due to industrial activities, vehicular emissions, and construction. Poor air quality is a significant public health concern in many cities, contributing to respiratory diseases such as asthma, bronchitis, and chronic obstructive pulmonary disease, and presenting a risk factor for other non-communicable diseases. As a matter of fact, cities are estimated to produce almost 70% of global CO_2 emissions (Luqman et al., 2023). In addition, due to the UHI, further exacerbated by global warming, residents of urban areas are more susceptible to the effects of high temperatures on adverse health events, including CV emergencies in particular.

Regarding the UHI phenomenon in particular, while it is well-studied at the urban versus rural scale (Shahmohamadi et al., 2011; Tan et al., 2010; Wong et al., 2013), recent years have seen increased attention to intra-city analysis (Heaviside et al., 2017; Deilami et al., 2018; Kim and Brown, 2021). This shift is due to the diverse socio-urban structure of large cities, which results in varying exposure to heat-related health hazards. These hazards include not only heat exposure but also access to healthcare services, prevalence of heat mitigation infrastructures, characteristics of built infrastructure, and the presence of green spaces. As the intra-city approach is still emerging, no standardized methodology has been established. Consequently, various methodologies have been implemented to assess the spatial variations of UHI, its interaction with social, economic, and urban factors, and their combined impact on human health (Deilami et al., 2018; Almeida et al., 2021).

Such analyses have served as initial attempts to create a vulnerability map of a city, resulting in the development of various indices describing the vulnerability to heat (Bao et al., 2015; Niu et al., 2021; Li et al., 2022; Szagri et al., 2023; Cheng et al., 2021). These static maps are valuable for urban planners, local policymakers, and medical services, as they provide insights into the spatial distribution of environmental risk and offer a tangible numerical value, comparable among spatial units. However, specifically regarding the medical dimension, the lack of easily accessible medical data makes the real-world application of such indices a big challenge, especially at a detailed geographical level (Heaviside et al., 2017; Conlon et al., 2020; Niu et al., 2021). Such data are necessary either for the creation of the index itself, or for its validation, as greater exposure to hazard (i.e., heat in this case) does not always result in a proportionally increased risk of adverse health event (Niu et al., 2021). While data on mortality or hospitalizations can be useful to this purpose, their spatial granularity is usually limited to the hospital level or, at best, the patient's residence zip code. In this context, data from ambulance dispatches could offer promising insights, as they provide more precise geolocation of where emergencies occur.

Heat-resilient smart cities

The term "smart city" first emerged in the late 1990s, encapsulating the vision of urban environments enhanced by advanced technologies to improve quality of life, efficiency of services, and sustainability (Anthopoulos, 2015). Smart cities leverage information and communication technologies (ICT) to collect, analyse, and act upon data from various sources

such as sensors, devices, and infrastructure. The ultimate goal is to create a more connected, efficient, and responsive urban environment that meets the diverse needs of its residents, also in the context of their health.

Regarding data-driven techniques relevant to human health, smart cities can leverage wearable devices, Internet of things (IoT) sensors, and official medical services providers' data to monitor residents' health in real-time (Ghazal et al., 2021; Mishra and Singh, 2023). Data collected from these sources provide insights into heart rate, blood pressure, and physical activity levels, as well as into adverse health outcomes requiring medical intervention, such as ambulance arrival or hospitalization, which can be used by researchers to identify at-risk individuals and implement targeted interventions, thereby improving public health outcomes. However, the use of sensitive personal data in this context is complicated by stringent data protection regulations, and the potential uncertainty of wearable devices regarding whether the same individual is consistently using their device, as well as contextualization of the acquired data.

Environmental sensing instead, one of the crucial components of smart city, is relatively easy to access and implement (Ramírez-Moreno et al., 2021). By deploying a network of sensors to monitor conditions such as temperature, air quality, and humidity, cities can better understand the impact of environmental factors on residents' health outcomes. For example, correlating heatwaves with spikes in CV emergencies enables the development of early warning systems and preparedness plans to protect vulnerable populations.

Furthermore, predictive modelling, through the analysis of historical data and current trends, allows smart cities to forecast extreme weather events, such as heatwaves, as well as health outcomes, including ambulance calls and emergency department visits (Ghazal et al., 2021; Mishra and Singh, 2023). In addition, statistical analysis and unsupervised machine learning can provide useful insights into ongoing trends in the impact of environmental factors (e.g., of heat) on human health (e.g., on CV emergencies), enabling cities to implement measures to safeguard residents from potential risk before its occurrence, with strategies covering issuing heat warning messages, opening cooling centres, or adjusting public services. These proactive strategies are essential for mitigating the health impacts of global warming.

By combining insights from advanced mathematical modelling performed on real-world data with domain knowledge, in order to create heat-resilient cities, urban planners, local policymakers, and medical services providers can also implement long-term targeted strategies to mitigate the impact of heat on human health in particular areas of a city. Such strategies can include the incorporation of green spaces, cool roofs, pavements and walls, water installations, and energy efficiency plans into urban projects, as well as the fostering of community engagement and education about heat-related health risks. Such strategies encourage proactive measures, safeguarding urban populations from health risks associated with environmental factors before they become severe and require medical intervention. This represents a necessary paradigm shift from a reactive approach, which relies solely on retrospective analysis and omits the provision of tangible metrics, essential for developing a healthy smart city.

1.2. Research questions and methodology overview

1.2.1 Research objectives and research questions

In response to the escalating threat of climate change and its implications for public health, there has been a growing recognition of the need to develop adaptive strategies and mitigation measures. International initiatives such as the United Nations Framework Convention on Climate Change (UNFCCC), Intergovernmental Panel on Climate Change (IPCC), Conference of the Parties (COP) meetings and the Sustainable Development Goals (SDGs) have underscored the urgency of addressing climate-related health risks. One of the most significant international agreements aimed at addressing climate change is the Paris Agreement, adopted in 2015 and signed by 195 countries, which aims to limit global warming to well below 2 °C above pre-industrial levels and to pursue efforts to limit the temperature increase to 1.5 °C. To achieve these goals, countries have pledged to, among others, reduce greenhouse gas emissions and enhance climate resilience, which can be largely achieved through initiatives targeted to urban environments. In addition, the importance of climate change, resilient urban environments and human well-being is underscored by three SDGs, in particular: SDG3 ("Ensure healthy lives and promote well-being for all at all ages"), SDG11 ("Make cities and human settlements inclusive, safe, resilient and sustainable"), and SDG13 ("Take urgent action to combat climate change and its impacts").

However, despite global efforts to mitigate the anthropogenic climate change and adapt to the warming trend, gaps remain in understanding the interactions between heat, health, and urban environments, as described in section 1.1. In particular, these gaps include:

- Absence of a static, periodically updated, health-related index or indicator, allowing for frequent analysis of national performance and comparisons at municipal level, as well as necessary for the validation of more specific heat-health related indices.
- Lack of a globally standardized definition of heat or heatwave, which hinders comprehensive analysis of trends and their comparison across different geographical locations.
- Predominant focus on patient-level analyses regarding the impact of heat on CV health, representing a reactive approach. This leaves population-level risk assessment underdeveloped, which is crucial for shifting towards a proactive approach in managing vulnerability to heat, aiming to prevent residents from becoming patients.
- Insufficient spatial resolution in analyses of the impact of meteorological, social, and urban characteristics on CV health, as well as of their interdependencies, preventing to fully capture the spatial dynamics within urban environments.

This PhD thesis seeks to address the above gaps by leveraging data-driven approaches to examine the achievement of SDG3 in all the Italian municipalities, and in particular by proposing a reproducible spatio-temporal framework of analysis of the impact of passive heat stress on CV emergencies in an urban environment, extending the focus to align with SDG11 and SDG13 as well. Recognizing the interconnections among these SDGs enhances the thesis's relevance to contemporary challenges. Specifically, it addresses the following research questions (RQs):

1) Is it possible to construct a national municipality-level SDG3 index and how do Italian municipalities differ from each other?

2) What are currently applied definitions of heat in CV health context, do they influence the results, and how to standardize them?
3) How to quantify the impact of heat on CV events on a certain area by analysing the geolocalized data relevant to CV ambulance dispatches?
4) What are the socio-urban characteristics that could influence CV health in presence of heat?
5) How can artificial intelligence be used to forecast CV emergencies in a big city considering meteorological parameters?

By answering the above RQs, this study aims to:

- contribute to the state-of-the-art by:
  - developing the first-ever SDG3 index for all Italian municipalities to quantify their overall health vulnerability, proposing standardized methods for assessing the representativeness of open data and downscaling them to finer geographical resolutions (RQ1);
  - proposing a universal approach for selecting temperature threshold for defining heat in health-related studies, based on the most common strategies identified in relevant literature (RQ2);
  - introducing original methodological approaches for a holistic analysis of the influence of heat on CV emergencies in urban environments, using geolocalized ambulance dispatches as a proxy (RQ3, RQ4, RQ5).
- provide actionable short- and long-term insights for:
  - Emergency medical services (EMS) which can benefit from comprehensive maps that highlight areas where shifts in the spatial distribution of ambulance calls for CV problems occur on heat days compared to non-heat days, and from a predictive model for next-day CV ambulance calls. These short-term insights can enhance EMS preparedness during extreme weather conditions, thereby improving overall efficiency (RQ3, RQ4, RQ5).
  - Urban city planners who can gain insights into the urban characteristics that significantly impact vulnerability to heat in the CV context. These findings can inform long-term strategies regarding greenery and infrastructure development to reduce this vulnerability (RQ4).
  - Local policymakers who can access an overview of the achievement of SDG3 across all Italian municipalities. By comparing scores between municipalities, targeted public health strategies can be implemented to foster the improvement of health services (RQ1).

1.2.2. Methodology overview

In order to answer the RQs, there is a need to properly define hazard, exposure, and vulnerability. In the specific context of this thesis, following the definitions provided by Cardona et al. (2012), hazard, defined as a factor that can potentially cause harm (i.e., a CV emergency), is represented by passive heat, i.e., the temperature above some threshold. Exposure refers to the collection of elements within an area that may be affected by hazardous

events, i.e., degree to which the residents of the city under consideration are subjected to passive heat. Vulnerability is the inherent susceptibility of exposed residents to experience CV emergency when subjected to passive heat, which can be measured, to some extent, by a standardized index such as SDG3. Finally, the risk, i.e., the likelihood of harm occurring, is determined by hazard, exposure and vulnerability.

In quantitative research, numerous approaches have been developed over the past decades to assess risk and its determinants (Aven, 2016; Zio, 2018; Rausand, 2013). Among these, the odds ratio (OR) is one of the most frequently used statistical methods in epidemiology, providing a measure of association between two binary variables (Bland and Altman, 2000). The odds represent the probability of an event occurring versus not occurring, and the OR is the ratio of the odds between two groups, such as a CV emergency in individuals exposed to passive heat versus those not exposed. OR are typically estimated using logistic regression models, which are well-suited for proportions and binary outcomes (Knol et al., 2012).

A related concept is relative risk (RR), often mistakenly used interchangeably with OR. RR is the ratio of incidence rates (i.e., risks) of an event, such as a CV emergency, between two population groups, such as those exposed and not exposed to passive heat (Bland and Altman, 2000). The statistical models commonly employed to estimate RR include Poisson, quasi-Poisson, or negative binomial regression which deal with counts and ratios (Frome and Checkoway, 1985; Gardner et al., 1995). Both RR and OR are interpreted as follows: a value below 1 indicates that the event is less likely to occur with exposure to the hazard, a value above 1 indicates the event is more likely to occur with exposure to the hazard, and a value of 1 implies no difference between exposure to the hazard and non-exposure.

In the specific context of estimating health risks associated with environmental factors, Gasparrini et al. (2010) introduced distributed lag non-linear model (DLNM), which estimates cumulative RR over specific lags, acknowledging that the health response to a risk factor may be delayed. Despite its stringent mathematical assumptions, as detailed in Chapter 4, the DLNM has rapidly become a gold standard in environmental epidemiology, with its statistical robustness validated through both simulated and real-world data (Gasparrini, 2014; Wang et al., 2021a).

Traditional statistical languages, such as R, provide a straightforward framework for implementing models to estimate OR and RR. The prevalence of each method to estimate the risk of a CV emergency in passive heat will be further overviewed in Chapter 3, and DLNM and Poisson regression will be applied in a case study in Chapter 4.

While the use of OR and RR provides valuable and intuitive insights into the association between exposure and outcome, particularly for medical stakeholders, the growing significance of health geomatics highlights the necessity of incorporating spatial components in the assessment of vulnerability and risk. Health geomatics involves the use of geoinformatics in health-related research, covering the geography of the disease and of the healthcare system (Boulos et al., 2001), with both concepts being interconnected and relevant to the contents of this thesis. The former refers mostly to the exploration of spatial patterns of the disease itself, while the latter aims to manage the spatial distribution of the health services, such as EMS supply. Although intuitively health geomatics is well-suited for analysing communicable diseases, it has also demonstrated significant potential for non-communicable diseases (Jia et

al., 2019; Blangiardo et al., 2020; Tuoane-Nkhasi and van Eeden, 2017; Sogno et al., 2020; Andrees et al., 2024). Despite the recognition of spatial dependencies in epidemiology for centuries - exemplified by John Snow's 1854 cholera map, which helped him to identify the source of contamination in London - the systematic integration of spatial analysis into health research has been still underused in recent years (Boulos et al., 2001; Ostfeld et al., 2005; Sogno et al., 2020). Consequently, there remains a lack of consensus on the optimal spatial approaches in health research, particularly those that includes environmental factors as well.

One of the fundamental challenges in spatial analysis is defining the spatial unit for performing analyses. In this study, official administrative boundaries will be used as reference polygons to ensure the real-world applicability of the results, along with point data on medical events. In the absence of predefined polygons, alternative spatial partitioning approaches include introducing an ad-hoc grid or applying a partitioning algorithm, such as the Voronoi diagram (Zlatanova et al., 2020; Novaes et al., 2009). While dealing with polygons, before statistically quantifying various aspects, the subsequent step often involves defining spatial neighbours, for which three primary strategies are recognized: rook, queen, and bishop contiguity (Dubin et al., 2009), named after chess piece movements, as illustrated in Figure 1.4.

Figure 1.4. Rook, queen, and bishop contiguity first order neighbours

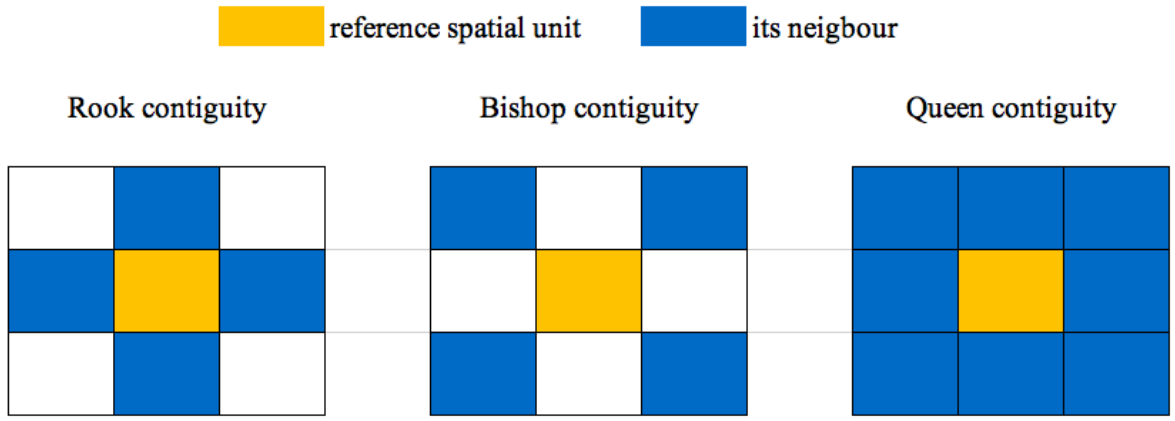

To quantify spatial associations among polygons, the most common method is Moran's Index, which assesses spatial autocorrelation, i.e., the clustering (or dispersion) tendency of the data, at both local and global levels (Kirby et al., 2017). Despite its simplicity, the index has been successfully implemented to gain valuable health-related insights (Auchincloss et al., 2012; Lorant et al., 2001; Saffary et al., 2020). The mathematical details of this statistic will be discussed in Chapter 2.

A more advanced approach for determining spatial relationships between independent variables and a target variable (e.g., quantifying population vulnerability to a hazard) is the regression modelling. Two main theoretical frameworks are commonly employed: geographically weighted regression (GWR) and spatial regression (Kirby et al., 2017). GWR operates on the principle that the relationship between independent and dependent variables varies across locations, and therefore, it estimates ordinary least squares (OLS) regression separately for each spatial unit, defined by a spatial bandwidth. In contrast, spatial regression

models account for three types of spatial dependencies: local (referring to the spatial unit and its neighbours), global (referring to the spatial unit and all other spatial units), and in the error term. These models estimate both direct and spillover effects of each independent variable on the target variable, and they are further described in Chapter 5.

Spatial analysis is applicable to various aspects of this study, from analysing the spatial clustering tendency of health indices to examining the spatial determinants of population vulnerability to heat in the context of CV emergencies. From a software perspective, these analyses can be implemented using traditional programming languages such as R or Python, as well as specialized geographic information system (GIS) software like QGIS.

While traditional statistical methods provide valuable static results, such as for the development of health indices or the estimation of risk and vulnerability, the current era of big data necessitates more dynamic approaches that can be easily generalized and updated with new information. To address this need, machine learning (ML) models are increasingly utilized for public health problems for their ability to automatically learn and improve over time (dos Santos et al., 2019; Mooney and Pejaver, 2018; Kino et al., 2021). In this study, ML techniques are employed for spatio-temporal analysis in particular. These techniques, which integrate statistical methods with computer science principles, are typically implemented using the Python programming language.

Initially, unsupervised ML models will be applied for distance- and density-based clustering to uncover underlying patterns in the data. Distance-based algorithms, such as k-nearest neighbours (k-NN) and support vector machines (SVM), aim to group data points into clusters by minimizing the distance between point within each cluster, and maximizing the distance between separate clusters. The choice of distance metric, such as Euclidean, cosine, Manhattan, Chebyshev, or other (Pandit and Gupta, 2011), depends on the nature of the data. Density-based clustering, on the other hand, identifies densely populated regions within the data space, classifying remaining points as noise. Therefore, both clustering approaches inherently incorporate spatial dimension, making them particularly relevant for health-related analyses, as explored in this study. These clustering techniques are further detailed and implemented in Chapter 5 of this thesis.

Supervised ML, which covers regression and classification, is another paradigm applied in this study. The focus in the following analyses is on regression models, which are commonly based on linear and non-linear OLS regression, decision trees, SVM, or neural networks. In the context of this thesis, supervised ML is utilized for time-series prediction, with the spatial dimension predefined by clustering, as discussed in Chapter 6. Additionally, there is growing recognition of the importance of explainable artificial intelligence (XAI; Gerlings et al., 2022; Loh et al., 2022), which enhances interpretability by providing insights into the contribution of individual variables to the model's output, offering a significant advantage over complex statistical models. Accordingly, XAI framework is included in supervised ML modelling for the purposes of this thesis.

In conclusion, to achieve the objectives outlined in section 1.2.1, this thesis will employ a quantitative approach to assess the risk and vulnerability of the exposed population under investigation, focusing on both general health outcomes and CV emergencies triggered by passive heat hazard. Traditional statistical methods will be integrated with ML modelling to develop a comprehensive analytical framework and enhance the robustness of the results.

The analyses use Italy and in particular the city of Milan as applicative case studies. The data for this research include CV ambulance dispatch records provided by *Agenzia Regionale Emergenza Urgenza Lombardia*, alongside open datasets encompassing various meteorological, health, social, demographic, and urban indicators.

1.3. Thesis outline

In light of ongoing global warming and urbanization, this thesis aims to address the research questions outlined in section 1.2.1 by applying the quantitative methodology detailed in section 1.2.2. The structure of the thesis is as follows.

Chapter 2 presents the calculation of an SDG3 index for all Italian municipalities. This chapter offers a methodological overview of the index calculation and assesses the current status of human health and well-being across Italian municipalities, addressing RQ1.

After assessing the overall health vulnerability, Chapters 3 through 6 focus specifically on the relationship between elevated temperatures and CV outcomes. Chapter 3 provides a systematic review of recent literature on the influence of passive heat on adverse CV outcomes, with particular attention to the definitions of heat used and their impact on results. In addition, a framework for selecting the percentile threshold for defining heat is proposed. This chapter addresses RQ2.

From Chapter 4, the focus narrows to the city of Milan, Italy. Building on the previous chapter, a framework for defining heat is applied to data on ambulance dispatches for CV problems in Milan from May to September 2017-2022. These data are coupled with meteorological data, including air temperature, relative humidity, and wind speed. The chapter estimates the risk of CV emergencies during heat events, accounting for potential delayed effects, and addresses both RQ2 and RQ3.

Chapter 5 introduces a finer spatial analysis of Milan by clustering its administrative districts based on various socio-urban features. The impact of these features on CV vulnerability to heat, defined following the results from the previous chapter, is quantified using spatial regression. A socio-urban vulnerability to heat index is then developed and applied to each district. The chapter also confronts this index with density-based clustering of CV emergency data, revealing spatial shifts in their distribution during heat days. This chapter addresses RQ4.

Chapter 6 presents a forecasting model to predict the number of CV emergencies across the city and within specific clusters, integrating methodologies from the previous chapters. Additionally, a XAI analysis is conducted to assess the impact of meteorological variables on predictions during heat and non-heat days, addressing RQ5.

Chapters 2 to 6 begin with a list of the publications on which they are based, followed by a “Highlights” box outlining the RQ addressed and the main findings.

The thesis concludes with Chapter 7, summarizing the findings from Chapters 2-6, highlighting their contributions to the state of the art, and discussing their implications for medical, urban planning, and policymaking stakeholders. Future directions for spatio-temporal research on the effects of heatwaves on public health in urban areas are also outlined.

Chapter 2. Development of SDG3 index for Italian municipalities and geospatial analysis of the results

The content of this chapter is an elaborated version of the following publications:

- Nawaro, J., Gianquintieri, L., & Caiani, E. G. (2024). Developing a Sustainable Development Goal 3 (SDG3) index for Italian municipalities. In *Medical Sciences Forum* (Vol. 25, No. 1, p. 6). MDPI. https://doi.org/10.3390/msf2024025006

- Nawaro, J., Gianquintieri, L., & Caiani, E. G. (2024). Analysis of the Sustainable Development Goal 3 index for Italian municipalities. *Public Health*, *236*, 386-395. https://doi.org/10.1016/j.puhe.2024.08.014

Highlights:

- RQ1: Is it possible to construct a national municipality-level SDG3 index and how do Italian municipalities differ from each other?
- Substantial geographical variations in municipal performance across 13 official SDG3 targets were highlighted, with municipalities in central, far Northeast and far Northwest Italy performing the best.
- Methodological framework for calculating the SDG3 index under conditions of data scarcity was established.
- Municipality-level SDG3 index for 7,900 Italian municipalities could provide a valuable tool for local policymakers to inform evidence-based decision-making and tailor public health interventions.

2.1. Introduction

Urban indices can be a valuable tool in highlighting inequalities among the vulnerability level of municipalities, and consequently identifying geographical areas where substantial action needs to be taken. In this context, many complex urban health indices, also accounting for environmental, social, and economic factors, have been proposed in literature, and five main purposes for their utilization have been defined: 1) informing policy and decision-making, 2) monitoring and evaluation, 3) research, 4) benchmarking, and 5) communication with non-specialists, with most studies focusing on the first category (Kaltenthaler et al., 2004; Pineo et al., 2018a). Such urban health indices have been commonly developed either for a single city, to provide an overview of health indicators and their determinants, or for several ones, in order to perform a score-based quantitative comparison. Additionally, in recent literature an increasing attention has been given to the application of attributing a score to lower urban partitions than the whole city, such as neighbourhoods or districts (Pineo et al., 2018a).

Several attempts to provide a standardized set of indicators for the construction of an urban health index were made by organizations such as the United Nations (UN), the United States Department of Health and Human Services, the World Bank and the World Health Organization (Rothenberg et al., 2015), with the latter also proposing the calculation of a specific index called The Urban Health Index (Weaver et al., 2014). However, no universally recognized standard exists, neither for the indicators nor for the methods used for the urban health indices' computation, thus existing indices are characterized by a large heterogeneity in these terms. Moreover, the lack of index validation is a very diffused limitation in the development and use of such urban health indices (Jiang et al., 2018; Kaltenthaler et al., 2004; Pineo et al., 2018b).

After a 15-years period (2000-2015) in which the UN formulated the Millennium Development Goals (MDGs), a set of eight international objectives, the Sustainable Development Goals (SDGs) were adopted on 1st January 2016. The SDGs extend the MDGs by the formulation of 17 goals, described by 169 targets, and since their establishment, multiple studies have been developed with the purpose of assessing the current progress towards their achievement (Lamichhane et al., 2021; Lim et al., 2016; Schmidt-Traub et al., 2017; Stanujkic et al., 2020). Additionally, in 2012, the UN established the Sustainable Development Solutions Network (SDSN) to foster innovation and collaboration towards achieving the SDGs at global, regional, national, and local levels (SDSN, 2024). The SDSN contributes to this aim by publishing the Sustainable Development Report, which provides an overview of the total progress towards achieving all 17 SDGs across 166 countries. In its most recent version (Sachs et al., 2023), Italy was classified as 24 out of 166 countries, preceded by 22 European states and Japan. However, when accounting for the spillover effect, measuring the environmental and social impact of actions within each country on trade, economy and finance, and security of other countries, Italy's ranking shifted to 127 out of 166, with only six European Union members characterized by a more positive global spillover effect. In addition, since 2018, the Italian National Institute of Statistics (Istat) has been publishing yearly reports on the SDGs' progress in Italy, accounting for all the official goals and reporting scores individually for all the available indicators, implementing diverse geographical aggregations, including national,

regional and provincial levels (Istat, 2023b). However, a municipal overview of the SDGs progress is still missing.

The SGD3 (i.e., Ensure healthy lives and promote well-being for all at all ages), is described through 13 targets including 28 indicators, addressing various factors relevant to public health access, non-communicable and communicable diseases, maternal and child health, risk factors prevalence, and health financing and research. Additionally, a previous study has identified SDG3 as one of the four fundamental SDGs (Fenner and Cernev, 2021). According to the Sustainable Development Report (Sachs et al., 2023), Italy's progress toward SDG3 is described as “moderately improving”, yet “challenges remain”. Within SDG3, one of three indicators showing no progress is the “Gap in life expectancy at birth among regions”, highlighting considerable local disparities in Italy. Existing empirical analyses on SDGs in Italy have tried to address this challenge by focusing on provincial level as the smallest geographical unit; however, they have only covered a subset of targets and/or indicators.

Considering the above-mentioned research gaps, both in relation to SDG3 and more broadly to urban health indices, the aim of this chapter is to develop a heath vulnerability index based on SDG3 targets, to be computed at municipal level for a whole country (Italy in this study case). In order to enhance reproducibility, only official open data are used. Main objectives of this index are to provide an overview of the current spatial distribution in the level of achievement of SDG3 goals (i.e., health vulnerability) and to highlight possible geographical disparities along the territory through statistical comparison. Such index also aims at overcoming the challenges in constructing an urban health index covering an entire country, ultimately providing a standardised measure to validate other spatial analyses of health status. Regardless of the specific study case, this work is relevant to international research as it proposes original methodological solutions to overcome the challenges posed by limited data availability and insufficient geographical granularity, that represent very common issues when addressing the country-wise computation of urban health indices and, in particular, SDG3 assessment at municipality level. Accordingly, in this chapter, the RQ1 is addressed, i.e., is it possible to construct a national municipality-level SDG3 index and how do Italian municipalities differ from each other?

2.2. Materials and methods

2.2.1. Study area

Italy is the 10th largest country on the European continent, with an area of more than 300,000 km^2 and a population of nearly 60 million. As of 1st January 2023, the country is administratively divided into 20 regions, 107 provinces (including two autonomous provinces of Trento and Bolzano) and 7,901 municipalities (Figure 2.1). The median number of municipalities per region is 294 (25th-75th percentile: 223-394), spanning from 74 in Aosta Valley to 1,504 in Lombardy, with a median population per municipality of 2,394 residents (25th-75th percentile: 977-6,223). For statistical purposes, the following classification of municipalities have been defined by Istat:

- 12 municipalities in the centre of the metropolitan area: Turin (Piedmont region), Milan (Lombardy), Venice (Veneto), Genoa (Liguria), Bologna (Emilia-Romagna), Florence

(Tuscany), Rome (Lazio), Naples (Campania), Bari (Apulia), Palermo (Sicily), Catania (Sicily), Cagliari (Sardinia);

- 1,051 municipalities located in the same provinces as the above-mentioned metropolitan areas, constituting the 13.3% of all Italian municipalities;
- 3,253 municipalities with up to 2,000 residents (41.2%);
- 2,755 municipalities with 2,001-10,000 residents (34.9%);
- 733 municipalities with 10,001-50,000 residents (9.3%);
- 97 municipalities with more than 50,000 residents (1.2%).

Figure 2.2 illustrates the geographical distribution of the abovementioned categories, while Table 2.1 provides additional details on the largest municipalities in the centre of the metropolitan areas and the largest provinces within these areas. According to this classification, the regions of Molise, Aosta Valley, and Abruzzo have the highest proportion of municipalities with fewer than 2,000 inhabitants, while Tuscany, Apulia, and Emilia-Romagna are characterized by the highest percentage of municipalities with more than 50,000 inhabitants. Additionally, almost one in five Italians lives in a municipality with 10,001-50,000 residents, making this category the most populous nationwide.

Among both the centres and the provinces of the metropolitan areas, Rome emerges as the most populous, followed by Milan and Naples. In terms of land area, aside from the municipality of Rome and its province, municipalities of Venice and Genoa rank among the top three largest centres, while provinces of Turin and Palermo place among the top three largest provinces. Concerning the number of municipalities within the province of the metropolitan area, the provinces of Turin and Milan in the north of Italy precede the province of its capital, Rome.

Figure 2.1. Administrative division of Italy on 1st January 2023

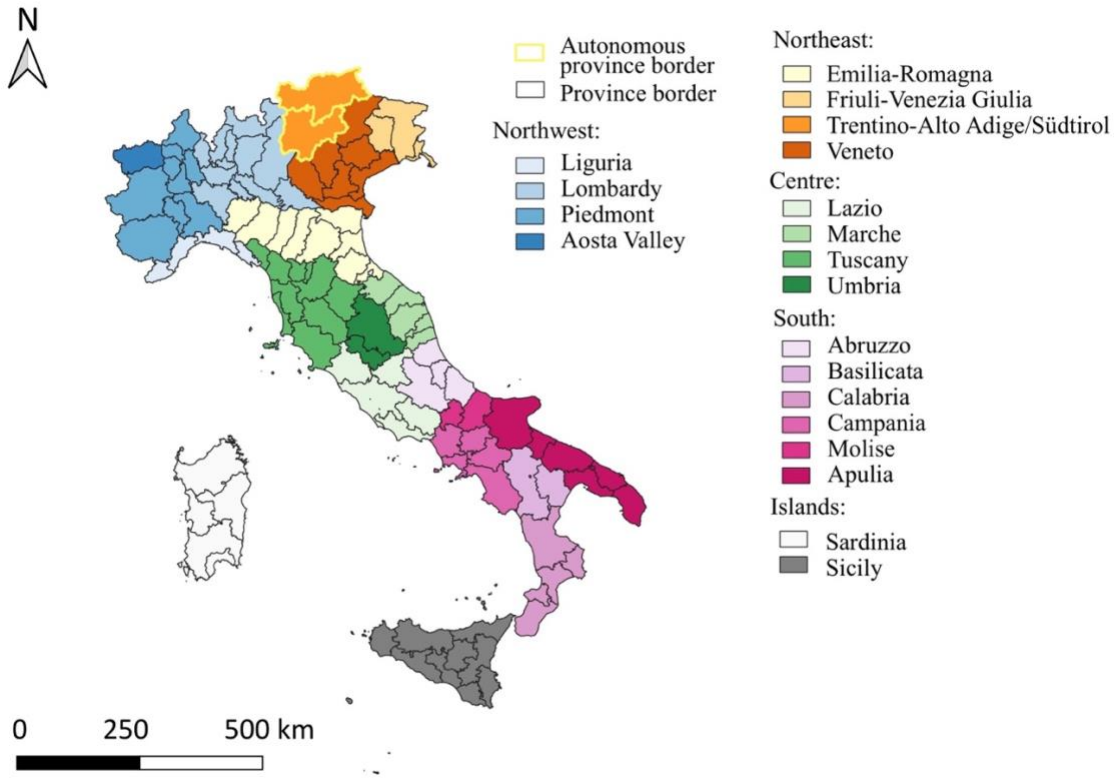

Figure 2.2. Geographical distribution of classes of municipalities defined by the Italian National Institute of Statistics (Istat)

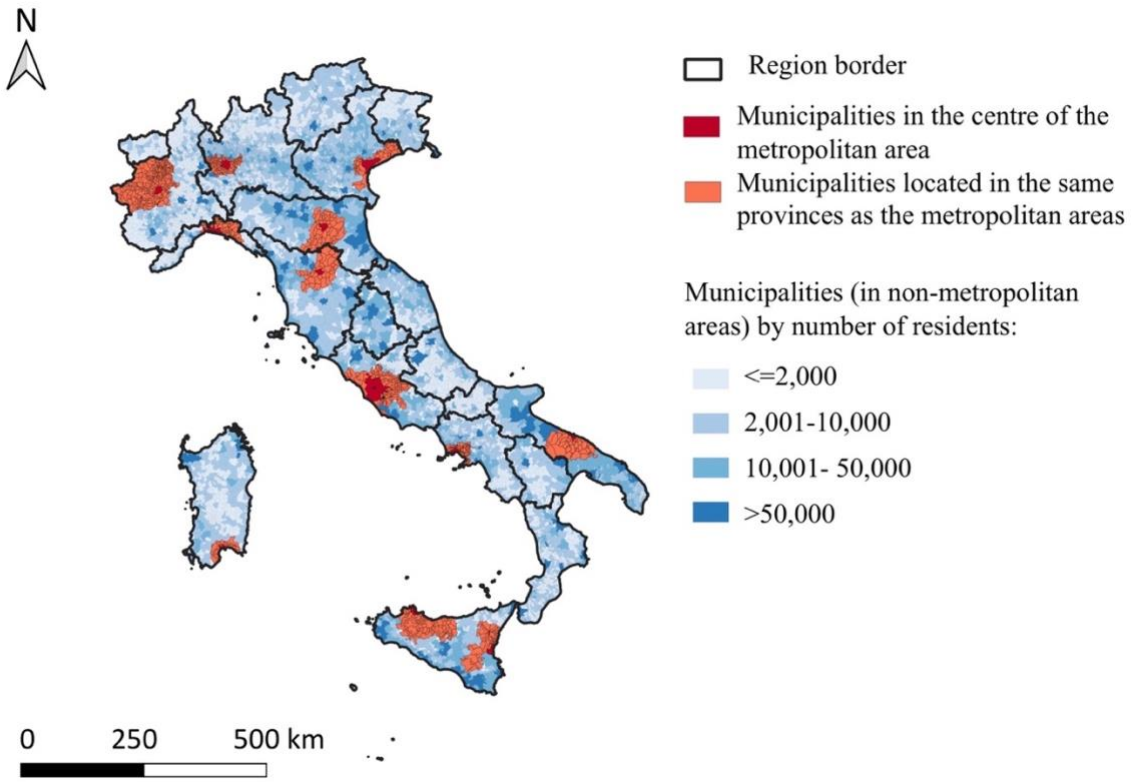

Table 2.1. The largest municipalities and provinces of metropolitan areas in terms of population, area covered and number of municipalities

	Municipality in the centre of the metropolitan area			Province of the metropolitan area		
Population (number of residents; % of all region's residents)	Rome (2,748,109; 48.2%)	Milan (1,354,196; 13.6%)	Naples (913,462; 16.3%)	province of Rome (4,216,553; 73.9%)	province of Milan (3,219,391; 32.4%)	province of Naples (2,969,571; 53.1%)
Area (area; % of all region's area)	Rome (1,285 km²; 7.5%)	Venice (416 km²; 2.3%)	Genoa (240 km²; 4.4%)	province of Turin (6,828 km²; 26.9%)	province of Rome (5,361 km²; 31.1%)	province of Palermo (5,005 km²; 19.5%)
Number of municipalities (number; % of all region's municipalities)	N/A	N/A	N/A	province of Turin (311; 26.4%)	province of Milan (132; 8.8%)	province of Rome (120; 31.7%)

2.2.2. SDG3 data sources

To develop the SDG3 index, as a first step the indicators of each of the 13 SDG3 targets, officially defined by WHO, were matched to available open data, published by Istat, Ministry of Health, and Italian National Institute of Health (i.e., Istituto Superiore di Sanità; - ISS), henceforth referred to as "Italian indicators". The process resulted in matching the Italian indicators with the official ones except for:

- four cases in which multiple Italian indicators were assigned to one official indicator because the latter was specified with finer details (by age group – 3.7.2 or by disease – 3.4.1), or because it was too generic in its description (3.8.1 and 3.c.1);
- eight cases in which the official indicator (3.3.1, 3.5.2, 3.7.2, 3.8.1, 3.8.2, 3.a.1, 3.b.2, 3.c.1) was matched to a proxy, due to lack of specific available data among the Italian indicators;
- 11 cases in which no Italian indicator was assigned to an official one (3.1.1, 3.1.2, 3.3.3, 3.3.5, 3.5.1, 3.7.1, 3.9.1, 3.9.2, 3.b.3, 3.d.1, 3.d.2) due to lack of data.

Coherently, data were available for 11 out of 13 official SDG3 targets. In Table 2.2, for each SDG3 target and indicator, the corresponding Italian indicator is reported, together with the relevant source, the latest temporal update and the most detailed spatial level available.

Table 2.2. SDG3 targets and indicators, together with the details of corresponding Italian indicators, when available. ICD - International Classification of Diseases; Istat - Italian National Institute of Statistics, ISS - Italian National Institute of Health. Regional data refer to 19 regions and two autonomous provinces of Bolzano and Trento.

SDG3 target	SDG3 official indicator	Italian indicator	Data source	Latest availability	Spatial granularity
3.1. Maternal mortality	3.1.1. Maternal mortality ratio	N/A	N/A	N/A	N/A
	3.1.2. Proportion of births attended by skilled health personnel	N/A	N/A	N/A	N/A
3.2. Neonatal and child mortality	3.2.1. Under-five mortality rate	3.2.1. Mortality rate of children 0-4 years old per 1,000 births	Istat	2019	municipal
	3.2.2. Neonatal mortality rate	3.2.2. Neonatal (0-29 days old) mortality rate per 10,000 live births	Ministry of Health	2018	regional
3.3. Infectious diseases	3.3.1. Number of new HIV infections per 1,000 uninfected population, by sex, age and key populations	3.3.1. Number of new HIV infections per 1,000 residents >=15 years old	ISS	2019[1]	regional
	3.3.2. Tuberculosis incidence per 100,000 population	3.3.2. Tuberculosis incidence rate per 100,000 residents	Ministry of Health	2008	geographical areas[2]
	3.3.3. Malaria incidence per 1,000 population	N/A	N/A	N/A	N/A
	3.3.4. Hepatitis B incidence per 100,000 population	3.3.4. Hepatitis B incidence rate per 100,000 residents	ISS	2022	regional
	3.3.5. Number of people requiring interventions against neglected tropical diseases	N/A	N/A	N/A	N/A
3.4. Noncommunicable diseases	3.4.1. Mortality rate attributed to cardiovascular disease, cancer, diabetes or chronic respiratory disease	3.4.1(1). Mortality rate attributed to cardiovascular diseases (ICD10: I00-I99) per 1,000 residents	Istat	2019	municipal
		3.4.1(2). Mortality rate attributed to malignant neoplasms (ICD10: C00-C97), per 1,000 residents	Istat	2019	municipal
		3.4.1(3). Mortality rate attributed to diabetes mellitus (ICD10: E10-E14) per 1,000 residents	Istat	2019	municipal

		3.4.1(4). Mortality rate attributed to respiratory diseases (ICD10: J00-J99) per 1,000 residents	Istat	2019	municipal
	3.4.2. Suicide mortality rate	3.4.2. Suicide mortality rate (ICD10: X60-X84) per 1,000 residents	Istat	2019	municipal
3.5. Substance abuse	3.5.1. Coverage of treatment interventions (pharmacological, psychosocial and rehabilitation and aftercare services) for substance use disorders	N/A	N/A	N/A	N/A
	3.5.2 Alcohol per capita consumption (aged 15 years and older) within a calendar year in litres of pure alcohol	3.5.2. Residents >11 years old who consume alcohol between meals (%)	Istat	2022	regional and category of municipality
3.6. Road traffic	3.6.1. Death rate due to road traffic injuries	3.6.1. Mortality rate in road accidents per 10,000 residents	Istat	2021	municipal
3.7. Sexual and reproductive health	3.7.1. Proportion of women of reproductive age (aged 15-49 years) who have their need for family planning satisfied with modern methods	N/A	N/A	N/A	N/A
	3.7.2. Adolescent birth rate (aged 10-14 years; aged 15-19 years) per 1,000 women in that age group	3.7.2(1). Maternal age-specific fertility rates per women 10-14 years old (%)	Istat	2021	regional
		3.7.2(2). Maternal age-specific fertility rates per women 15-19 years old (%)	Istat	2021	regional
3.8. Universal health coverage	3.8.1. Coverage of essential health services	3.8.1(1). Beds in public hospitalisation facilities (ordinary hospitalization) per 1,000 residents	Ministry of Health	2021	provincial
		3.8.1(2). Pharmacies per 10,000 residents	Ministry of Health	2021	municipal
		3.8.1(3). Places in residential social-welfare and social-health facilities per 100,000 residents	Istat	2020	regional
		3.8.1(4). Anti-influenza vaccination coverage (%)	Ministry of Health	2022/2023	regional

	3.8.2. Proportion of population with large household expenditures on health as a share of total household expenditure or income	3.8.2. Households who do not have enough money for health care (%)	Istat	2022	geographical areas[3] and category of municipality
3.9. Environmental health	3.9.1. Mortality rate attributed to household and ambient air pollution	N/A	N/A	N/A	N/A
	3.9.2. Mortality rate attributed to unsafe water, unsafe sanitation and lack of hygiene (exposure to unsafe Water, Sanitation and Hygiene for All (WASH) services)	N/A	N/A	N/A	N/A
	3.9.3. Mortality rate attributed to unintentional poisoning	3.9.3. Mortality rate (ICD-10 =X40, X43-X44, X46-X49) per 1,000 residents	Istat	2019	municipal
3.a. Tobacco control	3.a.1. Age-standardized prevalence of current tobacco use among persons aged 15 years and older	3.a.1. People >=14 years old who smoke cigarettes (%)	Istat	2022	regional and category of municipality
3.b. Medicines and vaccines	3.b.1. Proportion of the target population covered by all vaccines included in their national programme	3.b.1. Children obligatory vaccination coverage (poliomyelitis, diphtheria, tetanus, whooping cough, hepatitis B, hemophilus influenzae type B, measles, mumps, rubella, chicken pox) (%)	ISS	2020	regional
	3.b.2. Total net official development assistance to medical research and basic health sectors	3.b.2. Expenditure for social home care, home care integrated with health services, social and health vouchers, contributions for health benefits, contributions for mental illness, day care centers for people with mental distress per resident (EUR)	Istat	2020	municipal
	3.b.3. Proportion of health facilities that have a core set of relevant essential medicines available and affordable on a sustainable basis	N/A	N/A	N/A	N/A
3.c. Health financing and workforce	3.c.1. Health worker density and distribution	3.c.1(1). Specialist practitioners per 10,000 residents	Istat	2021	regional
		3.c.1(2). General practitioners per 10,000 residents	Istat	2021	regional

		3.c.1(3). Dentists per 10,000 residents	Istat	2021	regional
		3.c.1(4). Doctors in public hospitalization facilities per 10,000 residents	Ministry of Health	2021	provincial
		3.c.1(5). Nurses in public hospitalization facilities per 10,000 residents	Ministry of Health	2021	provincial
		3.c.1(6). Pharmacists per 10,000 residents	Istat	2021	regional
3.d. Emergency preparedness	3.d.1. International Health Regulations (IHR) capacity and health emergency preparedness	N/A	N/A	N/A	N/A
	3.d.2. Percentage of bloodstream infections due to selected antimicrobial-resistant organisms	N/A	N/A	N/A	N/A

[1] Data available also for 2020, but ignored due to COVID-19 effect.
[2] North, Centre, South, Islands.
[3] Northwest, Northeast, Centre, South, Islands

Furthermore, the International Organization for Standardization (ISO) developed the ISO/TS 21564:2019 standard to ensure consistency and clarity in communication among stakeholders involved in healthcare management and policymaking. Therefore, to obtain a measure of the matching quality between terminology resources in the official and in the Italian indicator, the ISO/TS 21564:2019 standard was applied, in which matching is defined as four possible levels (ISO, 2023):

- 0: Exact match on semantic domain,
- 1: Fully inclusive overlap of semantic domain,
- 2: Non-inclusive overlap of semantic domain,
- 3: No overlap.

2.2.3. SDG3 index computation

As the final goal was to obtain an SDG3 index able to describe the achievements at municipal level, in case the data of the Italian indicators were available at a less detailed spatial level (i.e., provincial, regional, or in bigger areas) the same value was assigned to all the municipalities being part of such geographical partition. In case the data were available only at regional or bigger geographical area level, but they were separately reported for the different classes of municipalities (see description in section 2.2.1), an original mathematical approach was proposed. The value corresponding to such class was assigned as baseline to each municipality in that class, then weighted by a coefficient calculated as follows:

$$coefficient = \frac{value_a * number\ of\ municipalities_a}{\sum(value_b * number\ of\ municipalities_{b\ within\ a})} \tag{2.1}$$

where *a* is the less detailed geographical partition (i.e., regional or bigger geographical area), and *b* is the more detailed geographical partition (i.e., class of municipality).

For example, for the Lazio region, the distribution of the 378 municipalities in the six classes is: 1, 120, 121, 101, 32, 3. Assuming an Italian indicator (% of smokers in 2022) measuring 0.205 for the whole region, and baseline values of 0.185, 0.214, 0.188, 0.188, 0.192, 0.209 for each of the classes, respectively, the regional coefficient for Lazio is equal to:

$$coefficient = \frac{0.205 * 378}{0.185 * 1 + 0.214 * 120 + 0.188 * 121 + 0.188 * 101 + 0.192 * 32 + 0.209 * 3} = 1.04 \tag{2.2}$$

Accordingly, to each of the 378 municipalities in Lazio, the baseline value corresponding to its class, weighted by 1.04, was assigned.

For each Italian indicator, once having derived the values for each municipality, data were normalised between 0 and 1, with 0 representing values related to poor health outcomes and 1 being the best outcome.

Regarding the calculation of scores relevant to each official indicator and target, if multiple Italian indicators were used together for the computation of one official indicator, they were averaged to compute the unique output, according to the equation 2.3:

$$official\ indicator\ score = \frac{\sum_i^n Italian\ indicator_i}{n} \tag{2.3}$$

where *n* is the total number of Italian indicators forming the official indicator.

Similarly, the score of each target was then calculated as the average of the official indicators' scores included in it (equation 2.4):

$$target\ score = \frac{\sum_j^m official\ indicator_j}{m} \tag{2.4}$$

where *m* is the total number of official indicators forming the SDG3 target.

To compute the final SDG3 index, as no specific guidelines for weighting are provided by the UN, the output value was defined as the average of all the available targets (equation 2.5), an approach widely adopted in relevant literature (Guijarro and Poyatos, 2018; Lafortune et al., 2018), including in particular the SDSN Sustainable Development Report (Sachs et al., 2023):

$$SDG3\ index = \frac{\sum_k^l target_k}{l} \tag{2.5}$$

where *l* is the total number of SDG3 targets.

As a result, the final index can range from 0 to 1, with higher values corresponding to a greater fulfilment of the SDG3 targets in the corresponding municipality. The workflow of the index computation is graphically summarized in Figure 2.3.

Figure 2.3. Workflow of SDG3 index computation for the Italian municipalities

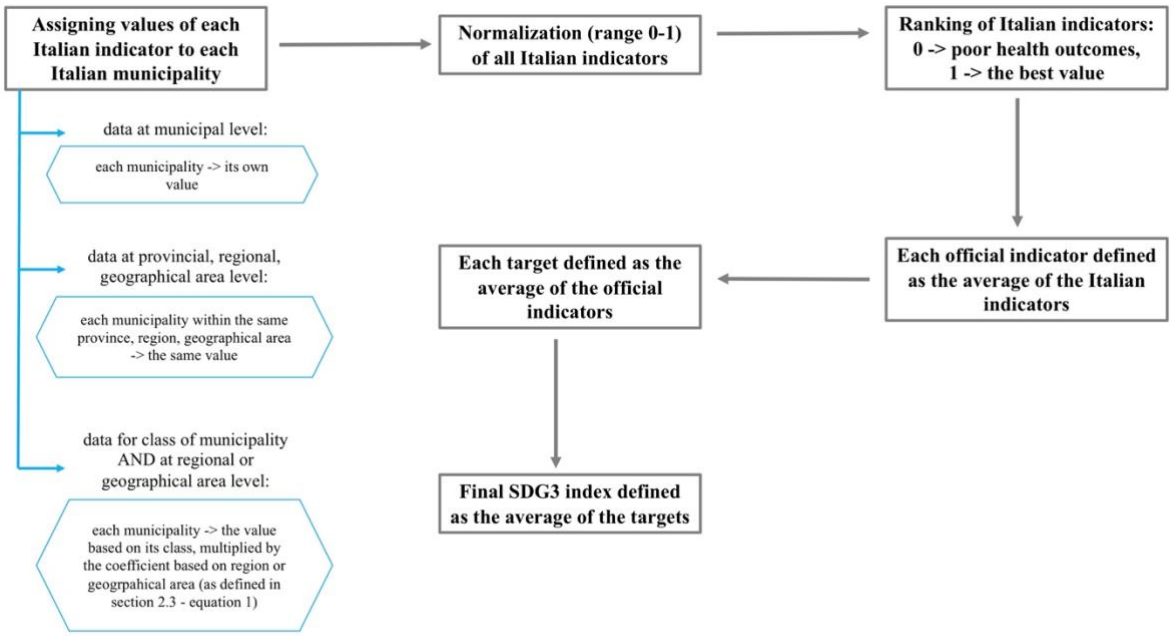

Considering the hierarchical structure of the proposed SDG3 index, the contribution of each i-th Italian indicator to the final index can be defined as follows:

$$w_{i,j,k} = \frac{1}{N} * \frac{1}{M} * \frac{1}{L}$$

where *N* is the number of Italian indicators in the corresponding j-th official indicator, *M* is the number of official indicators in the corresponding k-th official target, and *L* is the total number of targets covered by available Italian data.

Consequently, the weight of each official indicator (covered by at least one Italian indicator, otherwise its weight is zero) included in the SDG3 index can be calculated by the following formula:

$$w_{j,k} = \frac{1}{M} * \frac{1}{L}$$

and the weight of each target (covered by at least one Italian indicator, otherwise its weight is zero) can be expressed by the equation below:

$$w_k = \frac{1}{L}$$

Accordingly, these formulas allow to calculate the relative contributions of national indicators, official indicators, and targets when applying the framework to other countries, with varying data availability.

2.2.4. Statistical analysis and visualization

To analyse the characteristics of the indicators and the final index, data were summarised using descriptive statistics, i.e., mean, population-weighted mean, standard deviation, minimum, 25th percentile, median, 75th percentile, maximum. Additionally, the Kolmogorov-Smirnov test was applied to evaluate whether the final index and targets' scores followed a normal distribution. Subsequently, Kruskal–Wallis test with Bonferroni correction was performed to determine if

the final index for all regions, and for all provinces within each region, originated from the same distributions.

The legends on the maps describing quantitative outcomes were generated using the quantile method, ensuring an equal distribution of municipalities across each class, with a total of five or 10 classes set arbitrarily. In case this method led to a poor visualization due to the values' distribution, the Jenks natural breaks method (Chen et al., 2013) was used. This technique classifies data minimizing the variance within categories and maximizing the variance between categories, and a total number of either nine or 10 classes was applied, arbitrarily selected to optimize the visualization. Values displayed on the legends were rounded to three decimal places, or, when the difference in values of the subsequent classes was <0.001, to four.

To analyse the clustering tendency of the final SDG3 index, and of the three targets composed entirely of the Italian indicators with original data provided directly at municipal level, Moran's Index (both global and local), with queen contiguity method (Getis and Aldstadt, 2004) used to define neighbours, was applied. The global Moran's I statistic quantifies the overall tendency to cluster by measuring the correlation coefficient between the variable values in each municipality and its neighbours. This statistic corresponds to the slope of the ordinary least squares (OLS) line fitted to the normalized scatterplot depicting the relationship between the variable values in each municipality and the mean value of its neighbours. Significance (at level equal to 0.05) was determined using the pseudo p-value derived from Monte Carlo simulation, with a default value of 999 permutations (equation 2.6).

$$pseudo\ p - value = \frac{number\ of\ permutations\ yielding\ a\ more\ extreme\ Moran's I\ statistic}{1000} \qquad (2.6)$$

To analyse local dependencies, Local Indicators of Spatial Autocorrelation (LISA) clusters were derived from the local version of Moran's I and mapped. The scatterplot, with the variable value in each municipality on the x-axis and the mean of its neighbours' values on the y-axis, can be divided into four quadrants by drawing a horizontal and a vertical line corresponding to the mean values for each axis. Quadrants define the following clusters:

- top right corner, high-high (HH) cluster, where the municipality with high variable value is surrounded by municipalities with high mean of the values;
- bottom right corner, high-low (HL) cluster, where the municipality with high variable value is surrounded by municipalities with low mean of the values;
- bottom left corner, low-low (LL) cluster, where the municipality with low variable value is surrounded by municipalities with low mean of the values;
- top left corner, low-high (LH) cluster, where the municipality with low variable value is surrounded by municipalities with high mean of the values.

Also in this case, the Monte Carlo simulation was used to assess the significance of observations. In each permutation for local Moran's I, the value for the municipality being assessed for significance remained fixed while all other values were shuffled. Similar to the global version, the pseudo p-value was calculated according to equation 2.6.

2.3. Results

The SDG3 index was calculated for the Italian municipalities existing at the 1st January 2023, excluding Misiliscemi in Sicily region, formerly part of Trapani municipality, as the computation of indicator values was impossible for such municipality created by disaggregating a city's district. Therefore, the proposed index was computed for a total of 7,900 municipalities.

2.3.1. Mapping between SDG3 official indicators and Italian indicators

Based on the ISO/TS 21564:2019, the results of the matching quality were the following: for 11 of the 28 official SDG3 indicators, no corresponding Italian indicator was found (level 3), as presented in Table 2.2. For the remaining 17 official indicators, 29 Italian indicators were matched, of which 11 represented the exact match on semantic domain (quality level 0), while nine indicators were assigned a quality level of 1, and nine indicators a quality level of 2. The resulting quality of the matching process for each Italian indicator to each SDG3 official indicator, based on ISO/TS 21564:2019, is summarized in Figure 2.4.

Figure 2.4. ISO/TS 21564:2019 measures of the quality of matching (represented by the colours where 0 is the best and 3 is the worst) of each Italian indicator included in the computation for each of the 28 official SDG3 indicators, here summarized in the 13 SDG3 targets.

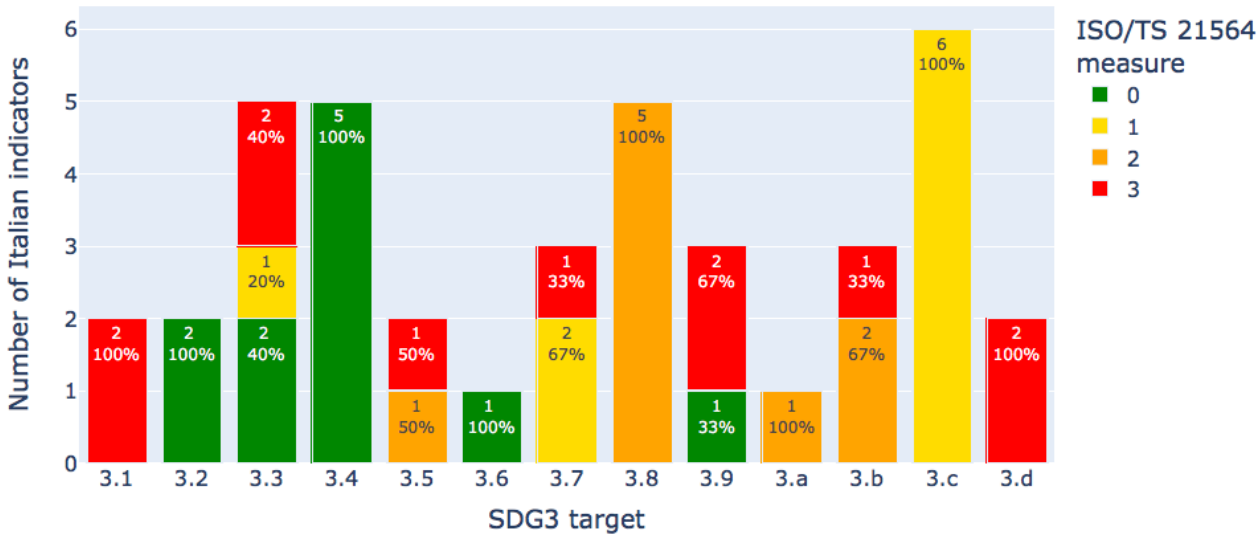

A description of the basic statistical properties of the raw values (i.e., values assigned to each municipality, as described in the first black box in Figure 2.3) for the 29 Italian indicators, as well as relative weight of each Italian indicator, official indicator, and target in the final SDG3 index, is summarized in Table A2.1 in Appendix, while the median, 25th, and 75th percentile of the raw values of selected Italian indicators, is reported in Table 2.3. Considering the 29 Italian indicators, their contribution to the final SDG3 index varied from 1/88 (1.14%) for all the national indicators forming official indicators 3.4.1 and 3.8.1, to 1/11 (9.09%) for Italian indicators covering 3.5.2, 3.6.1, 3.9.3 and 3.a.1. Regarding the official indicators, covered by Italian data, their weight ranged from 1/33 (3.03%) for indicators in target 3.3. *Infectious*

diseases to 1/11 (9.09%) for indicators in target 3.5. *Substance abuse*, 3.6. *Road traffic*, 3.7. *Sexual and reproductive health*, 3.9. *Environmental health*, 3.a. *Tobacco control*, and 3.c. *Health financing and workforce*. Each target score contributed by 1/11 (9.09%) to the final SDG3 index for Italy. The distribution of all the Italian indicators after normalization and ranking, as described in section 2.2.3 (i.e., value 0 corresponding to the poorest health performance, and value 1 – to the best performance), and of the SDG3 targets (calculated according to equation 2.4 in section 2.2.3), is graphically presented in Figure 2.5, as boxplots of the values obtained for 7,900 municipalities.

The maximum value exceeded the value of the 75th percentile by one order of magnitude in four indicators (the number of pharmacies (indicator 3.8.1(2) in Figure 2.5), municipality expenditure for health services (3.b.2), mortality due to diabetes mellitus (3.4.1 (3)), and mortality for respiratory diseases (3.4.1(4))), relevant to 56 unique municipalities, all with less than 4,000 residents. This characteristic is illustrated in Figure 2.5 (top panel) by a narrow interquartile range and a large number of outliers, represented by dots.

When considering *Infectious diseases* (target 3.3), the lowest values were achieved by hepatitis B (median incidence 0.189 infections per 100,000 residents; indicator 3.3.4 in Figure 2.5), followed by HIV (3.86 for indicator 3.3.1), with both indicators available at regional level. Tuberculosis instead had the highest incidence among the analysed diseases (10.8 for indicator 3.3.2), but data were only available for multi-regional aggregations (into four geographical areas) and not recently updated (2008); consequently, its boxplot is characterised by the largest interquartile range among all the Italian indicators.

With regards to *Noncommunicable diseases* (target 3.4) whose data were accessible at municipal level, suicide reached the lowest median value (<0.1 per 1,000 residents; indicator 3.4.2 in Figure 2.5), followed by diabetes mellitus (0.205 for 3.4.1(3)), respiratory diseases (0.785 for 3.4.1(4)), malignant neoplasms (2.70 for 3.4.1(2)), and cardiovascular diseases (3.80 for 3.4.1(1)). As the interquartile range of all indicators of this target was relatively narrow, with a high number of outliers, these characteristics are also reflected in the boxplot for the SDG3 targets (bottom panel of Figure 2.5).

For target 3.c. (*Health financing and workforce*), at regional level, the number of specialists resulted in the highest median value (31.27 per 10,000 residents; indicator 3.c.1(1) in Figure 2.5), followed by pharmacists (13.05 for 3.c.1(6)), dentists (8.35 for 3.c.1(3)) and general practitioners (8.01 for 3.c.1(2)). The minimum number of specialists (24.2 per 10,000 residents) was also much higher than the other three groups, characterised by a minimum of 6.0 pharmacists, 5.71 dentists and 6.07 general practitioners. When considering the staff of public hospitals, a median value of 16.04 doctors (indicator 3.c.1(4)) and 23.24 nurses (indicator 3.c.1(5)) per 10,000 inhabitants at the provincial level was obtained.

The characteristics of indicators' distribution are reflected in the boxplots of each SDG3 target (bottom panel of Figure 2.5), defined as the average of the indicator scores. In particular, four targets (i.e., 3.4, 3.6, 3.9, 3.b) show relatively narrow interquartile ranges and a large number of outliers, with the first three composed entirely of mortality rates provided at municipal level. Of all 11 normalised and ranked targets, only four (i.e., 3.3, 3.8, 3.b, 3.c) had a median below 0.5, with the lowest median of 0.59 (target 3.5) among the remaining targets.

Table 2.3. Median (25th – 75th percentile) of raw values (i.e., values assigned to each municipality, as described in the first black box in Figure 2.3) of selected Italian indicators

Italian indicator	Median (25th – 75th percentile)
3.3.1 HIV infections (per 1,000 residents)	0.039 (0.032 – 0.064)
3.3.2 Tuberculosis incidence rate (per 100,000 residents)	10.80 (2.60 – 10.80)
3.3.4 Hepatitis B incidence rate (per 100,000 residents)	0.189 (0.079 – 0.191)
3.4.1(1) Mortality rate: cardiovascular diseases (per 1,000 residents)	3.80 (2.59 – 5.37)
3.4.1(2) Mortality rate: malignant neoplasms (per 1,000 residents)	2.70 (1.89 – 3.58)
3.4.1(3) Mortality rate: diabetes mellitus (per 1,000 residents)	0.205 (0.000 – 0.533)
3.4.1(4) Mortality rate: respiratory diseases (per 1,000 residents)	0.785 (0.277 – 1.286)
3.4.2 Suicide mortality rate (per 1,000 residents)	0.000 (0.000 – 0.000)
3.8.1(2) Pharmacies (per 10,000 residents)	4.16 (2.80 – 8.14)
3.b.2 Municipality expenditure for health services (per resident) (EUR)	11.70 (5.32 – 21.48)
3.c.1(1) Specialist practitioners per (10,000 residents)	31.27 (29.32 – 34.81)
3.c.1(2) General practitioners (per 10,000 residents)	8.01 (7.51 – 8.63)
3.c.1(3) Dentists (per 10,000 residents)	8.35 (8.25 – 8.73)
3.c.1(4) Doctors in public hospitalization facilities (per 10,000 residents)	16.04 (12.70 – 18.64)
3.c.1(5) Nurses in public hospitalization facilities (per 10,000 residents)	23.24 (10.83 – 31.47)
3.c.1(6) Pharmacists (per 10,000 residents)	13.05 (12.46 – 15.85)

Figure 2.5. Top panel: Boxplots of the considered 29 Italian indicators after normalization and ranking, as described in section 2.2.3. Bottom panel: Boxplots of the 11 SDG3 targets (i.e., the average of official indicators as described in equation 2.4 in section 2.2.3).

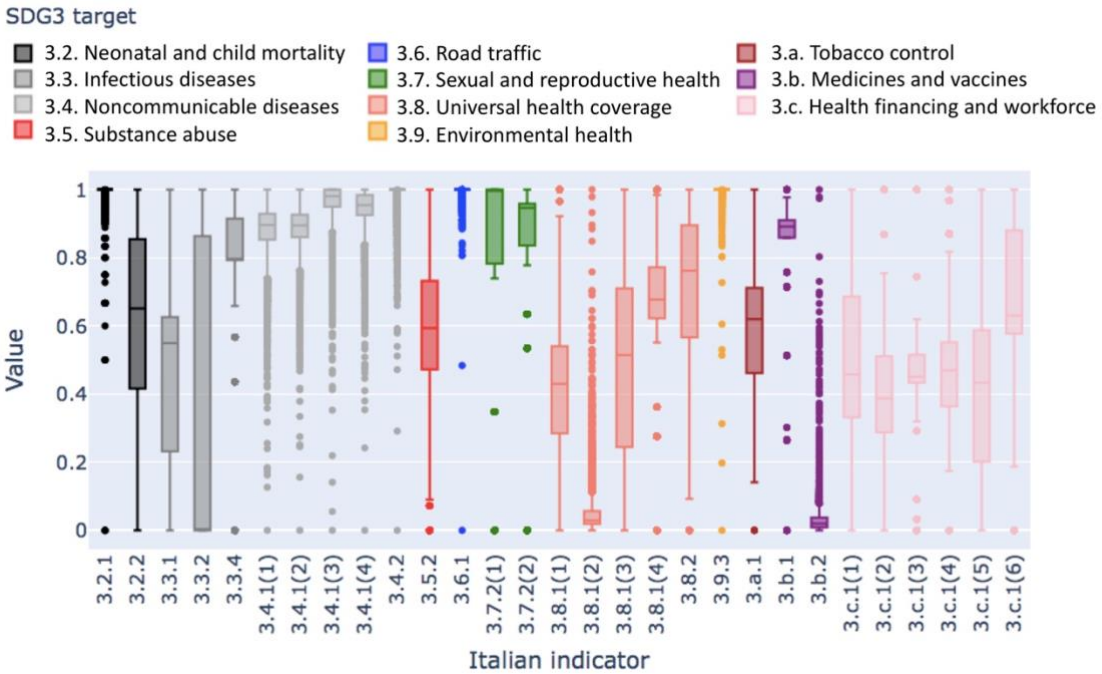

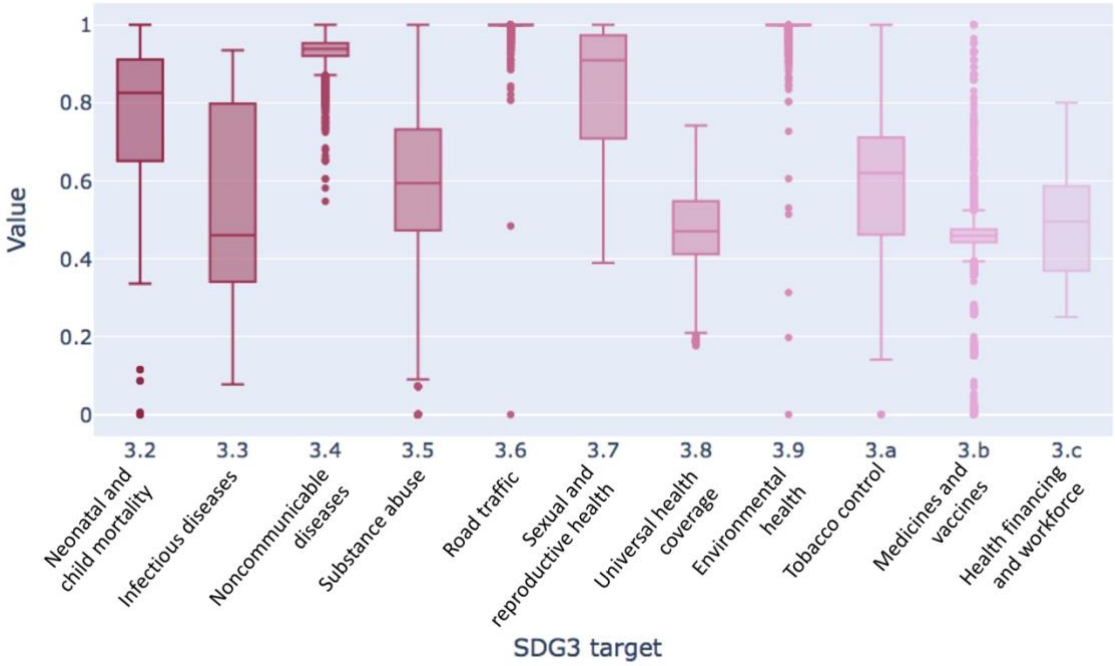

2.3.2. SDG3 index for Italian municipalities

The values of the final index, i.e., the average of all available targets' scores, ranged from 0.595 to 0.81. The lowest value was reached by Terragnolo in the province of Trento (Trentino-Alto Adige/Südtirol region), with a population of 707, and the highest by Girasole in the province of Nuoro (Sardinia region) with a population of 1,350. The median value of the index was 0.697 (25th-75th percentiles = 0.681 - 0.719). When considering classes of municipalities (as described in section 2.2.1), the highest median was achieved by municipalities in the centre of the metropolitan area (0.709), not much higher compared to those with up to 2,000 residents (0.707), followed by those between 10,001 and 50,000 inhabitants (0.698), municipalities in the province of the centres of the metropolitan areas (0.691), municipalities between 2,001 and 10,000 inhabitants (0.690), while the lowest score was achieved by those with a population of more than 50,000 (0.683). In particular, among municipalities at the centre of the metropolitan area, the highest score was obtained by Cagliari, Sardinia (0.785), then Turin, Piedmont (0.729), followed by Florence, Tuscany (0.726). The computed final index for each municipality is visualized as colour-coded information in Figure 2.6 (legend of categories obtained with quantiles method) for the whole country, and in Figure A2.1 for each region separately.

Figure 2.6. Final SDG3 index computed for all the 7,900 Italian municipalities

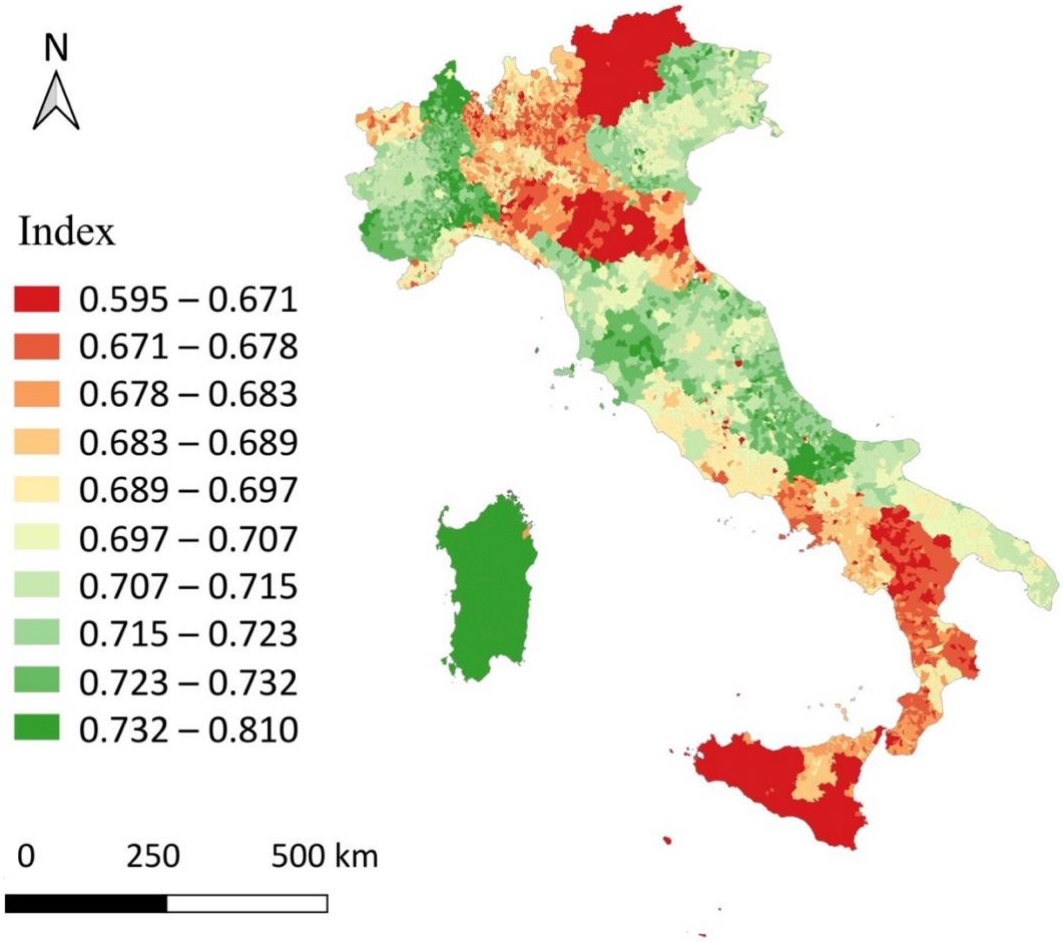

At the regional level, the highest population-weighted mean of the SDG3 index was obtained for Sardinia (0.775), Molise (0.737) and Piedmont (0.721), while the lowest for the autonomous province of Trento (0.635), the autonomous province of Bolzano (0.637), and Sicily (0.667). The same order was also reflected in the distribution of index's median across regions. The highest max-min range within the same region was noted for Piedmont (0.154), Marche (0.131) and Abruzzo (0.092). In general, municipalities located in the central, far Northeast, and far Northwest regions of Italy reached relatively high values. The boxplots of the SDG3 index at regional level are plotted in Figure 2.7.

Figure 2.7. Boxplots of the SDG3 index in the Italian regions. The width of the boxplot is represented as proportional to the resident population.

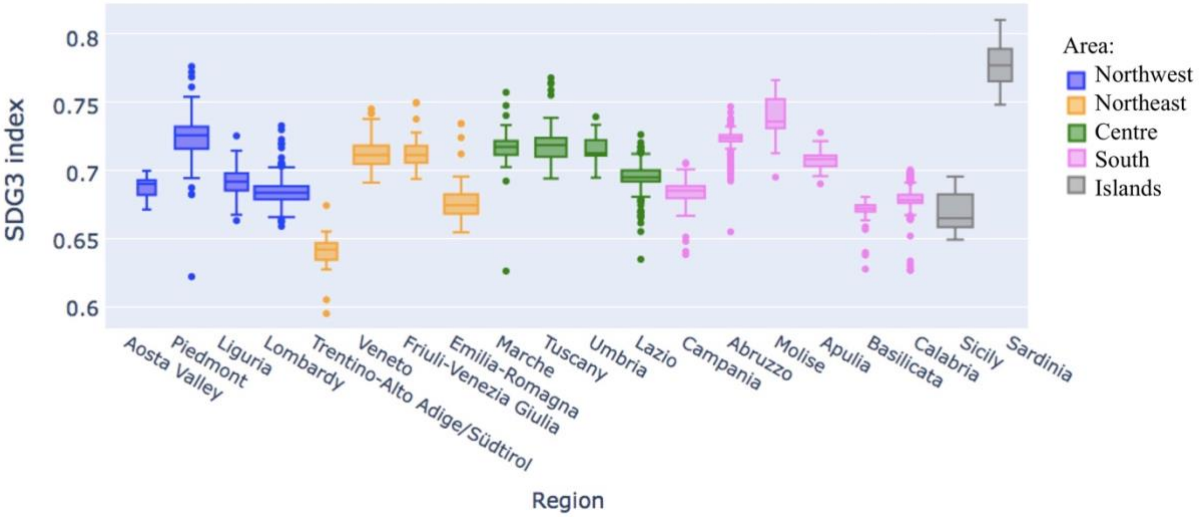

The global Moran's I (gMI) for the SDG3 index showed a strong tendency to cluster within the Italian territory, with a value of gMI=0.91 against the expected gMI=$-1.3*10^{-4}$. Concerning the three targets with municipal granularity (i.e., 3.4, 3.6, 3.9), the outcome was significant only for target 3.4. *Noncommunicable diseases* showing a small tendency to cluster (gMI=0.16). The four types of spatial autocorrelation deriving from local Moran's I (lMI) for the final SDG3 index and for target 3.4 are plotted in Figure 2.8.

Figure 2.8. Final SDG3 index and target 3.4. *Noncommunicable diseases* spatial autocorrelation types (from local Moran's Index as defined in section 2.2.4)

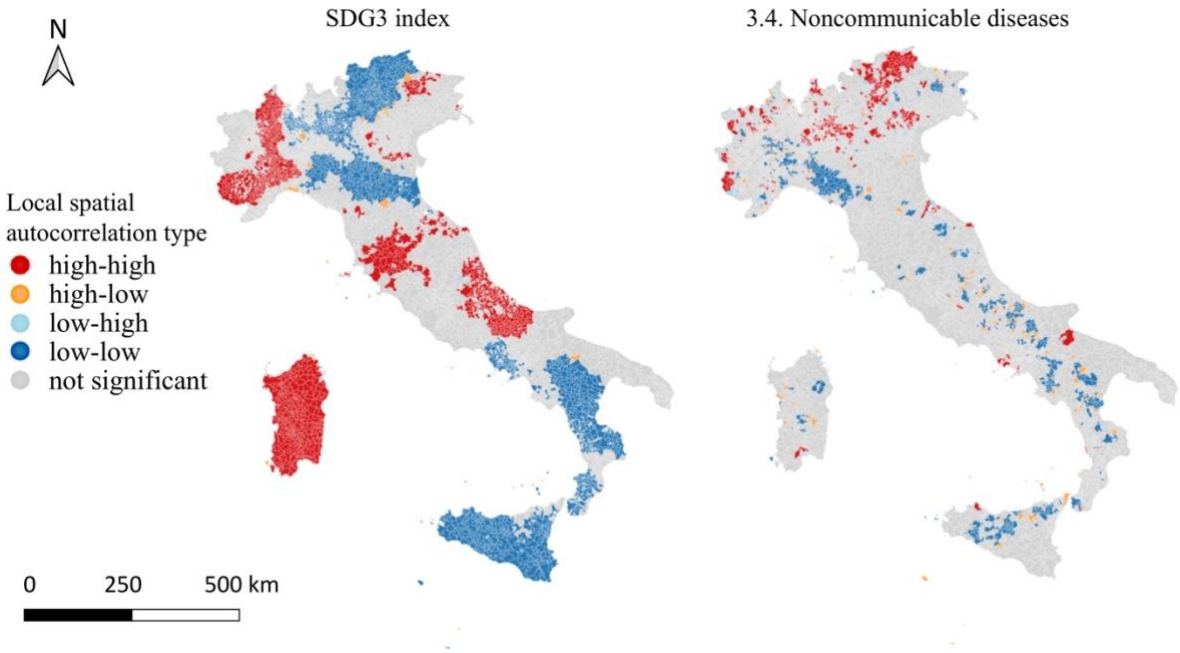

Scores of single targets are presented in Figures 2.9-2.11. Based on the geographical distribution of the resulting values of the 11 SDG3 targets, it was possible to identify three groups:

1) G1 - high scores in northern municipalities, low scores in southern municipalities: 3.7. *Sexual and reproductive health*, 3.8. *Universal health coverage*, 3.b. *Medicines and vaccines*.
2) G2 - low scores in northern municipalities, high scores in southern municipalities: 3.3. *Infectious diseases*, 3.5. *Substance abuse*.
3) G3 - no clear geographical trend: 3.2. *Neonatal and child mortality*, 3.4. *Noncommunicable diseases*, 3.6. *Road traffic*, 3.9. *Environmental health*, 3.a. *Tobacco control*, 3.c. *Health financing and workforce*.

Figure 2.9. SDG3 targets' scores for 7,900 Italian municipalities: targets for which northern municipalities scores are high and southern municipalities scores are low

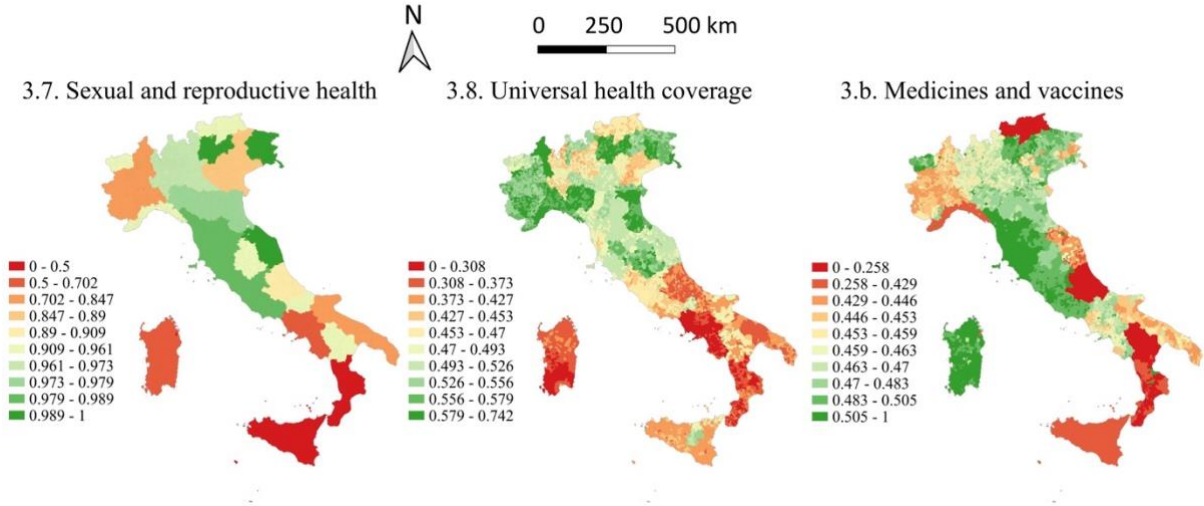

Figure 2.10. SDG3 targets' scores for 7,900 Italian municipalities: targets for which northern municipalities scores are low and southern municipalities scores are high

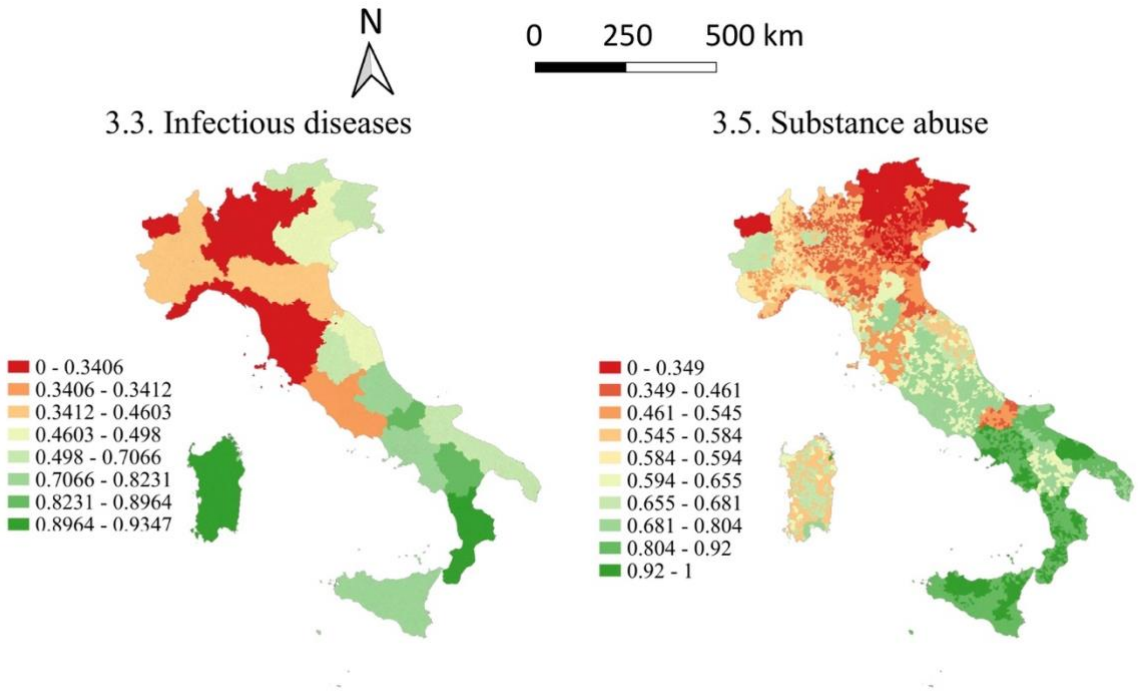

Figure 2.11. SDG3 targets' scores for 7,900 Italian municipalities: targets for which no clear geographical trend emerges. For targets 3.6. *Road traffic*, and 3.9. *Environmental health*, Jenks natural breaks method was used to optimize the visualization; for 3.9. *Environmental health*, nine classes instead of 10 were used to optimize the categorization.

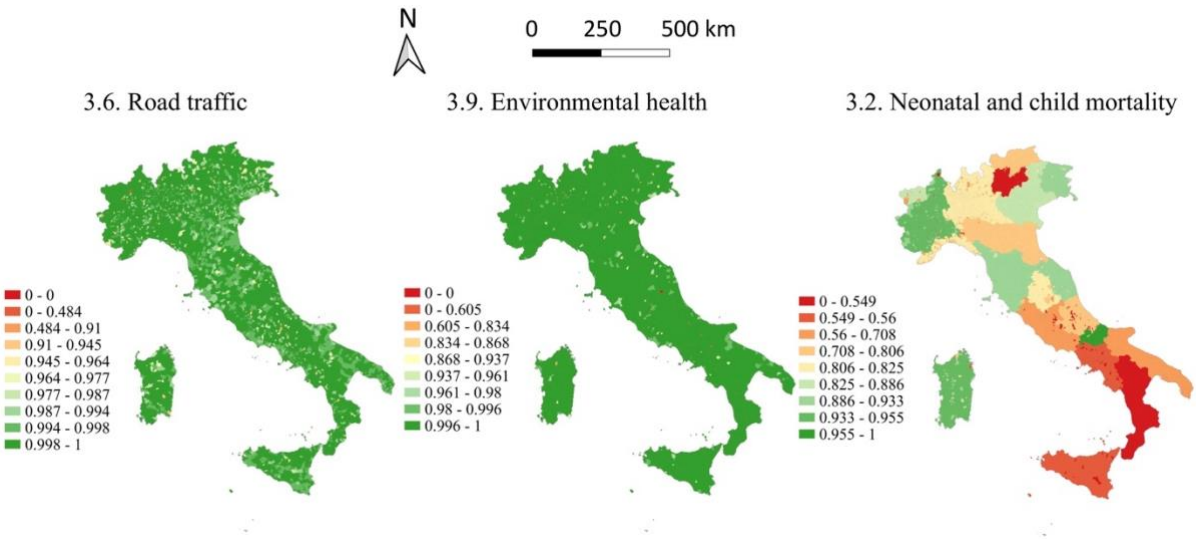

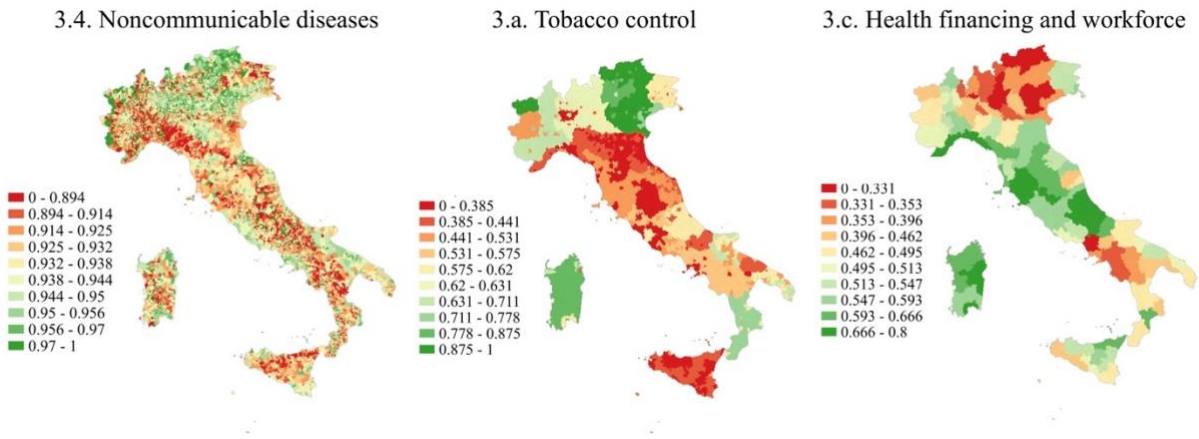

At municipal level, the standard deviation of all targets' scores ranged from 0.192 in Alice Bel Colle (Piedmont region) to 0.391 in Bresimo (Trentino-Alto Adige/Südtirol region). The standard deviation for each Italian municipality is plotted in Figure 2.12.

Figure 2.12. Standard deviation across all targets' scores

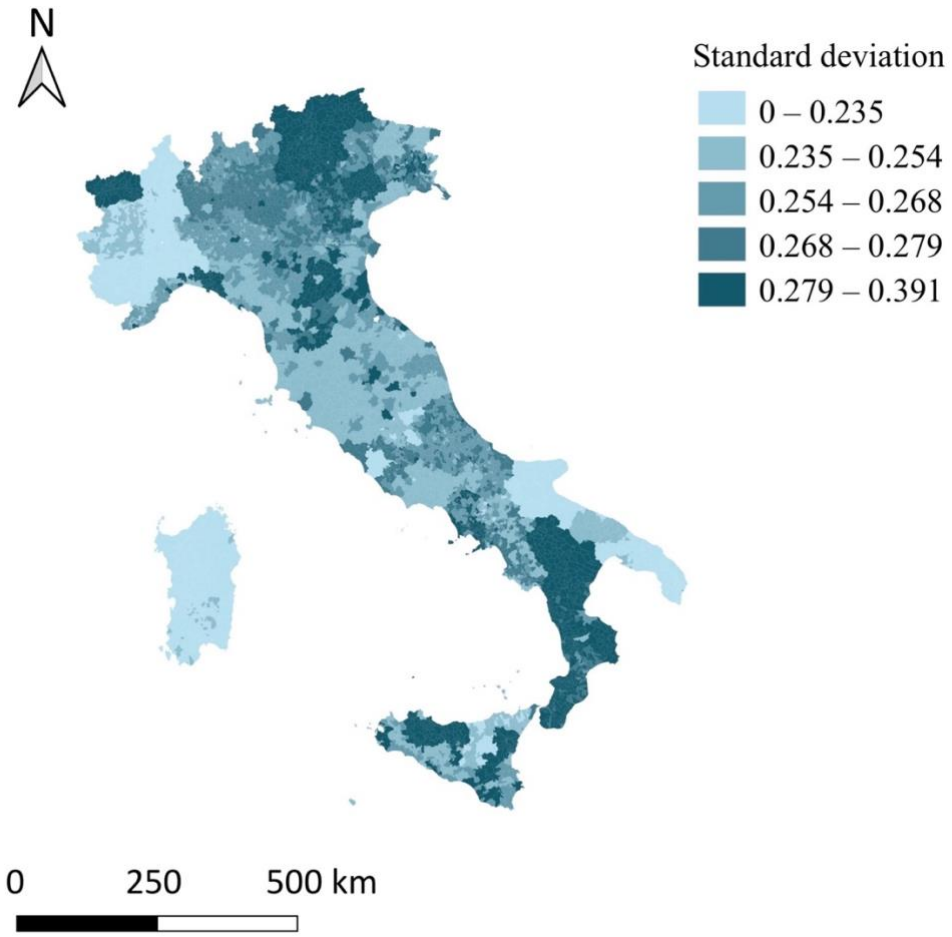

Both the final SDG3 index and the target scores resulted not normally distributed. Therefore, the municipal scores across regions, and across provinces in the same region, were statistically compared using the Kruskal–Wallis test. The municipal scores resulted differently distributed

across regions with statistical significance, both for single targets and for the final index. The analysis of spatial patterns across provinces within each region was limited to the final SDG3 index, as the geographical granularity of the data hindered the analysis of each target separately. The only regions where the distribution of municipal index did not vary among provinces are Trentino-Alto Adige/Südtirol and Abruzzo.

2.3.3. SDG3 index and cardiovascular mortality in Milan, Italy

As the forthcoming chapters of this thesis will centre on Milan, Italy, this section aims to contextualize Milan's performance within this framework, highlighting the general health vulnerability and in particular CV vulnerability of its residents. Therefore, the following paragraphs provide an overview of Milan's position in the SDG3 index, specifically focusing on indicator 3.4.1(1) *Mortality rate: cardiovascular diseases (per 1,000 residents).*

Milan SDG3 index is equal to 0.702, with 3,575 municipalities (i.e., 45.25% of all considered Italian municipalities) achieving a better performance, and 4,324 (54.73%) characterized by a lower score. Milan ranked 8th among 12 municipalities in the centre of the metropolitan area, so ranked its province among other provinces of the metropolitan areas, while the Lombardy region, in which Milan is located, placed 15th among all the 20 regions of Italy. As previously illustrated in Figure 2.8, Milan is in high-low LISA cluster, meaning that it achieved a high SDG3 score, but it is surrounded by municipalities with low scores. Figure 2.13 provides a zoomed-in view of the SDG3 index values for the Lombardy region, with the boundaries of Milan's municipality and its province clearly marked.

Figure 2.13. Final SDG3 index computed for all the 7,900 Italian municipalities, with a focus on the Lombardy region

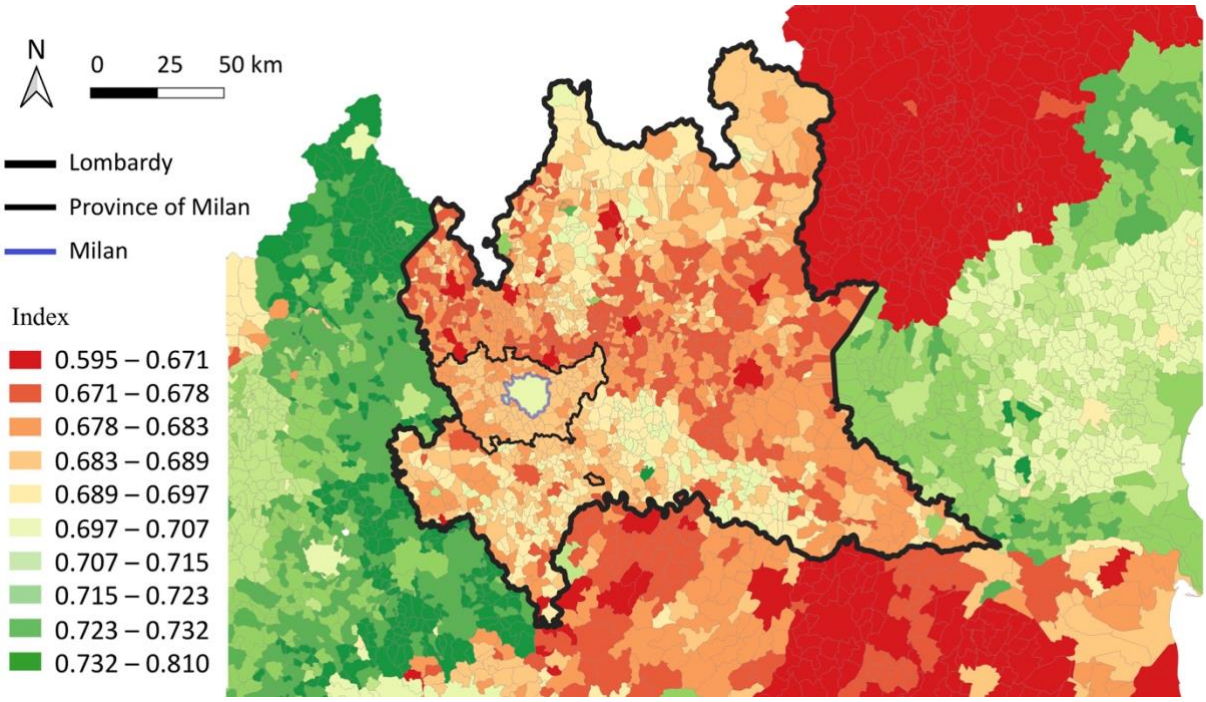

In particular, regarding the indicator 3.4.1(1). *Mortality rate: cardiovascular diseases (per 1,000 residents)*, for better interpretation, the following analyses will refer to its raw number, not normalized between 0 and 1. As highlighted in section 2.3.1, among all the non-communicable diseases included in indicator 3.4.1. *Mortality rate attributed to cardiovascular disease, cancer, diabetes or chronic respiratory disease*, CV mortality rate reached the highest median. The Italian median CV mortality rate was 3.80 per 1,000 residents, with the highest median equal to 4.31 CV deaths per 1,000 residents reached by the smallest municipalities (i.e., those with less than 2,000 residents), and with the lowest median of 3.42 reached by municipalities in the provinces of the metropolitan areas, as shown in detail in Table 2.4. Municipalities in the centre of the metropolitan area were characterised by the lowest standard deviation of the values, equal to 0.5, reaching the highest value of the 25th percentile among all the classes (i.e., 3.47 CV deaths per 1,000 residents), and the lowest 75th percentile (i.e., 4.09 CV deaths per 1,000 residents). As indicated by Kolmogorov-Smirnov test, mortality rate attributed to CV diseases was not normally distributed in any of the municipality class and, according to the Kruskal–Wallis test, the distributions were different among them.

Table 2.4. Mortality rate attributed to cardiovascular diseases (International Classification of Diseases code: I00-I99) per 1,000 residents

Municipality class	Mean	Standard deviation	Min	25th percentile	Median	75th percentile	Max
Municipalities in the centre of the metropolitan area	3.82	0.5	3.11	3.47	3.79	4.09	4.87
Province of the metropolitan area	3.78	2.28	0	2.55	3.42	4.57	20.2
<= 2,000 residents	4.84	3.95	0	2.14	4.31	6.84	36.53
2,001 – 10,000 residents	3.99	1.76	0	2.77	3.82	4.96	22.76
10,001 – 50,000 residents	3.50	1.02	0	2.79	3.47	4.16	7.25
> 50,001 residents	3.72	0.64	1.91	3.38	3.71	4.12	5.41

Specifically, CV mortality in Milan reached 3.11 deaths per 1,000 residents, placing Milan in the second quartile, at 35th percentile, among all 7,900 municipalities in respect to the lowest CV mortality rate, with 2,769 municipalities characterized by a lower rate. Milan had the lowest CV mortality rate among all the municipalities in the centre of metropolitan area. However, Milan's province, with a median rate of 2.86 CV deaths per 1,000 residents, was surpassed by the province of Cagliari, which had a lower median rate of 1.90 CV deaths per 1,000 residents. At the regional level, Lombardy had a median CV mortality rate of 2.93 deaths per 1,000 residents, making it the third-lowest among Italy's regions, following Trentino-Alto Adige (median rate of 2.53 deaths per 1,000 residents) and Valle d'Aosta (median rate of 2.71 deaths per 1,000 residents). The spatial distribution of CV mortality rates is illustrated in Figure 2.14, which zooms in on the Lombardy region and highlights the boundaries of Milan's municipality and its province.

Figure 2.14. (a) CV mortality rate (per 1,000 residents) computed for all the 7,900 Italian municipalities, (b) with a focus on the Lombardy region

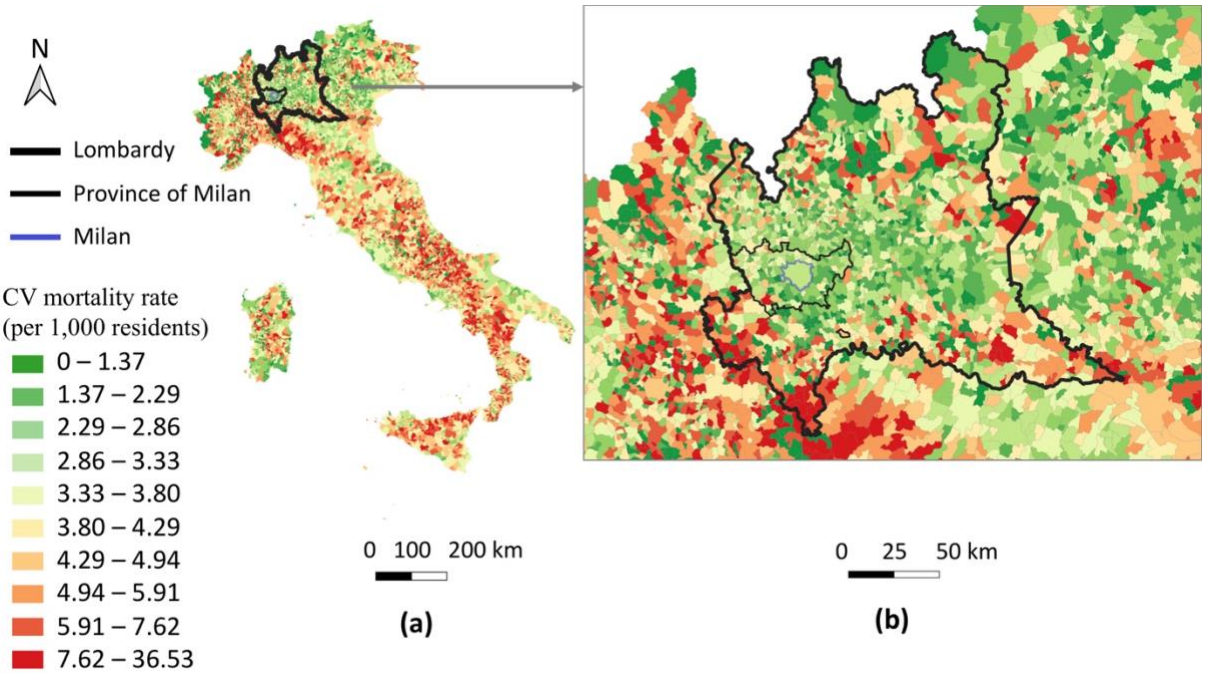

The gMI for CV mortality rates indicated a slight tendency for clustering within Italy, with a gMI value of 0.20 (expected gMI = -1.3×10^{-4}) and a p-value < 0.05. The LISA clusters derived from the lMI for CV mortality rates are presented in Figure 2.15. Milan is located in a low-low cluster, indicating that both the municipality of Milan and its surrounding municipalities exhibited relatively low CV mortality rates.

Figure 2.15. (a) LISA clusters for CV mortality rate for all the 7,900 Italian municipalities, (b) with a focus on the Lombardy region

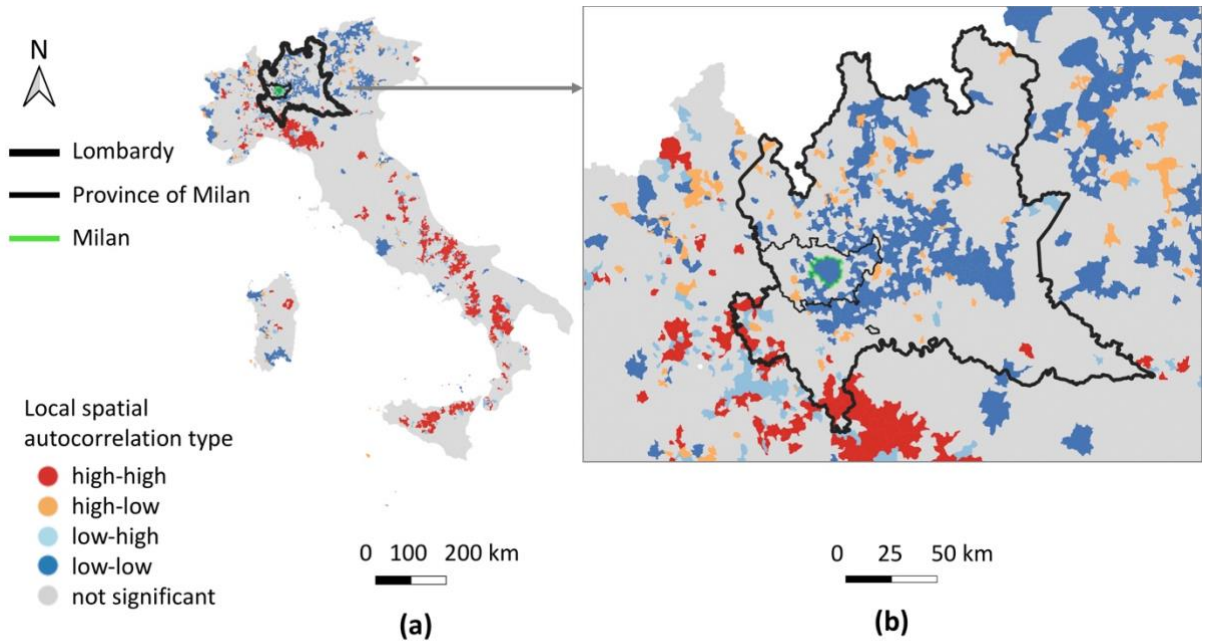

2.4. Discussion

In this study, a health vulnerability index based on SDG3 – Ensure healthy lives and promote well-being for all at all ages - was developed and applied at the granularity of the 7,900 Italian municipalities. To do so, open data relevant to 29 Italian indicators at either municipal, provincial, regional, population-based municipality class, and geographic area level were utilized, to be matched to 11 out of the 13 SDG3 targets, those for which open data were available. To the best of our knowledge, this is the first attempt to provide an SDG3 index at the municipal level for a whole country, using a standardised measure to assess the quality of the matching between officially defined indicators and available equivalents.

The scores for each municipality were calculated separately for the 11 SDG3 targets (eventually averaging the corresponding Italian indicators if multiple), and their average generated the final SDG3 index. In case of insufficient spatial granularity, the approach was to assign to each municipality the value of the corresponding lower available geographical level. Alternatively, if raw values were provided on two geographical levels, a multiplication factor was proposed to downscale the available data. Its simple statistical calculation enables extension also in cases where data are reported with more than two different granularities.

As the available data were sometimes approximative, the quality of the matching between the Italian and the official indicators was assessed using a common ISO standard, thus exploring the quality of national indices on the base of internationally indicated guidelines. This evaluation revealed that, even eight years after the adoption of the SDGs, a significant effort still needs to be made by the Italian institutions to properly provide information about all the SDG3 indicators, in particular at municipal level.

The statistical properties of the resulting indicators varied significantly and, consequently, the geographical distribution of the scores relevant to the SDG3 targets was heterogeneous, possibly described by three groups. Additionally, the proposed final SDG3 index showed a tendency to cluster. However, it may indicate a bias in the results, likely due to the heterogeneity of data granularity. In general, the computed SDG3 index values indicated that municipalities in the central portion of Italy are characterised by a relatively good fulfilment of SDG3. The significant differences in the score's distribution, even across provinces of the same region, emphasized the need to conduct the SDGs analyses at a detailed geographical level.

Originally, the establishment of SDGs was driven by the objective of ending deprivations, along with improving health and education, and fostering economic growth, with a particular attention to the challenges of ongoing climate change (UN, 2023). Upon adopting the SDGs, researchers identified issues with indicator relevance (Hák et al., 2016; Rickels et al., 2016), stating that out of the 169 targets which outline the 17 SDGs, 91 required further specification (Lu et al., 2015). Coherently, different limitations were encountered when creating the SDG3 index for Italy, including the following.

- Definition issues: It was unclear for two targets (3.8. *Universal health coverage* and 3.c. *Health financing and workforce*) what information should be taken into account, and hence the indicators were selected mostly based on the availability of relevant data sources. However, this can be partly explained considering that the SDGs were created for all UN member states, that are currently at different stages of development, without specifically identifying which

health services would need to be considered essential worldwide. The rest of the SDG3 targets are instead sufficiently well described by the official indicators, and they cover both the supply of health services (e.g., beds in hospitalization facilities or pharmacies) and the expected demand for them (e.g., by monitoring smoking prevalence or the spread of infectious diseases).

- Spatial representativeness and information robustness: When gathering data for specific indicators, especially regarding mortality in developed countries, information is accessible through compulsory hospital record registration or administrative procedures, which also facilitate the collection of data at a municipal level. However, the process is more complex for other indicators. For instance, considering 3.9.1. *Mortality rate attributed to household and ambient air pollution*, such a cause of death is not standardised in the International Classification of Diseases (ICD). In addition, it should be noted that self-reported data present a range of challenges, notably with regard to their accuracy. While classifying oneself as a "smoker" or "non-smoker" can be simple, evaluating whether "healthcare expenses represent a significant portion of overall expenditures" is more complex, as household expenses are not typically precisely catalogued by their members, introducing a measurement bias; also, no definition of "significant portion" is given. Another important issue is that reporting certain SDGs indicators at the municipal level, such as hospital bed capacity, may not be practical. To address this problem, a possible solution is to implement a gravity model, designed to estimate the flow of goods or services between two or multiple locations, to assess the accessibility of the service based on physical distance (Shi et al., 2022; Ge et al., 2021; Delgado et al., 2022), or to use data provided directly at a lower granularity, which is the solution implemented in this study.

- Fluidity of the goals: The UN draws attention directly towards this issue, with each goal being linked to the others, considering both synergies and trade-offs amongst them, a topic that is furtherly discussed in the literature (Pradhan et al., 2017; Griggs et al., 2017; Bennich et al., 2020; Wu et al., 2022a; Alcamo et al., 2020; Scharlemann et al., 2020). The SDG3 shows positive interactions with the vast majority of goals worldwide, in particular with SDG1 – No poverty, SDG5 - Gender equality, SDG6 - Clean water and sanitation, and SDG10 - Reduced inequalities (Pradhan et al., 2017; Scharlemann et al., 2020). On the other hand, in Italy, SDG3 shows a major trade-off with SDG8 - Decent work and economic growth, a relationship that was also found, among others, in the United States, Spain and Sweden (Pradhan et al., 2017). While some trade-offs have been previously reported among different SDGs, no similar issues have been identified within single goals.

- Quantitative measurement: Out of the 13 officially defined targets of SDG3, a precise quantitative objective is formulated for only two of them, 3.1. *By 2030, reduce the global maternal mortality ratio to less than 70 per 100,000 live births*, and 3.2. *By 2030, end preventable deaths of newborns and children under 5 years of age, with all countries aiming to reduce neonatal mortality and under-5 mortality to, at least, as low as 12 per 1000 live births and 25 per 1000 live births*, respectively, thus providing a quantitative reference measure. For the remaining goals, instead, targets are described as aiming to "reduce", "increase", "strengthen" or "guarantee access to" the indicators concerned, without setting numerical outcomes. This same issue has been identified with reference to other objectives as well (Kubiszewski et al., 2022; Biermann et al., 2017; Mustajoki et al., 2022), which, again, can be partly explained by the global perspective of the SDGs. Under such circumstances,

rather than an index measuring indicators at a specific point in time, periodic changes in scores could be considered, an approach that, however, is at present hindered for municipal data available for Italian indicators by their temporal heterogeneity. Since 2018, Istat has released yearly reports on all SDGs (yet not at the level of municipalities), which enables periodic monitoring of the progress towards them in Italy. Nonetheless, there is a need to locally benchmark the targets (Swain and Ranganathan, 2021; Giles-Corti et al., 2020; Thomas et al., 2021), allowing the assessment of how far individual cities are from achieving concrete results, instead of a simple city-specific comparison of progress over time.

2.4.1. Comparison of the Italian results with literature

Since the establishment of the SDGs, various studies were conducted to measure progress towards SDG3 (or its single targets/indicators), mostly focusing on wide national or international geographical areas, such as OECD countries (Braithwaite et al., 2020), least developed Asian countries (Bedriñana et al., 2021) South Asia and Sub-Saharan Africa (Nwani and Ujah, 2023) or Latin America (Sanhueza et al., 2021). In particular for Italy, one study discussed the state-of-the-art in SDGs index development (Richiedei and Pezzagno, 2022), while another one analysed the contribution of the Italian National Healthcare System to the achievement of SDG3 (Pizzi et al., 2020). Additionally, six studies were published that developed and proposed national SDGs indices, including SDG3, with four of them providing it for the capital cities of each province (D'Adamo et al., 2022; Puertas and Marti, 2023; Cavalli et al., 2020; Farnia et al. 2019), while the remaining two applying regional (D'Adamo et al., 2021) or macro-area scale (Dello Strologo et al., 2021).

Focusing on single indicators that constitute SDG3 targets, five papers in which they are explicitly defined are available, with each of them covering different sets. The smallest one accounted for five indicators only (life expectancy at birth, life expectancy at 65 years old, road traffic deaths and injuries, suicide mortality and infant mortality (D'Adamo et al., 2022)), among which three were identical to those officially defined for SDG3. Two other studies accounted for one additional indicator: mortality rate (Cavalli et al., 2020), aligned with the official 3.4.1 indicator (mortality rates associated with non-communicable diseases such as cardiovascular diseases, cancer, diabetes, or chronic respiratory diseases), and support to elderly people (Farnia et al., 2019), not included in official SDG3 indicators. The above papers only included officially reported data, without any self-reported information. A single study (Dello Strologo et al., 2021), comparing the performance of Italy and Spain on macro-area divisions, defined SDG3 as a set of nine indicators, either corresponding to or proxying the following targets: 3.3. *Infectious diseases*, 3.4. *Noncommunicable diseases*, 3.6. *Road traffic*, 3.8. *Universal health coverage*, 3.9. *Environmental health*. Finally, one study (D'Adamo et al., 2021) has matched 28 Italian indicators to 11 official targets, thus closely aligning with the approach presented in this study. The main difference from this work is the geographical granularity, as the reference computes and reports the results at the regional level, while this study aimed at a municipal granularity that was never reported before. Additionally, compared to the state-of-art, a broader set of indicators was utilized, and the matching quality of indicators was assessed through an official standard (ISO/TS 21564).

With regards to the spatial perspective, two studies (D'Adamo et al., 2021; Farnia et al., 2019), with a large difference in the number of indicators included, generated maps for SDG3 scores. Interestingly, despite all indicators are referred to the same SDG3, substantial discrepancies could be observed in the geographical distribution of the performance scores reported for single targets, in particular internally to the northern regions (i.e., Piedmont, Trentino-Alto Adige/Südtirol and Liguria). Similar evidence emerges from our study (as also graphically represented in Figures 2.9-2.11), with the standard deviation of targets' scores exceeding 0.3 for selected northern municipalities. Also, for two of the three targets resulting higher in the northern municipalities (3.7. *Sexual and reproductive health*, and 3.b. *Medicines and vaccines*), those in Piedmont region were characterised by lower scores, despite this area had one of the highest median final SDG3 index score. Moreover, a previous mapping of the results at the provincial level (Farnia et al., 2019) revealed important score variations within regions, in agreement with our study, as confirmed by the statistical tests conducted on the SDG3 index. This strong spatial variability strengthens the need to conduct SDG3 analyses at a more detailed geographic level. Nonetheless, some clear trends also emerged from both the geographical analyses previously reported: the central areas of Italy demonstrated relatively strong performance for the final SDG3 indicator, while the south achieved the lowest scores. Once again, our results are in line and confirm these findings.

Several studies have quantitatively assessed the differences in various health, social, and economic indicators across Italian regions, particularly focusing on the North-South gap (Santana et al., 2020; Toth, 2014; Lynn, 2010; Mangano, 2010; Betti et al., 2023; Bosa et al., 2021). Notably, since the 1990s, the Italian National Health Service has been regionalized, which potentially contributes to the spatial differences in SDG3 scores. A previous study determined that this regionalization has further widened the already existing North-South gap in terms of residents' satisfaction with regional hospital services, patients' regional mobility, and regional healthcare deficits (Toth, 2014). Additionally, another study on Italian data found a significant correlation (r=0.936) between intelligence quotient (IQ) and geographical latitude, suggesting genetic admixture with populations that immigrated from the Near East and North Africa as a possible cause (Lynn, 2010). Furthermore, regional IQ showed a significant negative correlation with infant mortality and a positive correlation with income level (Lynn, 2010). The financial dimension has also been identified as a factor influencing regional inequalities in actual versus necessary spending on healthcare (Mangano, 2010). Southern, poorer regions are favoured in terms of publicly paid pharmaceuticals and medical visits, while Northern, richer regions benefit more in terms of residential and hospital care (Mangano, 2010). Beyond the North-South gap in the health sector, a recent study also highlighted considerable differences among regions in the Northeast, Northwest, and centre of Italy within prevention, community health services, and hospital areas (Betti et al., 2023), which aligns with our results. Besides the regionalization of the public health system, the COVID-19 pandemic was also cited as a possible cause of these disparities (Betti et al., 2023; Bosa et al., 2021).

Therefore, the existing spatial disparities in economic, social, and educational factors, along with the regionalization of the national health system, can be identified as the main drivers of the spatial differences in SDG3 targets found in this study. Despite considerable policy efforts towards SDGs achievement, which encompass, among others, accounting for the

SDGs in the national budget document, issuing an official governmental statement endorsing the implementation of the SDGs, and formulation of a lead government unit for the coordination and implementation of the SDGs across ministries (Sachs et al., 2023), there is still an important need for regional policy coordination.

2.4.2. Municipal SDG3 as an urban health index

Several urban health indices, not based on SDG3, have been developed since the early 20th century (Pineo et al., 2018a; Luo et al., 2022; Lima et al., 2022; Kåks & Målqvist, 2021; Rothenberg et al., 2014; Coles et al, 2017; Pampalon et al., 2010; Takano & Nakamura, 2001; Costa et al., 2019; Sadler et al., 2019; Jiang et al., 2018; Yanuar et al., 2010; Oliveira et al., 2019, Ogojiaku et al., 2020; Ho et al., 2019; Maclagan et al., 2014; Pineo et al., 2018b; Delaney et al., 2018; Yan et al., 2021; Remington et al., 2015 ; Green et al., 2018; Marek et al., 2021). A variety of topics were addressed, including oral health, child health, and distinguishing between health indicators and health determinants. To understand the underlying health components, diverse techniques were used, including principal component or factor analysis, regression, expert opinions, or entropy, while only a small fraction of studies utilized the arithmetic mean of the indicators. For SDG3 index, a complex data processing approach was not necessary, as the indicators were pre-defined, thereby making equal weighting appropriate. This approach might, however, hinder results reliability in countries where a consistent variability characterizes the distribution of the indicators composing a same target, as emerged for Italy. Also, the approach of equal weighting inherently penalizes health indicators for which there is an abundance of national data, as their contribution is weakened by the averaging process. Similarly, it equalizes the contribution of targets with numerous indicators and those with only a single indicator. Thus, this methodology is justifiable only under the assumption that the number of indicators included in each target does not reflect the relative importance of health aims within the framework of Agenda 2030.

Among the previously developed health indices, none considered the existing limits imposed by the regulations in a quantitative perspective, such as the numerical distance of pollution concentration from air quality thresholds. Similarly, the SDG3 targets are characterised by the lack of quantitatively defined objectives. Therefore, an index based on SDG3 can only be used for comparison among geographical units, but it is not representative of the distance from the actual fulfilment of SDG3 objectives.

The aforementioned indices were predominantly developed for individual cities/counties, with the purpose of providing a comprehensive overview of the overall health status. Alternatively, when they were computed on entire countries, they only included major cities, selected municipalities, provinces, or a few categories based on population size. Two studies only considered official geographic units more detailed than municipality level, namely meshblock in New Zealand (Marek et al., 2021) or lower layer super output areas in the United Kingdom (Green et al., 2018). Although such analyses used official administrative subdivisions, they were affected by the modifiable areal unit problem (MAUP), a significant possible source of bias (Schuurman et al., 2007). This issue also emerged in our work, with some of the indicators having a maximum value considerably higher than the 75th percentile, mostly due to rates resulting in municipalities with a very small number of inhabitants. Also,

certain health-related data, such as hospital bed capacity or the number of medical specialists, should be considered at a less detailed geographical level or be weighted with a gravity model, even if the data are available at the municipal level, as their meaning is lost with a high spatial granularity.

Previous studies have repeatedly identified a lack of national coverage at a more detailed level as a limitation, further highlighted by the possible variation in relationships among urban, village, and rural areas. In this work, only 10 out of 29 indicators could be inferred by data sources provided at municipal level; as a consequence, it is not surprising that the Moran's I indicated a tendency to cluster, with the clusters mostly corresponding to provincial or regional borders, as can be observed in Figure 2.8. This conclusion is corroborated by the fact that no correspondence with administrative boundaries can be observed for indicators inferred from data that are fully provided at municipal scale. Another common limitation of the above-mentioned urban health indices, potentially overcame by SDG3 index, is the impossibility to validate the results, with over half of them not being evaluated against any official health data. In contrast, an SDG3 index, as the one developed in this study, represents a worldwide standardized measure of health status and, as such, could potentially be set as the gold standard to validate other health indices, thus enabling a more comprehensive analysis of national health interdependencies.

2.4.3. Limitations and conclusions

To the best of our knowledge, this is the first attempt to propose a reproducible SDG3 index based on open data, computed at the municipal level, covering the whole territory of a country, specifically Italy in this study case. This index enlightened disparities in Italy's current sustainable health status, representing the underlying health vulnerability of the residents, thus potentially enabling local policymakers to use it to comparatively evaluate the territorial performance in terms of adoption of policies towards the fulfilment of SDG3 goals, and to identify areas that require substantial action. This analysis revealed that the central, far Northeast, and far Northwest parts of Italy were characterised by an overall good SDG3 performance, in contrast to the southern parts of the country; however, the results varied depending on the target. Considering the city of Milan in particular, that will represent an applicative case study in further chapters of this thesis, it placed in the middle of all Italian municipalities in SDG3 index, while it was characterised by relatively better performance in terms of CV mortality.

We highlighted the importance of calculating indices at the local level, as the results significantly varied at high geographical granularity. Within the scope of this study, one of the major challenges identified in advancing towards SDG3 achievement in Italy is the lack of data, compounded by their insufficient temporal and spatial granularity. This deficiency hinders the ability to conduct comprehensive statistical analyses, that are crucial for identifying specific areas where targeted actions are necessary. In general, the 2030 Agenda's promise of "Leave no one behind" necessitates increased attention towards a national analysis of SDG performance at a detailed geographical level. Nonetheless, this study has already yielded valuable insights which can guide local decisionmakers in developing and implementing targeted strategies, thereby serving as a call to action for effective policymaking.

This work holds global significance as well. It addresses the methodological difficulties associated with data limitations at the national level. While its primary focus is within the confines of a specific country, the study provides valuable insights into the management of limited data sets and the assessment of their alignment with officially defined indicators, such as those included in other SDGs. Therefore, its applicability extends beyond geographical boundaries and SDG3, providing a relevant resource for international researchers facing similar challenges.

The proposed framework, however, has some limitations. First, some of the data sources were not provided at the scale of single municipalities and were impossible to downscale, hindering a robust spatial statistical analysis of municipal performance, which is the main desirable application. Furthermore, the significant differences in the number of residents across municipalities resulted in computed rates that, despite being accurate, could not be fully representative (thereby exemplifying the MAUP issue). As a consequence, equal weighting, sensible to extreme values, may have further biased the results. Finally, differences in the availability of date over time made it impossible to analyse the temporal trend in the SDG3 index, which represents an essential aspect embedded in the official target definition. Also, possible indirect effects due to the COVID-19 pandemic could have affected some indicators, potentially biasing the results.

Consequently, the following challenges could be addressed in further research:

- Hierarchization of SDGs indicators and targets: The UN does not provide guidelines for weighting, possibly implying either that all targets and indicators hold equal significance, or that assigning specific weights universally across all UN member states proves unfeasible. In the latter scenario, future research could focus on assessing weights tailored to specific groups of countries, such as Mediterranean nations or European Union members, in particular by combining qualitative and quantitative methods, e.g., Delphi interviews, multiple-criteria decision analysis, dimensionality reduction, and regression analysis. Additionally, to this purpose, detailed sensitivity and statistical robustness analyses should be provided.

- Spatial monitoring of SDG3 achievement at local levels: Once detailed geographical granularity of the data is ensured, deeper quantitative and qualitative analyses to unravel the underlying drivers of spatial disparities will be crucial. Techniques such as spatial econometrics, geographically weighted regression, and spatial autocorrelation analysis can help identify and quantify the spatial patterns and influences of various health-related indicators. Furthermore, using mixed-effects models can allow for the assessment of both fixed and random effects across different spatial units, providing a more nuanced understanding of local variations.

- Temporal monitoring of SDG3 achievement at local levels: The findings of this study not only underscore the significant scarcity of available data but also highlight their temporal unavailability. Serving as a call for public institutes to provide more comprehensive and regularly updated data, this study can serve as a catalyst for initiating a systematic temporal assessment of annual progress at the municipality level for Italy. By establishing a robust framework for ongoing monitoring, future research could contribute to a deeper understanding of health and well-being trends within communities, thereby informing more targeted policy interventions and resource allocation strategies.

- Call for policymaking: Even with partial data, relevant quantitative studies provide insights that are sufficient for tailoring new local policies. Based on statistical results, future qualitative research can formulate localized policy interventions which can contribute to achieving the broader objectives of Agenda 2030 at national level.

Chapter 3. Heatwave definition and its impact on adverse cardiovascular events: a systematic review and a framework proposal

The content of this chapter is an elaborated version of the following publications:

- Nawaro, J., Gianquintieri, L., Pagliosa, A., Sechi, G. M., & Caiani, E. G. (2023). Heatwave definition and impact on cardiovascular health: A systematic review. *Public Health Reviews*, *44*, 1606266. https://doi.org/10.3389/phrs.2023.1606266

- Nawaro, J., Gianquintieri, L., Pagliosa, A., Sechi, G. M., & Caiani, E. G. (2024). A data-driven framework for the definition of heat in CV research for better comprehension of climate changes on human health. *European Heart Journal*, *45*(Supplement_1), ehae666-3578. https://doi.org/10.1093/eurheartj/ehae666.3578

Highlights:

- RQ2: What are currently applied definitions of heat in CV health context, do they influence the results, and how to standardize them?
- Systematic literature review of 54 studies analysing the impact of heat on CV health identified 21 different combinations of criteria, statistical methods, and comparison thresholds to define heat.
- Percentile-based thresholds were found to be the more commonly used method for defining heat, with thresholds ranging from the 90th to the 99th percentile.
- Standardized data-driven framework for selecting percentile threshold for defining heat in human health research, based on DLNM and Poisson regression, was proposed.

3.1. Introduction

Due to climate change, extreme weather hazards such as heatwaves, drought, hurricanes, and floods are becoming more frequent worldwide (Maxwell et al., 2019; National Academies of Sciences, 2016; Ummenhofer and Meehl, 2017). As discussed in the Chapter 1 of this thesis, one of the effects of climate change is global warming, due to the increasing concentration of greenhouse gases in the atmosphere (Houghton, 2005). The World Meteorological Organization reported that the years 2015-2022 were the warmest eight-year period since the beginning of the measurements in 1850 (WMO, 2023), with 2023 being the warmest year on record (Copernicus, 2024). Furthermore, apart from their frequency, heatwaves are increasing also in intensity and duration (Perkins-Kirkpatrick and Lewis, 2020; Steffen et al., 2014), with their climatological characteristics related to rainfall and weak pressure gradient events (Spensberger et al., 2020; Hunt, 2007). The Intergovernmental Panel on Climate Change identified the risk of death and illness from heatwaves, especially in the vulnerable population of urban areas, as one of the eight major risks related to global climate change (IPCC, 2022).

A negative impact of exposure to high temperatures on human health (i.e., cardiovascular (CV), cerebrovascular, infectious, mental and respiratory diseases) has been recognised by several studies (Liu et al., 2021a; Ballester et al., 2023; Schneider and Breitner, 2016). In particular, passive heat stress can affect the human CV system by increasing the heart rate and left ventricular contractility, and by reducing central blood volume, left ventricular filling pressures and cerebral perfusion (Crandall and Gonzalez-Alonso, 2010). Furthermore, people with a pre-existing CV disease have been found more vulnerable to high temperatures, as it reduces the organism's ability to thermoregulate (Zhang et al., 2026). A recent systematic review and meta-analysis provided evidence of the increased CV mortality and morbidity in heat conditions based on past data (Liu et al., 2022). Also, other aspects were explored in literature, from the projected effects of heat on health under different climate change scenarios (Dong et al., 2015; Gu et al., 2020; Hajat et al., 2014; Onozuka et al., 2019; Rodrigues et al., 2020), to the effectiveness of heat warning systems in decreasing mortality (Toloo et al., 2013).

However, despite the abundance of studies on heat effects on CV health, surprisingly there is not a unique definition of heat or heatwave, thus potentially hindering the comparison of epidemiological studies. Also, the conditions required to trigger an alert in heat warning systems vary by country, both in terms of meteorological indicators and applied thresholds (Casanueva et al., 2019). As a matter of fact, since the beginning of the 20th century, more than 150 thermal climate indices related to human health have been proposed in the scientific literature (de Freitas and Grigorieva, 2015). Moreover, several attempts to standardize the definition of heat were performed by comparing the prevalence and intensity of heatwaves within a country, using multi-percentile or absolute thresholds applied to a selected heat index, focusing on a particular time of day or on daily aggregates (i.e., mean, maximum, minimum value) (Perkins and Alexander, 2013; Robinson 2001; Smith et al., 2013; You et al., 2017). Other studies also focused on using different definitions of heat and comparing the effects on mortality in target population samples, reporting thresholds or meteorological indicators with the most significant impact (Chen et al., 2015a; Kang et al., 2020; Tong et al., 2015). However, all these attempts failed in the identification of a unique heat definition, even within the same

geographical area, with this lack of a common definition hindering the synergic analysis of trends and the comparison of reported results.

In light of the above considerations, the objective of this chapter is to conduct a systematic review considering open access papers published a 5-year period, when the attention towards this topic has increased worldwide. The focus of the analysis was on the effects of heat on CV health, primarily considering the applied definition of heat and, secondarily, assessing whether such definition had an impact on the applied methodology and on the reported results. In addition, based on these results, an attempt to standardize the definition of heat is made at the end of this chapter. These analyses address the RQ2: What are currently applied definitions of heat used in research analysing its impact on CV health, do they influence the results, and how to standardize them.

3.2. Methods: systematic review of the literature

In order to ensure transparency, reproducibility and effectiveness, a systematic review approach (Aromataris & Pearson, 2014; Wright et al., 2007) was applied to select relevant studies. The Preferred Reporting Items for Systematic Review and Meta-Analysis (PRISMA) guidelines (Page et al., 2021) were followed. Three online databases of scientific literature were examined– PubMed, ScienceDirect and Scopus – where the first one covers biomedicine and life science, while the other two provide an overview of multidisciplinary research. Databases were queried in the title, abstract or keywords using as keywords “heat*”, “high temperature*”, “extreme weather”, paired with “cardiovascular”, “heart”, “ischemic”, “cardiac”, “infarction”, “myocardial”, “hypotension”, “hypertension”. Only journal articles written in English, published between January 2018 and September 2022, and with full text open access availability were included.

Additional filtering was performed on the base of full-text content. First, papers without an explicit definition of heat were discarded. Then, only original studies with analytic study design (i.e., cohort study, case-control study or case-crossover study) based on official medical records (i.e., registered deaths, hospital admissions, emergency calls) were included, excluding those based on personal perception (i.e., questionnaires). Finally, for comparison purposes, only articles that reported the results as relative risk (RR), odds ratio (OR), or incidence density ratio (IDR) with a 95% confidence interval (CI) were kept. The characteristics of the included studies can be described with the following Population, Exposure, Comparison, Outcome – PECO statement (Morgan et al., 2018): (P) Among humans of all ages, genders and ethnicities, what is the effect of (E) exposure to heat versus (C) non-heat conditions on (O) CV morbidity and mortality.

The analysis of the resulting articles explored the following aspects:

1) Definition of heat, considering in particular three aspects:
   - Indicators: meteorological parameters and measures included in the definition;
   - Methods: statistical method applied for the comparison between exposure groups;
   - Comparison threshold: reference value applied to subdivide exposed and non-exposed groups.

   The computed values of different heat indices, in relation to different air temperatures, at the reference conditions, were also compared.

2) Main characteristics of the study design, such as the analysed outcome, medical data source, geographic distribution, sample size and meteorological data source.
3) Quantification of the impact on CV health, considering the statistical methods and the reported results, in relation to the applied definition of heat.

All-cause CV diseases refer to the International Classification of Diseases (ICD) codes 390-459 (ICD-9-CM) or I00-I99 (ICD-10-CM). To address disease-specific analyses, the results among six groups of pathologies were grouped: myocardial infarction (ICD-10 code I21-I23), ischemic (coronary) heart disease (including chest pain; I20-I25), stroke (I60-I69), hypertensive diseases (I10-I15), heart failure (I50) and other diseases (i.e., chronic rheumatic heart disease, out-of-hospital cardiac arrest, acute aortic dissection, arrhythmias).

In the following text, the term "heat" is used as abbreviation of "heatwave", while the term "outcome" describes the medical result (i.e., the received diagnosis or death), and "result" refers to the RR/OR/IDR reported in the studies. If a factor results in a "negative effect on health" it means that the risk of developing a health-related negative CV event is increased. All reported plots were created with Plotly library (version 5.11.0) in Python (version 3.8.5).

3.3. Results

The adopted query resulted in the identification of 11,783 articles (3,602 in PubMed, 2,390 in ScienceDirect and 5,791 in Scopus) in English language and published between January 2018 and September 2022. After title and/or abstract screening, 347 items were selected as possibly relevant articles, of which 232 resulted unique. During the phase of full text screening, 146 studies were excluded as not relevant, due to the lack of an explicit definition of heat, not focusing in the reported results on CV outcomes, or using a study design other than analytic. Lastly, considering only articles reporting results (i.e., the influence of heat on CV health) as RR, OR, or IDR with a 95% CI, 54 articles were finally selected for which full references are provided in Table A3.1. In this section, to ensure readability, references to these articles will be cited in square brackets, with numbers corresponding to those listed in Table A3.1. Figure 3.1 shows the summary of this literature systematic selection process.

Figure 3.1. Schematic of the results of the systematic literature selection process, including open access papers published between 2018 and 2022, written in English language, and resulting from the application of the selected query (see text for details)

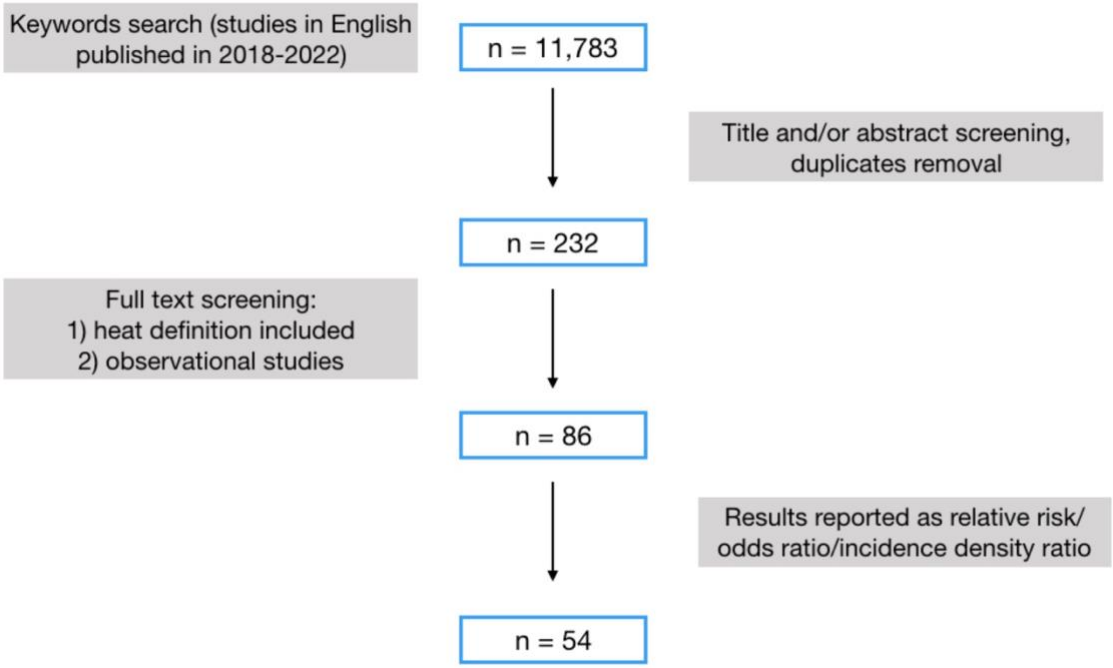

3.3.1. Definition of heat

In total, 21 different combinations of criteria to define heat were found (Table 3.1), with only three studies simultaneously testing and comparing more than one of them. The most frequently used meteorological measure as heat indicator was air temperature, applied in 56 of 57 cases. In 9 studies, air temperature was included in the computation of more complex indices, such as "Apparent Temperature" [8, 19, 26, 37, 42, 49], "Perceived Temperature" [5], "Pseudo-equivalent daily temperature" [54] or "Discomfort Score" [22], by combining it with relative humidity, water vapor pressure, dew point temperature, wind speed and/or heat radiation. The relevant calculation formulas are summarised in Table 3.2, except for Perceived Temperature [5] as it was not provided in the relevant study. Only one study [40] used air masses (excluding air temperature) to define heat days.

In the majority of cases (n=46), heat days were defined using thresholds on percentiles of temperature distribution over a certain period, with temperature defined by daily mean, minimum or maximum values. The three most frequent thresholds were 99th (n=17), 95th (n=13) and 97.5th (n=11) percentiles. In 8 cases, the thresholds were set on absolute temperature values, in the range 20-35 °C. In several studies, the threshold criterion was coupled with a duration requirement (e.g., temperature above the threshold for at least 2-5 days). When the study period was limited to the warmer months only, the considered temperature distribution was either annual or periodic. The lowest value of heat threshold reported in literature was a mean daily temperature of 20 °C [5], set in Austria, while the highest was a mean daily temperature of 43 °C, set in Kuwait [39].

As regards the threshold-based identification of the non-exposed groups for comparison, this was selected based on:

- the minimum mortality temperature (MMT) or its equivalent (minimum hospital admission temperature, minimum ambulance calls temperature etc.), derived from the relevant minimum of the mathematical function applied to the temporal series,
- another percentile (i.e., the 50th, 75th, 90th percentile of the temperature distribution or the 1st percentile of heat index values),
- defining non-heat days (i.e., all days not classified as heat),
- mean temperature or arbitrary absolute value.

Table 3.1. Summary of indicators used to define heat. MMT - minimum mortality temperature; EHF - Excess Heat Factor. The total amounts to 57 articles, as three of 54 studies applied more than one combination of different criteria. References as defined in Table A3.1.

Indicator	Method	Comparison threshold	Number of articles	References
air temperature	percentile	MMT or equivalent	21	[2, 9, 10, 12-17, 21, 23, 28, 32-34, 36, 39, 44, 46, 50, 52]
		another percentile	4	[8, 10, 30, 45]
		non-heatwave	3	[24, 25, 51]
		mean temperature	1	[18]
		arbitrary absolute value	1	[41]
		other	1	[27]
	percentile and duration	non-heatwave	8	[3, 4, 6, 11, 20, 29, 38, 48]
	absolute value	MMT or equivalent	1	[53]
		non-heatwave	1	[4]
	absolute value and duration	non-heatwave	4	[1, 31, 43, 47]
	other, i.e. EHF	another percentile	1	[35]
		non-heatwave	1	[7]
air temperature +relative humidity	percentile	another percentile	1	[22]
air temperature + water vapor pressure	percentile	non-heatwave	1	[42]
	absolute value and duration	non-heatwave	1	[54]
air temperature + dew point temperature	percentile	MMT or equivalent	1	[26]
		another percentile	1	[37]
air temperature + relative humidity + wind speed	percentile	MMT or equivalent	1	[19]
		another percentile	2	[8, 49]
air temperature, humidity, wind speed, heat radiation	absolute value	non-heatwaves	1	[5]

air masses	-	other air masses	1	[40]

Table 3.2. Calculation formulas for complex heat indices. References as defined in Table A3.1.

Heat index name	Formula	Abbreviations	References
Discomfort Score	$\frac{T + T_wetbulb}{2}$	T - air temperature, T_wetbulb - wet bulb temperature (derived from air temperature and relative humidity)	Kranc et al. [22]
Pseudo-equivalent daily temperature	$T + 1.5 * VP$	T - air temperature, VP - water vapor pressure	Perčič et al. [54]
Apparent Temperature 1	$-1.3 + 0.92 * T + 2.2 * VP$	T - air temperature, VP - water vapor pressure	Jiang et al. [42]
Apparent Temperature 2	$T + 0.33 * \frac{RH}{100} * 6.105 * e^{17.27 * \frac{T}{237.7+T}} - 0.7 * WS - 4$	T - air temperature, RH - relative humidity, WS - wind speed	Li et al. [19], Liu et al. [8], Zhai et al. [49]
Apparent Temperature 3	$-2.653 + 0.994 * T + 0.0153 * T_dewpoint^2$	T - air temperature, T_dewpoint - dew point temperature	Moghadamnia et al. [37], Parliari et al. [26]

It is worth noting that in four studies the heat definitions were used at national level for heat warning systems (Table 3.3).

Table 3.3. National definitions of heat. Country column refers to the country in which the definition is used at national level. EHF - Excess Heat Factor as defined in Nairn and Fawcett (2015). References as defined in Table A3.1.

Country	Heat definition	Reference
Australia	EHF >= 85th percentile of the distribution of its positive values; where $EHF = \frac{T_i+T_{i+1}+T_{i+2}}{3} - T_{95} * \max\left(1, \frac{T_i+T_{i+1}+T_{i+2}}{3} - \frac{T_i+T_{i-1}+\cdots+T_{i-30}}{30}\right)$, where T_i is the air temperature at day i and T_{95} is the 95th percentile of daily mean temperature distribution at day i. If a heatwave is detected for day i, days $i + 1$ and $i + 2$ are considered a heatwave as well.	Royé et al. [35]
Belgium	Daily maximum temperature > 25 °C for at least 5 consecutive days, including at least 3 days with daily maximum temperature >= 30 °C.	Alsaiqali et al. [1]
Latvia	1st level of heat: daily maximum temperature >= 27 °C and < 33 °C for at least 2 consecutive days. 2nd level of heat: daily maximum temperature >=33 °C.	Pfeifer et al. [43]

Sweden	Low intensity heat: daily maximum temperature >= 30 °C for 3 consecutive days. High intensity heat: daily maximum temperature >= 30 °C for 5 consecutive days and/or daily maximum temperature >= 33 °C for 3 consecutive days.	Oudin et al. [47]

For a deeper analysis and visual comparison of the different heat indexes summarised in Table 3.2, in Figure 3.2 they were plotted as a function of air temperature, with the other parameters arbitrarily set to standard conditions (relative humidity=50%, wind speed=1 m/s, water vapor pressure=2.34 kPa, dry bulb temperature equal to air temperature and dew point temperature calculated according to Lawrence (2005)).

From this graph, it can be noted that, in colder environments (i.e., 0-20 °C), Pseudo-equivalent daily temperature and Apparent Temperature 1, based on water vapor pressure, reach significantly higher values compared to the other indexes, with a maximum difference up to 7 °C. When the air temperature is closer to 30 °C, which is considered in many studies as the threshold for heat days, there are no big differences among the indexes, except the Discomfort Score, characterized by lower values. Above a value of air temperature equal to 30.4 °C, the differences among indexes increase progressively, with Apparent Temperature 2 and 3 rising to higher values due to their exponential/polynomial formulas.

Figure 3.2. Heat indexes as a function of air temperature as defined in Table 3.2, computed assuming relative humidity=50%, wind speed=1 m/s, water vapor pressure=2.34 kPa and dew point temperature calculated according to Lawrence (2005)

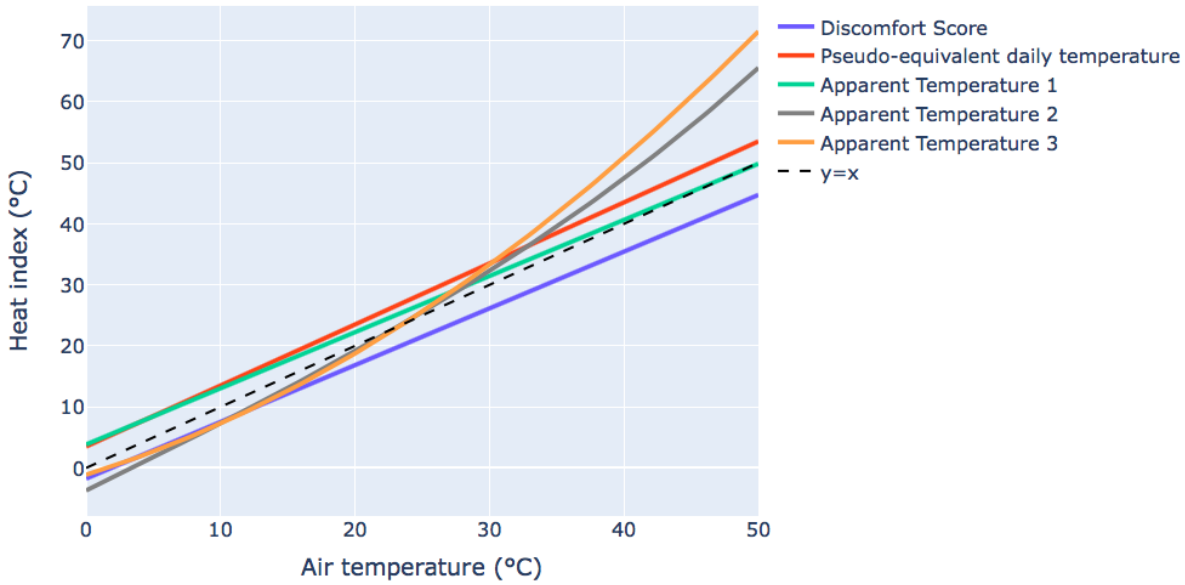

3.3.2. Study characteristics

Among the selected articles, 27 (50%) were targeting the analysis of mortality, 25 (46.3%) of morbidity and 2 (3.7%) of both these outcomes (Figure 3.3). In 21 (38.9%) studies, all-cause CV diagnoses were considered, while in the remaining 33 (61.1%) studies the results were stratified by specific CV disease. Additionally, regardless of the target outcome, in few studies the impact of heat was also studied on specific subgroups, stratified by age (9 studies; 16.7%),

by age adjusted for exposure to noise or chronic conditions (2 studies; 3.7%), or by presence of a chronic condition alone (1 study; 1.9%).

Figure 3.3. Summary of articles by the outcome

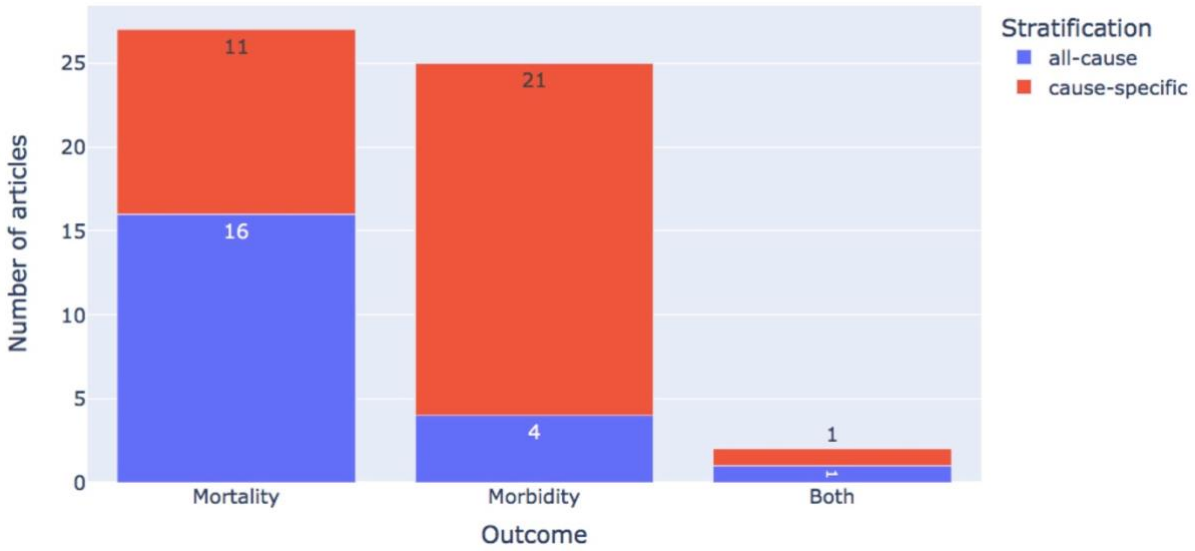

Among the studies including morbidity as a target, the majority (n=18) referred to hospital admissions (including three on emergency hospital admissions), while the rest considered emergency calls (n=4), emergency department visits (n=3), chest pain centre visits (n=1), or general practitioner consultations (n=1).

The sources of medical data were predominantly from national or regional public offices (e.g. Thai Ministry of Public Health [6], Canadian Institute of Health Information [10], Spanish Ministry of Health [36]), while other data providers included statistical bureaus (e.g. Hellenic Statistical Authority [26], Statbel [28], Swiss Federal Statistical Office [45]), hospital management systems (e.g. Hong Kong Hospital Authority [17]) and selected medical facilities or emergency service providers.

The geographical origin of the selected studies spanned areas from all six continents (Figure 3.4), with 25 (46,3%) articles from Asia, 15 (27.8%) from Europe, 8 (14.8%) from North America, 3 (5.6%) from Oceania, 2 (3.7%) from South America and 1 (1.9%) from Africa. The country covered with the highest number of studies was China, using either data from single cities [8, 18, 19, 31, 41, 49, 53], individual provinces [12, 14, 34], or multiple cities spread throughout the country [3, 13, 52]. Similarly, in the United States, studies alternatively focused on single cities, such as Atlanta [42], counties, such as Shelby County [4], states, such as New York [24], or wider geographic aggregations [27, 29, 48, 51]. In addition to the studies from China and the United States, three studies each were conducted using data from Australia [7, 11, 21], Hong Kong [17, 25, 32], and Spain [16, 35, 36].

Figure 3.4. Geographical distribution of the studies. Countries with at least three studies are labelled with the corresponding number of articles.

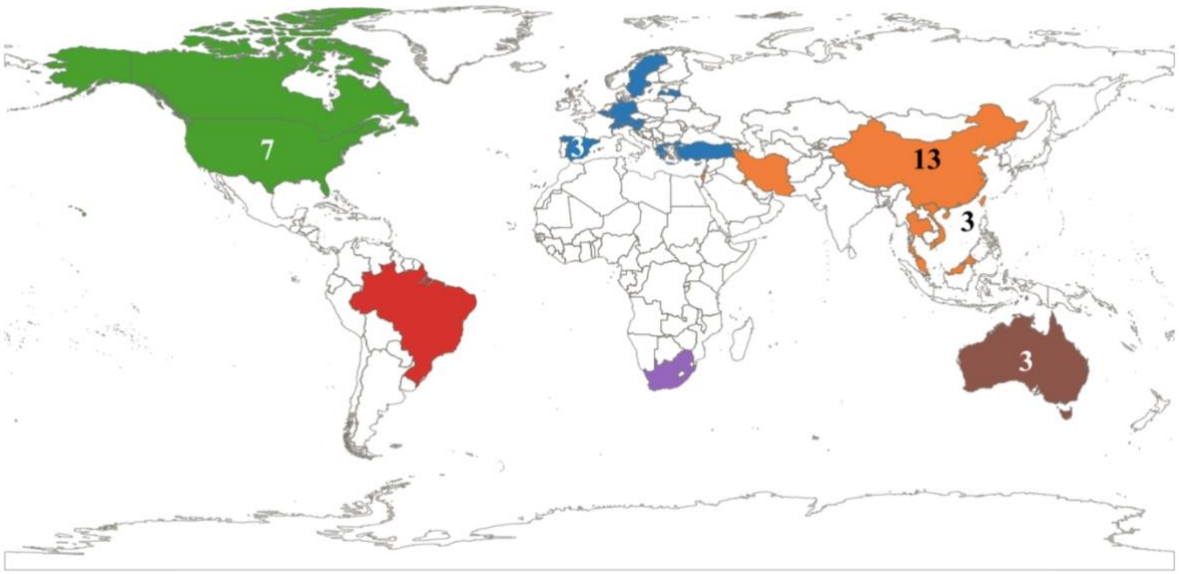

The sample size of the target study group was explicitly reported in 40 (74.1%) articles; alternatively, it was inferred multiplying the average daily incidence by the study period when both characteristics were specified in the article (n=10; 18.5%); in 4 (7.4%) studies it was not possible to infer any information about sample size. The median sample size was slightly above 40,000 subjects, with a minimum of 939 individuals in a study about congestive heart failure hospital admissions and mortality in Boston, New York and Philadelphia [51], and a maximum of 1,154,896 in an analysis of all-cause CV morbidity in South Africa [50]. Sample size distribution in the different geographical areas is reported in Figure 3.5.

Figure 3.5. Summary of selected articles divided by continent of interest for the analysis, stratified by sample size of the examined study group; in 10 (18.5%) studies, the sample size was inferred considering the average incidence and the study period.

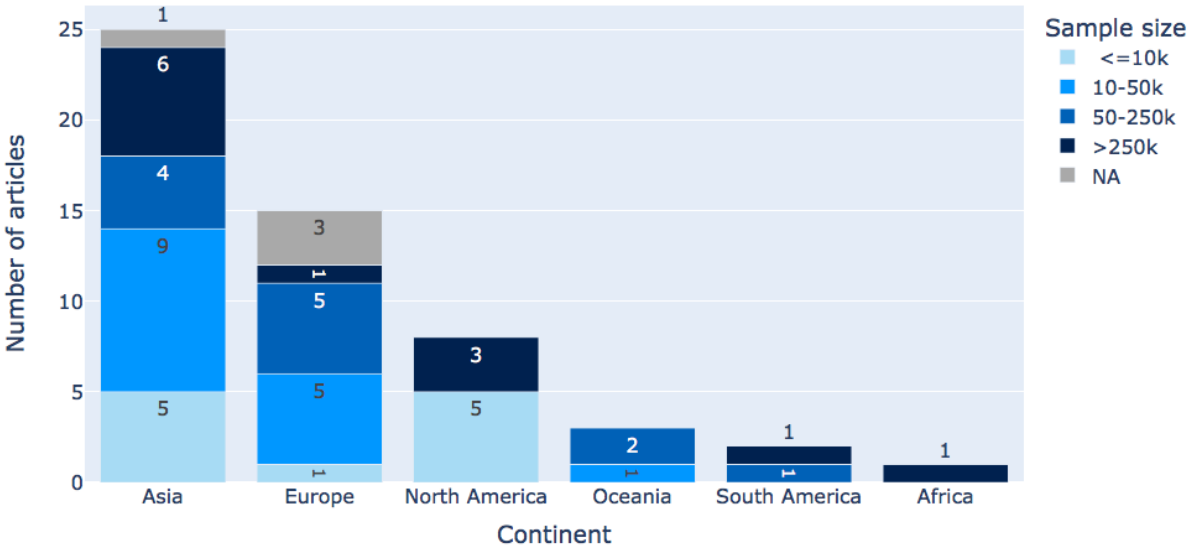

The median observation period was 10 years, with a minimum of 2 years for Israel [22], Slovenia [54] and a Chinese study [49], and a maximum of 28 years for Germany [23]. Several studies (n=22; 40.7%) analysed the influence of heat only in an arbitrarily defined warmer period of the year, beginning within March-June and ending within June-October for the Northern Hemisphere, while spanning from September-November to March for the Southern Hemisphere. When narrowing the study period, the most frequent interval was May-September (n=9; 16.7%).

Regarding the use of meteorological data as explicative attributes in the analysis, dew point/air temperature, relative humidity, wind speed, atmospheric/barometric pressure, precipitation, sunshine duration, solar radiation and air pollution were utilized. When the mean values for each factor were reported (n=36; 66.7%), they were calculated averaging all records from all measurement stations in the study area. In 9 (16.7%) studies, interpolated meteorological maps (e.g., maps at ZIP code level [48], district level [50] or at 2 km spatial resolution [2]) were alternatively used.

Among the 13 (24.1%) studies for which the events' location or patients' home address were available, only two [14, 22] associated them with the meteorological conditions at the event time, while Jiang et al. [52] linked the temperature with that at the hospital location, as the majority of patients did not report their complete address.

3.3.3. Quantification of heat impact on cardiovascular health

To assess the impact of heat on CV health, the majority of articles (n=39; 72.2%) applied the distributed lag non-linear model (DLNM), that describes the response to exposure accounting for a delayed effect (Gasparrini et al., 2010). The number of tested lags varies up to 30 days, with the most frequent choices being 21 (n=15; 27.8%), 3 (n=9; 16.7%) and 14 (n=5; 9.3%). Other applied techniques included the generalized linear models (n=13; 24.1%), or a simplified approach based on the comparison between incidence rates during heat and non-heat days (n=2; 3.7%). In several studies, mostly in those using only air temperature to define heat, the statistical models were further adjusted by meteorological factors (n=9; 16.7%), by air pollution (n=4; 7.4%) or by both (n=22; 40.7%).

In 14 studies (25.9%) a case-crossover design, as proposed by Maclure (1991) was applied. By using the same subjects as both cases and control at different points in time, this design allows to control for time-invariant characteristics, such as gender or medical history.

In the majority of studies, the results were reported as RR (n=44; 81.5%), and in the remaining studies as OR (n=7; 13%) or IDR (n=3; 5.6%). The values of these three indicators are approximately equal when the initial risk (i.e., prevalence of the disease in the population under study in non-heat conditions) is relatively small (Alsaiqali et al., 2022; Davies et al., 1998; Zhang and Kai, 1998), and are therefore comparable under this assumption.

Most of the results (n=37, 68.5%) showed a negative influence of heat for all-cause CV health (i.e., an increase in risk in relation to the comparison threshold as indicated in Table 3.1) in the range from 1.02 in Spain (95% CI: [1.00-1.04]) [36] and New York State (95% CI: [1.01-1.04]) [24] to 1.47 (95% CI: [1.43-1.51]) in Jiangsu Province, China [14], with two outliers equal to 4.61 (95% CI: [3.67–5.78]) [35] and 3.09 (95% CI: [1.72–5.55]) [39]. However, the studies differed in the applied heat definition (Table 3.1). All studies that reported a negative

effect of heat on CV health found this effect stronger if associated to a shorter lag, while this relation seemed to weaken over time.

In disease-specific analysis, the most consistent and significant results were reported for stroke, varying from 1.20 (95% CI: [1.02 – 1.40]) [45] to 1.62 (95% CI: [1.39 – 1.88]) [12], with the most frequently associated heat definition based on the combinations of air temperature, percentile and MMT equivalent. The strongest disease-specific result was found for myocardial infarction (5.22, 95% CI: [2.14 – 12.73]), with heat defined using Apparent Temperature 2, percentile and MMT equivalent [19].

However, in 11 studies (20.4%) no statistically significant results were found, while in 6 (11.1%) a statistically significant decrease in the risk of developing a CV acute event during heat was surprisingly reported. Of these 6, one study analysed all CV diseases together [49], on the base of hospital admissions in 2014-2015 in Pingliang, China, defining heat as the 95th percentile of annual Apparent Temperature 2 distribution and using the median of such distribution as comparison threshold. The other studies that reported a risk reduction during heat referred to specific diseases, i.e., myocardial infarction [45], hypertensive diseases [42, 45], heart failure [11, 29, 45] and acute aortic dissection [41].

A complete summary of these results is presented in Figure 3.6 for all-cause CV outcomes and in Table 3.4 for specific CV diseases.

Figure 3.6. Summary of the influence of heat on all-cause cardiovascular outcomes. The notation *e* in the last column means that the sample size was inferred as not directly specified in the relevant study. The letters *a–l* refer to the combination of criteria used to define heat (MMT – minimum mortality temperature): *a* – air temperature + percentile + MMT or equivalent, *b* – air temperature + percentile and duration + non-heatwave, *c* – air temperature +relative humidity+wind speed + percentile + MMT or equivalent, *d* – air temperature + percentile + non-heatwave, *f* – air temperature + dew point temperature + percentile + MMT or equivalent, *g* – air temperature + percentile + another percentile, *h* – air temperature + absolute value and duration + non-heatwave, *i* – air temperature + other + another percentile, *j* – air temperature +relative humidity+wind speed + percentile + another percentile, *k* – air temperature + absolute value + MMT or equivalent, *l* – air temperature +water vapor pressure + absolute value and duration + non-heatwave. References as defined in Table A3.1.

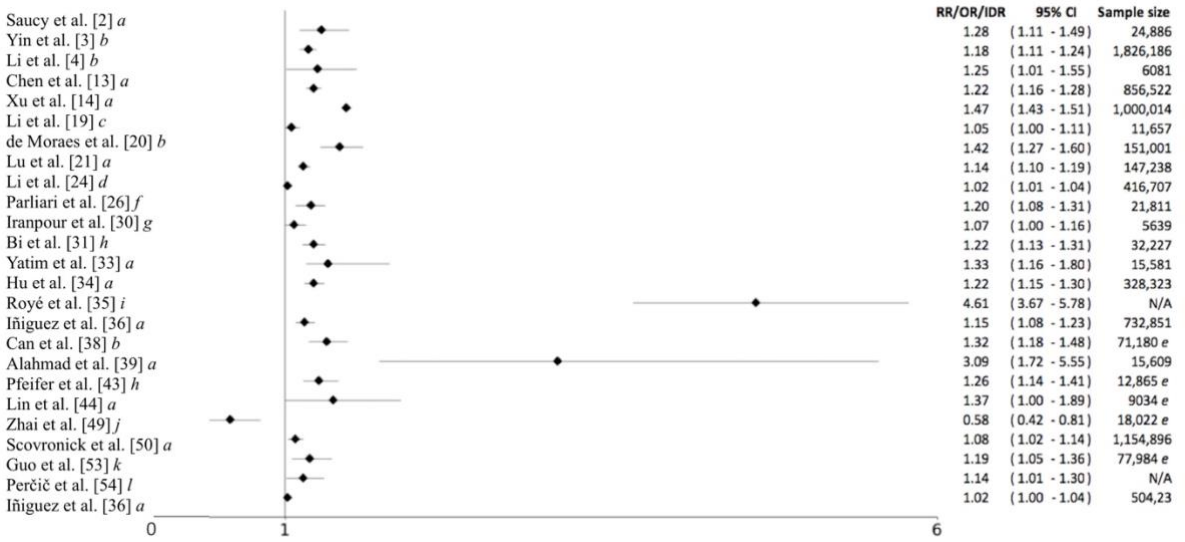

Table 3.4. Summary of the influence of heat on cause-specific cardiovascular outcomes. The notation e in the "Sample size" column means that it was inferred as not directly specified in the relevant study. MMT – minimum mortality temperature. References as defined in Table A3.1.

Study	RR/OR/IDR	95% CI	Sample size	Heat definition (indicator + method + comparison threshold)
Myocardial infarction				
Mortality				
Saucy et al. [1]	1.67	(1.09 - 2.55)	3248	air temperature + percentile + MMT or equivalent
Xu et al. [14]	1.52	(1.42 - 1.62)	169,886	air temperature + percentile + MMT or equivalent
Ma et al. [12]	1.40	(1.22 - 1.60)	98,516 *e*	air temperature + percentile + MMT or equivalent
Ferreira et al. [15]	1.24	(1.16 - 1.32)	118,898	air temperature + percentile + MMT or equivalent
Ferreira et al. [15]	1.07	(1.00 - 1.15)	131,394	air temperature + percentile + MMT or equivalent
Ferreira et al. [15]	1.05	(1.03 - 1.08)	118,898	air temperature + percentile + MMT or equivalent
Morbidity				
Li et al. [19]	5.22	(2.14 - 12.73)	3161	air temperature + relative humidity + wind speed + percentile + MMT or equivalent
Layton et al. [48]	1.53	(1.00 - 2.34)	608	air temperature + percentile and duration + non-heatwave
Dang et al. [9]	1.36	(1.06 - 1.73)	3328	air temperature + percentile + MMT or equivalent
Chen et al. [23]	1.14	(1.00 - 1.29)	27,310	air temperature + percentile + MMT or equivalent
Lam et al. [17]	1.14	(1.00 - 1.31)	53,769	air temperature + percentile + MMT or equivalent
Schulte et al. [45]	0.88	(0.82 - 0.95)	68,861	air temperature + percentile + another percentile
Ischemic (coronary) heart disease (incl. chest pain)				
Mortality				
Xu et al. [14]	1.52	(1.45 - 1.60)	295,829	air temperature + percentile + MMT or equivalent
Ma et al. [12]	1.49	(1.32 - 1.68)	164,980 *e*	air temperature + percentile + MMT or equivalent
Saucy et al. [2]	1.30	(1.04 - 1.62)	10,521	air temperature + percentile + MMT or equivalent
Huang et al. [6]	1.22	(1.13 - 1.21)	25,753 *e*	air temperature + percentile and duration + non-heatwave
Chen et al. [13]	1.19	(1.11 - 1.28)	306,601	air temperature + percentile + MMT or equivalent
Yin et al. [3]	1.17	(1.05 - 1.30)	306,601	air temperature + percentile and duration + non-heatwave

Oudin et al. [47]	1.10	(1.01 - 1.20)	68,299 *e*	air temperature + absolute value and duration + non-heatwave
		Morbidity		
Li et al. [19]	1.99	(1.12 - 3.51)	8006	air temperature + relative humidity + wind speed + percentile + MMT or equivalent
Lin et al. [44]	1.37	(1.00 - 1.89)	4455 *e*	air temperature + percentile + MMT or equivalent
Guo et al. [25]	1.22	(1.11 - 1.34)	N/A	air temperature + percentile + non-heatwave
Moghadamnia et al. [37]	1.09	(1.02 - 1.19)	15,094	air temperature + dew point temperature + percentile + another percentile
Li et al. [24]	1.07	(1.03 - 1.11)	64,262	air temperature + percentile + non-heatwave
Bai et al. [10]	1.06	(1.01 - 1.11)	1,389,057	air temperature + percentile + MMT or equivalent and air temperature + percentile + another percentile
Parry et al. [11]	1.04	(1.00 - 1.08)	68,334	air temperature + percentile and duration + non-heatwave
Li et al. [19]	1.01	(1.00 - 1.11)	14,447	air temperature + relative humidity + wind speed + percentile + MMT or equivalent
		Stroke		
		Mortality		
Ma et al. [12]	1.62	(1.39 - 1.88)	311,032 *e*	air temperature + percentile + MMT or equivalent
Chen et al. [13]	1.41	(1.26 - 1.59)	415,227	air temperature + percentile + MMT or equivalent
Xu et al. [14]	1.39	(1.31 - 1.47)	412,567	air temperature + percentile + MMT or equivalent
Yin et al. [3]	1.21	(1.04 - 1.40)	415,227	air temperature + percentile and duration + non-heatwave
Schulte et al. [45]	1.20	(1.02 - 1.40)	15,296	air temperature + percentile + another percentile
		Morbidity		
Alsaiqali et al. [1]	1.45	(1.04 - 2.03)	N/A	air temperature + absolute value and duration + non-heatwave
Jiang et al. [42]	1.26	(1.01 - 1.48)	70,380 *e*	air temperature + water vapor pressure + percentile + non-heatwave
		Hypertensive diseases		
		Mortality		
Saucy et al. [2]	1.91	(1.20 - 3.06)	2728	air temperature + percentile + MMT or equivalent
Ma et al. [12]	1.89	(1.41 - 2.54)	40,435 *e*	air temperature + percentile + MMT or equivalent
Xu et al. [14]	1.85	(1.68 - 2.04)	75,557	air temperature + percentile + MMT or equivalent

Schulte et al. [45]	1.18	(1.02 - 1.38)	17,142	air temperature + percentile + another percentile
		Morbidity		
Li et al. [24]	1.04	(1.01 - 1.07)	220,058	air temperature + percentile + non-heatwave
Jiang et al. [42]	0.99	(0.98 - 0.99)	1,502,460 *e*	air temperature + water vapor pressure + percentile + non-heatwave
Schulte et al. [45]	0.72	(0.64 - 0.81)	29,533	air temperature + percentile + another percentile
		Heart failure		
		Mortality		
Schulte et al. [45]	1.22	(1.05 - 1.43)	14,753	air temperature + percentile + another percentile
		Morbidity		
Hopp et al. [29]	0.94	(0.90 - 0.98)	19,498	air temperature + percentile and duration + non-heatwave
Parry et al. [11]	0.83	(0.76 - 0.90)	24,721	air temperature + percentile and duration + non-heatwave
Schulte et al. [45]	0.83	(0.76 - 0.90)	57,440	air temperature + percentile + another percentile
		Other (i.e., chronic rheumatic heart disease, out-of-hospital cardiac arrest, acute aortic dissection, arrhythmias)		
		Mortality		
Xu et al. [14]	1.82	(1.31 - 2.51)	8171	air temperature + percentile + MMT or equivalent
		Morbidity		
Kranc et al. [22]	3.24	(1.90 - 5.86)	12,401	air temperature +relative humidity + percentile + another percentile
Lin et al. [44]	1.67	(1.23 - 2.26)	4583 *e*	air temperature + percentile + MMT or equivalent
Wang et al. [46]	1.40	(1.25 - 1.57)	100,254 *e*	air temperature + percentile + MMT or equivalent
Li et al. [24]	1.06	(1.01 - 1.11)	81,290	air temperature + percentile + non-heatwave
Parry et al. [11]	1.06	(1.00 - 1.12)	32,682	air temperature + percentile and duration + non-heatwave
Yu et al. [41]	0.18	(0.01 - 0.55)	2120	air temperature + percentile + arbitrary absolute value

Finally, to identify a possible correlation between the applied definition of heat and the reported results relevant to the CV risk, an additional analysis was performed considering the percentage deviation of the reported heat threshold from the mean annual temperature, calculated as:

$$100 * \frac{heat\ threshold - mean\ annual\ temperature}{mean\ annual\ temperature} \quad (3.1)$$

This computation was feasible in 13 (24.1%) studies in which the absolute values of both parameters were explicitly specified, and relevant results are presented in Figure 3.7. Excluding three outliers (i.e., all-cause CV mortality in Kuwait [36], out-of-hospital cardiac arrest events in Israel [22], and acute aortic dissection morbidity in China [41]), a slight trend of higher risk with increasing deviation of the heat threshold from the mean annual temperature could be observed, yet not with robust statistical evidence, with the coefficient estimated by ordinary least squares linear regression equal to 0.002 (R^2=0.19).

Figure 3.7. Relationship between the percentage deviation of the considered heat threshold from the mean annual temperature and associated cardiovascular risk, subdivided as all-cause and cause-specific mortality or morbidity. RR - relative risk; OR - odds ratio; IDR - incidence density ratio. Dot size is proportional to the duration of the observation period expressed as number of years.

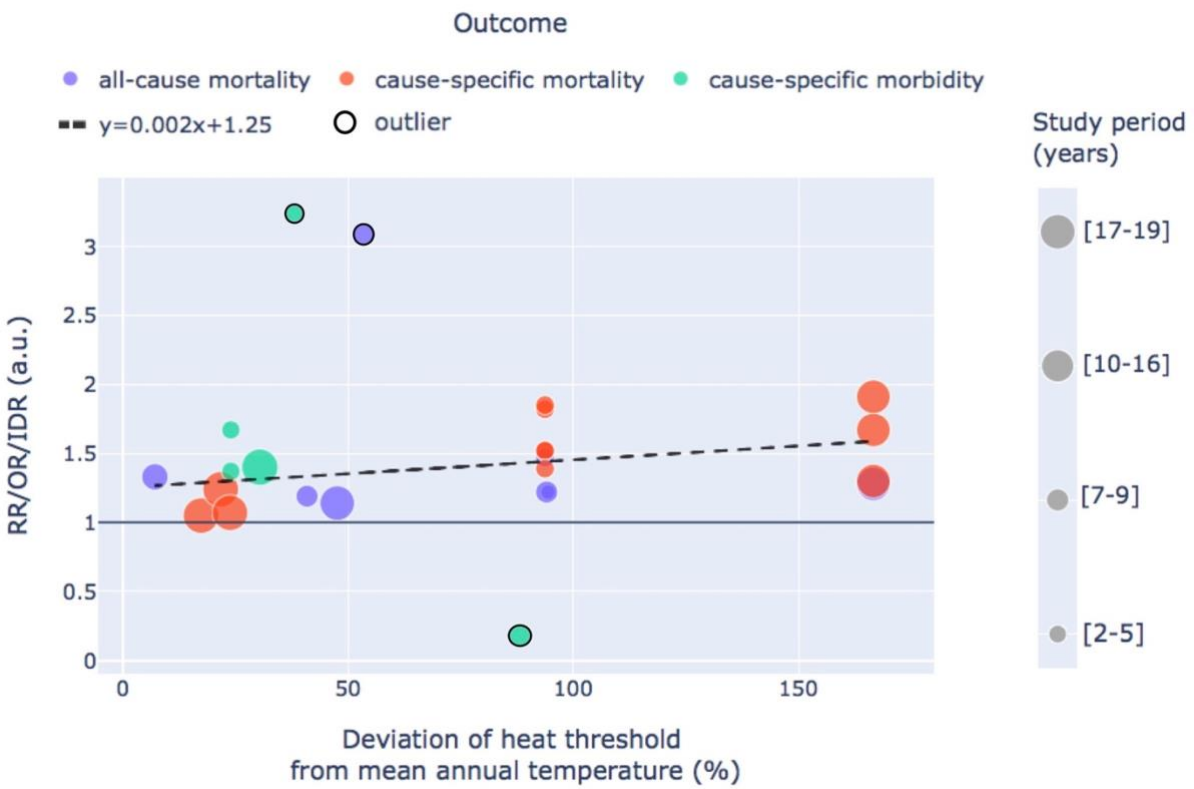

3.4. Discussion

In this chapter, a systematic review of studies focusing on the impact of heat on CV morbidity and/or mortality published in 2018-2022 period was performed, in order to assess the latest progresses made by the scientific community in this field. The identified studies were conducted across all six continents, with a leading role of Asia (both in terms of number of publications and of sample size), followed by Europe and North America. Source data spanned from 1987 to 2021.

Despite having the same goal, the examined study settings were extremely heterogeneous. Such heterogeneity could be noticed both in the definition of heat in the field of CV health, but also in other aspects, such as the medical and meteorological data used, the sample size, the observation periods, and the applied methodology for analysis. In addition,

biases due to measurement error (Obradovich et al., 2018) or spatial autocorrelation (Pramanik et al., 2022) could affect data generation and processing.

3.4.1. Applied definitions of heat

Already at the beginning of the 21st century, Robinson (2001) pointed out that, due to the lack of an unequivocal heat definition, it was difficult to assess if heatwaves varied in intensity or prevalence, which further hindered research into climate change. The majority of heat indices developed since the beginning of the 20th century was collected and organically presented in a theoretical framework (de Freitas and Grigorieva, 2015). However, to the best of our knowledge, a comparison of their viability in health-related studies is still missing. Moreover, only a small fraction of those indices uses exclusively meteorological factors, such as air temperature, relative humidity and solar radiation (Moran et al., 2001) or air temperature, dewpoint temperature, relative humidity, cloud cover, and wind speed (Watts and Kalkstein, 2004), whereas many other indices (e.g., Becker, 2000; Hamdi et al., 1999 ; Malchaire et al., 2001; Nagano and Horikoshi, 2011; Staiger et al., 2012) are based also on human thermal comfort factors (i.e., human metabolic rate), a type of data that is labour-intensive in terms of collection and processing, thus hindering their application in heat-health related research. In the examined recent literature, only one review focusing on heat definitions and addressing their heterogeneity was found (Xu et al., 2016). It included 60 studies published in 2001-2015 covering Asia, Australia, Europe and North America, considering the impact of heat on all-cause CV and respiratory mortality. As added value compared to that work, in this systematic review including studies published later, the morbidity dimension was considered as well and the stratification of risk by diagnosis was performed.

In line with this established knowledge, twenty-one unique combinations of indicators, methods and comparison thresholds, with the purpose of defining heat days and to distinguish them from non-heat days, were identified in the studies selected for this review. Differently from de Freitas and Grigorieva (2015), the majority of these studies used air temperature alone, averaging the values obtained from measurement stations without applying spatial interpolation. Other meteorological data (i.e., relative humidity, water vapor pressure, dew point temperature, wind speed and/or heat radiation) were eventually used only for a following adjustment of the statistical models. In addition, even when a combined indicator was applied, it is worth noticing that three different versions of “Apparent Temperature” were found, as a result of the application of simplified versions, depending on data availability, to the same original index (de Freitas and Grigorieva, 2015). Only the term “Perceived Temperature” can be referred directly to a specific and standardized heat index.

The choice of the index to be considered for the analysis is strongly relevant in terms of comparing results obtained in different studies. In fact, as shown in Figure 3.2, the values of the different indexes as a function of temperature cannot be assumed to be the same, except for a narrow range around 30 °C.

Two main methods for setting the heat threshold were identified, namely using a percentile of the indicator’s distribution or its absolute value. However, in this latter case, the reported threshold values varied in a range of 15 °C, making it impossible to formulate a universal threshold with this strategy. In addition, four national definitions implemented in heat

warning systems were identified, one of which applied to a territory different from the country when the criterion was defined.

These findings showing strong heterogeneity in heat definitions applied to research studied published from 2018 to 2022 indicated that, despite the increased international interest in climate change effects on health, there was no important progress in the harmonization and standardization process towards a singular heat definition to be applied in the CV health. A similar finding was already present in a former systematic review including 60 studies published in the period 2001-2015 (Xu et al., 2016), thus further highlighting the lack of action of the scientific community towards this problem.

It is important to assess if there is an overall trend, transversal to different settings, in the relationship between the selected definition of heat and the related results in terms of impact on CV health. In this perspective, Xu et al. (2016) noted that a modification of the threshold value led to a more important change in mortality than the modification of heatwave duration, which is consistent with our findings. In studies where multiple thresholds were tested, a higher risk was usually reported for higher thresholds. This trend is in agreement with Xu et al. (2018), who focused on heat definitions and five health events (i.e., ambulance service uses, all-cause and cause-specific emergency department attendances, all-cause and cause-specific hospitalizations) in Brisbane, Australia. In that study, multiple heat definitions were tested, combining three durations (2-4 days) and 10 percentiles (90th-99th) applied on mean and maximum air temperature. The authors concluded that, for three of these five health events, a threshold selection with the 97th percentile resulted in a significant association with heat (regardless of duration and temperature indicator), while for the other two a significant correlation was found with a threshold set to 98th or 99th percentile (depending on temperature indicator). Among the studies included in this review, it is worth noticing that two outliers with very elevated health risk in all-cause CV events were identified for Seville and Kuwait. The former compared the 99th percentile of a heat index distribution, accounting for the temperature in time windows of up to 30 days, to its 1st percentile. The latter compared the 99th percentile of daily mean air temperature distribution to the MMT. In both geographical areas, a very high percentile threshold was considered even though both these territories are characterized by particularly hot summers, thus focusing on extreme events only, in a set-up that could partly explain the outlier results.

3.4.2. Impact of heat on cardiovascular health

As a secondary target, this review also focused on the results of the analysis conducted in the included studies aiming at assessing the impact of heat on CV health, i.e., the risk, thus addressing the applicability and robustness of heat definitions towards this specific purpose.

On this topic, Xu et al. (2016) concluded, pooling the results of their review, that an increased mortality could be found in heat condition. Additionally, in the United States, the relationship between temperature and all-cause mortality resulted non-stationary from a spatial point of view (Yang and Jensen, 2017). Moreover, in previous research on the effect of heat on mortality and morbidity, both individual (e.g., age, gender, medical history, race, education level, occupation) and community-level (e.g., housing quality, medical care, air pollution) characteristics were identified as effect modifiers (Choi et al., 2022; Kim and Kim, 2017;

Madrigano et al., 2013; Medina-Ramón et al., 2006; O'Neill et al., 2003; Yang et al., 2012). In this regard, the case-crossover method should present an advantage over traditional cohort or case-study designs, as it overcomes the between-person confounding factors. In the studies here considered, the vast majority of results reported a negative impact of heat on all-causes CV health, yet using different parameters (mainly RR, but also OR and IDR) computed from different data sources (hospital admissions, emergency calls, emergency department visits). Regarding the spatial dimension, no specific information on the patient's home address could have been matched with the meteorological conditions at the time of the event, indicating a research gap in spatial analysis of the impact of heat on CV health.

In CV disease-specific analysis of both morbidity and mortality, an increased risk for stroke and ischemic (coronary) heart disease was evidenced in all the examined studies. In the case of the former, similar results have been previously reported, being particularly strong for ischemic stroke (Lavados et al., 2018; Lian et al., 2015), with possible explanations including dehydration, increased blood viscosity, hemoconcentration, and elevated cholesterol levels during heat (Lavados et al., 2018). In addition, indications that a sudden and large increase in temperature (i.e., Δtemperature>=5 °C) increases the risk of ischemic stroke events, rather than the absolute temperature values, were given (Kyobutungi et al., 2005). The increased risk of coronary artery disease could be explained with endothelial dysfunction expressed as a reduction of flow-mediated vasodilatation associated with increased temperature (Nawrot et al., 2005).

When patients are exposed to a hot environment, the CV system increases the cardiac output to augment blood flow to the skin for cooling (Sankoff, 2015), thus increasing the heart oxygen consumption and potentially generating a precipitation of events towards myocardial infarction. An increased risk for this pathology was reported in 11/12 analysed studies. Similarly, a previous study demonstrated that higher environmental temperatures were associated with an increased risk in myocardial infarction (Bhaskaran et al., 2012), with an influential effect during the first six hours after exposure. While it is known that acute myocardial infarction and higher mortality can be triggered by heat exposure (Wang et al., 2019), a recent study showed that patients taking anti-platelet medication and beta-receptor blockers had elevated risk for heat-related non-fatal MI compared to non-users of such medications (Chen et al., 2022).

The increased risk found in 5/7 studies on hypertension-related outcomes may seem contradictory as a response to heat, but it was explained with a possible interaction between heat and anti-hypertensive medications (Schulte et al., 2021).

When focusing on heart failure morbidity, a lower risk was apparently associated with heat. However, one of these studies analysed also heart failure mortality and reported a higher RR. This finding is in agreement with other reviews on the effects of heat on CV diseases, where a predominance of negative effects was reported for mortality, in contrast with an impact on morbidity that was not always consistent (Liu et al., 2022; Abrignani et al., 2022; Cheng et al., 2019; Cicci et al., 2022).

Among other causes, risk of aortic dissection was found reduced with heat, while risks of out-of-hospital cardiac arrest, chronic rheumatic heart disease and arrythmias were found increased.

3.4.3. Limitations and conclusions

This study has some limitations. Despite the selection of studies was conducted with the most possible uniform approach with regards to the methodology, the heterogeneity of resulting articles made any advanced meta-analysis unfeasible. The dissimilarities did not only concern the main target of this work, which was the definition of heat, but also affected other factors as well, such as the health outcomes or the characteristics of the studied population. The attempt to generalise the results, neglecting details such as the considered effect modifiers, may have led to miss some particular trend. Moreover, studying heat and heatwaves has consistent and complex climatological implications, that were not considered in detail in this review, as the focus was limited to the effects of heat on CV health. Lastly, an inherent limitation of this study is that it considered only open access publications over an arbitrarily selected short time frame of five years. However, this choice was made to increase accessibility and to focus on more recent studies to capture the state-of-the-art relevant to the topic, as a previous systematic review by Xu et al. (2016) covered previously published studies. Nonetheless, the exclusion of potentially relevant studies from high-impact subscription-based journals or from regions where open-access practices are less prevalent may have introduced additional bias (Logullo et al., 2024). Notably, articles from these high-impact journals could apply more standardized definitions of heat, reducing the heterogeneity observed in open-access publications. As literature search and data extraction was performed by a single person, this constitutes a possible methodological limitation of this study approach.

Despite the abundance of recent research in this field, there is no single definition of heat, together with a possible confusion introduced by the terminology and related different formulas for the utilized heat indices. An international effort should be conducted in order to harmonize a common standard in representing and evaluating such type of data including the definition of heatwave. This would allow better comparison among geographical areas and analysis of trends in heatwaves intensity, duration and prevalence, as well as the human heat adaptation capabilities. Such analyses could be incorporated into public health programs with a two-fold strategy: short-term intervention, by developing automated systems capable to analyse and predict, based on the current environmental variables on a given territory, the possible immediate impact of heatwaves, to guide emergency services in a better organization and deployment of available resources, as well as activating heat alert systems; mid-long term intervention, by highlighting those features for a certain territory that could influence the citizen's resilience, and planning accordingly urbanistic interventions.

3.5. Framework proposal for percentile threshold selection for heat definition

Accordingly, to fill the gap of lack of a standardized definition of heat, the following five-step data-driven framework for selecting the percentile threshold on temperature for defining heat in the context of studies on adverse CV outcomes is proposed, combining the most common approaches identified in the literature:

1) Selection of temperature lags based on the contour plot obtained by the DLNM.

   As argued in previous sections, the DLNM is one of the most common models for the analysis of the lagged effects of an environmental hazard, e.g., heat, on adverse health

events. In this context, lags are typically defined as days, representing the delay between exposure and the observed outcome. The model, usually fitted using Poisson regression, can be represented as follows:

$$Y_t = \alpha + \sum_{l=0}^{L} \beta_l(X_{t-l}) + \gamma \boldsymbol{Z}_t \quad (3.2)$$

where Y_t is the outcome at time t, α is the intercept, X_{t-l} is the exposure at time $t - l$, with l being the lag, β_l is the effect of the exposure at lag l, allowing for non-linear relationships, L is the maximum lag considered, $\boldsymbol{Z}_t$ is a vector of other covariates at time t (e.g., air pollution, calendar variables etc.) with associated coefficient γ.

The underlying idea of the DLNM is the inclusion of a cross-basis function, allowing the model to account for the effects of exposure over both the exposure level (non-linear effect) and time lag (distributed lag). Following the equation 3.2, this cross-basis can be described as follows:

$$\beta_l(X_{t-l}) = \sum_{i=1}^{m} \sum_{j=1}^{n} B_i(X_{t-l}) * C_j(l) \quad (3.3)$$

where $B_i(X_{t-l})$ are basis functions for the exposure (e.g., splines), capturing the non-linear effect, $C_j(l)$ are basis functions for the lag (e.g., splines or polynomial), capturing the distributed lag effect, m is the number of basis functions for the exposure dimension, and n is the number of basis functions for lag dimension.

The RR is estimated at each temperature step (e.g., 1 °C) with reference to previously defined baseline value, corresponding to the minimum of the best fitting function (i.e., the MMT or its equivalent), or to an arbitrary value. One of the graphical representations of the DLNM is the contour plot that visualises the interaction between the exposure and lag effects, showing how the risk, represented by RR, varies over both dimensions. Based on this plot, lags characterised by increased RR are selected for further analysis.

2) Estimation of the RR of having a CV emergency in heat versus non-heat days by Poisson regression considering the 90th-99th percentile of the temperature distribution for each lag.

Since DLNM involves a complex hyperparameter selection process and the inclusion of smoothing functions, the next step, after identifying the lags when the RR is elevated, is to perform Poisson regression. This regression model can estimate the RR of experiencing an adverse CV outcome specifically on heat days compared to non-heat days. For each lag, heat days are defined as those with temperatures exceeding the 90th to 99th percentiles of the annual distribution, i.e., 10 percentiles are tested. Non-heat days are defined as all days not classified as heat. Therefore, for each tested percentile and lag, the following model is applied:

$$Y_t = exp(\alpha + \beta * heat\ day_t + \gamma \boldsymbol{Z}_t) \quad (3.4)$$

where $heat\ day_t$ is the binary indicator (equal to 1 if a heat day, equal to 0 if a non-heat day), with its estimated coefficient β, α and, $\boldsymbol{Z}_t$ as defined in equation 3.2.

In order to derive the RR associated with a heat day compared to a non-heat day, the following formula is implemented:

$$RR = \exp(\beta) \tag{3.5}$$

This information is graphically represented as a line chart, with the percentiles (from 90th to 99th) on the x-axis and the associated RR on the y-axis, for each lag under consideration.

3) Selection of the final lag based on the curvatures of the 10 included percentiles.

   The final lag, at which the heat threshold will be set, is arbitrarily selected based on a visual and/or numerical comparison of the curves produced by the graph in the previous step.

4) Calculation of the percentage change in RR from percentile *i* to percentile *i+1*.

   For the selected final lag, a percentage change from percentile *i* to percentile *i+1* is calculated according to the following formula:

$$\forall i \in \{90, 91, \dots, 98\},$$
$$percentage\ change = \frac{RR\ at\ percentile\ i{+}1 - RR\ at\ percentile\ i}{RR\ at\ percentile\ i} * 100\% \tag{3.6}$$

5) Selection of the heat threshold, defined as the percentile from which all the next percentiles are associated with a higher percentage change (as defined in equation 3.6), or, if not existing, the percentile preceding the one with the highest percentage change.

   The two criteria above provide the final guidance for selecting the percentile threshold at which the heat threshold should be set.

The primary advantages of the proposed framework are its foundation in a systematic review of recent, relevant literature and its inherent flexibility, which allows for easy adaptation to various population sub-samples (e.g., females, elderly individuals) as well as to different environmental hazards (e.g., air pollution) and health outcomes (e.g., respiratory diseases). However, several arbitrary decisions remain regarding the selection of hyperparameters and non-linear functions in the DLNM, as well as the determination of the final lag. Additionally, the proposed guidelines exclude the possibility of selecting the 99th percentile, being one of the most common choices in recent literature. Furthermore, the definitions provided are heuristic and may not be applicable to all datasets; therefore, empirical testing is necessary. Accordingly, this framework will be tested and further discussed in the next chapter focusing on heat effects

on ambulance dispatches for CV problems in Milan, Italy in the period from May to September 2017-2022.

Chapter 4. Influence of passive heat stress on cardiovascular emergencies in Milan, Italy

The content of this chapter is an elaborated version of the following publications:

- Nawaro, J., Gianquintieri, L., Pagliosa, A., Sechi, G. M., & Caiani, E. G. (2024). A data-driven framework for the definition of heat in CV research for better comprehension of climate changes on human health. *European Heart Journal, 45*(Supplement_1), ehae666-3578. https://doi.org/10.1093/eurheartj/ehae666.3578

- Nawaro, J., Gianquintieri, L., Pagliosa, A., Sechi, G. M., & Caiani, E. G. (2023). Heatwaves and cardiovascular emergencies in our city, in Italy: pre-Covid-19, Covid-19 and post-Covid-19 characteristics and associated risk during heat days. *European Heart Journal*, 44(Supplement_2), ehad655-3009. https://doi.org/10.1093/eurheartj/ehad655.3009

Highlights:

- RQ3: How to quantify the impact of heat on CV events on a certain area by analysing the geolocalized data relevant to CV ambulance dispatches?
- Heat definition guideline was tested using Milan, Italy as a case study, emphasizing the importance of incorporating time-related factors and population exposure characteristics into statistical modelling.
- Key patient attributes, including gender, age, and emergency place and outcome, were examined, showing that fatal emergencies and those occurring on the street represented the highest risk subgroups during heat days.
- The COVID-19 pandemic significantly influenced CV ambulance dispatches, affecting daily demand, patient characteristics, and the RR of CV emergencies during heat days.

4.1. Introduction

In Chapter 2, a comprehensive calculation of the SDG3 index for Italy was conducted. The findings indicated that Milan's residents experience average overall health vulnerability, with relatively low vulnerability in terms of cardiovascular (CV) mortality rates. Subsequently, a systematic review of the literature explored the effects of heat on CV health in an international context and, due to the lack of standardized definition of heat, a framework for selecting percentile threshold to define heat days was proposed. The aim of this chapter is to empirically test this framework on the territory of Milan, Italy, and to retrospectively analyse the impact of heat on CV emergencies. Specifically, this chapter includes an overview of the data sources and preprocessing analyses, and a quantification of the relative risk (RR) of CV events on heat days compared to non-heat days. The analyses in Chapters 5 and 6 will also focus on the city of Milan, with the data preprocessing steps presented in this chapter being relevant to those analyses as well.

As discussed in Chapter 3, while most studies reported an increased risk of CV mortality with increased temperatures, the impact on morbidity remained less clear, thus highlighting the importance of conducting regional analyses. Emergency medical services (EMS), such as ambulance transportation, are a crucial component of the public healthcare system, and can serve as a proxy for morbidity. Recent literature has addressed a range of challenges in EMS management, including logistics, operations, effectiveness, and the balance between demand and supply (Aringhieri et al., 2017). Aringhieri et al. (2017) identified the greatest current challenge as the adoption of a holistic, data-driven framework for EMS management, highlighting a significant information gap regarding patients' conditions before an emergency event (e.g., pre-existing health conditions, exposure to risk factors) and after it (e.g., diagnosis details post-hospitalization).

However, despite these challenges, EMS data, characterized by the strength of providing near real-time information, have been successfully utilized in previous epidemiological studies as a proxy for morbidity, offering valuable insights for public health (Christensen et al., 2017; Petralli et al., 2012; Wang et al., 2021b; Wallgren et al., 2022), in particular while addressing specifically the impact of environmental hazards on EMS demand (Xu et al., 2022b; Sangkharat et al., 2019). Additionally, ambulance dispatch data are geolocalized, allowing for more spatially detailed analyses, which is often not possible with hospital data, as highlighted in Chapter 3. In light of the previously identified problem of lack of heat definition in the context of CV health, a recent scoping review analysing the impact of temperature on emergency ambulance calls for CV problems again highlighted the need to identify the temperature threshold from which the increase in EMS demand is noted (Gestal Romaní et al., 2023).

Accordingly, to address the RQ3: How to quantify the impact of heat on CV events on a certain area by analysing the geolocalized data relevant to CV ambulance dispatches, this chapter applies the framework for defining heat, described in Chapter 3, to ambulance dispatch data for CV emergencies in Milan using retrospective data from May to September during the years 2017-2022. After defining heat, the analysis assesses the risk to residents, and their specific subgroups, of having a CV emergency during heat with respect to non-heat days, applying mathematical modelling. Additionally, this chapter provides an overview of the

characteristics of CV emergencies and examines the exposure of Milan's residents to temperature-related hazards, establishing a foundation for the analyses in the subsequent chapters of this thesis.

4.2. Materials and methods

4.2.1. Study area

Milan, covering an area of 182 km^2, is located in northern Italy, at 45° North latitude and 9° East longitude. The city is situated in the Po Valley, thus with no significant differences in elevation within its area, which is equal to 120 meters above the sea level. Milan is bounded to the North by the Alps and to the South by the Apennines, a mountain barrier which protects it from the major circulations coming from the northern and coastal regions. The obstruction to air circulation, coupled with heavy traffic and industrialization, has made Milan one of the most polluted cities in Europe (European Environment Agency, 2024). The geographical location of Milan within national context is presented in Figure 4.1.

Figure 4.1. (a) The location of Milan in national and regional geographical context, and (b) borders of the city of Milan

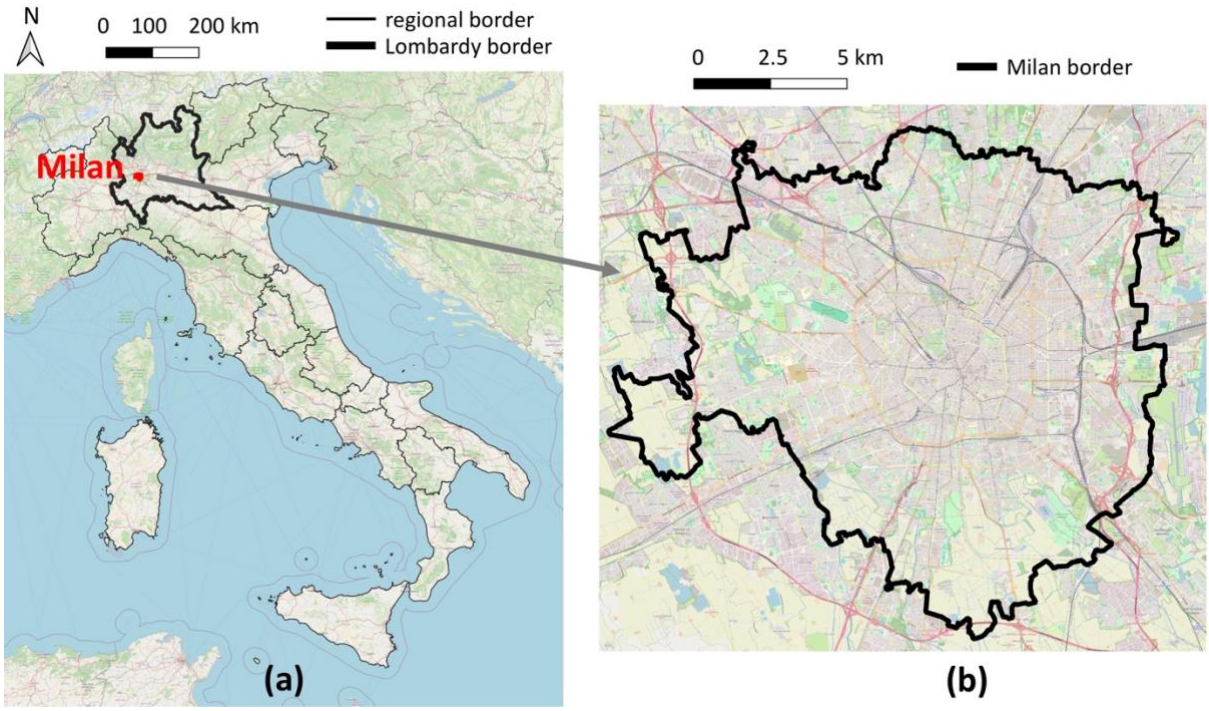

The Köppen-Geiger climate classification identifies five primary climate groups, i.e., *A* – tropical, *B* – arid, *C* – temperate, *D* – cold, *E* – polar, based on temperature and precipitation patterns, to which further specifications are applied, creating a total of 30 categories (Peel et al. 2007). Milan is located in the *Cfa* zone, where each letter corresponds to the following criteria:

- *C* (i.e., temperate climate) - the average temperature of the hottest month above 10 °C and the average temperature of the coldest month between 0 °C and 18 °C,

- *f* (i.e., without dry season) - the precipitation of the driest month in summer above 40 mm or above one third of the precipitation of the wettest month in winter, and the precipitation of the driest month in winter above one tenth of the precipitation of the wettest month in summer, where summer (winter) is defined as the warmer (cooler) six-month period of the year,

- *a* (i.e., hot summer): the average temperature of the hottest month above 22 °C.

Most of the northern and central-eastern regions of Italy exhibit the *Cfa* climate, which is also prevalent on a global scale in the southeastern part of the United States, South America and China, and the eastern part of Australia.

Milan has been characterized by a long-term increase in the mean annual temperature, albeit not consistent from year to year, from 13.16 °C in 2004 to 14.21 °C in 2015, with this trend being in line with global temperature increase and expected to continue in the future (Michetti et al., 2022).

On 1st January 2023, Milan had a population of over 1.3 million inhabitants, with a slight predominance of females (51.6%) (Istat, 2023a). Residents over the age of 65 accounted for 22.7% of Milan's total population, with 672 individuals surpassing the age of 100, while children (i.e., aged 0-18) covered 16% of the city's inhabitants. The population pyramid of Milan is contracting (Figure 4.2), characterizing populations with low birth and death rates and a long life expectancy, indicating an aging population. The dominant age class is 50-54 for both men and women, with a total of 54,464 and 56,181 residents of these genders, respectively, while the median age is 44 for men and 48 per women. Milan's population has experienced a relatively small but stable long-term increase, rising by slightly more than 8% between 2001 and 2023; in particular, the proportion of elderly people in the population has remained relatively constant during this period (Istat, 2024).

Figure 4.2. Population pyramid for Milan on 1st January 2023 (Istat, 2023a)

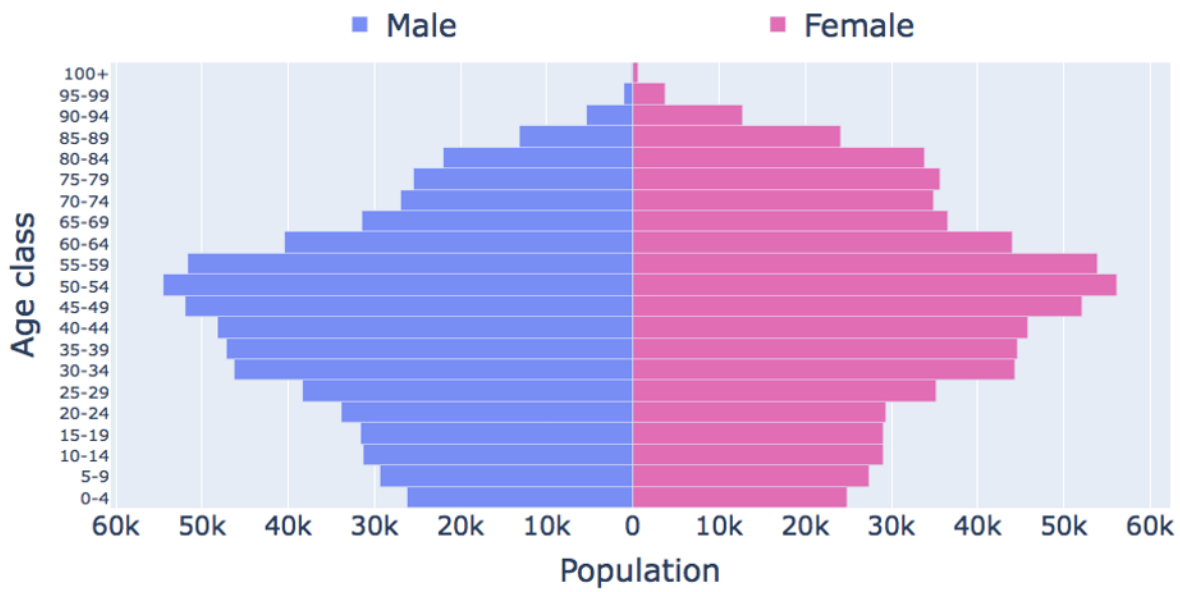

4.2.2. Emergency medical services data: ambulance dispatches

Ambulance dispatch data were provided upon request by the Regional Agency for Emergency and Urgency (in Italian: *Agenzia Regionale Emergenza Urgenza*; AREU) which is the EMS provider in the Lombardy region. Specifically, AREU is a public entity established under Regional Law no. 33 of 30th December 2009, with organizational, administrative, and financial autonomy (AREU, 2024). It is responsible for ensuring the delivery of essential healthcare services in EMS outside of hospitals, blood transfusions, and medical transports, including organ and tissue transplants, coordinating them primary at intra-regional scale, referring to the Lombardy region, and, secondarily, at inter-regional scale as well.

Additionally, AREU collaborates with civil protection authorities for large-scale emergencies, supports scientific research with healthcare organizations and research institutions, provides technical assistance to the regional government, liaises with national and regional health bodies, and partners with third sector and volunteer organizations to enhance emergency services and community healthcare, with a focus on training and education.

Data provided for the purposes of this thesis covered emergencies that occurred within the city of Milan between May and September in the period 2017-2022, and that were classified as CV upon receiving the emergency call through emergency numbers – 112 (European) or 118 (national), thus are used as proxy for CV morbidity. For each event, available information included:

- gender of the patient,
- age of the patient,
- state of the patient upon ambulance arrival (i.e., regular, dead, refuses to be transported, does not need transport, recedes, other)
- approximate location relevant to the place of call (i.e., geographical latitude and longitude),
- place of the event (i.e., home, street, socio-medical facility, other medical facility, workplace, hospital, public office, railway, school, sports facility, lake),
- time of the event (i.e., year, month, day and hour of the event).

The data were preprocessed to avoid inclusion of missing values in any of the above columns. Ambulance data were analysed both in their raw form, where each row represented an individual emergency, and in aggregated form, with each row corresponding to a day and columns representing the daily number of emergencies (total and in particular subgroups).

In addition, to estimate the actual presence of the city's resident population, accounting in particular for the holiday effect, average traffic data were used, provided by the Lombardy Region's Open Data portal (Regione Lombardia, 2022). This dataset included the daily number of vehicles passing through 10 Milan roads in 2016. For the purpose of estimating resident presence, the daily vehicle counts were averaged across all 10 roads to reflect an overall trend, rather than focusing on interpreting absolute daily values. Subsequently, mean traffic for the whole year was calculated, and for each day, the volume of traffic was standardized using the annual mean, according to the following equation:

$$standardized\ traffic = \frac{traffic_i}{mean\ traffic} \tag{4.1}$$

where $traffic_i$ is the averaged traffic from 10 roads for day *i*, and *mean traffic* is the mean traffic for the whole year 2016. The obtained values were matched in their raw form with annual ambulance data (in the months from May to September), without further adjustments for long-term trend, and their precise scope will be described in section 4.2.4.

4.2.3. Meteorological data

Open data for the years 2017-2022 relevant to the meteorological factors (i.e., temperature at 2 meters above the surface, relative humidity and wind speed), and the air pollution (i.e., carbon monoxide (CO), nitrogen dioxide (NO_2), sulfur dioxide (SO_2), ozone (O_3), particulate matters of less than 10 µm in diameter (PM10) and particulate matters of less than 2.5 µm in diameter (PM2.5)) were obtained from the website of the Regional Agency for Environmental Protection (in Italian: *Agenzia regionale per la protezione dell'ambiente;* ARPA) for the Lombardy region (ARPA, 2023a).

ARPA focuses on environmental prevention and protection, supporting regional and local institutions in areas such as air and noise pollution control, water protection, and monitoring meteorological parameters, electromagnetic fields and soil contamination (ARPA, 2023b). Established by Regional Law 16/1999, ARPA has administrative and financial autonomy and uses its scientific expertise to gather and analyse data, supporting environmental policy decisions for Lombardy's public entities.

ARPA promotes public transparency through information, communication, and environmental education, enabling citizens, researchers and businesses to understand and assess the state of their environment. It collaborates with regional and international research institutions and various local actors to address complex environmental issues. Additionally, ARPA contributes to technical-scientific working groups at the European, national, and local levels, supporting the development of environmental policies and measures for pollution control.

ARPA's services provide real-time weather information with data from 318 monitoring stations located within the Lombardy region. These data are publicly available in both raw and analysed formats. In air quality management, ARPA operates 85 monitoring stations across the region and uses mathematical models to predict and assess air pollution levels.

The choice of meteorological parameters enabled the calculation of apparent temperature (AT) in its most complete definition, i.e., accounting for the highest number of meteorological factors, as defined in Chapter 3 by "Apparent Temperature 2". Such heat index accounts not only for the air temperature, but also for cooling and heating capacities of relative humidity and wind speed, thus representing more accurate perception of the temperature by humans. The choice of air pollution variables was based on their influence on adverse CV outcomes, reported by both theoretical and empirical studies (Bourdrel et al., 2017; Lee et al., 2014). In particular, several previous works, as discussed in the previous chapter, adjusted the model assessing the impact of passive heat by air pollution in order to differentiate the impact of these two groups of environmental variables.

For each meteorological and air pollution variable, measurement stations were mapped, and the Lombardy region was partitioned using the Voronoi diagram (Boots et al., 2009). The Voronoi diagram is a way of dividing a plane into regions based on the distance to a specific

set of points, and it found application in different fields, including biology, geography, physics and social sciences (Ju et al., 2011). In this study, each point, called "seed", in this set represents an ARPA station for a particular variable. For each seed, there is a corresponding polygon that contains all the points on the plane that are closer to that seed than to any other seed. For each variable, minimum number of stations whose polygons allowed to cover the entire city of Milan was considered.

For each meteorological parameter, hourly data were downloaded from the selected stations. The final value of each parameter, i.e., air temperature, relative humidity and wind speed, was calculated for each hour as the arithmetic mean of values from all stations considered, ignoring missing values, as illustrated in Figure 4.3. Subsequently, for each hour, apparent temperature (AT) was calculated, according to the "Apparent Temperature 2" equation from Chapter 3:

$$AT = T + 0.33 * \frac{RH}{100} * 6.105 * \mathrm{e}^{17.27 * \frac{T}{237.7+T}} - 0.7 * WS - 4 \qquad (4.2)$$

where *T* is air temperature in °C, *RH* is relative humidity in %, and *WS* is wind speed in m/s.

Figure 4.3. Schema of calculation of hourly final value for each meteorological indicator. Absolute values are illustrative and do not represent true values of any of the indicators. NaN – missing value; n – number of stations considered; Station_i – non-missing value of an indicator for station *i*.

Time/station	Station_1	Station_2	...	Station_n
01-01-2017 00 h	5.1	5.9	...	5.2
01-01-2017 01 h	5.1	NaN	...	5.1
01-01-2017 02 h	5.0	6.0	...	4.9
...	...	...	...	...
01-01-2017 23 h	5.3	6.0	...	5.1

Time/station	Final value
01-01-2017 00 h	$\frac{\sum_{i=1}^{n} Station_i}{n}$
01-01-2017 01 h	$\frac{\sum_{i=1}^{n} Station_i}{n}$
01-01-2017 02 h	$\frac{\sum_{i=1}^{n} Station_i}{n}$
...	...
01-01-2017 23 h	$\frac{\sum_{i=1}^{n} Station_i}{n}$

Lastly, for each day from 1st January 2017 to 31st December 2022, mean, minimum and maximum daily AT was calculated, as illustrated in Figure 4.4.

Figure 4.4. Schema of calculation of mean, minimum and maximum daily apparent temperature (AT). T – temperature (°C), RH – relative humidity (%), WS – wind speed (m/s); AT_i - value of AT at hour *i*.

Time/final value	T	RH	WS
01-01-2017 00 h	T_0	RH_0	WS_0
01-01-2017 01 h	T_1	RH_1	WS_1
01-01-2017 02 h	T_2	RH_2	WS_2
...	...	...	...
01-01-2017 23 h	T_23	RH_23	WS_23
...	...	...	...
31-12-2022 23 h	T_23	RH_23	WS_23

Time/AT	AT
01-01-2017 00 h	$T_0 + 0.33 * \frac{RH_0}{100} * 6.105 * e^{17.27 * \frac{T_0}{237.7+T_0}} - 0.7 * WS_0 - 4$
01-01-2017 01 h	$T_1 + 0.33 * \frac{RH_1}{100} * 6.105 * e^{17.27 * \frac{T_1}{237.7+T_1}} - 0.7 * WS_1 - 4$
01-01-2017 02 h	$T_2 + 0.33 * \frac{RH_2}{100} * 6.105 * e^{17.27 * \frac{T_2}{237.7+T_2}} - 0.7 * WS_2 - 4$
...	...
01-01-2017 23 h	$T_23 + 0.33 * \frac{RH_23}{100} * 6.105 * e^{17.27 * \frac{T_23}{237.7+T_23}} - 0.7 * WS_23 - 4$
...	...
31-12-2022 23 h	$T_23 + 0.33 * \frac{RH_23}{100} * 6.105 * e^{17.27 * \frac{T_23}{237.7+T_23}} - 0.7 * WS_23 - 4$

Time/AT	Mean_AT	Min_AT	Max_AT
01-01-2017	$\frac{\sum_{i=o}^{23} AT_i}{24}$	$\min_{0 \le i \le 23} AT_i$	$\max_{0 \le i \le 23} AT_i$
02-01-2017	$\frac{\sum_{i=o}^{23} AT_i}{24}$	$\min_{0 \le i \le 23} AT_i$	$\max_{0 \le i \le 23} AT_i$
...	...	...	...
31-12-2022	$\frac{\sum_{i=o}^{23} AT_i}{24}$	$\min_{0 \le i \le 23} AT_i$	$\max_{0 \le i \le 23} AT_i$

For air pollutants, due to the absence of higher temporal granularity, their daily mean values from each measurement station were directly considered. Similar to the meteorological parameters, the final daily value for each pollutant was the average of non-missing values of all stations considered. Accordingly, in this case, no minimum and maximum daily value was calculated, and the final value represented the mean daily value for each pollutant.

4.2.4. Statistical methods

Percentile threshold for defining heat

In this chapter, the framework for selecting temperature threshold for defining heat formulated in the previous chapter was tested. To this purpose, mean daily AT was selected as the meteorological indicator representing the environmental hazard, which was merged with the time series of daily number of CV emergencies in Milan in May-September period of 2017-2022. The first step of the framework required fitting the distributed lag non-linear model (DLNM) to estimate the relative risk (RR) of having a CV emergency depending on AT with respect to the reference AT value (estimated directly by the DLNM as the fitted function minimum), accounting for a possible delayed effect. Fitting the DLNM required some arbitrary choices to be made regarding the distribution family, the covariates inclusion, the smoothing functions, and the hyperparameters. Based on previous literature, outlined in Chapter 3, the following arbitrary choices were made:

- distribution family – quasi-Poisson distribution,
- covariates – to account for long-term trend and seasonality: day of year, observation order, day of week, and to account for air pollution effects: CO, NO_2, SO_2, PM10, O_3, PM2.5,
- smoothing functions – natural spline for day of year, observation order and lags,

- hyperparameters – 6 degrees of freedom for day of year, 2 degrees of freedom for observation order, 3 lags with 2 equally placed knots and 3 degrees of freedom.
Accordingly, the DLNM can be described in a form of the following equation:

$$y \sim cb.temp + ns(doy,6) + ns(order,2) + dow + CO + NO_2 + SO_2 + PM_{10} + O_3 + PM_{2.5} \quad (4.3)$$

where *y* – CV dispatches in May-September 2017-2022 in Milan, *cb.temp* – cross basis matrix for AT for 3 lags, *ns(doy, 6)* – natural spline of day of year with 6 degrees of freedom, *ns(order, 2)* – natural spline of the observation order with 2 degrees of freedom, *dow* – day of week, *CO*, NO_2, SO_2, PM_{10}, *O3*, $PM_{2.5}$ – mean daily pollutant levels (optional inclusion, as explained in the following paragraph).

The resulting contour plot was reported for all the CV emergencies, as well as separately for those in women, in elderly (i.e., above 65 years old), and stratified by severity: requiring transportation to a hospital, fatal, and all others (henceforth referred to as "non-severe"). As sensitivity analysis, the model was repeated without the inclusion of air pollutants.

After selecting lags for further analysis based of the contour plot, the next step was to perform a Poisson regression which estimates the RR of having a CV emergency in heat days (with heat definition threshold tested for 10 percentiles, from the 90th to 99th) versus non-heat days, defined as all days not classified as heat. In case of data for Milan, traffic data were used in order to account for the actual daily presence of the residents, especially important during the holiday period. In particular, standardized traffic, as calculated in equation 4.1, was included as the offset for the Poisson regression model. The inclusion of traffic data was not necessary in the DLNM, as that model directly used spline functions for day of the year. In addition, a 95% confidence interval (CI) was reported for each RR. If the CI includes the value of 1, the RR is not statistically significant; otherwise, it is considered statistically significant.

The subsequent three steps, i.e., the selection of the final lag based on the curvatures of the 10 included percentiles, the calculation of the percentage change in RR from percentile *i* to percentile *i+1*, and the selection of the final heat threshold did not require any mathematical adjustments, thus they were performed following the descriptions in the Chapter 3, section 3.5.

Characteristics of meteorological, air pollution and ambulance data

Descriptive statistics, including the mean, standard deviation, minimum, 25th percentile, median, 75th percentile, and maximum, were reported at various stages of the analysis to summarise the distribution of meteorological, air pollution, and ambulance data. Spearman's correlation coefficient (ρ) was used to examine the correlation between each meteorological and air pollution variable, as the relationship between these factors was assumed to be non-linear (Zhang et al., 2017).

The Kolmogorov-Smirnov test was used to assess whether the daily number of CV emergencies followed a normal distribution. Time-related characteristics were visualized as boxplots, grouped by year, month, day of the week, and heat days. Differences in the distributions across these time dimensions were tested using the Kruskal-Wallis test with Bonferroni correction.

The characteristics (i.e., number and percentage) of emergencies were subsequently compared between heat and non-heat days, focusing on categories such as gender, age, severity (i.e., fatal, requiring transportation to a hospital, non-severe), and location (i.e., at home, on the street, and all other places). For each category, the percentage of emergencies occurring on heat days was compared to the percentage of total emergencies on heat days, with statistical differences tested using the chi-square test. Additionally, the RR of experiencing an emergency on heat versus non-heat days was calculated for each category using a Poisson regression model with the offset as defined in the previous section.

Special attention was given to the impact of the Coronavirus Disease 2019 (COVID-19) on CV health as studies have reported both direct and indirect effects of the pandemic on CV outcomes. Direct effects primarily included triggering acute myocardial injury and worsening health outcomes in patients with pre-existing CV conditions (Xie et al., 2022; Bansal, 2020; Zheng et al., 2020; Clerkin et al., 2020). Indirect effects, such as a decrease in emergency calls for CV issues, have been observed, likely due to fears of hospitalization and potential COVID-19 exposure (Goldberg et al., 2021; Chen et al., 2021; D'Ascenzi et al., 2021). This, in conjunction with delays or cancellations of CV examinations during the pandemic, further contributed to the worsening of CV outcomes within the population (Khan et al., 2023; Kiss et al., 2021).

Accordingly, three periods were defined: pre-COVID-19 (i.e., years 2017–2019), COVID-19 (i.e., years 2020–2021), and post-COVID-19 (i.e., year 2022). The pre-COVID-19 period served as the reference, and the characteristics of the emergencies, including their daily frequency, age distribution, percentage of female patients, and the percentages of fatal, requiring transportation to a hospital, and non-severe emergencies, were compared separately for the COVID-19 and post-COVID-19 periods relative to the reference period. These comparisons were conducted using the chi-square test for percentages and the Mann-Whitney U test for distributions. Additionally, the RR of experiencing an emergency on heat versus non-heat days was calculated for each of the three periods.

Lastly, to examine the spatial distribution of the ambulance data, their geolocation was visualized using heatmaps, with the radius arbitrarily set to 1,000 meters to ensure adequate visual clarity. Separate heatmaps were generated for heat days and non-heat days.

All maps were generated using QGIS software, while Python was employed for data preprocessing, statistical analysis, and non-spatial visualizations.

4.3. Results and discussion

In the analysed period of May-September 2017-2022, there was a total of 64,881 CV emergencies in Milan, of which 35,267 (54.36%) occurred in females, and 35,397 (54.56%) involved individuals above 65 years old. Among all these emergencies, 1,484 (2.29%) cases were fatal, 53,509 (82.47%) cases required hospitalization, and 9,888 (15.24%) cases were classified as non-severe. The mean daily AT during May-September period of the analysed years ranged from 6.86 °C to 36.03 °C, with an average of 23.54 °C. A more detailed description of CV emergencies and meteorological parameters is provided in sections 4.3.2 and 4.3.3.

4.3.1. Selecting temperature threshold for defining heat

The first step in heat definition framework applied in this study was to select the temperature lags based on the contour plot obtained by the DLNM. The estimated effect for different levels of AT, calculated with respect to the reference AT equal to 19.6 °C (estimated directly by the DLNM as the minimum of the resulting function) was the strongest at lag0, and persisted till lag1 (left panel of Figure 4.5). Interestingly, at lag2, the RR of a CV emergency was lower at high temperatures than in reference conditions, however, it was increased again at lag3. Accordingly, the lags selected for further investigation were lags 0 and 1. The version without the inclusion of air pollutants yielded very similar graph, as shown in the right panel of Figure 4.5; therefore, air pollutant will not be considered for further models.

Figure 4.5. Contour plot obtained through distributed lag non-linear model for cardiovascular emergencies in Milan, Italy in May-September 2017-2022, (a) with the inclusion of air pollutants, and (b) without the inclusion of air pollutants. RR – relative risk estimated against reference mean daily apparent temperature of 19.6 °C.

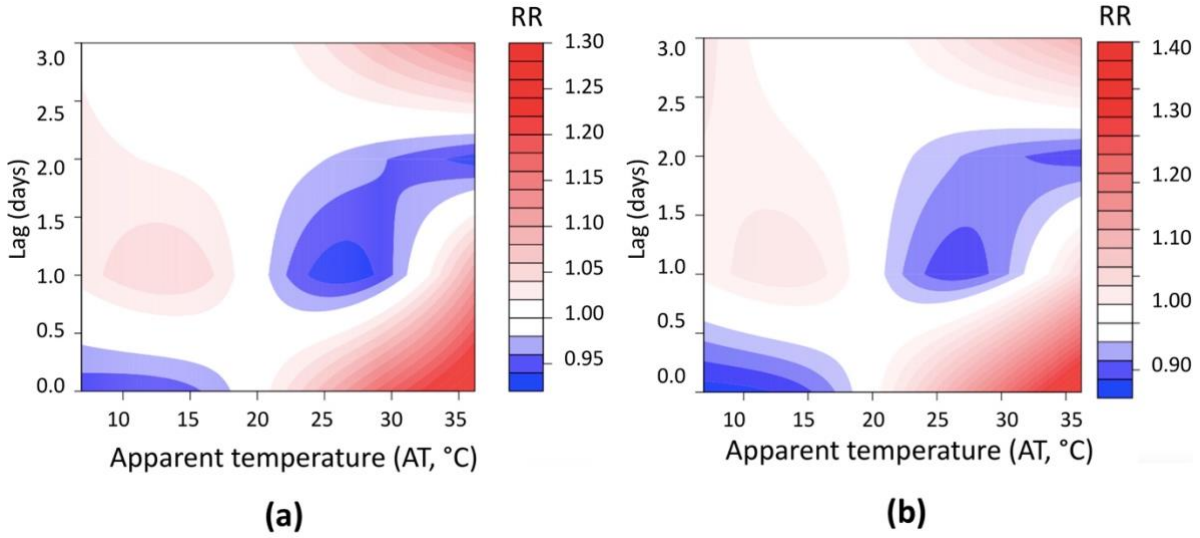

Interestingly, while the contour plot for emergencies in women had a similar shape as those including all the emergencies, it differed much when considering only elderly patients. For individuals over 65 years old, the RR associated with high temperatures remained increased across all lags, with the strongest effects observed at lags 0 and 3. When stratified by emergency severity, lag0 was most influential for cases requiring hospitalization, which accounted for the majority of the emergencies. However, lag1 was associated with the highest increase in RR for both fatal and non-severe emergencies. The contour plots for women, elderly patients, and the three levels of emergency severity are shown in Figure 4.6. When stratified by gender, age, or severity, the reference AT varied, ranging from 18.4 °C for emergencies requiring hospitalization to 23.5 °C for fatal emergencies. Additionally, the magnitude of RR differed substantially for fatal emergencies, where it exceeded the value of 3, compared to other cases, where the maximum RR was approximately 1.40.

Figure 4.6. Contour plot obtained through distributed lag non-linear model for cardiovascular emergencies in Milan, Italy in May-September 2017-2022 for (a) female patients, (b) above 65 years old patients, (c) non-severe emergencies, (d) emergencies requiring transportation to hospital, (e) fatal emergencies. RR – relative risk estimated against reference mean daily apparent temperature.

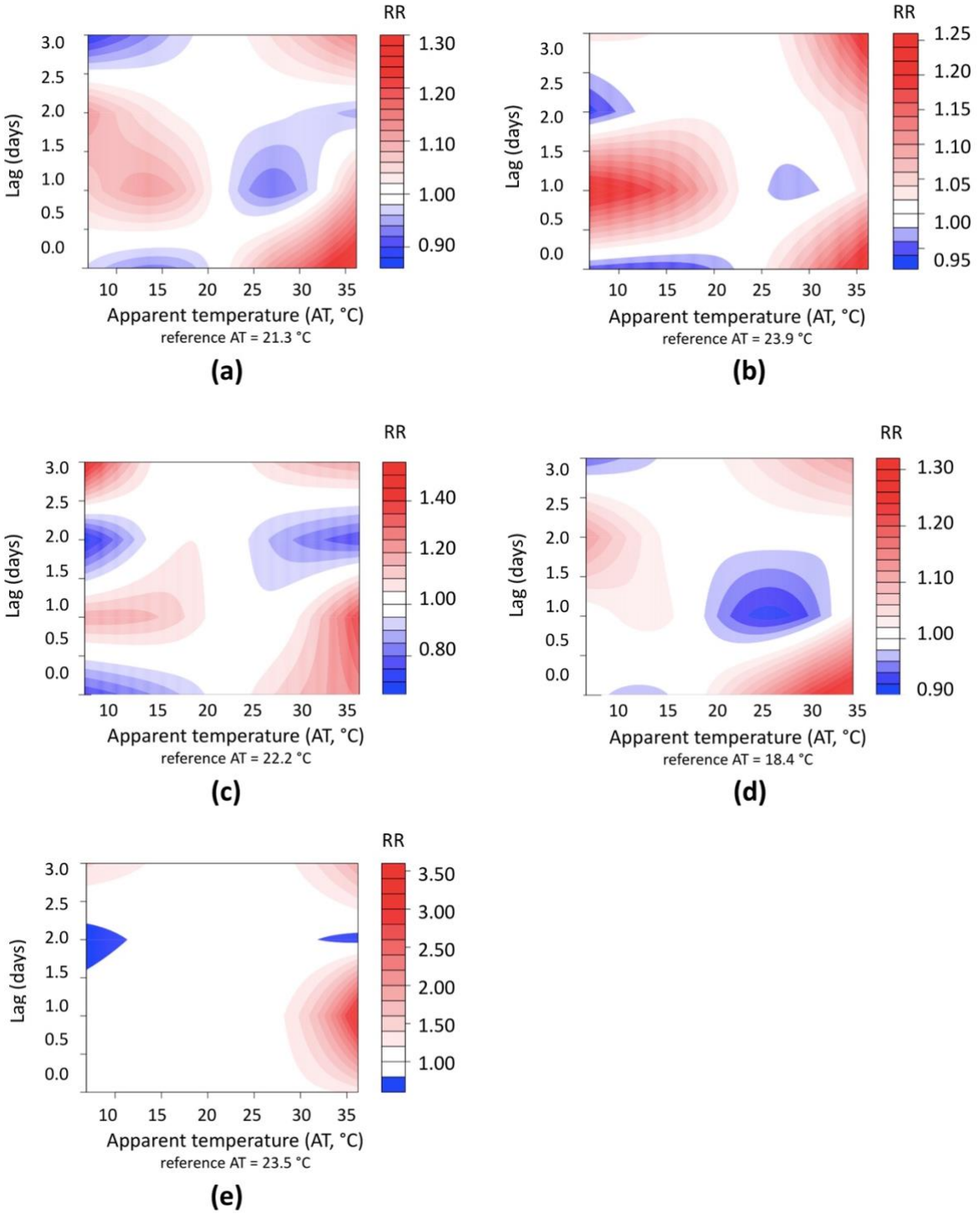

To ensure that the selected threshold for defining heat was applicable universally, Poisson regression was conducted on all CV emergencies, without stratifying by gender, age, or severity. Given that lags 0 and 1 were considered, the model was run using the following definitions of lags for heat days:

- only days when the mean daily AT exceeded the ith percentile (with i in range from the 90th to 99th) of its annual distribution (referred to as "lag0"),

- days when the mean daily AT exceeded the ith percentile (with i in range from the 90th to 99th) of its annual distribution and the following day, regardless of the second day's AT (referred to as "lags 0 or 1"),

- days when the mean daily AT exceeded the ith percentile (with i in range from 90th to 99th) of its annual distribution for that day and the following day (referred to as "lags 0 and 1").

As shown in Figure 4.7, the curves generated by these three criteria were similar, confirming the robustness of the approach. Accordingly, lag0 was arbitrarily selected for further analysis. Unsurprisingly, considering lags 0 and 1 (i.e., a minimum two-day heatwave) resulted in the highest RR.

Figure 4.7. Relative risk estimated by Poisson regression for heat thresholds set from the 90th to 99th percentile of annual apparent temperature distribution for three lags considered (see text for details). Shaded area represents 95% confidence interval.

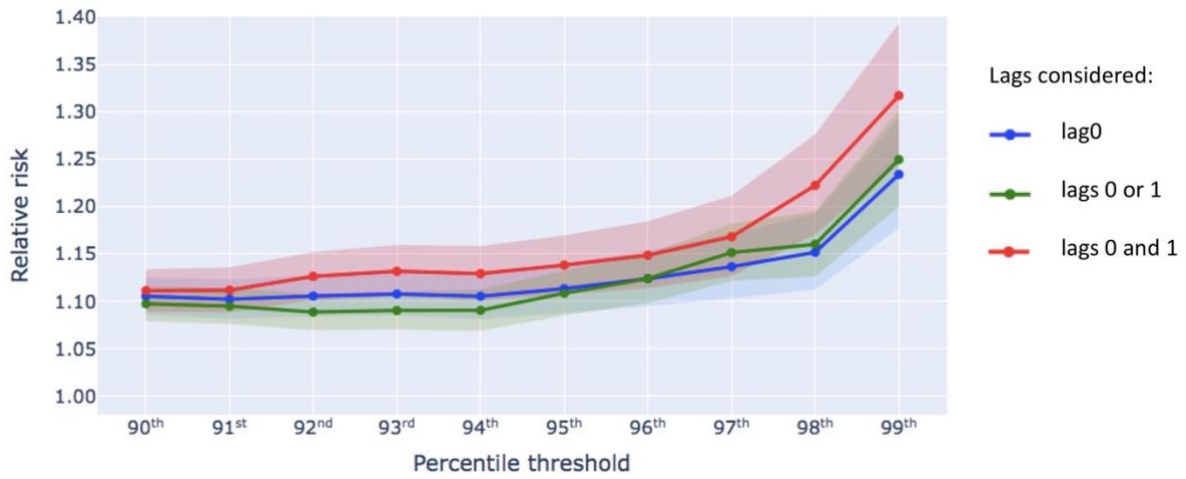

The percentage change from percentile i to $i+1$ ranged from -0.29% from the 90th to 91st percentile, to 7.14% from the 98th to 99th percentile (Figure 4.8). From the 95th percentile, all the next percentiles were associated with a higher percentage change. Therefore, for Milan, days with AT exceeding the 95th percentile of its annual distribution were selected as heat days. This approach classified 19 days as heat days each year, thus there were 114 heat days in total in the analysed period of 2017-2022, with all of them falling within the months from May to September. All other days were classified as non-heat days.

Figure 4.8. Relative risk of a cardiovascular emergency associated with each percentile of the apparent temperature distribution at lag0 in Milan, Italy. The blue shaded area represents a 95% confidence interval. RR – relative risk, CI – confidence interval.

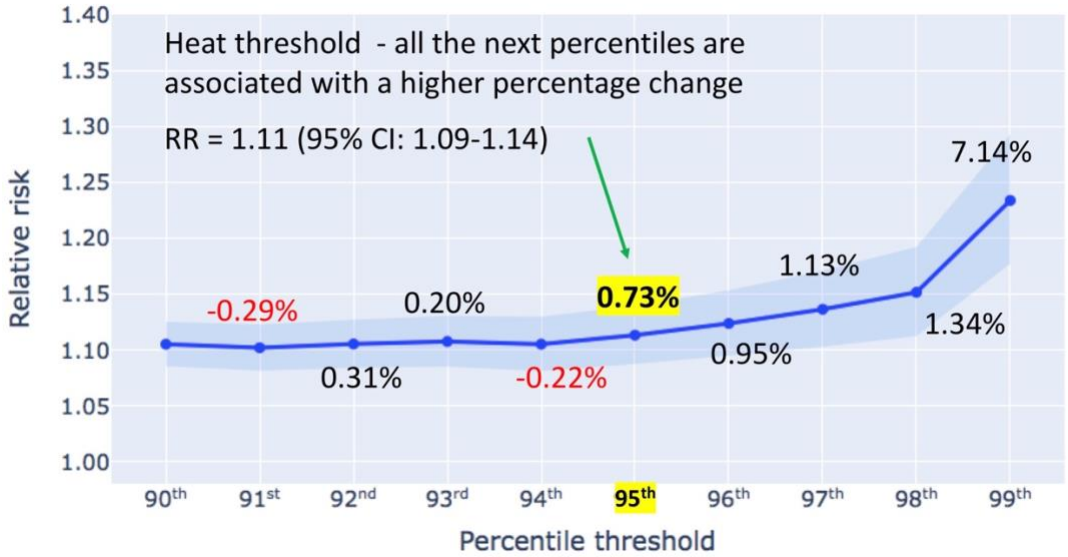

4.3.2. Meteorological characteristics and air pollution in the city of Milan

The approach for selecting the ARPA measurement stations resulted in the identification of 10 unique stations for meteorological parameters (nine for air temperature, eight for relative humidity, five for wind speed). In particular, one station ("Lacchiarella v. Molise") resulting from the application of the Voronoi diagram for wind speed was excluded, as it was located far from the borders of the city of Milan and yielded a polygon which covered only a very small area of the city. The polygons resulting from the Voronoi diagrams for each considered meteorological parameter are mapped in Figure A4.1 in Appendix.

For air pollutants, the selection of stations based on the Voronoi diagrams resulted in the identification of stations for which the majority of daily observations were missing values. Therefore, after the exclusion of these stations, a total of 10 unique measurement stations (seven for CO, nine for NO_2, two for SO_2, three for O_3, four for PM10, three for PM2.5) was selected. The geographical location of final ARPA measurement stations is mapped in Figure 4.9.

Figure 4.9. Geographical location of ARPA measurement stations for meteorological parameters and air pollutants. T – air temperature, RH – relative humidity, WS – wind speed, CO – carbon monoxide, NO_2 – nitrogen dioxide, SO_2 – sulfur dioxide, O_3 – ozone, PM10 – particulate matters of less than 10 µm in diameter, PM2.5 – particulate matters of less than 2.5 µm in diameter.

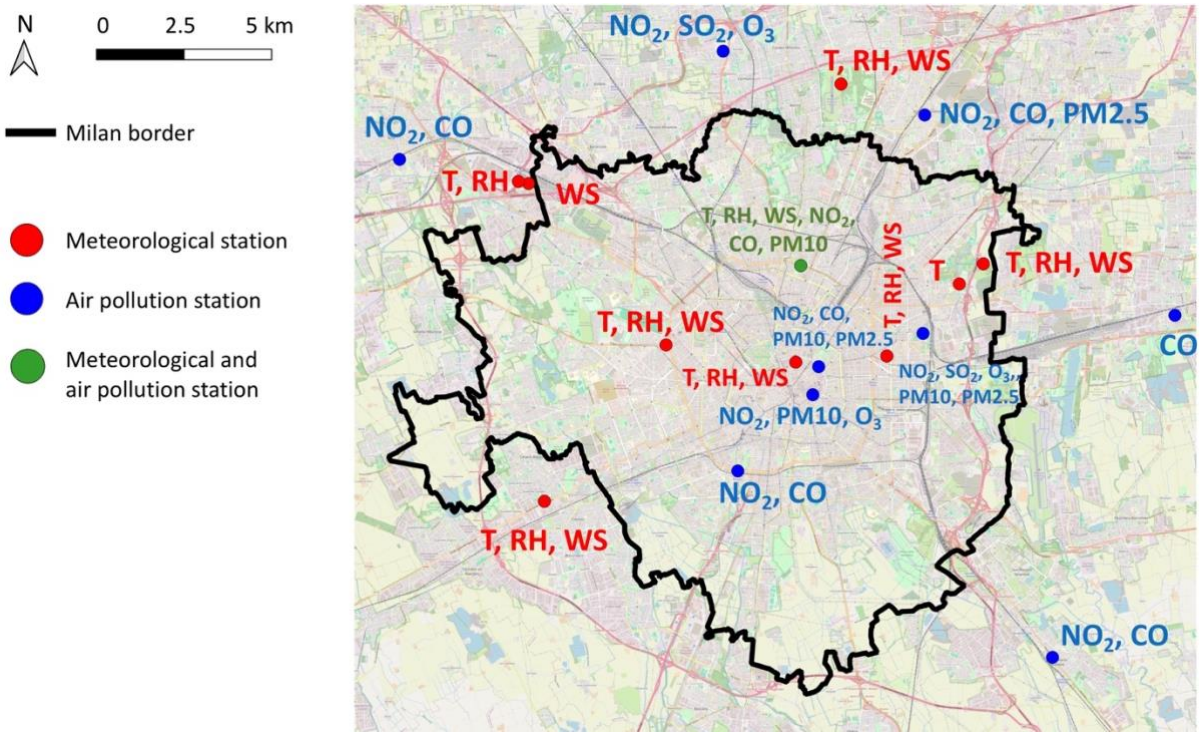

Overall, during the warmer months (i.e., from May to September) in the years 2017–2022, the mean daily AT was 23.54 °C, slightly higher than the mean daily air temperature over the same period, which was 23.25 °C. In general, the minimum and 25th percentile of AT were lower than the corresponding values for air temperature, while the median, 75th percentile, and maximum AT were higher. Milan was characterized by high humidity levels, with an average relative humidity of 59.07%. Wind speeds were relatively low and stable, ranging from 0.72 m/s to 3.15 m/s, with a 25th-75th percentile range of 1.30–1.81 m/s. A detailed summary of the descriptive statistics for meteorological parameters and air pollutants is provided in Table 4.1.

Table 4.1. Descriptive statistics of mean daily values of meteorological parameters and air pollutants in May-September 2017-2022 in Milan, Italy. CO – carbon monoxide, NO_2 – nitrogen dioxide, SO_2 – sulfur dioxide, O_3 – ozone, PM10 – particulate matters of less than 10 µm in diameter, PM2.5 – particulate matters of less than 2.5 µm in diameter.

Parameter/ statistics	Mean	Standard deviation	Minimum	25th percentile	Median	75th percentile	Maximum
Apparent temperature (°C)	23.54	5.00	6.86	20.27	24.38	27.24	36.03
Air temperature (°C)	23.25	4.19	9.84	20.42	24.03	26.30	32.17
Relative humidity (%)	59.07	11.79	27.63	50.92	58.69	66.56	96.12

Wind speed (m/s)	1.58	0.39	0.72	1.30	1.53	1.81	3.15
CO (mg/m^3)	0.52	0.11	0.28	0.44	0.51	0.59	1.07
NO_2 (µg/m^3)	29.49	9.68	8.50	22.25	28.51	35.30	77.17
SO_2 (µg/m^3)	2.82	1.36	0.34	1.74	2.64	3.73	12.92
O_3 (µg/m^3)	75.88	20.38	15.75	62.15	76.71	90.22	132.75
PM10 (µg/m^3)	21.77	8.23	5.00	16.00	20.47	26.00	62.50
PM2.5 (µg/m^3)	12.19	4.87	2.67	9.00	11.33	14.75	39.50

The correlation between air pollutants and AT was high only for O_3 (ρ=0.72), consistent with findings from previous studies (Abdullah et al., 2017; Porter and Heald, 2019). In contrast, the correlation coefficients for other pollutants ranged from -0.16 for NO_2 to 0.39 for PM2.5, as shown in Figure 4.10. This finding partially explains the minimal differences observed in the contour plots of DLNM results when comparing models with and without the inclusion of air pollutants.

Figure 4.10. Spearman correlation matrix for mean daily values of meteorological parameters and air pollutants in May-September 2017-2022 in Milan, Italy. AT – apparent temperature, T – air temperature, RH – relative humidity, WS – wind speed, CO – carbon monoxide, NO_2 – nitrogen dioxide, SO_2 – sulfur dioxide, O_3 – ozone, PM10 – particulate matters of less than 10 µm in diameter, PM2.5 – particulate matters of less than 2.5 µm in diameter.

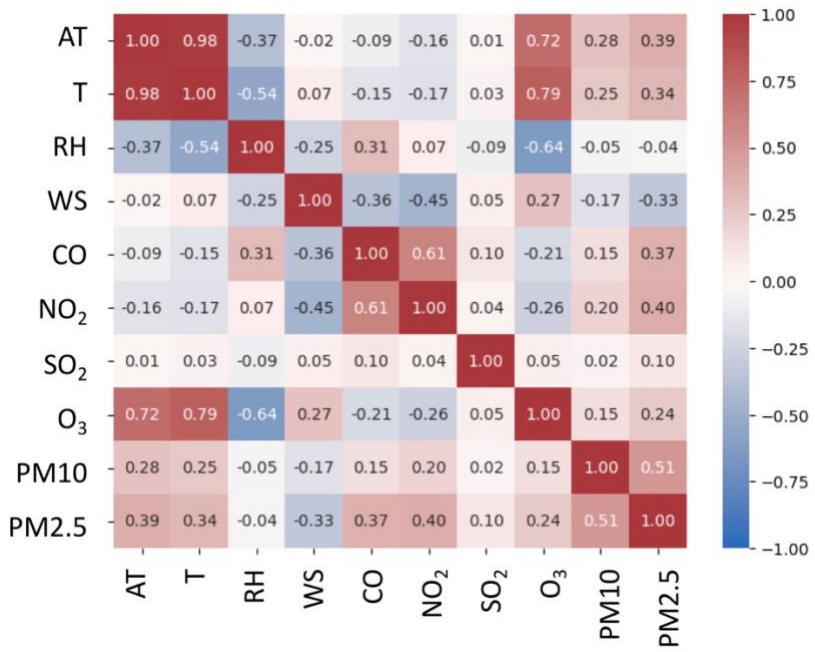

Table 4.2 provides a detailed annual overview of the mean daily AT statistics for the months from May to September, along with the corresponding annual heat thresholds. The year 2020 recorded the lowest median of mean daily AT, but no extremes in any of the other summary statistics. The warmest year in terms of the minimum, the 25th percentile and the median was 2022, while the 75th percentile and the maximum were higher in 2019. The lowest heat threshold, corresponding to the 95th percentile of the annual mean daily AT distribution, was observed in 2021 (27.68 °C) and the highest in 2022 (29.92 °C), with a difference of 2.24 °C

between these years. The record high mean daily AT of 36.0 °C was registered on 27th June 2019. Although the difference in AT value for heat threshold across years is relatively big, using separate thresholds each year is relevant as it reflects annual climate variability, making such approach sensitive to the specific conditions of each year, leading to a more accurate and meaningful identification of heat events.

Table 4.2. Descriptive statistics of the mean daily apparent temperature in May-September 2017-2022 in Milan, Italy. Heat threshold defined as the 95th percentile of annual daily mean apparent temperature distribution.

Year/statistics	Minimum	25th percentile	Median	75th percentile	Maximum	Heat threshold
2017	7.92 °C	19.07 °C	23.53 °C	27.04 °C	32.8 °C	28.34 °C
2018	11.82 °C	21.45 °C	24.8 °C	27.07 °C	32.19 °C	28.29 °C
2019	6.86 °C	19.26 °C	24.78 °C	28.13 °C	36.03 °C	29.27 °C
2020	10.46 °C	19.88 °C	23.12 °C	27.11 °C	33.36 °C	28.68 °C
2021	12.93 °C	20.01 °C	23.54 °C	26.08 °C	32.17 °C	27.68 °C
2022	13.61 °C	23.03 °C	25.96 °C	27.9 °C	32.86 °C	29.92 °C

Considering the five heat indices from the previous chapter, analysed under reference conditions (relative humidity=50%, wind speed=1 m/s) as a function of air temperature (Figure 3.2), 'Apparent Temperature 2' was lower than the air temperature up to approximately 25 °C. However, under warmer conditions, it exceeded the air temperature, reaching significantly higher values. As shown in Figure 4.11, during the warmest days of the period from May to September 2017–2022, AT was considerably higher than the air temperature, particularly when combined with high relative humidity. In contrast, during the cooler months of May and September, AT was lower than the air temperature.

Figure 4.11. Apparent temperature, air temperature and relative humidity in May-September 2017-2022 in Milan, Italy

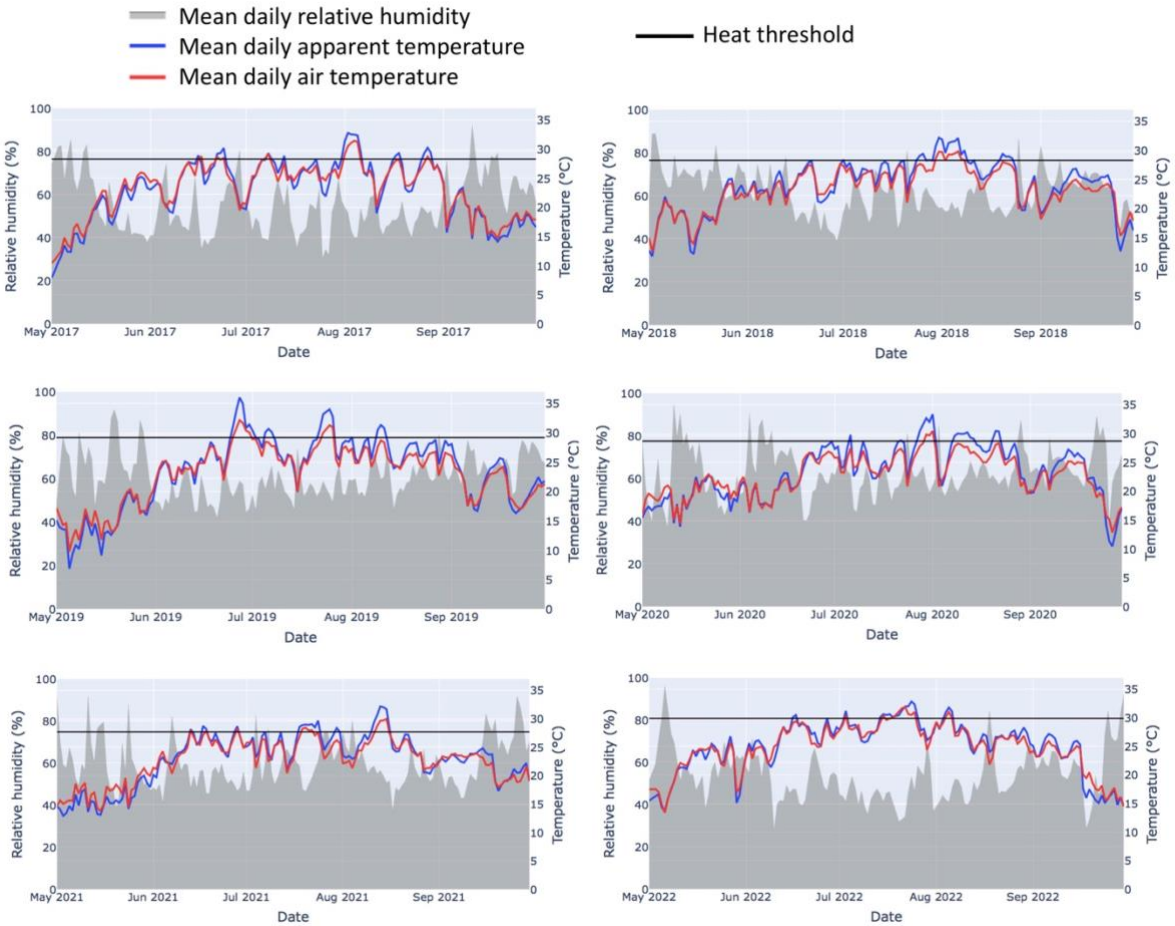

4.3.3. Ambulance dispatches for cardiovascular problems in the city of Milan

Of the 64,881 CV emergencies, 7,974 (12.29%) occurred during the 114 heat days. Figure 4.12 shows the daily number of CV emergencies and the mean daily AT throughout the period from May to September 2017-2022. A noticeable drop in the daily number of emergencies occurred each August, reflecting the holiday period for Italians. However, August was also characterized by relatively high temperatures and the occurrence of heat days. This highlights the importance of including traffic data in models that do not directly account for time trends. Specifically, in further analyses, traffic data were used as an offset in Poisson regression models to estimate the RR of CV emergencies on heat versus non-heat days.

Figure 4.12. Daily number of cardiovascular emergencies in May-September 2017-2022 in Milan, Italy and mean daily apparent temperature. Heat days are marked in red. CV – cardiovascular, AT – apparent temperature.

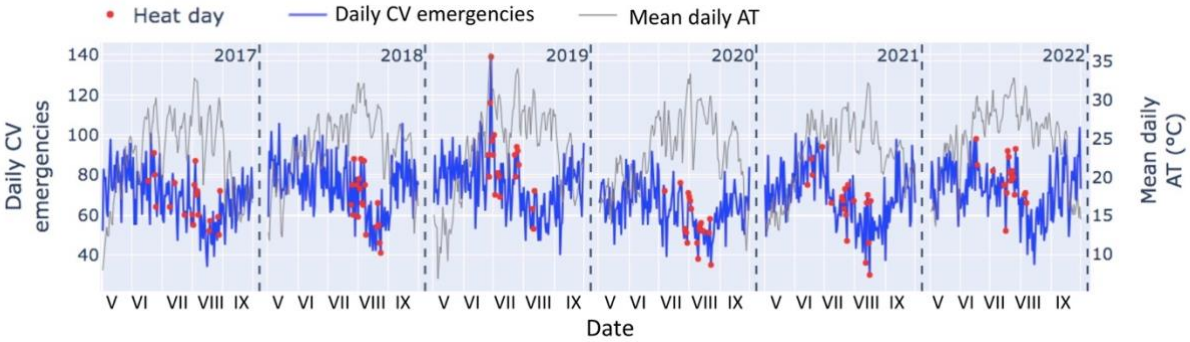

Based on the Kolmogorov-Smirnov test, the daily number of CV emergencies resulted not normally distributed. The median daily number of emergencies during the analysed period was 71 (25th-75th percentile 60-80). The highest median was reached in 2019 (76 emergencies), with two particularly elevated outliers equal to 116 and 139, while the lowest median was observed in 2020 (63 emergencies). In 2020, in addition to a low median, the distribution of daily emergencies was characterised by a relatively narrow interquartile range, as illustrated in Figure 4.13. As indicated by the Kruskal-Wallis test, the difference in the distribution across years was statistically significant.

In terms of months, there was a statistically significant difference in the distribution of daily CV emergencies across them. The highest median was observed in June (78 emergencies). On the contrary, August was the month with the lowest median daily number of emergencies (56 emergencies), exemplifying the holiday period effect, as shown in Figure 4.13.

The distribution of daily number of CV emergencies differed significantly also across the days of the week. The highest median daily number was observed on Monday (74 emergencies). Conversely, the lowest median number of emergencies was observed at the weekend - on Sunday (67 emergencies) closely followed by Saturday (68 emergencies). Moreover, the second half of the week was characterised by particularly high outliers, represented by dots in Figure 4.13.

When stratified by heat and non-heat days, the difference in the distribution of the daily number of CV emergencies was not significant. The median reached 71 emergencies during non-heat days, and 70 during heat days, but with two outliers equal to 116 and 139 emergencies. This similarity of median daily CV emergencies in both meteorological conditions further illustrates the holiday effect – while both DLNM and Poisson regression (both adjusted for time trends) estimated an increased RR with heat, absolute numbers for daily ambulance dispatches do not reflect such finding.

The distribution of the daily number of CV emergencies, stratified by temporal variables (i.e., year, month, day of the week and heat days) was graphically summarised as boxplots in Figure 4.13.

Figure 4.13. Summary of the distribution of the daily number of cardiovascular emergencies in May-September 2017-2022 in Milan, Italy, stratified by year, month, day of the week and heat days

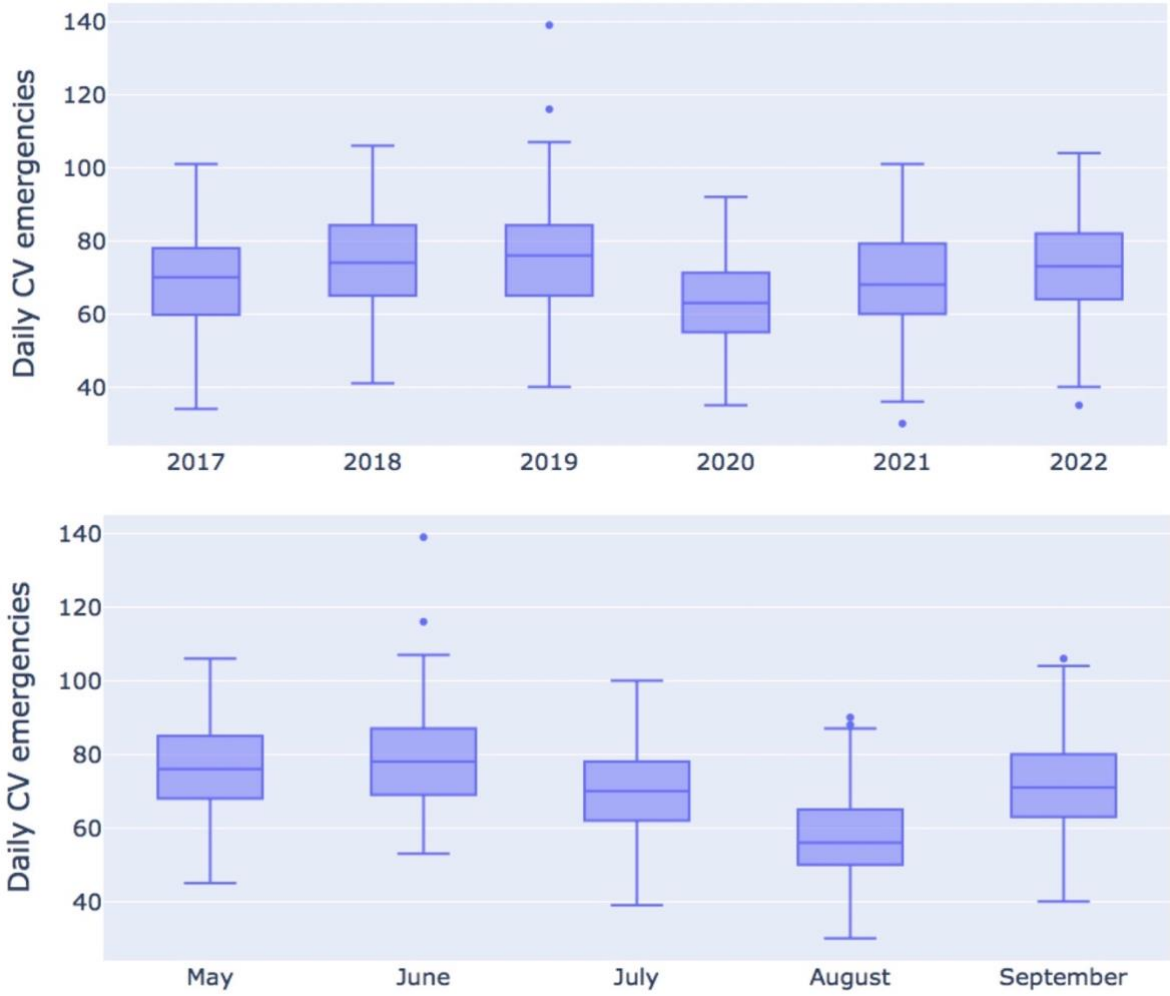

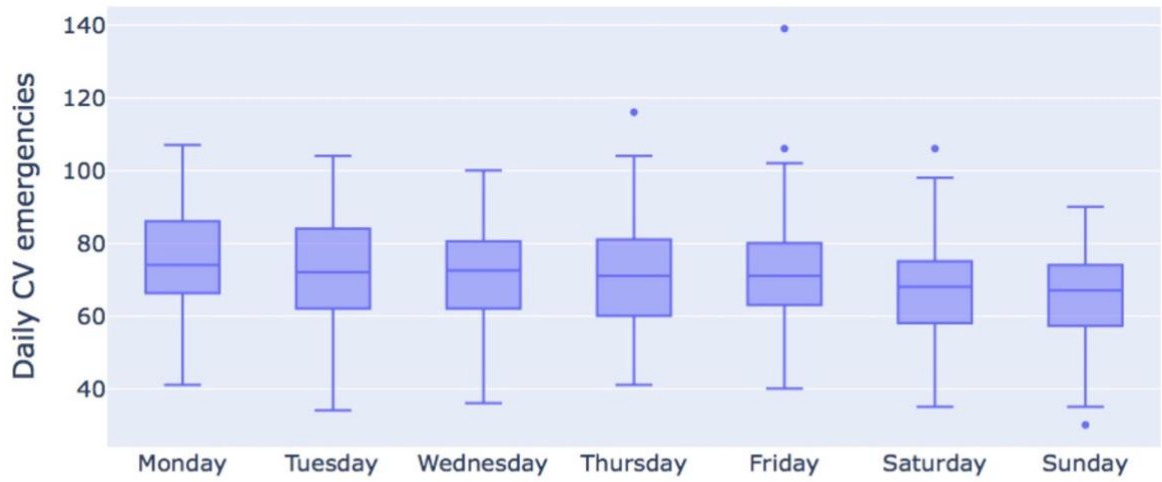

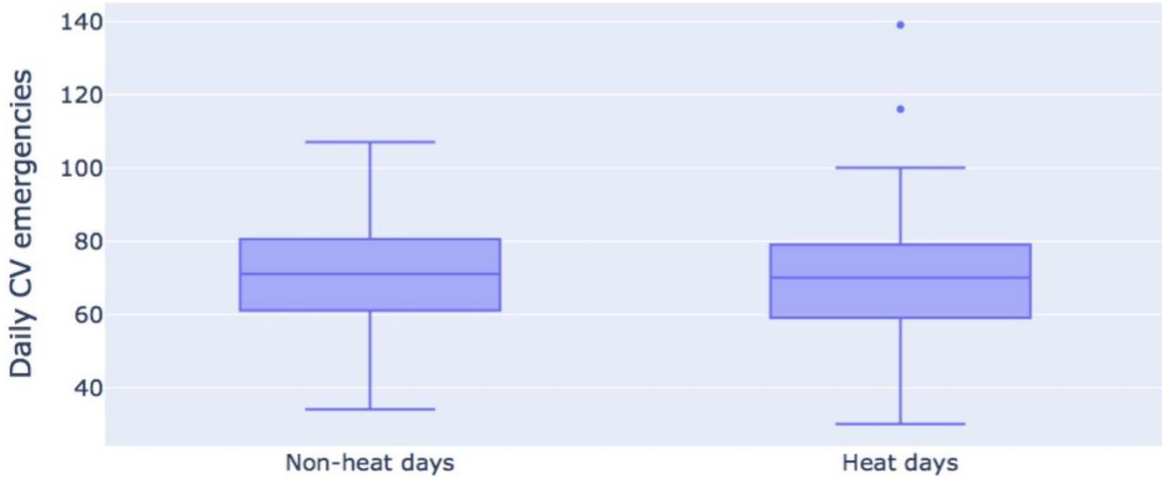

As estimated by Poisson regression with offset represented by traffic data, the RR of experiencing a CV emergency on heat days compared to non-heat days was 1.11, with a 95% CI of 1.09-1.14, indicating statistical significance. The same RR was observed for female patients, although with a slightly wider CI. Interestingly, the RR was slightly lower for elderly patients, at RR=1.10. The median age of elderly patients was 82 years for both heat and non-heat days, while for non-elderly patients, it was 45 on non-heat days and 46 on heat days.

When divided by emergency severity, the highest RR was observed for fatal emergencies (RR=1.56), followed by non-severe emergencies (RR=1.19), and those requiring transport to a hospital (RR=1.09). Furthermore, the percentage of fatal emergencies that occurred on heat days (16.37%) was significantly higher than the percentage of all emergencies that occurred on heat days (12.29%). These findings align with the results from the previous chapter and the existing literature, which consistently reports an increased risk for CV mortality during heat events, while the impact on morbidity remains less clear.

Regarding the place of emergency, the highest relative risk (RR=1.25) was observed for those occurring on the street, likely due to direct exposure to temperature hazard. Although only 6,117 emergencies occurred on the street, representing 9.43% of all cases, 13.52% of these emergencies occurred on heat days – a percentage significantly higher than the proportion of all the emergencies on heat days. The lowest RR equal to 1.08 was recorded for emergencies

occurring at home, which accounted for the largest share of all emergencies (43,939 emergencies; 67.72%). Emergencies at other locations, such as social/medical facilities, public offices, railways, schools, workplaces, sports facilities, or lakes, reached a RR of 1.17. The RR for all subgroups was statistically significant, and detailed results are provided in Table 4.3, providing evidence of increased morbidity risk in heat conditions for Milan.

Table 4.3. Summary of characteristics of cardiovascular emergencies during heat (as defined in section 4.2.1) and non-heat days of May-September 2017-2022 in Milan, Italy, and the corresponding relative risk of having a CV emergency in heat days in respect to non-heat days. RR – relative risk, CI – confidence interval.

	Non-heat days (% of total CV emergencies in each group)	**Heat days (% of total CV emergencies in each group)**	**RR (95% CI)**
Total	56,907 (87.71%)	7,974 (12.29%)	1.11 (1.09 – 1.14)[b]
Female	30,951 (87.76%)	4,316 (12.24%)	1.11 (1.08 – 1.15)[b]
Over 65 years old	31,107 (87.88%)	4,290 (12.12%)	1.10 (1.07 – 1.14)[b]
Non-severe	8,606 (87.03%)	1,282 (12.97%)	1.19 (1.12 – 1.26)[b]
Requiring transportation to a hospital	47,060 (87.95%)	6,449 (12.05%)	1.09 (1.07 – 1.12)[b]
Fatal	1,241 (83.63%)	243 (16.37%)[a]	1.56 (1.36 – 1.80)[b]
At home	38,692 (88.06%)	5,247 (11.94%)	1.08 (1.05 – 1.12)[b]
On the street	5,290 (86.48%)	827 (13.52%)[a]	1.25 (1.16 – 1.34)[b]
Other places (i.e., socio-medical facility, other medical facility, workplace, hospital, public office, railway, school, sports facility, lake)	12,925 (87.18)	1,900 (12.82%)	1.17 (1.12 – 1.23)[b]

a – significant difference in proportion of emergencies during heat days of a particular group with respect to all emergencies during heat days (chi-square test)
b – significant RR

In Milan, in pre- COVID-19 period, the median daily number of emergencies was 73, reduced to 66 in COVID-19, and back to the pre-pandemic level (73) in post- COVID-19. Also, the age of patients in post- COVID-19 was significantly reduced by 2 years. In both COVID-19 and post- COVID-19, compared to pre- COVID-19, a significant reduction of around 3% in events in women was observed. Additionally, stratifying by the severity of the emergencies, in both COVID-19 and post- COVID-19, the fraction of emergencies requiring transportation to a hospital decreased significantly, while the percentage of non-severe and fatal emergencies increased. The characteristic of CV emergencies in pre- COVID-19, COVID-19, and post-COVID-19 periods are summarized in Table 4.4.

The RR of experiencing a CV emergency on heat days was higher in the pre-COVID-19 period (RR=1.15) than during the COVID-19 period (RR=1.09) and post-COVID-19 period (RR=1.09), although all three RRs were statistically significant. Thus, despite a significant decrease in daily CV emergencies during the COVID-19 period, the negative impact of heat

on CV health persisted. Monitoring these trends in the coming years will be essential to fully understand the pandemic's effect on the demand for CV emergency services.

Table 4.4. Characteristic of cardiovascular emergencies in pre-COVID-19 (reference period), COVID-19, and post- COVID-19 periods. RR – relative risk, CI– confidence interval.

	pre-COVID-19 (reference)	**COVID-19**	**post-COVID-19**
Median number of cases per heat day (25th -75th percentile)	72 (60 – 85)	63 (51.25 – 69.75)[a]	78 (71 – 83.5)
Median number of cases per non-heat day (25th - 75th percentile)	73 (63 – 82)	66 (58.75 – 75)[a]	72 (63 – 81.75)
Median age (25th -75th percentile)	69 (48 – 83)	69 (48 – 83)	67 (46 – 83)[a]
Percentage of women	55.18%	53.44%[b]	53.56%[b]
Percentage of non-severe emergencies	13.6%	17.07%[b]	16.82%[b]
Percentage of emergencies requiring transportation to a hospital	84.43%	80.28%[b]	80.6%[b]
Percentage of fatal emergencies	1.97%	2.65%[b]	2.58%[b]
RR of CV emergency on heat versus non-heat days (95% CI)	1.15 (1.11 – 1.18)[c]	1.09 (1.04 – 1.14)[c]	1.09 (1.03 – 1.15)[c]

a – significant difference in distribution (Mann-Whitney U test)
b – significant difference in proportion (chi-square test)
c – significant RR

Chapters 5 and 6 will focus on the geographical dimension of CV emergencies. Figure 4.14 provides a simple overview of their spatial distribution through two heatmaps, one for heat days and another for non-heat days. A visual examination reveals distinct differences, highlighting the importance of conducting spatial analyses. As the absolute number of CV emergencies was considerably higher on non-heat days compared to the 114 heat days, the colour intensity on the heatmap for extreme temperatures is mostly lower, however this change is not uniform across the city. These differences will be further analysed, considering the official administrative divisions of Milan and various socio-urban characteristics of specific zones, which are essential for capturing the underlying trends. The precise geolocation obtainable from ambulance data offers a significant advantage over hospital data and can provide valuable insights at the local level, benefiting both EMS management and urban planning.

Figure 4.14. Heatmap of CV emergencies in May-September 2017-2022 in Milan, Italy (a) on non-heat days and (b) on heat days. Radius equal to 1,000 meters.

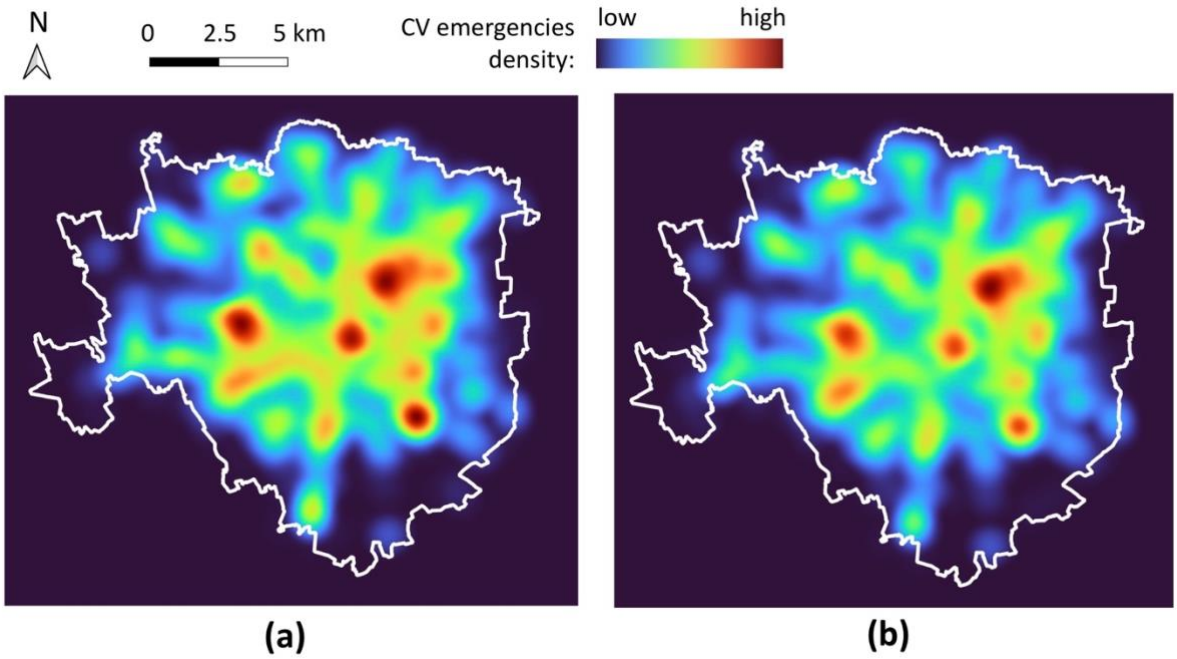

4.4. Limitations and conclusion

This chapter empirically tested the framework proposed for selecting a percentile threshold on the temperature to define heat, as formulated in the previous chapter. Utilizing retrospective data on ambulance dispatches for CV problems in Milan, covering the period from May to September in the years 2017-2022, the analysis led to the identification of the 95th percentile of the annual distribution of the mean daily AT as the heat threshold. Consequently, 19 days each year were defined as "heat days". Although the resulting temperature thresholds varied by more than 2 °C among the years, defining heat days based on annual thresholds effectively accounts for short-term (intra-annual) climate variability. Moreover, the corresponding RR of having a CV emergency on heat days with respect to non-heat days was estimated by Poisson regression, controlled by seasonal trend, and reported increased risk of CV morbidity for the city of Milan, regardless of gender and age of the patient, as well as place and severity of the emergency.

Furthermore, this chapter provided an overview of the data sources relevant to the subsequent chapters (Chapters 5 and 6), detailing their preprocessing and primary characteristics. It highlighted the utility of ambulance dispatch data as a proxy for morbidity, offering significant advantages over traditional medical data, such as hospital records or mortality statistics, which often lack detailed spatial information. The geographical dimension of ambulance data enables a deeper analysis pertinent to the urban context of this thesis, which will be further explored in the following chapters. Additionally, the meteorological data were examined, offering crucial climatic context for Milan and analysing the daily distribution of a heat index, i.e., apparent temperature, based on meteorological characteristics. Notably, it was also demonstrated that the model assessing the impact of heat on CV emergencies yielded

consistent results regardless of the inclusion of air pollutants, thus providing a rationale for their exclusion from future analyses.

As CV emergencies possess an inherent temporal dimension, this chapter also addressed time-related characteristics. The results indicated significant variations in the distribution of emergencies across years, months, and days of the week. Specifically, a considerable decrease in emergency calls during holiday period highlighted the effect of resident absence, while the COVID-19 pandemic resulted in a temporary decline in the daily number of emergencies. Adjusting for these temporal factors is vital for accurately estimating the RR, as neglecting them could lead to unrepresentative findings. The potential of utilizing traffic data as a proxy for resident presence in the city was also explored, offering a promising path for future research.

However, this approach is not without its limitations. The classification of emergencies as CV was based solely on the receiver's interpretation of the emergency call, which may not reflect an official medical diagnosis. This lack of rigorous classification necessitates closer collaboration between the EMS and hospitals to ensure accurate data for further research. Moreover, CV data for this thesis were restricted to ambulance dispatches, thereby excluding self-presentation at emergency departments. Such data could have provided additional insights or confirmed the robustness of results derived from ambulance records. In addition, meteorological data were subject to several limitations, primarily related to location sensitivity. For instance, these data were constrained by the limited and spatially dispersed number of measurement stations, which hindered the comprehensive averaging process required to derive a representative value for the entire city. The uneven spatial distribution of these stations impeded the calculation of daily AT values for different urban areas, limiting the analysis of the urban heat island effect. Future research may benefit from integrating satellite data to enhance the robustness of the methodology; however, such satellite data also present limitations, as remote sensing may be obstructed by cloud cover.

In conclusion, this chapter established a foundational understanding of the influence of passive heat stress on CV emergencies in Milan through statistical modelling. The subsequent chapters will delve into more comprehensive mathematical analyses, with a particular emphasis on the spatial dimension, aiming to offer a holistic perspective on the impact of heat on public health in urban environments.

Chapter 5. Socio-urban characteristics and cardiovascular vulnerability to heat: a geospatial perspective

The content of this chapter is an elaborated version of the following publications:

- Nawaro, J., Gianquintieri, L., Pagliosa, A., Sechi, G. M., & Caiani, E. G. (2024). Neighborhood determinants of vulnerability to heat for cardiovascular health: a spatial analysis of Milan, Italy. *Population and Environment*, *46*(4), 25. https://doi.org/10.1007/s11111-024-00466-3

- Nawaro, J., Gianquintieri, L., Pagliosa, A., Migliari, M., & Caiani, E. G. (2024). Geospatial analysis of socio-urban vulnerability to heat in the context of cardiovascular health. *Proceedings of* the *Sustainability in Energy and Buildings (SEB) conference* (in press).

- Nawaro, J., Gianquintieri, L., Pagliosa, A., Sechi, G. M., & Caiani, E. G. (2024, September). Spatial clustering of ambulance dispatches for cardiovascular problems during heat and non-heat days: Preliminary study for Milan, Italy. In *2024 IEEE 8th Forum on Research and Technologies for Society and Industry Innovation (RTSI)* (pp. 66-71). IEEE. https://doi.org/10.1109/RTSI61910.2024.10761157

Highlights:

- RQ4: What are the socio-urban characteristics that could influence CV health in presence of heat?
- K-means clustering identified three geographically coherent clusters of Milan, Italy, i.e., Central, Residential, and Peripheral, differing by socio-urban features.
- Spatial and non-spatial regression models assessed the direct and spillover effects of socio-urban characteristics on CV vulnerability to heat, identifying significant effects of mean summer temperature, density of drinking water fountains, and demographics (percentages of elderly, female, and graduate residents).
- Socio-urban vulnerability to heat index derived from regression coefficients enabled the creation of a vulnerability map highlighting highly and low vulnerable districts of the city.

5.1. Introduction

Currently, more than half of the world's population lives in cities, with this percentage being projected to reach 70% by 2050 (World Bank, 2022). Urbanization, despite driving economic development due to cities' higher productivity, creates many challenges. These challenges include increased air pollution due to vehicles' emissions and industrial development, noise pollution generated from human activities, and heat waste from buildings, with all these factors being associated with adverse health outcomes (Ebi et al., 2021; OECD, 2020; Zhang, 2016). Moreover, higher temperature has been observed in cities compared to their surroundings (i.e., urban heat island), and within the city comparing central districts to more peripherical neighbourhoods (Kim & Brown, 2021), exposing urban populations to an intensified risk factor for their CV health. Big cities, as centres of human activity, are not only experiencing the physical manifestation of climate change, but they are also confronted with the complex interplay of socio-urban vulnerabilities that could exacerbate the impact of heat events on human health.

The effect of urbanisation on human health can be twofold: on one hand, the facilitated access to healthcare allows for timely and appropriate assistance; on the other hand, the typical conditions of polluted environment, social depravation and stressful lifestyle can undermine health (Ebi et al., 2021; Münzel et al., 2022). While most of the research focuses on understanding and treating diseases in patients, there is a growing recognition of the need for preventive measures to keep urban residents from becoming patients in the first place (Tong and Ebi, 2019; WHO, 2021). Clinical research is vital, but the challenges posed by climate change and urbanization require a proactive approach, aiming to anticipate and address health issues before they manifest in a severe way.

In particular, different patterns of social, cultural and physical segregation can be recognised within large cities, each having its own particular health-relevant characteristics (Münzel et al., 2022; Godfrey & Julien, 2005). Such inequalities highlight the need to analyse the determining factors with more spatial detail. For example, Bakhtsiyarava et al. (2023) argued that further investigation is needed towards the spatial analysis of the impact of socio-urban factors on health vulnerability to heat, as they found unexpected effects of population density and income inequality on heat-related mortality at the city level. Indeed, studies conducted at higher geographical resolution have yielded clearer conclusions regarding all-cause, CV and cardiorespiratory mortality, particularly concerning the effects of age, greenery, and wealth (Morais et al., 2021; Murage et al., 2020; Silveira et al., 2021).

Spatial relationships in epidemiology have been known for centuries, however, advanced geomatics methods were still rarely used in the first decade of the twenty-first century (Auchincloss et al., 2012). Nevertheless, in recent years, spatial analysis, including techniques such as clustering and spatial correlation detection, has been recognised as crucial in epidemiological research (Baptista & Queiroz, 2019; Mena et al., 2018). Such spatially disaggregated approaches can inform strategies to increase the resilience of the population living in large cities to heat waves, in particular relating to CV diseases. Towards this goal, it is important to assess whether the urban area can be clustered into smaller zones based on socio-urban features, and what is the effect of these features and clusters on population vulnerability to heat in the context of CV health.

In recent years, numerous indices to assess socio-urban vulnerability to heat were developed (Ellena et al., 2020a; Li et al., 2022; Cheng et al., 2021; Krellenberg et al., 2017; Dong et al., 2020; Macintyre et al., 2018; Sera et al., 2019). The most common methodologies for the index calculation (Li et al., 2022; Cheng et al., 2021), however, lack direct connection to real-world health outcomes, making theoretical assessments that may not reflect actual trends in mortality or morbidity during heat events. Furthermore, validation is a significant limitation of the relevant articles, with only about one in four study testing their indices against real-world health data, covering heat-related, cardiovascular, cerebrovascular, respiratory, or all-cause morbidity or mortality data as reference (Li et al., 2022; Cheng et al., 2021). While conducting geospatial analysis with aggregated morbidity and mortality data is very difficult, as argued in previous chapters, the use of geolocalized information on the CV burden of heat, along with advanced spatial modelling, could enable this kind of study. Specifically, geolocalized data originating from the local emergency medical system (EMS) could be used. Despite the lack of information on official clinical diagnoses, information on health events from EMS data can be considered as a valid proxy for the spatio-temporal analysis of a pathologic condition (in this case, CV health problems), as previously validated in the context of COVID-19 (Gianquintieri et al., 2022; Gianquintieri et al., 2021).

Another major research gap of socio-urban vulnerability indices is the lack of practical guidelines for applying them (Chen et al., 2021). Many studies do not provide specific recommendations for urban areas needing urgent intervention. Addressing this gap is essential for improving the indices' accuracy and practical utility in guiding urban planning and public health responses.

Accordingly, to align with the proactive approach, the aim of this chapter is to propose an analysis that identifies clusters of a large urban area based on socio-urban characteristics of its neighbourhoods, and subsequently studies the direct and indirect effects of such characteristics on population vulnerability to heat for CV health. Beyond merely identifying the spatial and non-spatial behaviour of the determinants of vulnerability, the focus of this chapter lies in quantifying and mapping such vulnerabilities to create a comprehensive index that could serve as a tool for public health intervention and urban planning. As such, this chapter addresses the RQ4: What are the socio-urban characteristics that could influence CV health in presence of heat?

5.2. Materials and methods

The following analyses will be performed for Milan, Italy, whose main climatic and demographic characteristics were overviewed in Chapter 4. For administrative purposes, the city is officially divided into 88 Nuclei of Local Identity (NIL) (Figure 5.1), which represent different districts with varying urban and socio-demographic characteristics (Comune di Milano, 2023a). In order to ensure real-world applicability of this study, the NIL, which represent the principal spatial division of Milan for local policymaking, are the units used in the following analyses, with the NIL 3 and 8 excluded as being entirely covered by city parks. The official names of each NIL are listed in Table A5.1 in Appendix.

Figure 5.1. The 88 Nuclei of Local Identity (NIL) of Milan

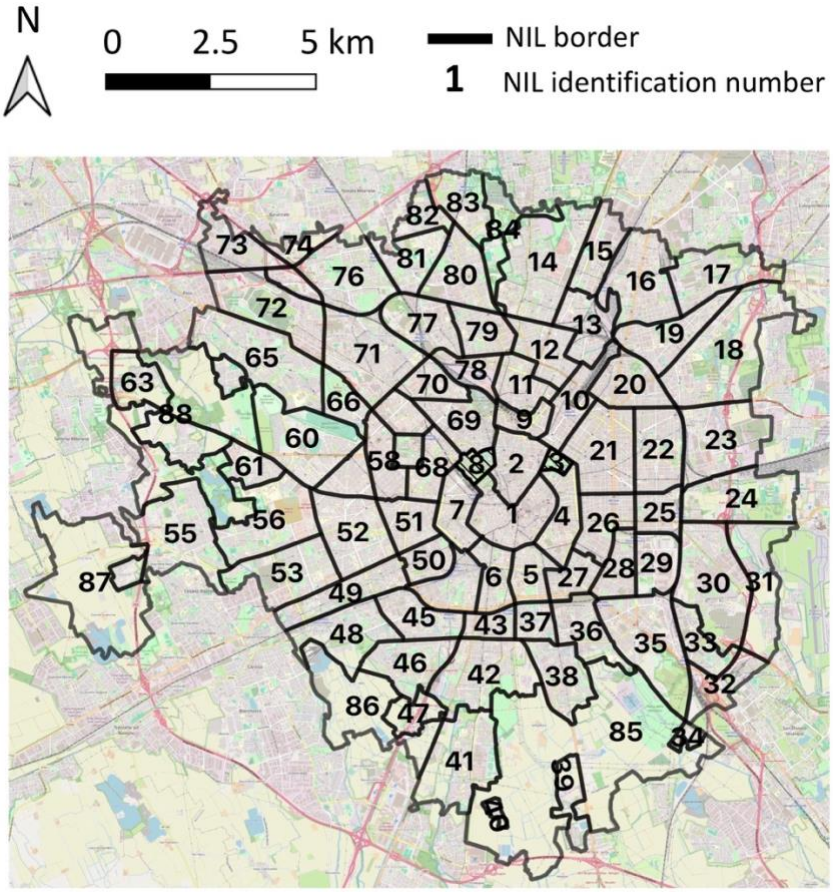

Regarding the meteorological parameters and ambulance dispatches, data from the Regional Agency for Environmental Protection (ARPA) for the years 2017-2022 and the Regional Agency for Emergency and Urgency (AREU) for the period May-September 2017-2022, overviewed in the previous chapter, were used. Following previous results, heat days were defined as those with the mean daily apparent temperature (AT) exceeding the 95th percentile of its annual distribution, i.e., 114 days were classified as heat days in the years 2017-2022.

5.2.1. Cardiovascular vulnerability to heat

For the purpose of calculating the CV vulnerability to heat (CV_VtoH), ambulance data were limited to the events that occurred at home only, in order to ensure consistency between each emergency and the characteristics of the NIL of residence of the patient. The CV_VtoH for each NIL was defined as the percentage of emergencies that happened during heat days and the day after (in order to account for delayed effect of heat on fatal emergencies, as previously illustrated in Figure 4.6), with respect to the total number of ambulance interventions in that NIL during the whole observation period (May-September 2017-2022). The following formula was used for this purpose:

$$CV_VtoH = \frac{\sum_i^n number\ of\ in{-}home\ emergencies\ during\ heat\ day_i\ and\ the\ day\ following\ heat\ day_i}{number\ of\ total\ in{-}home\ emergencies} * 100\% \qquad (5.1)$$

where n is the total number of heat days.

5.2.2. Socio-urban characteristics

Although there is not a standard set of socio-urban characteristics to be included in heat-health related research, a significant impact of several features on CV health has been consistently reported in relevant literature (Kreatsoulas & Anand, 2010; Mena et al., 2018; Nieuwenhuijsen, 2018; Sharma et al., 2004; Son et al., 2019). These features include: demographic characteristics (e.g., gender (Achebak et al., 2019), age (Cicci et al., 2022)), socio-economic status (e.g., education level (Zhou et al., 2017)), environment variables (e.g., temperature (Liu et al., 2022), greenery (Murage et al., 2020)) and urban planning (e.g., connectivity (Adhikari et al., 2021)). Accordingly, also accounting for open data availability relevant to Milan (Comune di Milano, 2023b; Milano Geoportale, 2023), for each NIL, 11 socio-urban features were computed, according to the formulas presented in Table 5.1.

Table 5.1. Description of the socio-urban features computed for each Nucleus of Local Identity (NIL), with the relevant formula and the reference year(s) for which the data were available

Feature	Formula/description	Data reference year(s)
Built-up area (%)	$\frac{built-up\ area}{total\ area} * 100\%$	2012
Non-residential buildings' volume (m^3/m^2)	$\frac{non-residential\ buildings' volume}{built-up\ area}$	2018
Green roofs (%)	$\frac{green\ roofs\ area}{built-up\ area} * 100\%$	2016
Population density (people/km^2)	$\frac{number\ of\ residents}{total\ area}$	2020
Vegetation index	$\frac{N(green\ area)+N(tree\ avenue)+N(\ tree\ number)}{3}$, where N is the normalization ($\frac{x-x_{min}}{x_{max}-x_{min}}$) of all NIL's values, $green\ area$ is $\frac{green\ area}{total\ area}$, $tree\ avenue$ is $\frac{length\ of\ tree\ avenues}{total\ area}$, $tree\ number$ is $\frac{number\ of\ isolated\ trees}{total\ area}$.	2012
Mean summer land surface temperature (LST) (°C)	mean daytime June-August land surface temperature	2013-2017
Density of drinking water fountains (n/ km^2)	$\frac{number\ of\ drinking\ water\ fountains}{total\ area}$	2019
Cycle paths (km/km^2)	$\frac{cycle\ paths\ length}{total\ area}$	2022
Residents >=65 (%)	$\frac{number\ of\ residents \geq 65\ years\ old}{total\ residents} * 100\%$	2020

Female residents (%)	$\frac{number\ of\ female\ residents}{total\ residents} * 100\%$	2020
Graduate residents (%)	$\frac{number\ of\ graduate\ residents}{total\ residents} * 100\%$	2011 (graduate $residents$), 2020 ($total\ residents$)

5.2.3. Statistical methods

Descriptive statistics (i.e., minimum and maximum, mean and standard deviation, median, 25th percentile and 75th percentile) was used to summarize the data. The Kolmogorov-Smirnov test was used to test whether the data follow normal distribution (alpha=0.05). Relative risk (RR) was estimated by Poisson regression with traffic offset as defined in Chapter 4. In order to graphically represent the distribution of a continuous variable on a map, colour-coded classes were computed on the basis of the equal quantile method for a total of 5 classes. Spatial autocorrelation was assessed using both global and local Moran's Index (Moran's I; described in detail in Chapter 2, section 2.2.4). Given the relatively small sample size (i.e., the number of NIL), in order to balance type I and type II errors, the significance level for both global (gMI) and local (lMI) Moran's I was set at 0.1 (Kim and Choi, 2021).

K-means clustering of socio-urban characteristics

The NIL were grouped into clusters, defined by their socio-urban characteristics, applying the k -means algorithm. This approach divides *M* points in *N* dimensions into *k* clusters, with the objective of minimizing the within-cluster and maximizing the between-cluster scatter (Hartigan & Wong, 1979). The k-means algorithm has been previously applied to cluster cities' neighbourhoods in a range of problems, including evaluating cities' mobility or accessibility (Rahimi, 2022; da Silva et al., 2016), identifying urban sprawl (Liu et al., 2018b), finding heat-prone neighbourhoods (Wu et al., 2022b) or tackling districts' evolution based on a set of social, economic, and demographic variables (Delmelle, 2015).

The optimal value of *k* was chosen within an arbitrarily selected range of values from 2 to 10, by comparing the outputs of the elbow method (Syakur et al., 2018), the silhouette method (Yuan & Yang, 2019), the Davies Bouldin index (Bolshakova & Azuaje, 2003) and the hierarchical clustering with Ward's linkage (Murtagh & Legendre, 2014). The former method graphically compares the difference in the error sum of squares (which equals 0 when *k*=*M*) of clustering with each *k*, and the *k* for which the curve's angle forms the elbow is the optimal value. The silhouette coefficient, based on intra-cluster distance (i.e., mean distance among points within the same cluster) and inter-cluster distance (i.e., mean distance between a point and the nearest cluster other than that to which the point belongs), ranges between -1 and 1, where the higher the score, the more dense and well separated are the clusters. In this study, the Euclidean distance metric was used. The Davies Bouldin index calculates the average similarity between clusters, accounting for their diameter, i.e., mean distance between points and the cluster centroid, and for the distance between clusters' centroids. It reaches non-negative values, and lower score indicates better partition. The last method used to select the optimal value of *k*, i.e., hierarchical clustering, is in fact another clustering algorithm which aims at building a hierarchy of clusters. For the purpose of this study, the agglomerative

approach with Ward's linkage was implemented, meaning that observations were successively merged together minimizing the total within-cluster variance, and the optimal number of clusters was read directly from the dendrogram.

After choosing the *k* value, non-parametric Kruskal–Wallis and Mann–Whitney U tests were applied to investigate the significance of the differences in the distribution of each socio-urban variable among clusters (henceforth referred to as "socio-urban clusters"). For Kruskal-Wallis test, the Bonferroni correction was implemented.

Regression analysis

To assess the impact of socio-urban characteristics on NIL's CV_VtoH, several regression models were applied and compared, and the best performing one was chosen based on goodness of fit measures.

The simplest model (linear multiple regression model with ordinary least squares (OLS), m1) was defined as:

$$Y = X\beta + \varepsilon \tag{5.2}$$

where Y is the target variable to be modelled (in this study, CV_VtoH, as defined by equation 5.1 in section 5.2.1), X is a matrix of independent variables (in this study, socio-urban features described in Table 5.1, section 5.2.2), β is a vector of coefficients estimated using OLS technique, and ε is a vector of random error terms. The fulfilment of the OLS linear regression assumptions was assessed by the Ramsey Regression Equation Specification Error Test (RESET) test (linearity assumption), Shapiro–Wilk test (error normality), Breusch–Pagan test (homoscedasticity), Durbin-Watson test (error independence), and variance inflation factor (VIF) (multicollinearity).

As we hypothesized a spatial relationship between the socio-urban variables and the CV_VtoH, this was tested by incorporating a spatial component into the statistical models. In regression analysis, three forms of spatial interactions have been identified: among the independent variables (i.e., local), among the dependent variables (i.e., global) and among the error terms (Halleck Vega & Elhorst, 2015). In order to potentially account for all these interactions, the following models were applied, respectively:

- spatially lagged X model (SLX; m2):

$$Y = X\beta + WX\theta + \varepsilon \tag{5.3}$$

- spatial autoregressive model (SAR; m3):

$$Y = \rho WY + X\beta + \varepsilon \tag{5.4}$$

- spatial error model (SEM; m4):

$$Y = X\beta + u, \quad u = \lambda Wu + \varepsilon \tag{5.5}$$

where W is a matrix of spatial weights, θ is a vector of response parameters, and ρ and λ are scalar parameters measuring the strength of spatial dependence. Accounting for mathematical details, the assumptions of linear regression could be statistically tested only for the SLX model.

Furthermore, three additional nested models obtained combining the above spatial interactions were considered:

- spatial Durbin error model (SDEM; m5), combining SLX and SEM:

$$Y = X\beta + WX\theta + u, \quad u = \lambda Wu + \varepsilon \tag{5.6}$$

- spatial Durbin model (SDM; m6), combining SAR and SLX:

$$Y = \rho WY + X\beta + WX\theta + \varepsilon \tag{5.7}$$

- Kelejian-Prucha model (m7), combining SAR and SEM:

$$Y = \rho WY + X\beta + u, \; u = \lambda Wu + \varepsilon \tag{5.8}$$

All these spatial models except SEM result in an estimation of the direct effect of a change in the independent variable (i.e., one of the socio-urban features) on the dependent variable (i.e., the CV_VtoH) for each unit (i.e., the NIL), along with an estimation of the indirect effect of such change (limited to one specific unit) on the dependent variable in the neighbourhood (in local models) or in all units (in global models) (Golgher & Voss, 2016; Halleck Vega & Elhorst, 2015). The total effect is defined as the sum of both direct and indirect effects (Golgher & Voss, 2016). While the coefficient (i.e., the β) estimated in OLS non-spatial regression represents the change in the dependent variable associated with a one-unit change in an independent variable, the direct and indirect effects of spatial models do not have a straightforward numerical meaning, and they will be analysed with respect to their direction (sign) and relative strength. To create the matrix of spatial weights between the NIL, i.e., to define neighbours, the queen contiguity method was used (Getis & Aldstadt, 2004).

To determine the best model, the following two-step method was applied: 1) the goodness- of-fit for each candidate model (non-spatial OLS plus six selected spatial models) was computed using the Akaike information criterion (AIC), and the model with the lowest value was selected; 2) for the selected model, the likelihood ratio test was further applied to decide if it should be restricted to its simpler version (either it is spatial or non-spatial) or not.

Socio-urban vulnerability to heat

Coefficients (i.e., the β for non-spatial model or the direct effect for spatial models) estimated by the best regression model for statistically significant variables (p-value<0.05) were used to calculate the socio-urban vulnerability to heat (SU_VtoH) for each NIL. Pearson correlation (r) was applied to examine the correlation between each significant socio-urban variable and CV_VtoH. Moreover, the OLS regression was fitted to SU_VtoH (i.e., independent variable)

and CV_VtoH (i.e., dependent variable), and the proportion of variation in CV_VtoH explained by SU_VtoH was assessed by R^2.

Final map of low and highly vulnerable NIL was created combining the CV_VtoH and SU_VtoH. Specifically, high values were defined as >=60th percentile of the distribution of both vulnerabilities, while low values were defined as <=40th percentile. This map was colour-coded, with green and red tones indicating positive and negative health outcomes, respectively, and with colour intensity representing the resident population of each NIL.

Hierarchical density-based spatial clustering of applications with noise of ambulance dispatches

Previous research has applied various techniques, including k-means, density-based and deep learning clustering, to analyse ambulance dispatches in urban areas, focusing on their response time optimization, patient characteristics analysis, and high-demand areas identification (Desai et al., 2023; Kamireddy and Keshavamurthy, 2016; Bharsakade et al., 2022). Density-based clustering algorithms are particularly well-suited for this task as they identify clusters of varying shapes and sizes and are robust to noise in the data, making them flexible and adaptive to the inherent data structure (Campello et al., 2013). When combined with maps of additional neighbourhood characteristics, such as SU_VtoH and CV_VtoH, these algorithms can provide a comprehensive view capable to integrate socio-economic factors, environmental conditions, and urban infrastructure. Accordingly, to cluster the CV ambulance dispatches (in this case not limited to in-home emergencies) separately for heat and non-heat days, the hierarchical density-based spatial clustering of applications with noise (HDBSCAN) algorithm was employed and visualized coupled with the map of low and highly vulnerable NIL, in order to further confirm the robustness of the results.

Density-based spatial clustering of applications with noise (DBSCAN) directly clusters points based on their density. It requires two hyperparameters: epsilon, which specifies the maximum distance between two points to be considered neighbours, and the minimum number of points (m_pts) required to form a dense region. The algorithm defines core objects as points containing at least m_pts within the epsilon distance, with all non-core objects classified as noise. A cluster consists of all points 1) within the epsilon distance from the core point, or 2) connected to a core point by a chain of points, each within the epsilon distance from the others.

HDBSCAN does not require specifying the epsilon parameter as it constructs the mutual reachability graph, which stores the relationship between data points based on their mutual reachability distance. Subsequently, it builds a minimum spanning tree, which is hierarchically clustered using the single-linkage method. The optimal number of clusters is then determined based on their stability (i.e., persistence of the cluster in the hierarchy) and coherence (i.e., tightness and separation of data points within the cluster). The estimated clusters include the dense clusters and the noise cluster.

For the purpose of this chapter, HDBSCAN was selected primarily for its automatic tuning of hyperparameters. Moreover, it offers advantages relevant to emergency modelling, including the capability to form arbitrarily shaped clusters robust to outliers, particularly important in the urban context (Cesario et al., 2023). Since the CV ambulance dispatches need to be clustered based on longitude and latitude coordinates, the Haversine distance, measuring

the angular distance between two points on the surface of the Earth, was chosen as the distance metric. Two hyperparameters were explicitly specified: the distance metric and the minimum cluster size. For the latter, the following arbitrary values were tested: 45, 50, 60, 70, 80, 90, 100 for the emergencies during heat days, and 300, 350, 400, 450 for the emergencies during non-heat days. The optimal minimum cluster size was determined based on the Davies–Bouldin index and visual examination.

For the map representing the non-noise HDBSCAN clusters of CV emergencies for heat and non-heat days, the underlying map included the classification in low and highly vulnerable NIL regarding the CV_VtoH and SU_VtoH. Points representing individual emergencies were displayed with 70% transparency to provide an overview of their density.

Once the emergencies that occurred during heat and non- heat days were clustered, differences in the geographical locations of the clusters were visually assessed, and three groups of zones (one zone does not necessarily correspond to one cluster) were defined:

- A: zones where clusters exist during non-heat days but not during heat days;
- B: zones where clusters exist in both meteorological conditions, but with a considerable spatial shift in point concentration;
- C: zones where clusters experience a considerable increase in spatial coverage during heat days compared to non-heat days.

Subsequently, differences in the fraction of elderly (i.e., above 65 years old) and female patients, as well as of fatal emergencies in heat days with respect to non-heat days for the zones belonging to the second (i.e., B) and the third (i.e., C) group defined above were tested for significance at alpha=0.05 using the chi-square test.

5.3. Results

The number of residents in the observed 86 NIL of Milan ranged from 104 (for NIL 84, located in the northern part) to 62,347 (for NIL 21, in the north-eastern part), with a median value of 15,170 residents (25th-75th percentile: 4,855 - 23,405). The NIL median area was 1.64 km^2 (1.09 km^2 - 2.66 km^2), with the districts located further from the centre tending to have a larger area. In the analysed period, there were a total of 64,881 CV emergencies, of which 43,919 (67.69%) occurred at home and could be mapped to the NIL of occurrence (20 emergencies happened at the NIL border and they were excluded from CV_VtoH calculation). Of these emergencies, 6,669 (15.18%) happened during heat days and the following day, of which there were a total of 145 days in the analysed period.

5.3.1. Socio-urban characteristics and cardiovascular vulnerability to heat

The distribution of the focal socio-urban characteristics among the 86 NIL, along with their CV_VtoH, are summarised in Table 5.2. It is possible to notice a wide range (min-max) of values for each feature in all parameters, evidencing the large spatial differences that are typical of a big city such as Milan. This finding corroborates the hypothesis that, in order to highlight possible differences in the distribution of heat-related CV events within a big city, the utilization of a more detailed geographical partition can result in more interpretable and accurate results than city-level analyses.

Table 5.2. Descriptive statistics of the distribution of values among the 86 Nuclei of Local Identity (NIL) in the city of Milan for each selected socio-urban feature and the cardiovascular vulnerability to heat (CV_VtoH)

Feature/statistic	Mean	Standard deviation	Minimum	25th percentile	Median	75th percentile	Maximum
Built-up area (%)	19.34	11.31	0.72	10.51	18.16	27.84	47.34
Non-residential buildings' volume (m^3/m^2)	5.46	3.45	0.59	3.86	4.55	5.96	21.27
Green roofs (%)	3.10	2.7	0.0	1.27	2.77	4.08	17.14
Population density (people/km^2)	9,131	6,418	32	3,888	8,434	13,630	26,993
Vegetation index	0.30	0.15	0.01	0.21	0.29	0.37	0.75
Mean summer land surface temperature, LST (°C)	35.58	1.17	31.31	35.06	35.86	36.28	37.78
Density of drinking water fountains (n/ km^2)	4.29	2.73	0.0	2.28	4.07	5.80	12.72
Cycle paths (km/km^2)	1.81	1.29	0.0	0.85	1.69	2.37	7.46
Residents >=65 (%)	20.86	5.29	5.53	17.61	21.72	24.38	31.80
Female residents (%)	49.85	6.73	12.54	48.90	51.67	52.86	54.99
Graduate residents (%)	17.54	9.57	0.0	10.42	14.63	25.11	39.71
CV_VtoH (%)	15.05	4.59	0.0	13.99	15.05	16.08	33.33

To aggregate NIL that are similar by the considered features, an optimal number of socio-urban clusters needs to be defined. The silhouette method indicated k=3, with a coefficient equal to 0.25; although the elbow point was not distinctly visible, that method also resulted in k=3 as the best choice (sum of the squared error equal to 555.15). As well, the dendrogram of hierarchical clustering showed three clusters, while the Davies Bouldin index reached a local minimum equal to 1.36 for k=3 (in the range k=2÷4), while the score was lower for any k>=5. As the value k=3 resulted viable or optimal according to all applied techniques, this was assumed as the final choice for the number of clusters to be set in the k-means clustering algorithm. As a result, 32 NIL, mainly located in the central portion of the city, were classified as part of the first socio-urban cluster – Central (inhabited by 720,244 residents). 45 NIL surrounding the city centre were part of the second socio-urban cluster – Residential (663,995 residents), and finally, 9 NIL in the periphery of the city were assigned to the third socio-urban cluster – Peripheral (8,227 residents). Each of these three socio-urban clusters showed a strong geographical cohesion, and their spatial distribution is visualized in Figure 5.2. The Pearson correlation coefficient between each pair of 11 socio-urban features in the whole city and in the three socio-urban clusters is presented in Table A5.2.

Figure 5.2. Geographical distribution of the Central, Residential, and Peripheral socio-urban clusters obtained through k-means clustering of socio-urban features of Milan's 86 Nuclei of Local Identity (NIL)

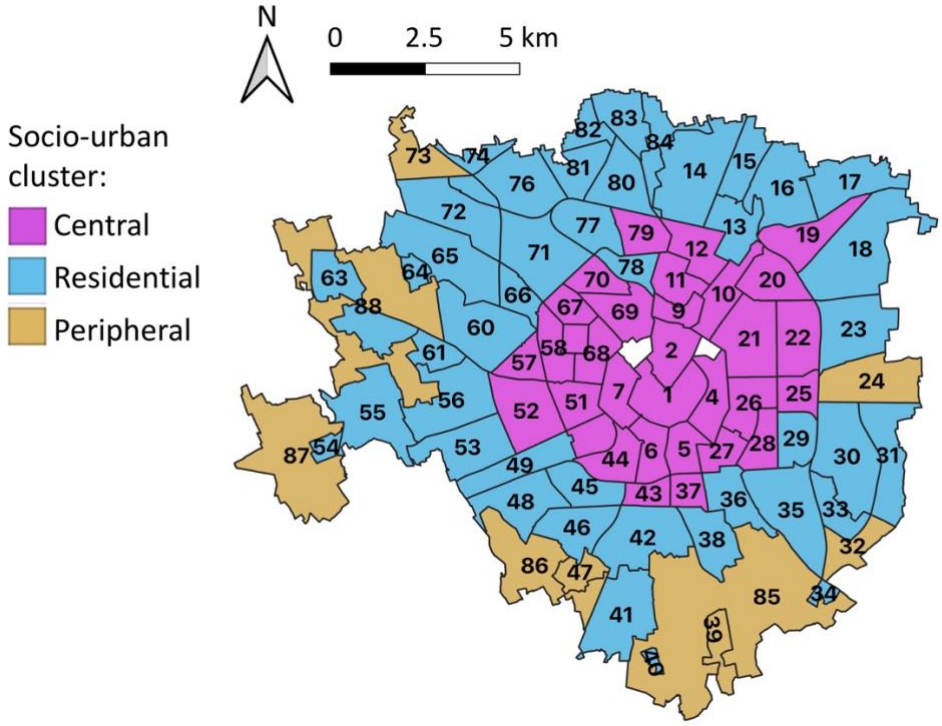

In Table 5.3, the median, the 25th, and the 75th percentiles of the distribution of the 11 socio-urban features among NIL are reported separately for each socio-urban cluster. The results of the Mann-Whitney U test, followed by the Kruskal-Wallis test for multi-group comparison, at the cluster level showed significant differences ($p<0.05$) in all the considered socio-urban parameters, except for: % of elderly residents, similar for the Residential and the Central clusters; cycle paths length and % of graduate residents, similar in Residential and Peripheral clusters; vegetation index, similar in the Central and Peripheral clusters. However, no significant difference was observed in the CV_VtoH among the three clusters.

Overall, the Central cluster was characterised by the highest values in median built-up area, green roofs, population density, density of drinking water fountains, cycle paths, and percentages of elderly, female and graduate residents. In addition, the highest mean summer LST was registered in that cluster. On the contrary, the Peripheral cluster was characterized by the highest values of non-residential buildings' volume and by the lowest values for all the remaining socio-urban features. Values for the Residential cluster were intermediate, except for vegetation index, which had the maximum level.

Table 5.3. Median (25th-75th percentile) of the distribution of the socio-urban features and the cardiovascular vulnerability to heat (CV_VtoH) for the Nuclei of Local Identity (NIL) composing each socio-urban cluster

Feature/cluster	Central	Residential	Peripheral
Built-up area (%)	29.32 (27.64-35.51)[ac]	13.5 (10.29-17.98)[ab]	2.2 (1.33-4.82)[bc]
Non-residential buildings' volume (m^3/m^2)	4.15 (3.57-4.59)[ac]	4.85 (4.14-6.12)[ab]	8.68 (6.66-16.97)[bc]
Green roofs (%)	3.84 (3.26-4.72)[ac]	1.9 (1.23-3.64)[ab]	0.0 (0.0-0.11)[bc]
Population density (people/km^2)	16,056 (11,911-17,534)[ac]	7,155 (3,816-8,641)[ab]	540 (82-828)[bc]
Vegetation index	0.25 (0.19-0.33)[a]	0.34 (0.27-0.46)[ab]	0.12 (0.07-0.24)[b]
Mean summer land surface temperature, LST (°C)	36.22 (35.98-36.5)[ac]	35.62 (34.99-36.16)[ab]	33.62 (33.21-34.4)[bc]
Density of drinking water fountains (n/ km^2)	5.59 (4.98-7.19)[ac]	3.26 (2.27-4.94)[ab]	0.07 (0.0-1.37)[bc]
Cycle paths (km/km^2)	2.34 (1.41-3.24)[ac]	1.5 (0.69-1.96)[a]	0.85 (0.24-1.29)[c]
Residents >=65 (%)	22.4 (20.44-23.84)[c]	22.21 (17.72-25.66)[b]	12.26 (8.77-15.55)[bc]
Female residents (%)	52.94 (52.16-53.78)[ac]	51.11 (49.46-52.40)[ab]	43.39 (26.24-46.64)[bc]
Graduate residents (%)	26.16 (20.87-32.34)[ac]	11.51 (9.58-14.56)[a]	9.55 (7.38-14.7)[c]
CV_VtoH (%)	14.80 (13.49-15.41)	15.47 (14.29-16.40)	16.67 (8.33-22.22)

a - significant difference between Residential and Central clusters (Mann-Whitney U test, p-value<0.05)
b - significant difference between Residential and Peripheral clusters (Mann-Whitney U test, p-value<0.05)
c - significant difference between Central and Peripheral clusters (Mann-Whitney U test, p-value<0.05)

Although differences in the distribution of CV_VtoH were found not significant, its highest median was observed in the Peripheral cluster (16.67%), followed by the Residential (15.47%), and then the Central (14.80%), with the same order considering the interquartile range of the CV_VtoH (equal to 13.89, 2.11 and 1.92, respectively). The RR instead was the highest in the Residential cluster (RR=1.13, 95% CI [1.10-1.17]), followed by the Central cluster (RR=1.11, 95% CI [1.07-1.15]), and the Peripheral cluster, for which the result was not statistically significant (RR=1.06, 95% CI [0.85-1.32]). Moreover, in the Peripheral cluster, the observed values of CV_VtoH were only either above the 80th percentile or below the 20th percentile of the distribution of CV_VtoH for all NIL considered in the whole city of Milan. The CV_VtoH in each NIL, together with the boxplots for each socio-urban cluster, is shown in Figure 5.3.

Considering the whole city of Milan, the cumulated CV_VtoH, calculated dividing CV emergencies in the whole city that happened during heat days and the following day by all CV emergencies, was equal to 15.2%. This value was found exceeded in 24 out of 45 (53.3%) NIL belonging to the Residential cluster, in 11 out of 32 (34.4%) NIL belonging to the Central cluster, and in 5 out of 9 (55.6%) NIL belonging to the Peripheral cluster.

The gMI=0.218 (p-value<0.01) revealed a small clustering tendency of the CV_VtoH considering the whole city of Milan, and the LISA clusters were composed solely of the NIL close to the city outside border.

Figure 5.3. Top panel: (a) Map of cardiovascular vulnerability to heat (CV_VtoH) in each Nucleus of Local Identity (NIL), with reference to three socio-urban clusters, and (b) LISA clusters derived from local Moran's Index. HH – high-high, LL – low-low, HL – high-low, LH – low-high, gMI – global Moran's Index. Bottom panel: Boxplots of the CV_VtoH in each of three socio-urban clusters. The width of the boxplots is proportional to the logarithm of the number of residents. Dashed lines within boxplots represent standard deviation.

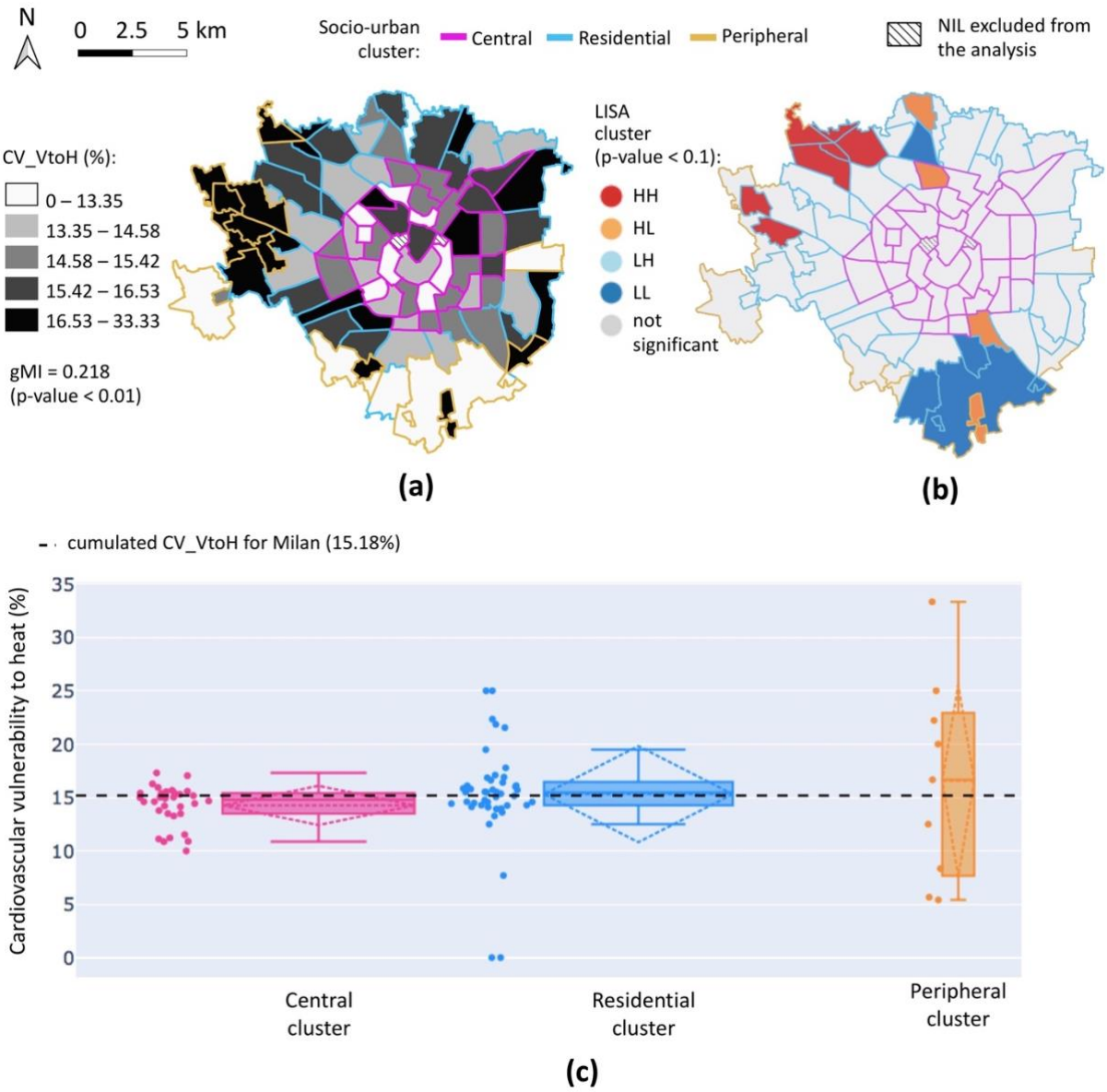

The regression modelling aimed at assessing the impact of the 11 socio-urban features on NIL's CV_VtoH. For clarity of interpretation, the terms 'negative' and 'positive' effect are used based on their mathematical meaning and are not representative of qualitative health outcomes: a socio-urban feature will be described to have a negative effect if an increase in its value is related to a decrease in the CV_VtoH, while it will be described to have a positive effect if an increase in its value is related to an increase in CV_VtoH.

First, the analysis was performed considering the whole city (i.e., on the 86 NIL). Both AIC and likelihood ratio test indicated the SLX (m2) as the best model ($p<0.05$). For the SLX model, statistical tests indicated that the homoscedasticity and error independence assumptions

were satisfied; however, there was statistical evidence that assumptions of linearity and error normality might be violated. Additionally, selected variables (built-up area in non-spatial and spatially lagged versions, spatially lagged mean summer LST and spatially lagged percentage of graduate residents), yielded VIF>10, suggesting that the model may, to some extent, suffer from multicollinearity (for full model diagnostics see Figures A5.1-A5.3 in Appendix). To ensure the robustness of the results despite potential multicollinearity in the SLX model, the sign and significance of all independent variables were compared with those from the OLS model, which reached VIF<10 for all the independent variables. The sign and significance were identical in both models. Additionally, the modelling approach was repeated with a trimmed set of independent variables, excluding the built-up area variable. In this case as well, the best model was the SLX model, with the sign and significance remaining identical in both its original and trimmed versions.

At alpha=0.05, the SLX model estimated a significant direct effect for five features: positive for mean summer LST and the percentages of elderly and graduate residents, and negative for the percentage of female residents and the density of drinking water fountains. Only the percentage of elderly and female residents showed a significant indirect effect, and together with the prevalence of density of drinking water fountains, they had a significant total spatial effect for the 86 NIL of Milan. It is worth noting that the percentage of elderly and female residents reached particularly low p-values ($p<0.01$) and their total impact was the strongest.

The regression analysis was also performed separately for each of the obtained socio-urban clusters. However, it was not possible to perform it on the Peripheral cluster, due to the low number of NIL it contained.

For the Residential cluster, the best model determined to be the non-spatial OLS regression (m1). This model satisfied the assumptions of independence of errors and no multicollinearity, but the statistical test suggested possible problems in regard to linearity, error normality and homoscedasticity. In case of this cluster, two urban (i.e., green roofs area and density of drinking water fountains) features had a significant negative effect while two social features (i.e., percentage of elderly and female residents) had a positive and negative effect, respectively, confirming the results obtained for the whole city.

For the Central cluster, the AIC and likelihood ratio test indicated the SDEM (m5) as the best model. Also in this case, a possible multicollinearity problem emerged for spatially lagged models. Therefore, the modelling approach was repeated, subsequently trimming the set of independent variables by those characterized by elevated VIF values. This led to the confirmation of the robustness of the initial results, specifically by comparing them with the SEM model, which included nine variables. The SEM results closely aligned with the initial p-values and reported an identical direction of impact for all significant independent variables.

Features with significant effects estimated by the SDEM model for the Central cluster were non-residential buildings' volume, green roof area and population density, with a direct negative effect, and mean summer LST, which had a direct positive effect on CV_VtoH. No significant indirect effects emerged.

The results from the regression analysis, either in the whole city or in the Residential and Central clusters, is presented in Table 5.4. Additionally, the Appendix contains the results of each of seven tested models in each of three geographical partitions (Figures A5.1-A5.3).

Table 5.4. Results of the regression analysis considering coefficient, direct, indirect and total effects in all districts, and in districts grouped in Central and Residential socio-urban clusters. SLX – spatially lagged X model, SDEM – spatial Durbin error model, OLS – ordinary least squares.

Feature/Cluster (model)	**All (SLX)**			**Central (SDEM)**			**Residential (OLS)**		
Direct effect (spatial models) / estimated coefficient (non-spatial model)	effect	p-value	std error	effect	p-value	std error	β	p-value	std error
Built-up area (%)	-0.28	0.35	0.29	0.07	0.64	0.15	-0.53	0.18	0.39
Non-residential buildings' volume (m^3/m^2)	0.16	0.26	0.14	-1.27*	<0.01	0.29	0.17	0.58	0.30
Green roofs (%)	-0.18	0.15	0.13	-0.29*	0.04	0.15	-0.32*	0.02	0.13
Population density (people/km^2)	0.26	0.09	0.15	-0.5*	0.02	0.22	0.52	0.16	0.36
Vegetation index	-0.13	0.35	0.14	0.08	0.64	0.17	-0.1	0.52	0.15
Mean summer LST (°C)	0.71*	<0.1	0.18	1.11*	<0.01	0.36	0.38	0.07	0.20
Density drinking water fountains (n/ km^2)	-0.24*	0.03	0.11	0.29	0.08	0.17	-0.73*	<0.01	0.21
Cycle paths (km/km^2)	-0.1	0.35	0.10	0.1	0.12	0.06	-0.1	0.66	0.22
Residents >=65 (%)	0.37*	<0.01	0.12	0.23	0.54	0.37	0.39*	0.02	0.17
Female residents (%)	-0.29*	0.02	0.13	-0.07	0.91	0.60	-1.16*	0.05	0.56
Graduate residents (%)	0.46*	0.01	0.18	-0.12	0.25	0.10	0.17	0.58	0.31
Indirect effect									
Built-up area (%)	0.06	0.93	0.70	-0.07	0.93	0.81			
Non-residential buildings' volume (m^3/m^2)	-0.1	0.72	0.28	2.4	0.15	1.66			
Green roofs (%)	-0.11	0.71	0.31	-0.14	0.8	0.55			
Population density (people/km^2)	-0.44	0.21	0.35	0.74	0.18	0.55			
Vegetation index	0.06	0.8	0.26	-0.16	0.71	0.42			
Mean summer LST (°C)	-0.16	0.69	0.40	0.65	0.52	1.01			
Density drinking water fountains (n/ km^2)	-0.52	0.08	0.30	0.35	0.4	0.41			
Cycle paths (km/km^2)	0.27	0.34	0.28	0.11	0.76	0.38			
Residents >=65 (%)	0.64*	0.01	0.26	1.5	0.07	0.83			
Female residents (%)	-0.82*	0.02	0.35	0.13	0.94	1.66			
Graduate residents (%)	-0.2	0.59	0.38	-0.14	0.83	0.63			
Total effect									
Built-up area (%)	-0.21	0.76	0.70	0.0	1	0.80			
Non-residential buildings' volume (m^3/m^2)	0.06	0.88	0.36	1.13	0.52	1.74			
Green roofs (%)	-0.29	0.43	0.37	-0.44	0.37	0.49			
Population density (people/km^2)	-0.18	0.61	0.35	0.24	0.63	0.50			

Vegetation index	-0.07	0.8	0.27	-0.08	0.85	0.41	
Mean summer LST (°C)	0.55	0.16	0.40	1.76	0.13	1.18	
Density drinking water fountains (n/km^2)	-0.76*	0.02	0.32	0.63	0.22	0.52	
Cycle paths (km/km^2)	0.17	0.53	0.28	0.21	0.59	0.39	
Residents >=65 (%)	1.01*	<0.01	0.29	1.72	0.12	1.10	
Female residents (%)	-1.11*	<0.01	0.40	0.07	0.98	2.13	
Graduate residents (%)	0.26	0.5	0.38	-0.26	0.67	0.6	

* significant results at alpha=0.05

5.3.2. Socio-urban vulnerability to heat

Following the regression results, the SU_VtoH was computed separately for the Central, Residential, and Peripheral clusters, as described in the following equations (equations 5.9 – 5.11). For each neighbourhood, the standardized values (the same as used for the regression models) of the significant independent variables were multiplied by the coefficients estimated from the regression models, i.e., by direct effect or by β coefficient. For the Peripheral cluster's NIL, the variables resulting significant for the entire city were utilized (equation 5.9), while for the Central and Residential clusters, the variables significant for their respective models were applied (equations 5.10 and 5.11, respectively). Subsequently, the obtained values of SU_VtoH for all the 86 considered NIL were normalized between 0 and 1.

$$\begin{aligned} &Peripheral\ Cluster\ SU_VtoH \\ &\quad = 0.37 * \%\ elderly\ residents - 0.29 * \%\ female\ residents - 0.24 \\ &\quad * drinking\ water\ fountains + 0.71 * LST + 0.46 * \%\ graduate\ residents \end{aligned} \tag{5.9}$$

$$\begin{aligned} &Central\ Cluster\ SU_VtoH \\ &\quad = 1.11 * LST - 0.29 * green\ roofs - 1.27 * non\ residential\ buildings \\ &\quad - 0.5 * population\ density \end{aligned} \tag{5.10}$$

$$\begin{aligned} &Residential\ Cluster\ SU_VtoH \\ &\quad = 0.39 * \%\ elderly\ residents - 1.16 * \%\ female\ residents - 0.73 \\ &\quad * drinking\ water\ fountains - 0.32 * green\ roofs \end{aligned} \tag{5.11}$$

Examining the Pearson coefficient of each significant independent variable with CV_VtoH, in the Central cluster population density reached the strongest value (r=0.54), followed by non-residential buildings' volume (r=-0.52), mean summer LST (r=0.46), and green roofs (r=-0.22). In contrast, in the Residential cluster the r was lower, with the highest value for drinking water fountains (r=-0.45) and green roofs (r=-0.42), followed by % of female residents (r=-0.18) and the % of elderly residents (r=0.08). In the Peripheral cluster, the r ranged from 0.60 for mean summer LST, to -0.01 for % of graduate residents, with intermediate values for % of female residents (r=-0.45), drinking water fountains (r=-0.20), and % of elderly residents (r=0.13).

Focusing on the Central and Residential clusters, the gMI did not yield statistical significance in the Central cluster for CV_VtoH; however, its local version identified 8

significant NIL – two high-high (HH), four high-low (HL), and two low-low (LL). For each significant independent variable, the gMI was significant, ranging from 0.165 for green roofs to 0.308 for population density. This resulted in the identification of geographically varying LISA clusters for each feature.

In contrast, in the Residential cluster the spatial distribution of CV_VtoH exhibited a statistically significant but small tendency to cluster, with the statistic equal to 0.150. At local level, only 6 significant NIL were identified. Among the four examined independent variables, the gMI was significant only for the % of female residents (gMI=0.166). This resulted in the identification of 12 NIL forming LISA clusters at the local level, with six in HH cluster.

Global Moran's I and the numerosity of each LISA cluster for CV_VtoH and for each significant independent variable in the Central and the Residential clusters are summarized in Table 5.5.

Table 5.5. Global Moran's Index (gMI) and significant LISA clusters numerosity for cardiovascular vulnerability to heat (CV_VtoH) and each significant independent variable in the Central and the Residential socio-urban clusters. HH – high-high, LH – low-high, HL – high-low, LL – low-low, n/a – not applicable.

Variable/cluster	**Central**					**Residential**				
	gMI	HH	LH	HL	LL	gMI	HH	LH	HL	LL
CV_VtoH	0.056	2	0	4	2	0.150*	3	0	1	3
Non-residential buildings' volume	0.197*	2	0	2	4	n/a	n/a	n/a	n/a	n/a
Population density	0.308*	4	0	1	3	n/a	n/a	n/a	n/a	n/a
Mean summer LST	0.193*	4	1	2	4	n/a	n/a	n/a	n/a	n/a
Green roofs	0.165*	3	2	0	1	-0.036	1	4	0	9
Drinking water fountains	n/a	n/a	n/a	n/a	n/a	0.046	0	3	2	2
Elderly residents	n/a	n/a	n/a	n/a	n/a	0.013	3	1	5	2
Female residents	n/a	n/a	n/a	n/a	n/a	0.166*	6	1	2	3

* significant result (p-value<0.1)

The SU_VtoH across the city of Milan (thus without considering clusters separately) resulted not normally distributed, with median value equal to 0.596 (25th-75th percentile: 0.498-0.667). The gMI=0.147 (p-value <0.1) revealed a tendency to cluster, which was less pronounced than the clustering tendency for CV_VtoH, however, the resulting LISA clusters were located in more central parts of Milan. In particular, within the Central cluster, a substantial portion of the eastern NIL exhibited a significant HH local spatial autocorrelation in SU_VtoH, totalling 7 HH neighbourhoods. Conversely, in the southern part of the city, within the Residential cluster, 6 neighbourhoods formed LL clusters, covering a considerable area. The SU_VtoH and the resulting LISA clusters for the city of Milan are mapped in Figure 5.4.

Figure 5.4. (a) Geographical distribution of the socio-urban vulnerability to heat (SU_VtoH) in the whole city of Milan, and (b) the corresponding LISA clusters. HH – high-high, LL – low-low, HL – high-low, LH – low-high, gMI – global Moran's Index.

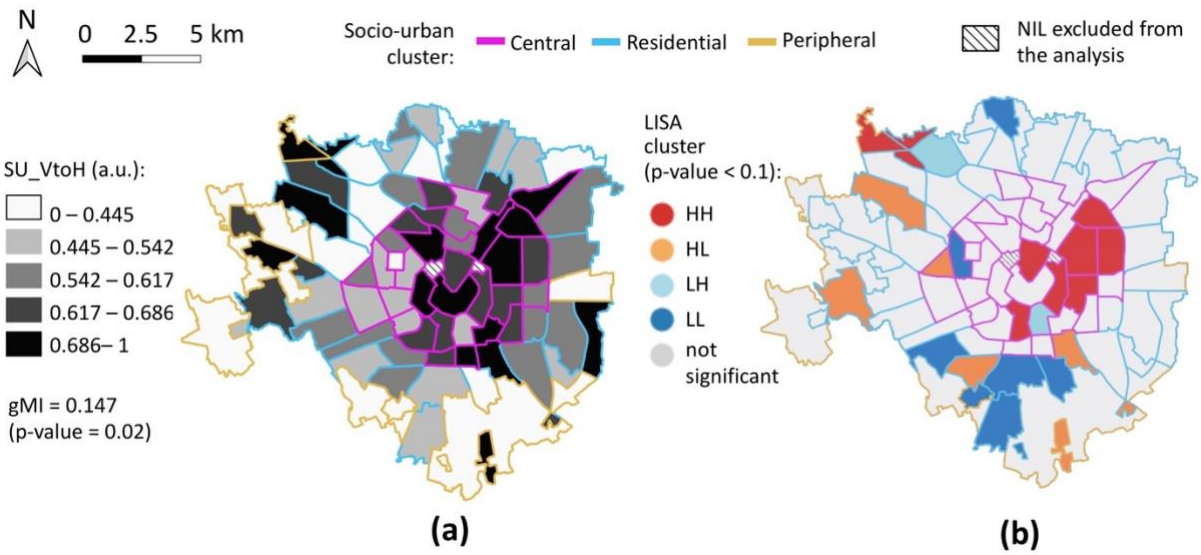

The r between CV_VtoH and SU_VtoH resulted equal to 0.489. In particular, the highest coefficient was observed in the least populous Peripheral cluster (r=0.72), followed by the Residential (r=0.711) one, and then the Central cluster with a lower value (r=0.461). The relationship between CV_VtoH and SU_VtoH is shown in Figure 5.5, accounting for the number of residents in each NIL. The most populated NIL tended to achieve SU_VtoH values similar to its median, with corresponding CV_VtoH levels around 15%, whereas smaller, in terms of population, NIL showed a greater dispersion of values. The OLS regression model, applied to both the entire city and separately to each cluster, indicated that SU_VtoH was able to explain more than 50% of the CV_VtoH variance in the Residential and Peripheral clusters, but only slightly above 20% in the Central cluster.

Figure 5.5. Relationship between cardiovascular vulnerability to heat (CV_VtoH) and socio-urban vulnerability to heat (SU_VtoH). Dot size is proportional to the logarithm of the number of residents. Dashed lines represent the ordinary least squares regression line in the whole city and in the three socio-urban clusters.

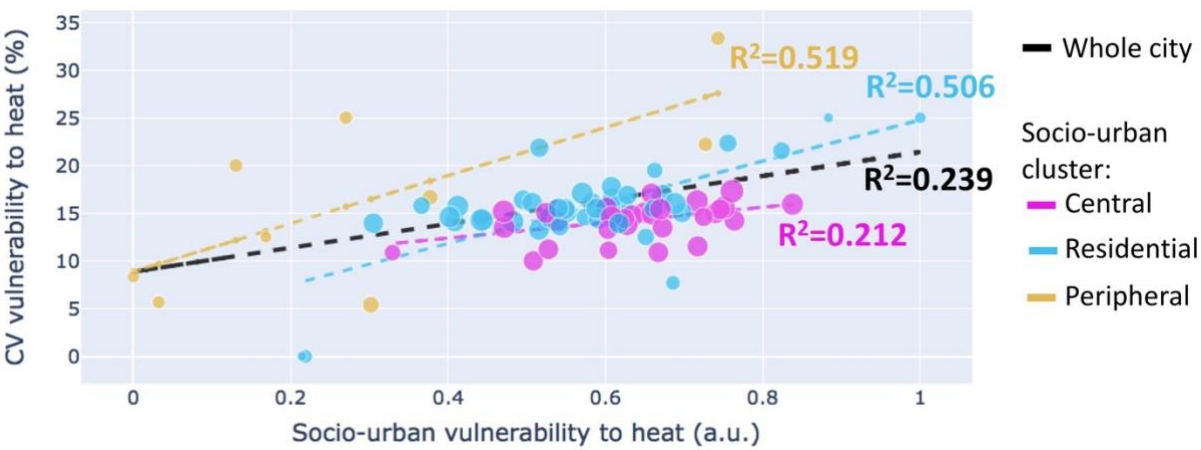

5.3.3. Mapping of low and highly vulnerable districts

In Figure 5.6, the NIL with high and low values for both CV_VtoH and SU_VtoH were highlighted. Specifically, high values were defined as >=60th percentile of the distribution, while low values were defined as <=40th percentile. This categorization resulted in 18 highly vulnerable and 20 low vulnerable NIL, inhabited by a total of 322,068 and 278,005 residents, respectively, accounting for 23% and 20% of Milan's population.

Examining the 18 highly vulnerable NIL, the majority, i.e., 10 NIL, were located in the Residential cluster, 6 were part of the Central cluster, and the remaining 2 belonged to the Peripheral cluster. However, in terms of population exposure, more than 210,000 residents (211,926 people; representing 65.8% of the total residents in highly vulnerable NIL) were concentrated in the Central cluster, with less than 110,000 (108,251; 33.61%) living in the Residential cluster, and less than 2,000 (1,891; <1%) in the Peripheral part of the city.

A similar trend in terms of the number of NIL was observed for low vulnerable zones – the majority (11 out of 20 neighbourhoods) belonging to the Residential, 5 to the Central, and 4 to the Peripheral clusters. However, in this case, the majority of the population, almost 200,000 residents (194,834; 70.08% of the least vulnerable NIL population), lived in the Residential part of the city, with only 80,000 (79,718; 28.68%) in the Central cluster, and slightly over 3,000 (3,453; 1.24%) in the Peripheral cluster.

Figure 5.6. Geographical distribution of the Nuclei of Local Identity (NIL) with both cardiovascular vulnerability to heat (CV_VtoH) and socio-urban vulnerability to heat (SU_VtoH) above the 60th percentile of their distribution (red tones; highly vulnerable NIL), or below the 40th percentile of their distribution (green tones; low vulnerable NIL).

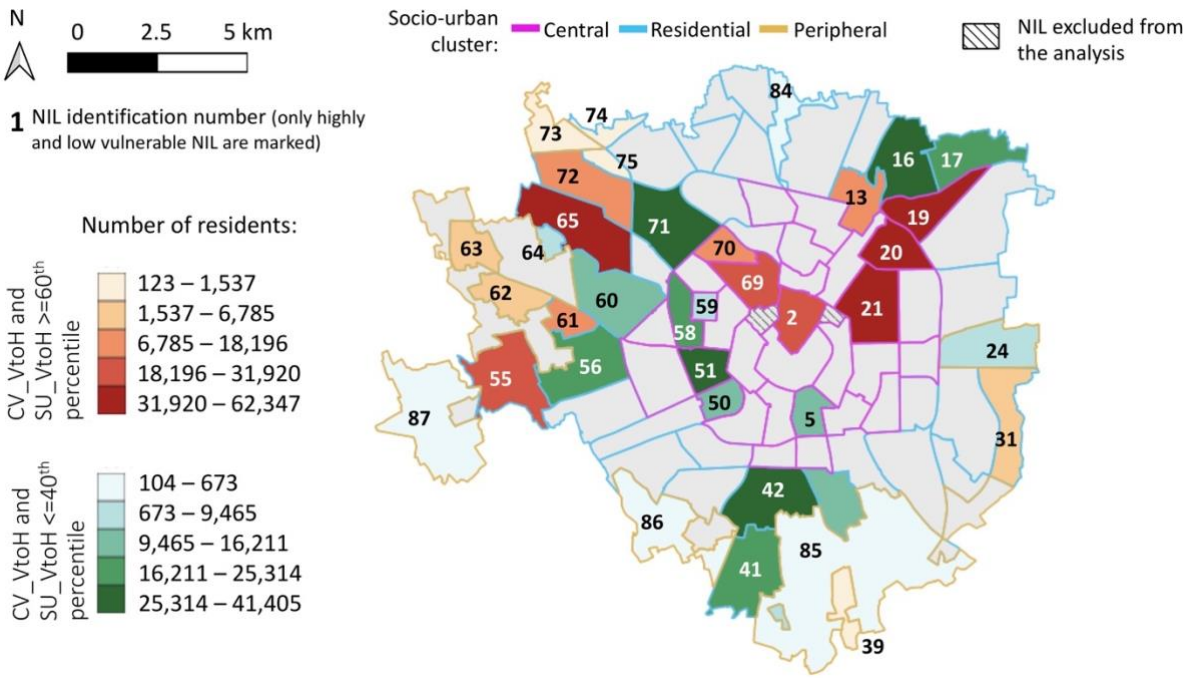

In order to further validate the above map, and to use the geolocalized ambulance data at their finer resolution (i.e., the resolution of a single emergency), CV emergencies were spatially

clustered accounting for their density by the HDBSCAN algorithm, considering separately the emergencies that happened on heat days and on non-heat days.

During non-heat days, HDBSCAN, with minimum cluster size equal to 300, estimated 25 non-noise clusters of CV emergencies, with 24,108 ambulance dispatches (42.36% of total dispatches during non-heat days) included in them. No significant cluster was identified within the Peripheral socio-urban cluster. When considering CV emergencies during heat days, 18 non-noise clusters were found, with minimum cluster size equal to 60, where a total of 3,294 emergencies (41.31% of all emergencies in heat days) happened. The emergencies forming clusters during heat and non-heat days are mapped in Figure 5.7. The underlying map highlights highly and low vulnerable NIL, but it does not use colour intensity to represent the number of residents in order to avoid visual clutter.

Figure 5.7. Emergencies forming non-noise HDBSCAN clusters during heat and non-heat days. Zone A - zone where HDBSCAN clusters exist during non-heat days but not during heat days; zone B - zone where HDBSCAN clusters exist in both meteorological conditions, but with a considerable spatial shift in point concentration; zone C - zones where HDBSCAN clusters experience a considerable increase in spatial coverage during heat days compared to non-heat days. CV_VtoH – cardiovascular vulnerability to heat, SU_VtoH – socio-urban vulnerability to heat.

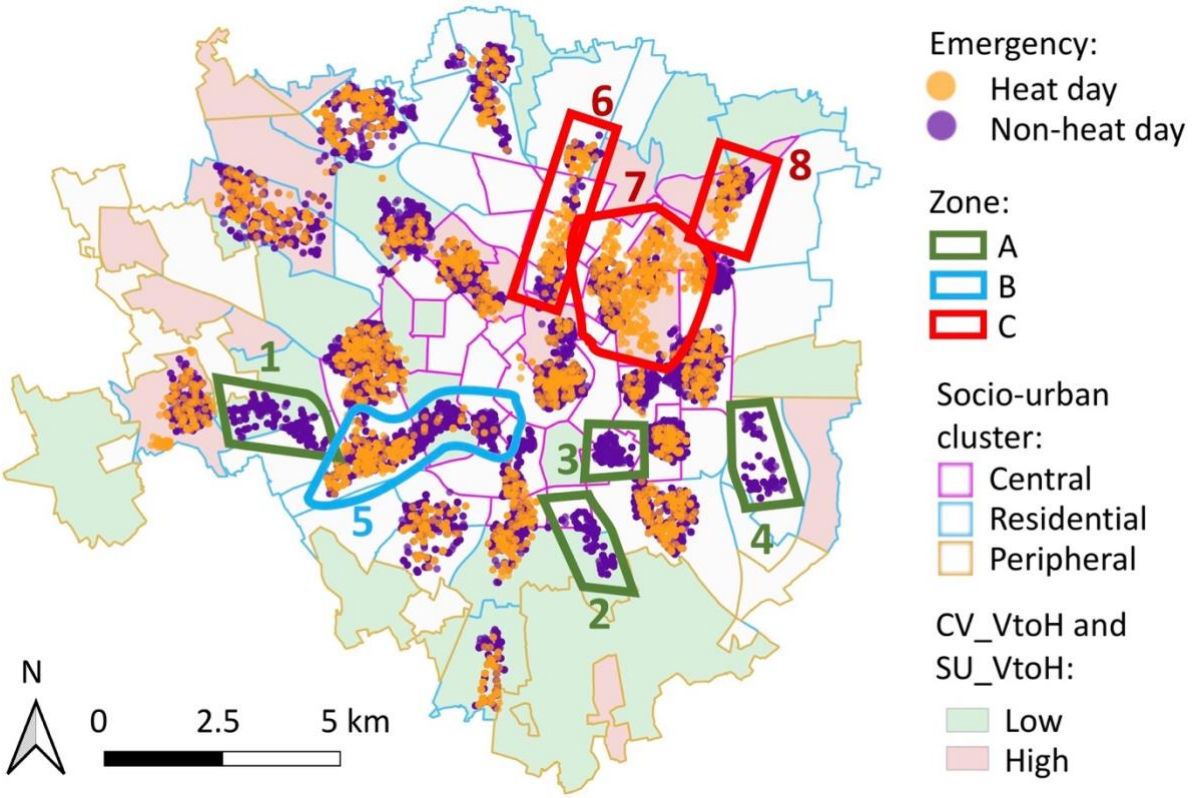

Following the categorization defined in section 5.2.3, four zones where HDBSCAN clusters were identified during non-heat but not during heat emerged, denoted as zones A1-A4 in Figure 5.7. In this case, they corresponded to four HDBSCAN clusters, in which 3,668 emergencies happened, mostly within the area of the NIL 27 (“Porta Romana”), 30 (“Mecenate”), 37 (“Ex Om Morivione”), 38 (“Ripamonti”), 53 (“Lorenteggio”), and 56 (“Forze Armate”). Out of

these six NIL, two (NIL 38 and 56) were classified as low vulnerable in terms of CV_VtoH and SU_VtoH.

In one zone (i.e., B5 in Figure 5.7) there was a considerable spatial shift between emergencies in heat (270 emergencies) and non-heat days (2,101 emergencies). In non-heat weather conditions, an HDBSCAN cluster of emergencies was identified along the common border of the NIL 49 ("Giambellino") and 52 ("Bande Nere"), 50 ("Tortona") and 51 ("Washington"), and 7 ("Magenta- San Vittore") and 44 ("Navigli"). During heat days, however, the vast majority of emergencies occurred only along the border of NIL 49 and 52, thus with the exclusion of two low vulnerable NIL (50, 51).

In the northern part of Milan, three zones were detected where the HDBSCAN clusters showed a considerable increase in spatial coverage during heat days compared to non-heat days. Starting from the most western zone (i.e., C6 in Figure 5.7), two HDBSCAN clusters were identified during non-heat days, covering a strip over the NIL 9 ("Garibaldi-Repubblica"), 11 ("Isola"), 12 ("Maciachini-Maggiolina"), and 14 ("Niguarda- Cà Granda"). The 737 emergencies were most densely located in the upper and lower parts of the highlighted zone. However, during heat days, only one HDBSCAN cluster of emergencies has been identified, with 176 emergencies covering as densely the area of two previous HDBSCAN clusters, as the area between them, corresponding to NIL 11.

The largest increase in spatial coverage during heat days compared to non-heat days was observed in the most central of the three zones (i.e., C7 in Figure 5.7). In non-heat meteorological conditions, two identified HDBSCAN clusters of 1,480 emergencies densely covered specific, but relatively small, areas of the NIL 10 ("Centrale"), 20 ("Loreto"), and 21 ("Buenos Aires-Venezia"). During heat days, however, a large HDBSCAN cluster of 518 ambulance dispatches was identified, with this cluster including emergencies that covered the entire area of the three above-mentioned districts, of which two (i.e., NIL 20 and 21) were considered as highly vulnerable.

Finally, in highly vulnerable NIL 19 ("Padova") one cluster was identified in both heat and non-heat days. It included 424 emergencies in non-heat days and 109 emergencies in heat days, while the area where the ambulances were called was larger during the extreme temperatures.

In terms of age, gender, and mortality outcome, as shown in Table 5.6, significant differences were observed in the proportion of elderly patients only for zone C7, with 13.21 percentage points more elderly patients during heat days compared to non-heat days. Across all other zones examined, a trend of higher proportions of patients above 65 years old during heat days was also observed. No significant difference was found in the proportion of females, and varying trends were noted depending on the zone. Across all zones examined, during heat days a higher fraction of emergencies resulted in fatalities compared to non-heat days, with a significant difference in percentage observed in zones B5 and C6, with 2.29 and 2.22 percentage points more for both locations respectively.

Table 5.6. Fraction of elderly patients, female patients, and fatal emergencies in heat days with respect to non-heat days in zones B5, C6-C8

Condition/characteristics	Number of emergencies	% elderly	% female	% fatal
Zone B5				
Heat	270	61.11%	54.07%	4.81%*
Non-heat	2,101	60.73%	56.31%	2.52%
Zone C6				
Heat	176	53.41%	55.11%	3.98%*
Non-heat	737	52.1%	53.87%	1.76%
Zone C7				
Heat	518	45.37%*	52.90%	2.32%
Non-heat	1,480	32.16%	51.76%	1.42%
Zone C8				
Heat	109	55.05%	55.96%	1.83%
Non-heat	424	54.95%	54.95%	1.42%

* significant difference in proportion with respect to non-heat days (chi-square test, p-value<0.05)

5.4. Discussion

In this study, a framework based on the application of different spatial models, designed to analyse geolocated data originating from the EMS was proposed to estimate the direct and indirect influence of socio-urban characteristics on CV_VtoH in different parts of the city, and to subsequently calculate a vulnerability index accounting for both socio-urban factors and CV emergencies, highlighting neighbourhoods where substantial action needs to be taken to protect the residents. This framework aimed to answer fundamental research questions concerning urban resilience to heat waves by proposing the further subdivision of a major urban area based on socio-urban characteristics of its neighbourhoods, and by estimating the effects of such socio-urban features on populations' vulnerability to heat for different clusters within the city, aligning with the proactive approach to climate change and human health.

5.4.1. Novelties of the proposed framework

The use of geolocalized ambulance dispatches for CV events as a proxy signal represents, to the best of our knowledge, a novel approach for the evaluation of the effects of neighbourhood characteristics on CV health during heat. Such data allowed the computation of the CV_VtoH with relatively high spatial granularity within a big city (i.e., at the level of the 86 NIL in which Milan was subdivided). This approach highlights local differences among NIL, also those within the same socio-urban cluster, in terms of their CV_VtoH. These insights contrast to models considering only the whole city, in which such differences would be smoothed out. In fact, the CV_VtoH was characterized by high variability in its values (from 0% to 33%) among NIL, thus confirming the importance to study and quantify local disparities within a big city.

Multiple studies have analysed the influence of diverse neighbourhood characteristics on human health (Arcaya et al., 2016; Malambo et al., 2016; Pérez et al., 2020; Roux et al., 2016; Yen et al., 2009). However, few studies addressed the particular problem of CV_VtoH

in this context (Bakhtsiyarava et al., 2023; Morais et al., 2021; Murage et al., 2020; Silveira et al., 2021; Wu et al., 2011). This issue is particularly important due to the increasing prevalence and intensity of heat waves. In previous research, neighbourhood-level factors were examined mainly using non-spatial approaches, while few studies that accounted for geographical dimension implemented spatial regression or geographically weighted regression (GWR) (Morais et al., 2021; Wu et al., 2011). The GWR aims to examine spatial heterogeneity of the analysed phenomenon by estimating the parameters in each unit of analysis; in contrast, spatial dependences and patterns are modelled by spatial models (Düzgün & Kemeç, 2008) listed in section 5.2.2. In the field of human health, considering the exposure to risk factors only in the district of residence might limit the interpretation of the results (Tamura et al., 2019), and applying spatial regression, a method that accounts for both direct and indirect effects, partly overcomes this limitation. Moreover, by applying the spatial models separately for clusters of relatively similar districts, both the spatial non-stationarity of the explicative variables (i.e., the socio-urban features) and the spatial behaviour of the target measure (i.e., CV_VtoH) were taken into account and adjusted for.

In this study, a comprehensive guideline for the calculation of an urban vulnerability to heat index tailored to human health was proposed. As such approach is relatively recent, there is still a lack of a common standard in terms of methodology. Relevant vulnerability indices proposed so far used different calculation techniques, from simple equal weighting to more advanced spatial and non-spatial models, and covered a range of demographic, social, urban, economic, infrastructural and environmental factors (Ellena et al, 2020a; Shrestha et al., 2016; Macintyre et al., 2018; Sera et al., 2019; Krellenberg et al., 2017; Dong et al., 2020). The methodology proposed in this study aligns with the urgent call for cross-sectorial collaboration (Tong and Ebi, 2019; Sharifi et al., 2021; Ebi and Hess, 2020), as the SU_VtoH calculation explicitly accounts for the interdependencies among climate change, CV health, and social, urban and demographic factors. Additionally, validation of the results with density-based clustering conducted separately for heat and non-heat days is another novelty with respect to existing research.

5.4.2. Influence of socio-urban characteristics for the whole city of Milan

Considering the whole city of Milan, a significant positive effect (i.e., increased CV_VtoH with larger values of the feature) was associated with the average summer land surface temperature, to the percentage of elderly and graduate residents, along with a negative effect of the density of drinking water fountains and to the percentage of female residents. For two social features (i.e., percentage of elderly and female residents), both the direct and indirect effects were significant, resulting in a particularly strong and significant total effects.

A higher risk of CV pathologies, as well as a more frequent use of EMS during heat has been repeatedly reported for older people compared to younger individuals (Cicci et al., 2022; Katayama et al., 2022). A recent review (Son et al., 2019), which assessed the factors that modify the influence of heat on CV mortality, reported the strongest and significant effects for age and sex, a weaker but significant effect for the education level, green space and neighbourhood's socio-economic status, and a non-significant evidence concerning population density. In 107/142 (75.4%) studies, a higher mortality risk from heat exposure was found for

the elderly, with a decrease in heart rate variability and maximum heart rate, and a series of observed pathological alterations in aging CV tissues (North & Sinclair, 2012) proposed as possible explanation.

In the same review, higher heat-related mortality was reported for women in 37 (26.1%) studies, for men in 12 (11.2%) studies, and without gender differences in 25 (17.6%) studies. Several hypotheses to explain a greater vulnerability to heat in women, especially pre-menopausal women, are discussed in the literature. For fertile females, compared to men, a lower blood's viscosity, aggregation of red blood cells and their deformability, as well as different levels of hormones (Kameneva et al., 1999; Stramba-Badiale et al., 2006) are described, together with a higher heart rate increase and body heat storage, and a lower sweat rate (Burse, 1979). The estimation of higher increase in CV risk in heat for women is opposite of our results. However, several studies highlighted that, if standardizing CV fitness level, body size, and acclimation state, gender differences tended to disappear, and if a lower sweat rate in women is disadvantageous in hot-dry environments, it could result advantageous in hot-wet environments (Kenney, 1985). This could be the case of the Milan hot climate, characterized by high humidity, as overviewed in Chapter 4.

In this study, the strongest direct impact on CV_VtoH for Milan was recorded for the average mean summer LST, which is concordant with established scientific knowledge. This result is not surprising as CV vulnerability specifically to heat is addressed. A harmful influence of high temperature on the risk of CV diseases has been found in many studies, as reported in Chapter 3, especially after the 2003 European heatwave. This literature includes a recent study analysing the mortality in Europe in summer 2022, during which multiple record-breaking temperatures were registered, and over 60 thousand heat-related deaths in 35 European countries were estimated (Ballester et al., 2023).

Two additional features were found to have a significant direct or total influence on CV_VtoH for the whole city. The first one is the density of drinking water fountains, having a negative direct and total effect, thus indicating how this simple urban feature could result in effective benefits for health. This finding is in agreement with previous research reporting the importance of accessibility to drinking water fountains outside the house in reducing urban CV_VtoH (Aminipouri et al., 2016; Komac et al., 2016; Arnberger et al., 2017). In fact, it is recommended to increase cool fluid intake during heat, to reduce the high body temperature by internal conductive heat transfer through cold ingested fluid (Jay et al., 2021).

The second relevant feature is the percentage of graduate residents, with an apparent positive effect. This finding contrasts with other studies reporting a predominantly lower risk of heat-related morbidity or mortality among people with higher level of education (Huang et al., 2015; Zhou et al., 2017). In their review of 142 studies, Son et al. (2019) found 16 (11.3%) studies in which higher risks were associated to those with no or lower education compared to those with more education, with 3 (2.1%) studies finding the opposite and 7 (4.9%) studies finding no difference. However, in a recent study focusing on heat-attributable all-cause mortality in the city of Turin in the Northwest of Italy, for the period 1982–2018, a mixed-effect of gender and education was found. Heat increased the relative risk among men (RR=1.66) with higher level of education and among women (RR=1.93) with lower level of education (Ellena et al., 2020b). In our study, the impact of the percentage of graduate residents was significant only as a direct effect. A possible explanation could be related to the fact that

more educated people tend to live closer to the city centre, where the highest temperatures are recorded, negatively influencing the human health as discussed in one of the previous sections. Another possible interpretation is related to our proxy variable used in the analysis (i.e., the ambulance dispatches), as individuals with higher levels of education may be able to identify symptoms more accurately and quickly leading to prompter calls to emergency services (Yan et al., 2009).

5.4.3. Influence of socio-urban characteristics for particular clusters of Milan

In addition to the features with significant impact for the whole city, the percentage of green roofs, population density and non-residential buildings' volume showed a significant effect in particular clusters of Milan. Goodness-of-fit measures indicated that socio-urban cluster-specific regression models performed better than whole-city models.

The non-spatial regression model proved to be the best fit for the Residential cluster, characterised by intermediate median values for almost all socio-urban features, compared to other two socio-urban clusters. In this case, it is possible that the spatial relationship was lost with the clustering process. Spatial interactions were instead detected in the Central cluster, where both local dependencies and dependencies in the error term emerged. These results suggest the occurrence of more complex spatial relationships in this area, not eliminated by the clustering process.

The percentage of green roofs had a direct negative impact of similar strength for both the Residential and the Central clusters. Green roofs contribute significantly to the decrease in roof temperature and, to smaller extent, to the decrease in ground temperature and in temperature at 2 meters above the surface, with the highest reduction observed in the hottest parts of cities (Black-Ingersoll et al., 2022; Sharma et al., 2018). This is in agreement with our results, that estimated a significant direct impact in clusters with high mean summer LST.

The observed influence of non-residential buildings' volume on CV_VtoH could be interpreted in two opposite directions. On one side, such buildings could host service and commercial centres, which are equipped with air conditioning, where people can thus temporarily reduce the perceived heat during hot weather. On the other hand, these same systems also produce additional heat outside; furthermore, non-residential buildings include factories as well. Their presence is significantly correlated, in the territory of Lombardy region, with high concentration of pollutants (Gianquintieri et al., 2023), such as PM2.5, that can increase CV risk (Cambra et al., 2011). This second condition seems to characterize the Peripheral cluster, where the highest non-residential buildings' volume was found, as possibly corresponding to the usual location of factories in big cities. On the opposite, in the Central cluster, composed by the areas including the core of commercial retail, the non-residential buildings' volume had a negative direct effect on CV_VtoH. In this case we might infer that it reflects more the cooling efficiency rather than an increase in temperature and industrial pollution's impact on human health.

Interestingly, population density was found to have a significant negative direct impact on CV_VtoH for the Central cluster, while a positive direct effect emerged when considering the whole city (though only marginally significant, p-value=0.09). Using population density as an indicator in human health-related studies lacks a clear rationale (Greenberg, 2023). It can

correlate with various characteristics, such as social deprivation or the provision of health services. Based on our findings, we hypothesize that when considering the entire city of Milan, population density primarily reflects the attractiveness of the neighbourhood. This attractiveness may include factors such as safety, green spaces, and proximity to various services, which influence where people choose to reside. However, in the Central cluster, comprising commercial and transportation hubs, and tourist zones, the calculated resident population density may not fully capture the actual population density. As a result, this discrepancy could potentially alter the regression results.

5.4.4. Highly and low vulnerable districts of Milan

In Milan, over 300,000 citizens resulted residing in highly vulnerable areas, with approximately two-thirds living in the central part of the city. Interestingly, these vulnerable neighbourhoods are located along the tracks of two major railway stations, i.e., the Central station and the Garibaldi station. These areas exhibit elevated mean summer LST, and four NIL, in the vicinity of the Central train station, formed HH LISA clusters. Conversely, the less vulnerable zones were primarily situated in the western part of the Central socio-urban cluster. This low vulnerable area encompassed two and three NIL in significant LISA clusters of non-residential buildings' volume and mean summer LST, respectively, with these features highly contributing to the SU_VtoH in this part of the city. The Residential and Peripheral clusters exhibited less geographical coherence in spatial distribution of highly vulnerable NIL. This observation aligns with the non- significant clustering tendency of most independent variables, and it can also be partly explained by unique geometries and particular patterns of shared boundaries among neighbourhoods in these two clusters. Nonetheless, a considerable number of highly vulnerable NIL belonging to Residential or Peripheral cluster was situated in the western part of the city.

The obtained results emphasize the need for geospatially analysing socio-urban vulnerability to heat concerning CV health in a major European urban area, while underscoring the associated challenges. The most spatially coherent results were observed in the central part of the city, predominantly including historic districts where socio-urban characteristics extended beyond current neighbourhood boundaries, where, however, some undiscovered spatial patterns persist (as indicated by spatial dependencies in the error term estimated by SDEM). Conversely, residential neighbourhoods appeared more independent among each other, lacking geographic clustering in the considered features.

Additionally, validation of the final map (i.e., Figure 5.6) with density-based clustering of CV emergencies revealed some noteworthy disparities in spatial distribution patterns under varying weather conditions, underscoring the importance of considering such factors in emergency management strategies. In particular, central-northern districts exhibited larger zones of high CV emergency density during heat-days with respect to normal conditions. Notably, zones C6-C8 encompassed only either neutral or highly vulnerable, in terms of CV_VtoH and SU_VtoH, areas, mainly located along the tracks of Central railway station, characterized by particularly high temperature and low vegetation. Conversely, several central-southern neighbourhoods demonstrated significant HDBSCAN clusters of emergencies exclusively during non-heat days, suggesting potential shifts in emergency patterns with

climate conditions. All these clusters encompass either neutral or low vulnerable areas. Interestingly, the part of the zone B5, where few significant points were identified during heat, was characterized by a relatively high percentage of elderly people but also with a high prevalence of cycling paths and green roofs, with both NIL belonging to low vulnerable categories. These findings further support the evidence that environmental and infrastructural factors, such as temperature, vegetation cover, and urban design, significantly influence the spatial distribution of CV emergencies during different weather conditions, and they should be taken into account for optimizing EMS. Moreover, effective clustering serves as a foundational step towards the development of advanced models for optimizing ambulance stationing and arrival times, essential for ensuring timely responses to emergencies under both normal and extreme weather conditions, potentially leading to increased survival rates and improved patient outcomes.

5.4.5. Limitations and conclusions

The proposed framework has some limitations. The first is related to the accuracy, temporal validity and synchronicity of some of the included open data. The number of graduate residents was available, but with latest update in 2011, and it was used in relation to the total number of residents in 2020, thus possibly producing biased percentages. Also, the mean summer LST was obtained as an average for the period 2013-2017, thus not reflecting possible recent changes in the vegetation coverage and land-use, which could significantly impact local temperature variations. Moreover, the relationship between LST and air temperature has been found to be subject to spatial inconsistencies (Reiners et al., 2023), so it is still unclear if this indicator can be used as a proxy of urban heat exposure. The retrieved open data was put into relation with the ambulance dispatches in the period 2017-2022, eventually resulting in an additional, partial or total, temporal mismatch. Still, socio-urban features can be considered to have a relatively low frequency of variability, and the use of data collected within just a few years of each other could therefore be considered as an acceptable error; nonetheless, the use of updated data would be still recommendable and, when possible, should be addressed in future studies.

Furthermore, in this analysis, the NIL served as the reference unit of analysis. Their boundaries were officially established by the city of Milan, yet without any specific consideration for health-related aspects. Therefore, the NIL application may exemplify the modifiable areal unit problem (Flowerdew et al., 2008) in relation to socio-urban features and CV vulnerability which indeed did not differ significantly across socio-urban clusters. This problem arises due to the inherent variability in spatial data that can occur when point (e.g., CV emergencies) or continuous (e.g., LST) observations are aggregated into different areal units, leading to potential changes in statistical relationships and outcomes. Different aggregation schemes can yield different patterns and associations, as smaller units may capture local variability more accurately but could also introduce noise, while larger units may oversimplify spatial patterns, smoothing or averaging continuous spatial patterns and thus masking fine-scale variability or hotspots. Also, the incorporation of the mean, affected by outliers and non-normal distributions, in Moran's Index may have introduced biases in the identification of spatial correlations Sensitivity analyses could help assess the robustness of

results. However, in light of the practical relevance of our analysis for decision-makers, the NIL division was chosen as the official reference partition for local policymaking.

While our findings offer a map highlighting highly and low vulnerable zones, representing a proactive approach, a notable challenge emerges regarding the practical application of these results in real-time scenarios, especially those regarding the HDBSCAN. This challenge arises from the definition of heat days, which are identified as those with the AT surpassing a percentile threshold of its annual distribution; accordingly, the classification of a heat day could not be made in advance, posing difficulties in planning strategies. Moreover, not only the annual distribution of AT is unknown in advance, but also the mean daily AT for future days could only be derived from weather forecasts, which introduces an additional source of bias into the classification process. Consequently, relying on meteorological forecasts and an approximative heat threshold, it could lead to inaccurate a priori determinations, resulting in the preparedness for an incorrect spatial distribution of emergencies.

As the k-means algorithm is a common technique for a series of problems, many approaches for the selection of the optimal number of clusters have been proposed beyond what was used here, including the gap statistic (Tibshirani et al., 2001), canopy clustering (Yuan, & Yang, 2019) and the Calinski-Harabasz index (Maulik & Bandyopadhyay, 2002). However, no method allows the deterministic identification of a unique optimal solution (Ikotun et al., 2023). In this study, the optimal number of clusters k was defined using a combination of four decisional methods, all of them indicating of k=3 as an appropriate dimensioning, yet, some uncertainty was still present. In fact, while the elbow point was not distinctly visible, the Davies-Bouldin index was relatively high, and the silhouette coefficient was close to zero, thus indicating that the clusters may not be very well separated, and the observations may therefore be close to the decision boundaries. Nonetheless, the results of the statistical tests showed the merits of such choice, with almost all the considered features showing significant differences among the three clusters.

As real geographical coordinates were utilized for HDSCAN, the Haversine distance was employed to account for Earth's curvature. This approach limited the density-based clustering analysis to just two features (i.e., longitude and latitude), while the inclusion of other factors and potential confounders might have provided further insights. Nevertheless, research by Maria et al. (2020) indicates that the difference between the Haversine and Euclidean distances, with the latter allowing for the inclusion of multiple features, is small for relatively small areas such as a city. Furthermore, as illustrated in Table 5.6, significant differences were observed in the fraction of elderly patients and fatal emergencies, which suggests that incorporating such features into the clustering process could yield valuable insights. Additionally, an arbitrary range of minimum cluster size for both heat and non-heat days, without any scientific rationale, was tested. Also, the identification of zones of interest relied solely on visual analysis, potentially resulting in overlooked findings. Future research could address these limitations by conducting further spatial distribution analyses relevant to HDBSCAN results using statistical methods such as Ripley's L function or Moran’s Index. Additionally, adjustments to the clustering algorithm could be made, including sensitivity analyses of DBSCAN with respect to epsilon and m_pts based on the quantity of ambulances and reachability time specifically for the city of Milan. Moreover, the implementation of fuzzy

clustering could be considered for increased flexibility, as well as a more detailed temporal dimension, which could greatly benefit EMS management problems.

Regarding the regression analysis, due to the insufficient number of observations, the socio-urban cluster including the most peripheral NIL had to be excluded from cluster-level analysis, thus impeding the evaluation of possible differences in urban and suburban zones. Given the underexplored nature of spatial regression modelling in socio-urban studies related to health, common guidelines for model selection and restriction have yet to be established. Consequently, our choice of a combination of AIC and likelihood ratio for model selection may have led to the selection of an unsuitable equation. Furthermore, the failure to meet several model assumptions could introduce bias into our findings.

Finally, previous research showed that the spatial distribution of either mortality or morbidity of CV diseases is heterogeneous (Mena et al., 2018), and in our study we did not differentiate between fatal and non-fatal emergencies. Further research should continue addressing the spatial analysis of CV_VtoH and SU_VtoH, especially stratifying for morbidity and mortality, which is crucial for the efficient management of EMS in the city.

In conclusion, in this study, a novel holistic framework to assess the direct and indirect impact of socio-urban characteristics on population CV_VtoH in different parts of a big city was proposed, taking into account local variability through the application of different spatial models, and considering the geolocalized data originating from the EMS as a spatially dis-aggregated proxy for CV health issues. The proposed framework has the potential not only to delineate areas of elevated CV and socio-urban vulnerability to heat but also to empower policymakers, urban planners, and healthcare professionals with a tangible metric that informs targeted interventions and resource allocation, ultimately equitably preventing urban citizens from becoming patients.

Further research on relevant topic could address several underexplored areas in the literature. First, incorporating behavioural factors like mobility patterns and access to cooling resources into spatial vulnerability assessments could provide additional insights for equitable heat resilience strategies. Second, conducting comparative studies across cities with different socio-urban and historical contexts could reveal commonalities and differences in vulnerability, helping identify transferable best practices for global urban heat resilience. Finally, engaging stakeholders, such as policymakers, urban planners, and community members, ensures that findings are relevant, actionable, and tailored to local needs through participatory approaches.

Chapter 6. Impact of meteorological variables on daily cardiovascular emergencies forecast: an explainable artificial intelligence approach

The content of this chapter is an elaborated version of the following publication:

- Nawaro, J., Gianquintieri, L., Pagliosa, A., Sechi, G. M., & Caiani, E. G. (2024). Impact of meteorological variables on daily cardiovascular emergencies forecast during heat and non-heat days: an explainable artificial intelligence approach. Manuscript submitted to *ACM Transactions on Computing for Healthcare*.

Highlights:

- RQ5: How can artificial intelligence be used to forecast CV emergencies in a big city considering meteorological parameters?
- XGBoost, CatBoost and LSTM algorithms demonstrated strong predictive performance for CV emergency volume, with error rates nearing the random noise component of the time series.
- XAI revealed minimal effects of temperature on CV emergency volume prediction on most days but a significant increase during the hottest days.
- Trade-off between prediction accuracy and spatial resolution suggests that further optimization of ML-based solutions is needed to capture the dynamics of urban environments.

6.1. Introduction

The term “artificial intelligence" (AI) has been defined by John McCarthy as "the science and engineering of making intelligent machines" (Azer and Guerrero, 2023). The main task of machine learning (ML), a subset of AI, largely combining computer science and statistics, is to build systems that automatically improve with experience. For many learning problems, this approach represents a more time- and cost-efficient scenario compared to designing frameworks by anticipating every possible input-output pair (Helm et al., 2020). One of the three main ML paradigms, along with unsupervised and reinforcement, is supervised ML that handles labelled data in the attempt to predict or classify the correct output given the input, finding potential applications in time series forecasting. Recent research has increasingly focused on the implementation of ML models in this predicting task, providing evidence that AI-based methods, that often do not require rigorous assumptions regarding the data, can outperform traditional approaches, such as the autoregressive integrated moving average model (ARIMA) or seasonal ARIMA (SARIMA), particularly when applied to large datasets (Masini et al., 2023; Cerqueira et al., 2019; Parmezan et al., 2019).

Nonetheless, even when ML algorithms achieve satisfactory performance, they are often criticised for their lack of explainability and/or interpretability, especially in high-risk applications, such as those related to healthcare (Leichtmann et al., 2023; Praveen and Joshi, 2022). However, since 2018 there has been a considerable increase in articles implementing AI to address various problems in emergency medicine (Piliuk and Tomforde, 2023). While traditional white-box ML models, such as linear regression or decision trees, are easily interpreted by humans, more complex black-box algorithms, including ensemble methods and neural networks, often achieving better performance, sacrifice interpretability (Loyola-Gonzalez, 2019). To address this issue, recent research applying AI techniques has underlined the role of explainable artificial intelligence (XAI) capable of providing insights into the decision-making process of the algorithm (Praveen and Joshi, 2022; Angelov et al., 2021). Through the application of XAI approaches, the transparency and trustworthiness of AI-driven systems is enhanced, potentially leading to their wider adoption in real-world scenarios. The fundamental taxonomy of XAI techniques distinguishes between methods based on their stage of implementation (i.e., ante-hoc and post-hoc methods) and their scope (i.e., global and local methods), with selected methods being model-specific and the others model-agnostic (Leichtmann et al., 2023).

In the context of emergency medical services (EMS), the problem of forecasting the daily demand for hospital emergency department visits or ambulance calls has been studied extensively using both traditional statistical models and ML approaches (Jiang et al., 2023; Tang et al., 2021; Wargon et al., 2009). Due to the existing relation between environment and health, as reported through theoretical empirical analyses in previous chapters, it would be important to consider atmospheric variables in such forecasting. Interestingly, while in their systematic review of articles published up to 2007 Wargon et al. (2009) concluded that the inclusion of weather variables did not improve the model performance, a more recent review (Jiang et al., 2023) including articles published up to 2021 provided evidence that meteorological variables can influence the volume of patient arrivals in the emergency department.

As overviewed in Chapter 3, high temperatures have been shown to have a significant impact on adverse health outcomes and, as a result of ongoing climate change, heat days are becoming more frequent and intense, adding life-threatening risk. Accordingly, several recent papers have incorporated weather variables in the prediction of the demand for EMS (Sudarshan et al., 2021; Nakai et al., 2021; Ramgopal et al., 2021; Ramgopal et al., 2019; Hu et al., 2023; Martin et al., 2021; Wong 2023; Murtas et al., 2022), but relevant research implementing XAI techniques in this context remains limited (Piliuk and Tomforde, 2023). In addition, to the best of our knowledge, no study has specifically addressed the difference in the algorithm's decision-making process between extreme and normal weather conditions. Furthermore, there is still a limited consideration of the spatial dimension in EMS demand forecasting, despite its recently acknowledged significance (Martin et al., 2021).

Given the escalating trend in global temperatures and the consequential strain on EMS during heatwaves (Xu et al., 2023), it seems critical to consider weather variables in emergency demand modelling, and to explain their role in the inference process. To address the research gaps described above, and to answer the RQ5: How can artificial intelligence be used to forecast CV emergencies in a big city considering meteorological parameters, the aim of this chapter is two-fold: 1) to propose an XAI framework for the prediction of the daily demand for ambulance services; 2) to analyse the impact of the meteorological variables on the predicted output with a focus on explaining the decision-making process, separately for heat and non-heat days.

6.2. Materials and methods

The framework was tested on the city of Milan and separately on its three socio-urban clusters, i.e., Central, Residential and Peripheral, obtained though k-means clustering of the socio-urban features of 86 Nuclei of Local Identity of Milan, as described in the previous chapter. In this chapter, EMS data covering the period May-September 2017-2023 were used (i.e., including one additional year than all the previous analyses). All CV emergencies were included, with no further inclusion/exclusion criteria based on emergency place, patient's age, gender, condition on ambulance arrival, etc. Accordingly, meteorological data to calculate apparent temperature (AT) included the year 2023 as well (for calculation details please refer to Chapter 4). While heat days were defined as those with mean daily AT above the 95th percentile of its annual distribution (19 warmest days each year i.e., coherently with previous analyses), for the purposes of this study non-heat days were selected as the 19 coldest days in the period May-September for each year.

6.2.1. Statistical processing and time series analysis

Basic summary statistics of the data were computed: mean, median, minimum, maximum, 25th percentile and 75th percentile. The Kolmogorov-Smirnov test was used to test whether the data were normally distributed. Subsequently, the non-parametric Mann-Whitney U test and Kruskal-Wallis test with Bonferroni correction were performed to compare the distributions of two or multiple groups, respectively, with the significance level set to 0.05.

The stationarity of the data on daily CV emergencies represented as a time series was assessed by the Augmented Dickey-Fuller test (alpha=0.05). The data relevant to the whole

city was then decomposed into trend, seasonal component and residual, assuming the additive trend. Subsequently, the distribution of the emergencies with regard to time-related characteristics (i.e., year, month, day of week and heat or not-heat day) was graphically summarised as boxplots for each of the three socio-urban clusters.

6.2.2. Feature selection for predictive models

The choice of independent variables for the prediction models was determined on the basis of previous relevant studies that outlined four main groups of features: (i) temporal variables, (ii) lagged versions of the target variable, (iii) weather variables and (iv) socio-economic variables (Sudarshan et al., 2021; Petsis et al., 2022).

Temporal features selected as independent variables for predictive modelling, allowing to control for seasonality and long-term trend, based on descriptive analyses included in Chapter 4, were: year, month, day of the week, day of the year and summer break period (i.e., traditionally in August for Italy). As for the latter, a binary variable indicating the month of August was considered (i.e., the value of 1 was assigned to all days in August, while 0 was set for all the other days). In addition, a binary variable indicating the Coronavirus disease 2019 (COVID-19) period (i.e., 2020 and 2021) was included as independent variable for forecasting models, as it was shown in Chapter 4 that it had a significant impact on the volume of daily CV emergency calls.

As for the second group of features, the lagged version of the daily CV emergencies expressed by its autocorrelation function (ACF) up to lag 30 was examined, both for the whole city and separately for its three socio-urban clusters. The delay values included in the modelling were then determined based on the ACF.

Regarding the weather variables, the AT represented the relevant meteorological feature of which three aggregates (i.e., mean, minimum and maximum), and three lags (i.e., lag0, lag1 and lag2) were considered. In this case, a “lag” refers to the past (i.e., lag1 describing the previous day), not to the future (i.e., lag1 describing the next day), as in the case of distributed lag non-liner model performed in Chapter 4. Two common univariate feature selection methods were applied (Remeseiro & Bolon-Canedo, 2019):

- based on Pearson correlation: it calculates the correlation coefficient between the daily CV emergencies and each of the candidate meteorological features, and the best variables are those with the highest correlation with the target;
- based on mutual information: it calculates the mutual information by determining how the joint distribution of the daily CV emergencies with each of the candidate meteorological features is different from the product of the marginal distributions of these variables, and it selects the variables that bring the highest information gain.

Lastly, as the predictive models were computed for the whole city and separately for its three socio-urban clusters obtained already accounting for 11 socio-urban characteristics, as described in Chapter 5, no additional socio-economic feature was considered as an independent variable.

6.2.3. Predictive modelling

Three ML algorithms, being a common choice for time series forecasting task, were tested and compared: eXtreme Gradient Boosting (XGBoost), CatBoost and Long Short-Term Memory neural network (LSTM) (Han et al., 2019; Kontopoulou et al., 2023; Karingula et al., 2021). Both XGBoost and CatBoost use ensemble methods on decision trees, while LSTM is a type of recurrent neural network with increased memory capacity. All three algorithms are black-box models, meaning that their architectures do not give as output an explainable decision-making process. As the objective of the prediction was the number of CV emergencies expected for the next day, Mean Absolute Error (MAE) was selected to assess the model performance, while Mean Absolute Percentage Error (MAPE) was also reported for better comparison among geographical partitions.

To examine the changes in the performance metrics due to the inclusion of weather variables, each model was evaluated separately with and without their inclusion, both for the whole city and separately for its socio-urban clusters.

The dataset, consisting of the time series for the target variable (i.e., daily number of CV emergencies) and for a set of independent variables, was divided into a training set, covering the period May-September 2017-2022, and the test set, consisting of May-September 2023. Each of the three models, for the whole city or for each socio-urban cluster, and with the inclusion or exclusion of the weather variables, underwent hyperparameter tuning. For XGBoost and CatBoost, a randomized search strategy with 5-fold cross-validation was implemented, training the models with a random combination of the defined hyperparameters, while for LSTM, due to the computational effort, the hyperparameters were optimized by randomized search without cross-validation. For LSTM, the Adam optimizer, the rectified linear unit (ReLu) activation function and one hidden layer were arbitrarily chosen. The hyperparameters resulting in the lowest MAE on the test set were selected as optimal for the predictive models. The tested ranges of hyperparameters are summarized in Table 6.1, where the hyperparameters' names correspond to the names defined in the *xgboost* (Chen & Guestrin, 2016), *catboost* (Prokhorenkova et al., 2018) and *keras* (Chollet et al., 2015) Python packages.

Table 6.1. Range of values considered in setting the hyperparameters for each tested prediction model

Model	Hyperparameters set
XGBoost	n_estimators: [300, 500, 1000, 1500, 2000] max_depth: [3, 5, 7] learning_rate: [0.01, 0.1, 0.2, 0.3] subsample: [0.8, 0.9, 1.0] colsample_bytree: [0.8, 0.9, 1.0]
CatBoost	iterations: [300, 500, 1000, 1500, 2000] depth: [3, 5, 7] learning_rate: [0.01, 0.1, 0.2, 0.3] subsample: [0.8, 0.9, 1.0] colsample_bylevel: [0.8, 0.9, 1.0]
LSTM	batch_size = [8, 16, 32, 64] num_epoch = [50, 100] neuron number = [32, 64, 128]

	dropout = [0.1, 0.2, 0.3]

For each model, the difference in predictive accuracy on the test set between its version with and without the inclusion of the meteorological variables was assessed by the Diebold-Mariano test at 0.05 significance level. This test was also used to assess the pairwise difference in predictive accuracy on test set between each combination of the models (i.e., XGBoost and CatBoost, XGBoost and LSTM, CatBoost and LSTM) in each geographical partition. Considering the performance of the models including the weather variables, the one resulting in the lowest MAE on the test set was selected as the final prediction model, whose decision-making process was then explained by XAI.

A sensitivity analysis of the final models for each geographical partition was conducted by creating its five additional versions for the May-September period of the years 2017-2018, 2017-2019, 2017-2020, 2017-2021, and 2017-2022. In each iteration, the last year was used as the test set, while the remaining years formed the training set. Each of the five models underwent separate hyperparameter tuning.

In addition, the MAE on the test set from the ML models was compared against five simpler prediction models. These simpler models included: (1) predicting the number of CV emergencies during the test period as (1) the mean and (2) the median number observed between May and September 2017–2022; an autoregressive model forecasting the number as the same as (3) on the previous day and (4) as observed 7 days earlier; and (5) a moving average model that calculates the number as the arithmetic mean of the values from the two preceding days.

6.2.4. Explainable artificial intelligence

To investigate the impact of the meteorological variables on the algorithm's decision-making process, the SHapley Additive exPlanations (SHAP) technique, which is among the most commonly used XAI techniques (Saranya & Subhashini, 2023), was selected.

The SHAP method applies the concept of Shapley values from cooperative game theory, representing the average marginal contribution of each player in a game considering all possible cooperations (Lundberg & Lee, 2017). The SHAP values estimated post-hoc (i.e., after model training) are the Shapley values for a conditional expectation function of the model and they represent the contribution of each feature to the model prediction (Lundberg & Lee, 2017). Specifically, the baseline prediction was the average of the target variable (i.e., daily CV emergencies) in the training set along May-September 2017-2022, while the actual model prediction consisted in the sum of the baseline prediction and the SHAP values for all features.

The SHAP value is calculated for each feature for each prediction, making the SHAP a local XAI technique. However, it is also possible to use it on a global scale by summarising the impact of each variable on multiple predictions and visualising it as a summary plot. The technique is model agnostic, meaning that it can be applied to all the three tested algorithms, i.e., XGBoost, CatBoost and LSTM.

The summary plot is a scatterplot that ranks the variables according to the strength of their effect (i.e., the average of the absolute SHAP values), with the highest contributing variables at the top of the y-axis. Each dot in it represents the SHAP value associated with each

prediction for the relevant feature; in addition, the dots are color-coded on a continuous scale, with red corresponding to a high feature value and blue to a low feature value. In this study, the summary plot was shown separately for the predictions on heat days and non-heat days in each of the considered geographical partitions.

Another form of graphical representation is the dependence plot, showing the relationship between a feature value (on the x-axis) and its SHAP value (on the y-axis) for all the observations. For the purposes of this study, the dependence plot was used for the highest contributing meteorological variable. Predictions corresponding to heat days were highlighted, and the ordinary least squares (OLS) regression line was fitted to them.

6.3. Results

6.3.1. Characteristics of apparent temperature and cardiovascular emergencies

The summary statistics for AT each year from 2017 to 2022 were reported in Table 4.2 in Chapter 4. In 2023, heat threshold was set at AT=30.7 °C, i.e., the highest across all the years, while no extremes in any other statistic were found for 2023.

In the period May-September 2017-2023, there were a total of 75,728 CV emergencies in Milan, of which 37,942 (50.1%) occurred in the Central cluster, 36,865 (48.68%) in the Residential cluster and only 921 (1.22%) in the Peripheral cluster. During the analysed period, there were cumulatively 133 heat days, during which 9,268 (12.24%) CV emergencies occurred, while 9,805 (12.95%) occurred during non-heat days. Considering each cluster, 12.15% of the emergencies occurred on heat days in the Central cluster, 12.33% in the Residential cluster and 12.16% in the Peripheral cluster.

The Augmented Dickey-Fuller test indicated that the time series of daily CV emergencies were stationary for all the three socio-urban clusters. The time series of daily CV emergencies for the whole city of Milan, decomposed into trend, seasonal component and residual, are presented in Figure 6.1. The overall trend shows considerable decrease towards August, and a rising trend from the end of August, illustrating the holiday effect, analysed in Chapter 4. However, in 2020, possibly due to COVID-19 lockdowns and the fear of hospitalization, this characteristic was less apparent, with the daily number of emergencies relatively lower and stable throughout the months. In addition, a particularly large peak in the trend of 2019 is noticeable, occurring on 27-28/06/2019 when the mean daily AT recorded the highest and the second-highest value in the analysed period, respectively.

Figure 6.1. Time series of daily cardiovascular (CV) emergencies in Milan in May-September 2017-2023, decomposed into trend, seasonal component and residual. Red dots indicate heat days based on the applied criterion (see text for further detail). Mean daily apparent temperature (AT) is also shown overimposed to the daily emergencies.

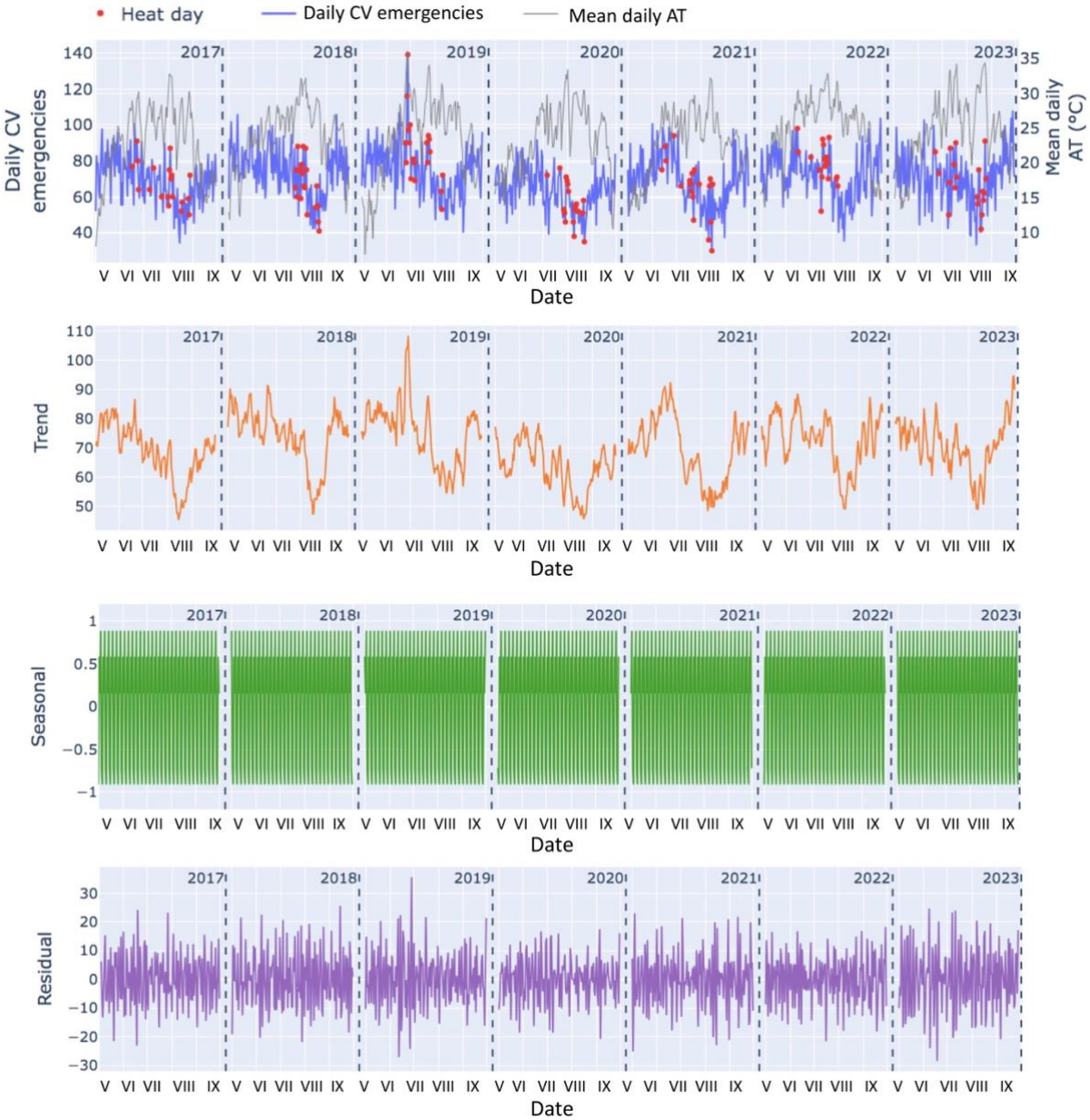

Based on the Kolmogorov-Smirnov test, the daily number of CV emergencies resulted not normally distributed in both the whole city and in its three socio-urban clusters. The median daily number of CV emergencies in the whole city during the analysed period was 71 (25th-75th percentile 61-80). Stratifying by socio-urban clusters and temporal variables, the highest median in the Central cluster was reached in 2019 (39 emergencies), while in the Residential cluster in both 2018 and 2019 (36 emergencies for both years). The lowest median was observed in 2020 in the Central cluster (29 emergencies), and in both 2017 and 2020 in the Residential cluster (33 emergencies for both years). For these clusters, in 2020, in addition to a low median, the distribution of daily CV emergencies was characterised by a relatively narrow interquartile range, as illustrated in Figure 6.2. The median daily number was equal to

1 for all years in the Peripheral cluster. As indicated by the Kruskal-Wallis test, the difference in the distribution across years was statistically significant for both the Central and Residential clusters, but not for the Peripheral cluster.

In terms of month, the highest median daily number of CV emergencies in both the Central and the Residential clusters was observed in June (39 and 37 emergencies, respectively). On the contrary, August was the month with their lowest median daily number for both the Central (27 emergencies) and the Residential (28 emergencies) clusters. Furthermore, May was the only month for which no outlier was observed in the Central and the Residential clusters, as shown in Figure 6.2. The median daily number was again the same for each month in the Peripheral cluster. There was a statistically significant difference in the distribution across months for both the Central and Residential clusters, while the difference was not significant for the Peripheral cluster.

The distribution of daily number of CV emergencies differed significantly across the days of the week only for the Central cluster, in which the day with the highest median was Tuesday (38 emergencies), while it was Monday for the Residential cluster (36 emergencies). Conversely, the lowest median number was observed at the weekend - on Sunday in the Central cluster (32 emergencies) and on Saturday in the Residential cluster (33 emergencies). In this case as well, the median daily number was the same for each day of week in the Peripheral cluster. Moreover, the second half of the week was characterised by particularly high outliers in all three socio-urban clusters, represented by dots in Figure 6.2.

When stratified by heat and non-heat days, the difference in the distribution of the daily number of CV emergencies was significant only in the Residential cluster, where the median reached 37 emergencies during non-heat days, and 34 during heat days, but with an outlier equal to 65 emergencies.

The distribution of the daily number of CV emergencies in each of the three socio-urban clusters, stratified by temporal variables (i.e., year, month, day of the week and heat days) was graphically summarised as boxplots in Figure 6.2. The difference in the distribution was statistically significant for the following variables, providing rationale for their inclusion in the forecasting models:

- in the Central cluster for year, month and day of week;
- in the Residential cluster for year and month;
- in the Peripheral cluster for none of the considered variables.

Figure 6.2. Summary of the distribution of the daily number of cardiovascular (CV) emergencies in May-September 2017-2023 for each of the three socio-urban clusters of Milan (i.e., Central, Residential, Peripheral), stratified by year, month, day of the week and heat days

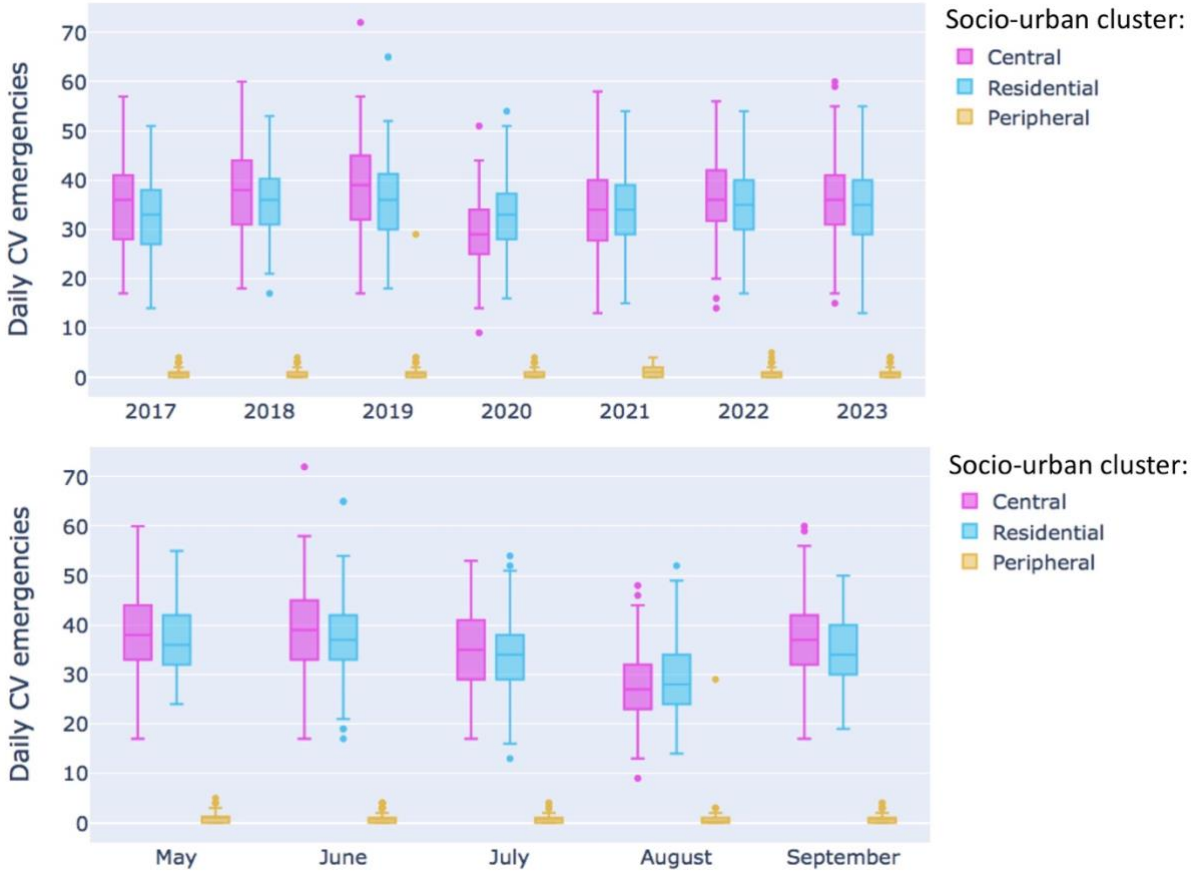

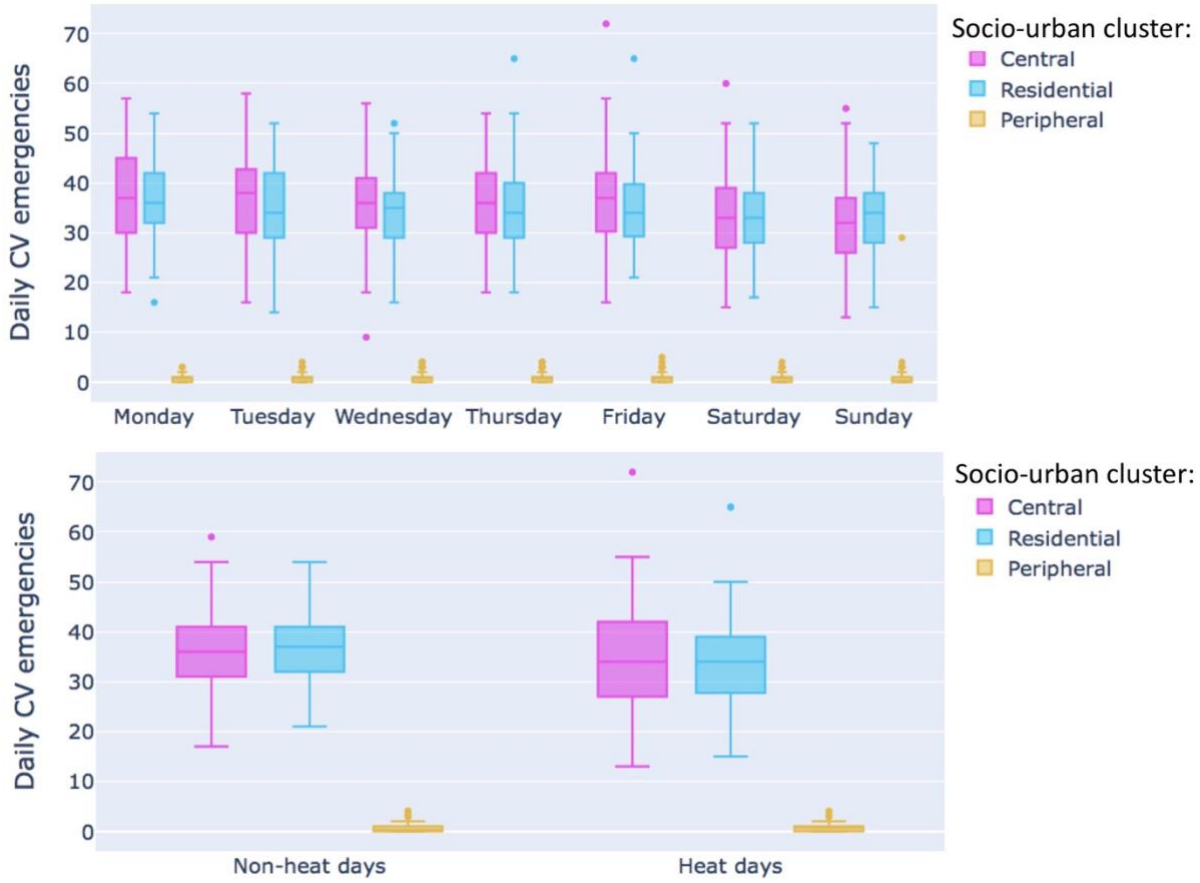

6.3.2. Feature selection for predictive modelling

The autocorrelation plots for daily CV emergencies for the whole city and separately for the three socio-urban clusters are presented in Figure 6.3. The ACF for the whole city showed a strong autocorrelation at lag 1, equal to 0.46, decreasing up to lag 5 when it reached the value of 0.34, and then increasing up to lag 7 at 0.41. The same pattern, although weaker in terms of values, was observed in the second week. From the third week, the autocorrelation started to decrease over time, again with a small peak at lag 21. In addition, in the fourth week, the autocorrelation became not significant.

A similar pattern was found in the Central cluster, in which the ACF was the strongest at lag 1 (0.43). For the next three lags, it reached similar values equal to 0.35, 0.36, and 0.34, respectively, and it peaked at lag 7 reaching the value of 0.39. From the second week, the autocorrelation began to considerably decrease, with small peaks at lags 14 and 21. Given these findings, the lags selected for the prediction model for both the whole city and for the Central cluster were lags 1, 2 and 7.

The autocorrelation in the Residential cluster was much weaker, with a maximum of 0.26 at lag 1 and similar (0.24) at lag 2. At lag 3, the autocorrelation dropped to 0.18 and it remained fairly stable and significant until lag 12, when it fell below 0.10 for the first time. Therefore, for this cluster, only lags 1 and 2 were considered in the forecasting model.

In the case of the Peripheral cluster, the ACF did not provide any significant lag. Given the very small number of daily CV emergencies and the lack of autocorrelation, no prediction model was performed for this cluster.

Figure 6.3. Autocorrelation plots for daily cardiovascular emergencies in May-September 2017-2023 in the whole city and for its three socio-urban clusters (i.e., Central, Residential, Peripheral). Results outside the shaded area are significant at alpha=0.05.

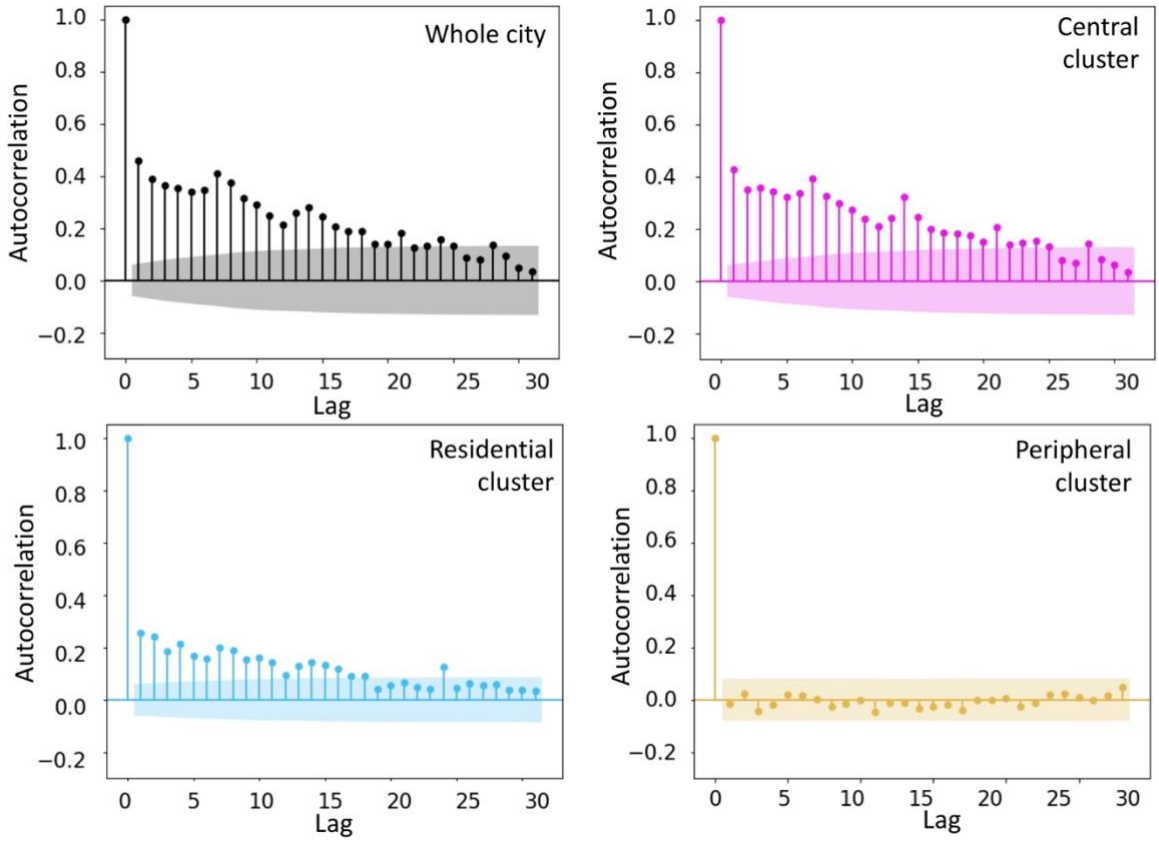

For the meteorological variables, three aggregates (i.e., mean, minimum and maximum), and three lags (i.e., lag0, lag1 and lag2) were considered. All six variables were highly correlated to each other, with Pearson correlations ranging from r=0.78 to r=0.99. The three best parameters obtained by the two applied feature selection methods for the whole city, the Central and the Residential clusters are summarised in Table 6.2. As the methods did not yield the same set of variables, and given a high correlation among the aggregates, the final three temperature indicators were chosen arbitrarily as mean daily AT (i.e., lag0), mean daily AT at lag1 (i.e., AT on the previous day), and mean daily AT at lag2 (i.e., AT two days before). In a real-world application of the forecasting model, the value of the mean daily AT at lag0 (i.e., the day for which the daily number of CV emergencies needs to be predicted) could be derived from existing meteorological forecasts.

Table 6.2. Apparent temperature aggregates returned by the feature selection methods in the whole city, the Central cluster and the Residential cluster

Method/socio-urban cluster	Whole city	Central cluster	Residential cluster
Pearson correlation	mean, minimum, maximum	mean, minimum, maximum	mean, minimum, maximum
Mutual information	lag1 minimum,	mean,	lag 1 mean,

	lag 1 maximum, lag 2 mean,	lag 2 mean, lag 2 minimum	lag 2 mean, lag 2 maximum

In conclusion, five temporal variables and the COVID-19 binary variable were included as independent variables in the prediction models. In addition, the lagged number of CV emergencies was considered, with the lags chosen on the basis of the ACF. Finally, for models with weather features, three meteorological variables were incorporated in the set of independent variables. The final variables included in each prediction model for the whole city, the Central and the Residential clusters, together with their description, are summarised in Table 6.3. To take into account the lag in the prediction of the number of CV emergencies assumed by the model, each annual time series for the prediction models started on May 3rd for the Residential cluster, and on May 8th for the whole city and the Central cluster. The total number of variables included in the models was 12 for the whole city and the Central cluster, and 11 for the Residential one.

Table 6.3. Final independent variables included in the prediction models for the whole city, the Central cluster and the Residential cluster. AT – apparent temperature, CV – cardiovascular.

Variable	Socio-urban cluster	Description
Year	Whole city, Central, Residential	An integer from 2017 to 2023
Month		An integer from 5 to 9
Day of the week		An integer from 0 to 6
Day of the year		An integer from 123 (Residential cluster) or 128 (whole city and Central cluster) to 273
COVID-19		A binary value of 1 for COVID-19 period (2020-2021) and 0 for other years (2017-2019, 2022-2023)
August		A binary value of 1 for August and 0 for other months
(optionally) Lag0 mean daily AT		A float value of mean daily AT
(optionally) Lag1 mean daily AT		A float value of mean daily AT a day before
(optionally) Lag2 mean daily AT		A float value of mean daily AT two days before
Lag1 CV emergencies		An integer number of CV emergencies which occurred a day before
Lag2 CV emergencies		An integer number of CV emergencies which occurred two days before
Lag7 CV emergencies	Whole city, Central	An integer number of CV emergencies which occurred seven days before

Accordingly, after excluding first eight days of May, 19 coldest days in the remaining period were classified as non-heat days. The mean daily AT on non-heat days varied from 9.12 °C in 2019 to 21.95 °C in 2022, with average mean daily AT equal to 16.61 °C (25th-75th percentile 15.12 °C-17.96 °C). Summary statistics of mean daily AT for heat and non-heat days separately for each year are reported in Table 6.4.

Table 6.4. Descriptive statistics of the mean daily apparent temperature during heat and non-heat days (as defined in section 6.2) in Milan, Italy.

Year	Heat/non-heat days	Minimum (°C)	25th percentile (°C)	Median (°C)	75th percentile (°C)	Maximum (°C)
2017	Heat	28.34	29.08	29.35	30.82	32.8
	Non-heat	14.14	14.97	16.41	17.28	18.37
2018	Heat	28.29	28.96	29.43	31.38	32.19
	Non-heat	12.22	15.74	17.93	18.97	20.32
2019	Heat	29.27	30.62	31.21	33.41	36.03
	Non-heat	9.12	13.82	16.56	16.98	18.07
2020	Heat	28.68	29.22	29.95	30.50	33.36
	Non-heat	10.46	16.01	17.40	18.14	19.05
2021	Heat	27.68	28.44	28.90	29.55	32.17
	Non-heat	13.10	15.20	16.32	18.47	19.06
2022	Heat	29.92	30.39	30.64	31.57	32.86
	Non-heat	14.52	15.34	16.42	17.46	21.95
2023	Heat	30.7	31.20	32.75	33.58	34.36
	Non-heat	14.57	16.43	18.96	20.06	21.07

6.3.3. Predictive modelling

The optimal hyperparameters, indicated by a randomized search, for XGBoost, CatBoost, and LSTM, are reported in Table 6.5, together with the resulting MAE on the test set (i.e., daily CV emergencies in May-September 2023). All models except for CatBoost in the whole city slightly improved their performance when also including weather variables. However, the difference in predictive accuracy between the model with and without meteorological features was statistically significant only for XGBoost for the Residential cluster. Considering each combination of geographical partition and inclusion of meteorological features, the resulting MAE showed minimal differences, and the differences in predictive accuracy among the models were not statistically significant in any of the three geographical partitions. As such, all the model diagnostics in the following parts will refer to the XGBoost model, including the AT features for the whole city, the Central and the Residential clusters.

Regarding the sensitivity analysis, performing XGBoost model with meteorological variables for different sets of year resulted in MAE on the test set ranging from 8.52 CV emergencies for the years 2017-2020 to 11.64 CV emergencies for the years 2017-2018 in the whole city (Table A6.1 in Appendix), from 5.83 to 7.34 CV emergencies for the years 2017-2022 and 2017-2018 respectively in the Central cluster (Table A6.2 in Appendix), and from 5.66 to 6.89 CV emergencies for the years 2017-2022 and 2017-2018 respectively in the Residential cluster (Table A6.3 in Appendix).

Table 6.5. The optimal hyperparameters for XGBoost, CatBoost and LSTM trained on train set (i.e., May-September 2017-2022), and the corresponding Mean Absolute Error (MAE) on the test set (i.e., May-September 2023)

Model	Socio-urban cluster	Weather variables	Optimal hyperparameters	MAE on test set
XGBoost	Whole city	yes	colsample_bytree = 1.0, learning_rate = 0.01, max_depth = 3, n_estimators = 500, subsample = 1.0	9.61
		no	colsample_bytree = 0.9, learning_rate = 0.01, max_depth = 7, n_estimators = 300, subsample = 0.8	9.82
	Central	yes	colsample_bytree = 0.8, learning_rate = 0.01, max_depth = 7, n_estimators = 500, subsample = 0.9	5.98
		no	colsample_bytree = 1.0, learning_rate = 0.01, max_depth = 7, n_estimators = 500, subsample = 0.8	6.07
	Residential	yes	colsample_bytree = 0.8, learning_rate = 0.01, max_depth = 7, n_estimators = 300, subsample = 1.0	6.34
		no	colsample_bytree = 0.9, learning_rate = 0.01, max_depth = 3, n_estimators = 500, subsample = 0.8	6.71
CatBoost	Whole city	yes	iterations = 1500, depth = 3, learning_rate = 0.01, subsample = 1.0, colsample_bylevel = 0.8	9.63
		no	iterations = 300, depth = 3, learning_rate = 0.01, subsample = 0.9, colsample_bylevel = 1.0	9.57
	Central	yes	iterations = 1500, depth = 3, learning_rate = 0.01, subsample = 0.8, colsample_bylevel = 0.8	5.67
		no	iterations = 500, depth = 3, learning_rate = 0.01, subsample = 1.0, colsample_bylevel = 0.9	5.77
	Residential	yes	iterations = 2000, depth = 3, learning_rate = 0.01, subsample = 0.8, colsample_bylevel = 0.9	6.44
		no	iterations = 1000, depth = 3, learning_rate = 0.1, subsample = 1.0, colsample_bylevel = 0.9	6.61
LSTM	Whole city	yes	batch_size = 64, num_epoch = 50, neuron number = 128, 64, 32, dropout = 0.3	10.01
		no	batch_size = 16, num_epoch = 50, neuron number = 128, 128, 64, dropout = 0.3	10.25
	Central	yes	batch_size = 64, num_epoch = 100, neuron number = 128, 64, 64, dropout = 0.1	6.32
		no	batch_size = 8, num_epoch = 50, neuron number = 128, 128, 128, dropout = 0.3	6.53
	Residential	yes	batch_size = 16, num_epoch = 50, neuron number = 128, 128, 64, dropout = 0.1	6.54
		no	batch_size = 16, num_epoch = 50, neuron number = 128, 128, 64, dropout = 0.3	6.64

Regarding the comparison with simpler models, all of them yielded bigger MAE in each socio-urban cluster compared to XGBoost (Table 6.6).

Table 6.6. The Mean Absolute Error (MAE) on the test set (i.e., May-September 2023) for five simpler models. For details see section 6.2.3.

Model – forecasted number of CV emergencies equal to	Socio-urban cluster	MAE on test set
Mean (of the training set)	Whole city	11.52
	Central	6.89
	Residential	6.73
Median (of the training set)	Whole city	11.61
	Central	6.92
	Residential	6.73
The previous day	Whole city	13.41
	Central	8.0
	Residential	8.78
7 days earlier	Whole city	12.53
	Central	7.85
	Residential	8.2
Arithmetic mean of two preceding days	Whole city	12.3
	Central	7.53
	Residential	7.47

In general, XGBoost forecast was able to capture the overall shape of the daily CV emergencies curve, but it was unable to accurately predict peaks in any of the geographical partitions, especially in the Residential cluster, as shown in Figure 6.4. The MAPE for all three geographical partitions was higher during heat days (14.56%, 16.57%, 22.21% for the whole city, the Central cluster and the Residential cluster respectively) than in non-heat days (10.89%, 15.93%, 16.68% respectively), but it was lower during the remaining days, i.e., days not classified as heat nor non-heat (16.14%, 19.29%, 22.98%). However, in each geographical partition, according to the Kolmogorov-Smirnov test, the absolute percentage errors for both heat and non-heat days were not normally distributed, and their distribution in both defined meteorological conditions was the same, as indicated by the Mann-Whitney U test. The distribution of the absolute percentage errors is summarized in Figure 6.5. Its lowest median during heat was reached for the whole city (10.71%), then for the Central cluster (11.55%), with the highest median for the Residential cluster (18.12%). Contrary to the mean (i.e., MAPE), the median absolute percentage error was lower during heat than non-heat days in one geographical partition – the Central cluster.

Figure 6.4. True and predicted values of daily cardiovascular (CV) emergencies in May-September 2023 in the whole city, the Central cluster and the Residential cluster. Red dots indicate heat days on the true values curve, orange dots – on predicted values curve. Violet dots indicate non-heat days on the true values curve, blue dots – on predicted values curve.

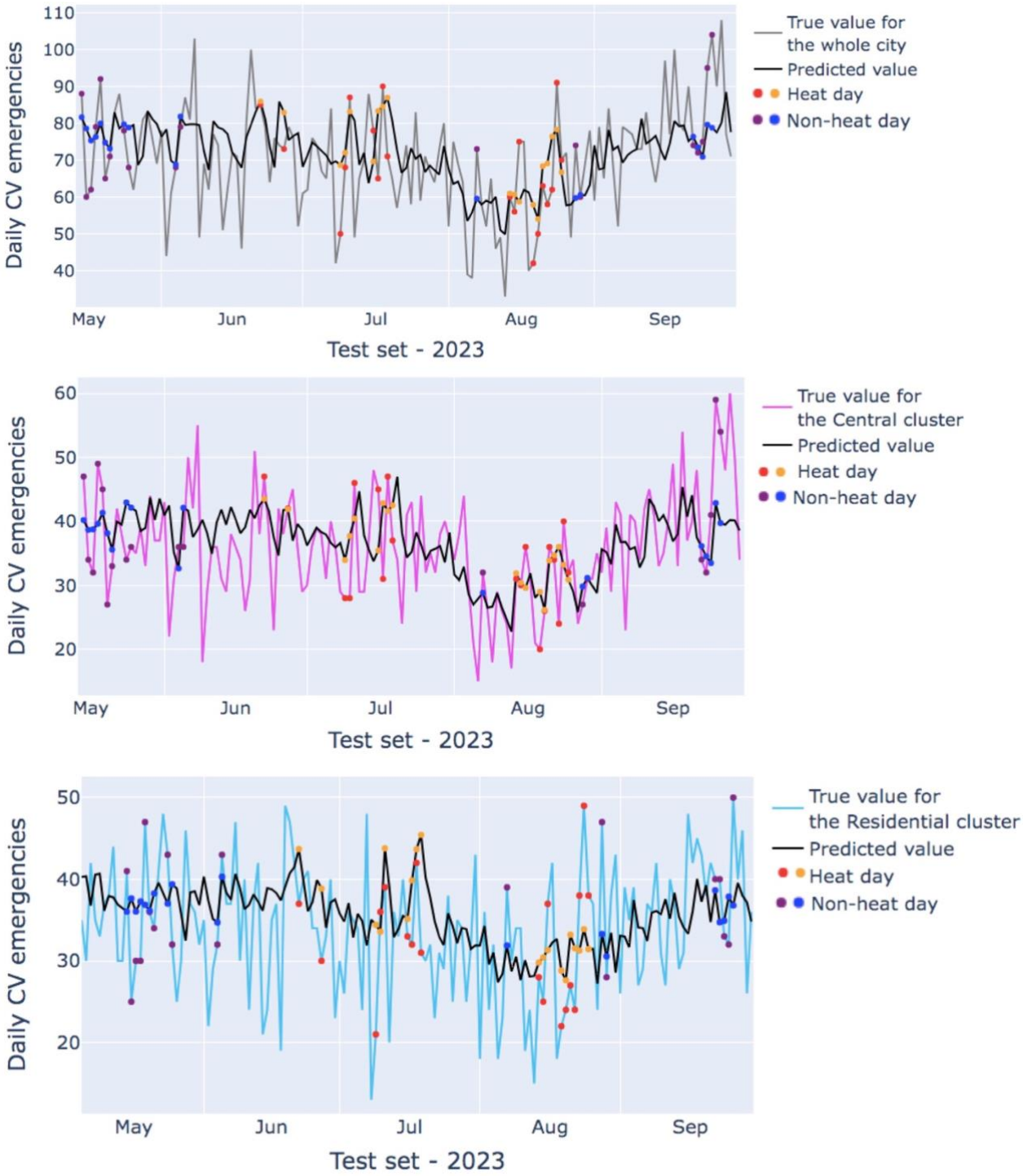

Figure 6.5. Density plot and rug plot of absolute percentage errors on test set (i.e., May-September 2023) in the whole city, the Central cluster and the Residential cluster

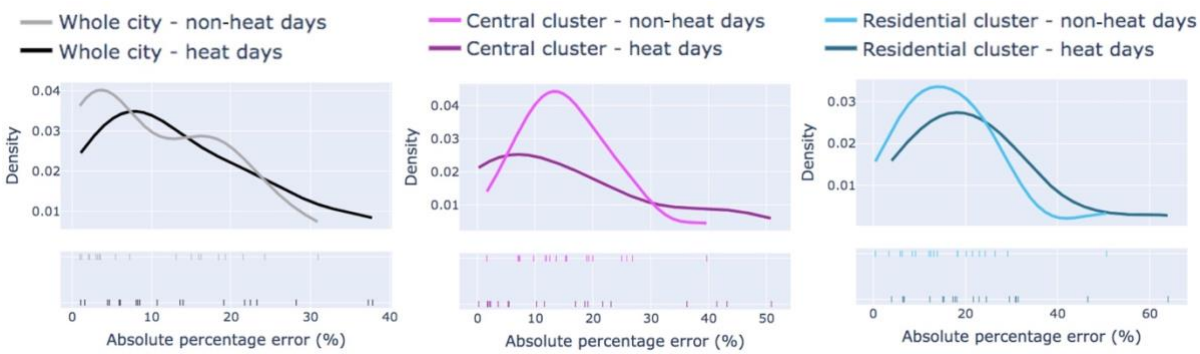

6.3.3. Explainable artificial intelligence

The final step in the analysis was to explain the XGBoost algorithm using the SHAP method. In the whole city and in the Residential cluster, the weather variables contributed more to the decision-making process during heat than non-heat days, with mean daily AT at lag0 being the strongest contributor. The distribution of SHAP values during heat and non-heat days was significantly different for the mean daily AT at all lags (i.e., lags 0, 1 and 2) in all three geographical partitions. Moreover, the varying contributions of temporal variables, as revealed by SHAP, partially account for the superior performance of the ML model compared to simpler forecasting approaches that rely exclusively on past values of the target variable during specific periods, such as one, two, or seven previous days, regardless of other characteristics, e.g., day of the year or holiday period. The summary plot of the SHAP values is presented in Figure 6.6.

In the whole city, the mean daily AT at lag0 was the strongest contributor among all the meteorological variables both during heat and non-heat days. Considering the strength of contribution of all the independent variables, it rose from fifth place during non-heat days to third place during heat days, with the difference of 0.8 in the median of the absolute SHAP values. Specifically, the median SHAP value changed from -1.3 during non-heat to 2.1 during heat days, with higher feature value associated with a higher positive contribution. The maximum contribution of the mean daily AT at lag0 during heat days was equal to 9.04, ranking as the fourth-highest among all variables, following the lag1 mean daily AT and the lag1 CV emergencies which exceeded the SHAP value of 12 for three observations. Additionally, while the lag1 of the AT was the second-lowest contributing variable during non-heat days, it rose by five positions during heat days. Interestingly, on non-heat days, lower values of the lag1 and lag2 mean daily AT increased the forecasted number of CV emergencies.

The mean daily AT at lag0 was the highest contributing variable in the Central cluster in non-heat days, and the third-highest during heat. On heat days, the SHAP values tended to be concentrated around the median of 1.82, with a relatively narrow min-max range from 0.54 to 4. While during non-heat days, the AT lagged by one day placed as the third-lowest contributor, during heat days, the impact of its highest values on the model prediction was considerable, reaching the maximum value of 6.04, the highest among all 12 considered variables.

In the Residential cluster, during non-heat days, the contribution of the mean daily AT at lag0 was the lowest among the three meteorological variables. Remarkably, it rose to the second place during heat days, with SHAP values ranging from -0.12 to 7.12. In this cluster, during heat days, all three meteorological variables were in the top five strongest contributors, along with the day of year and the August variable. In particular, the highest SHAP value equal to 8.58 was reached by the mean daily AT at lag1.

Figure 6.6. Summary plot of SHAP values for XGBoost algorithm on the training set (i.e., May-September 2017-2022) in the whole city, the Central cluster and the Residential cluster during heat and non-heat days

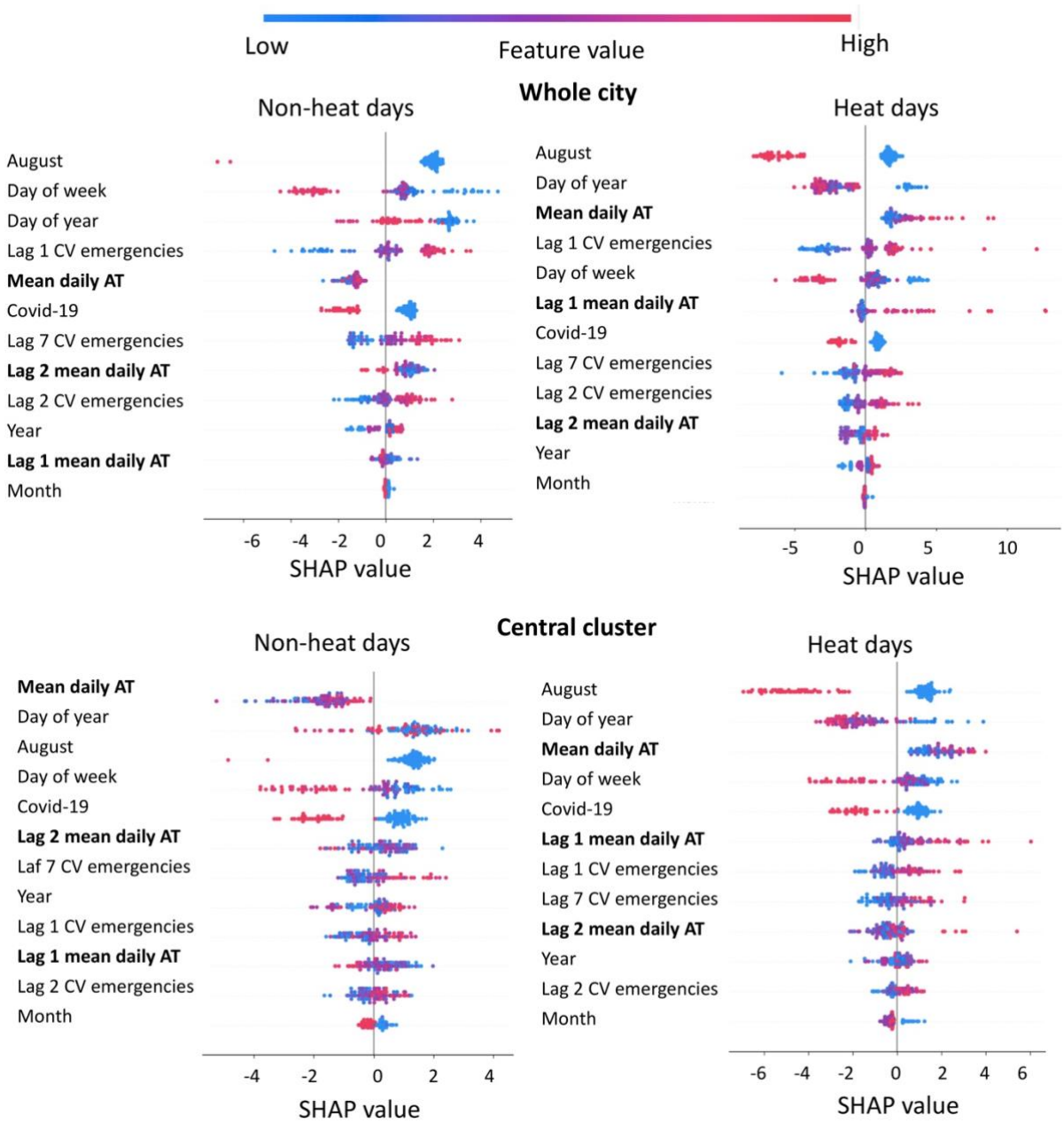

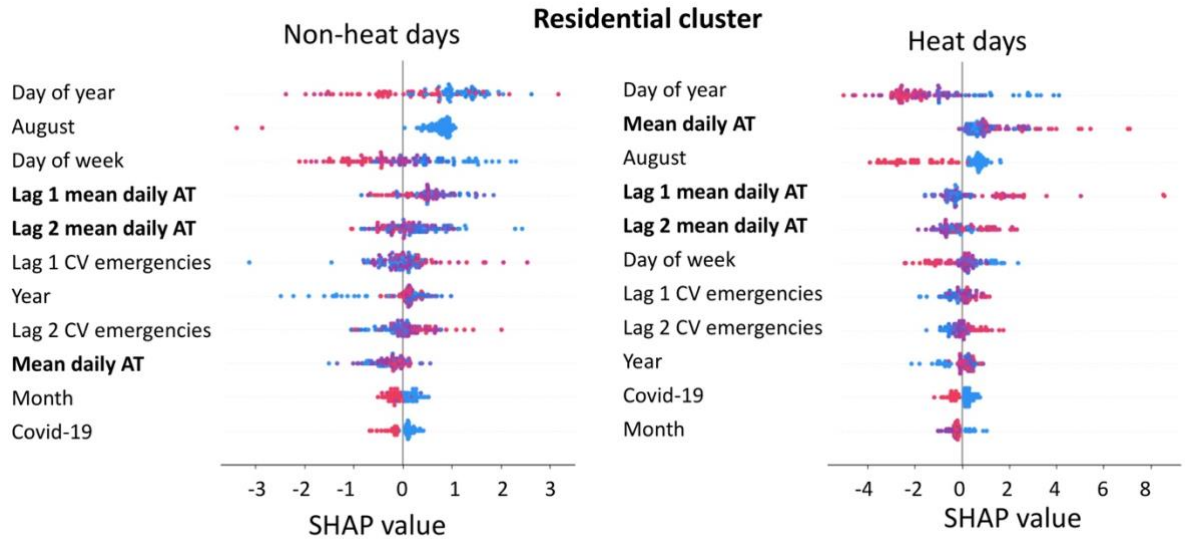

In Figure 6.7, the relationship between the mean daily AT at lag0 (i.e., the strongest contributor among the weather features) and the associated SHAP values is illustrated for all three geographical partitions. In the whole city, the plotted points initially exhibited a flat pattern until around 25 °C, beyond which higher values of AT corresponded to more elevated SHAP values. Considering heat days only, as defined in section 2.1, the relationship observed was well-captured by an OLS regression line, yielding an R^2 value of 0.79.

In the Central cluster, an increasing linear relationship was observed for the mean daily AT at lag0 below 20 °C, with the lowest AT values exhibiting relatively dispersed SHAP values. Then, between 20 °C and 25 °C, the points formed a rather flat shape, and again from the mean daily AT of 25 °C, another linear relationship began to emerge, albeit characterized by a lower slope compared to the entire city. The resulting R^2 for heat days in this cluster was equal to 0.67.

Finally, in the Residential cluster, a pattern similar to the whole city was noted. However, in this case, lower values of the mean daily AT at lag0 were characterized by a greater dispersion of SHAP values. Moreover, many observations corresponding to temperatures between the lowest 2017-2022 heat threshold, i.e., 27.7 °C, and around 32 °C were assigned to SHAP values below 2, not much higher than those below the heat threshold. The linear OLS regression for heat days in this cluster yielded an R^2 of 0.73.

Figure 6.7. Relationship between the mean daily apparent temperature (AT) and the SHAP values on the training set (i.e., May-September 2017-2022) in the whole city, the Central cluster and the Residential cluster, and the ordinary least squares regression line fitted to heat days.

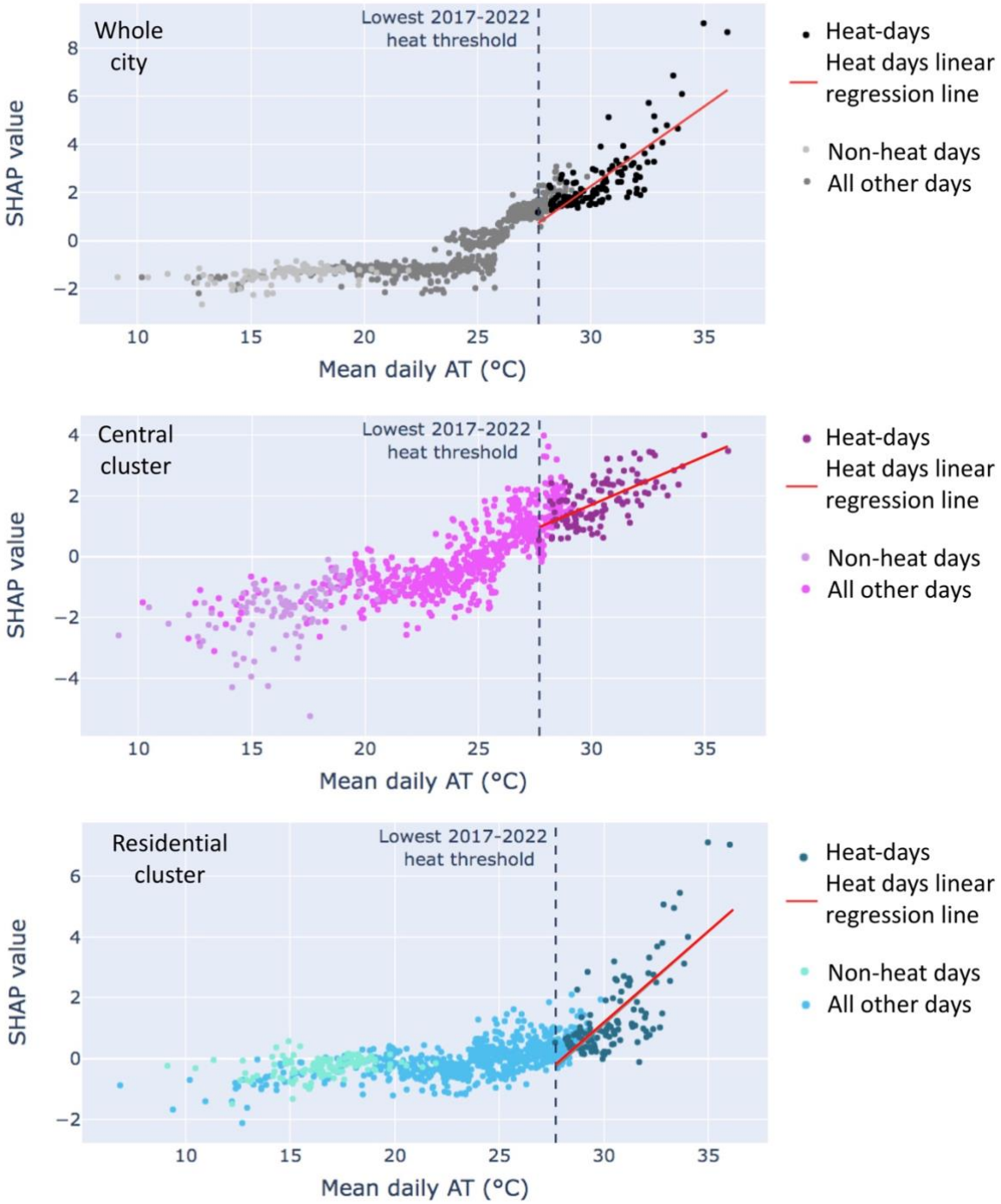

6.4. Discussion

In this chapter, the influence of apparent temperature on the forecast of daily ambulance dispatches for CV problems was analysed. Differently from existing studies, the focus was on examining heat days and non-heat days separately. Interestingly, the results show that while the effect of mean daily AT on the predicted number of daily CV emergencies during non-heat days was marginal, it considerably influenced the forecast during heat days. As adverse effects

of heat on the human CV system have been reported in the literature, and global temperatures are expected to increase, it is of great importance that the EMS are provided with accurate prediction models for extreme weather conditions in order to optimize their resources allocation and thereby potentially saving more lives.

6.4.1. Time series forecasting

The selection of XGBoost, CatBoost, and LSTM algorithms for daily CV ambulance dispatches forecast was driven by their strengths in handling time series prediction tasks, including those related to human health (Lim and Zohren, 2021; Liu et al., 2021b). XGBoost and CatBoost are gradient boosting algorithms which are able to capture complex patterns and nonlinear relationships in tabular data, making them well-suited for forecasting tasks with high-dimensional feature spaces, such as those used in our study, and potentially noisy input variables (Karingula et al, 2021). However, being based on decision trees, both algorithms are susceptible to overfitting the training data; moreover, they could overlook the long-term dependencies. On the other hand, LSTM is suitable for modelling temporal dependencies and capturing long-term trends in sequential data, which is crucial for predicting time series with intricate patterns and dynamic behaviours, but the training process requires data abundancy, and the algorithm can struggle to capture the interdependencies in high dimensions (Han et al., 2019). Moreover, not only the prolonged training time hindered cross-validation in hyperparameter tuning for LSTM in our study, primarily due to limited computational resources, but it also could pose a significant challenge in real-world applications within the EMS management.

For the specific task of predicting daily CV emergencies in Milan, XGBoost and CatBoost demonstrated superior, yet not statistically significant, performance in terms of MAE with respect to LSTM. In health-related applications, ensemble models have previously been recognized for their effectiveness compared to ARIMA and even neural networks (Kaushik et al., 2020; Gafni-Pappas and Khan, 2023; Qiu et al., 2020). However, in our study, the differences in MAE for the test set among the three tested algorithms were minimal, with values ranging from 9.57 to 10.25 CV emergencies (i.e., 10 CV emergencies rounded to the nearest integer) in the entire city of Milan. These values can be considered satisfactory, given the residual component's strength, predominantly falling within absolute values between 10 and 20, as shown in Figure 6.1. However, the distribution of absolute errors from XGBoost was not normal, suggesting that comparing the three tested algorithms using their mean value may not be fully appropriate.

Despite the capabilities of XGBoost in time series forecasting, it struggled to accurately predict peaks in CV ambulance dispatches, possibly due to the inherent uncertainty associated with emergency events, and a relatively small set of training data, both in terms of number of observations and number of daily emergencies. Similar issue, irrespective of the algorithm applied, has been reported in previous studies on predicting daily EMS demand, both with (Gafni-Pappas and Khan, 2023; Hermansen and Mengshoel, 2021; Sudarshan et al., 2021) and without (Rostami-Tabar and Hyndman, 2024; Xie et al., 2021; Álvarez-Chaves et al., 2023) the inclusion of the meteorological variables. One study, which specifically addressed the problem of peak prediction in CV hospital admissions, concluded that ensemble-based

algorithms achieve significantly better performance than logistic regression, support vector machine and artificial neural network (Qiu et al., 2020). On the contrary, in our study, XGBoost model primarily captured the general trend and underlying patterns in the CV EMS data, which may be influenced by factors such as seasonal variations, demographic changes, and environmental conditions. Peaks in ambulance dispatches often arise from stochastic events, which may not be fully captured by the historical data and the features included in the predictive model. Although MAPE achieved by XGBoost was higher during the 19 hottest days than during the 19 coldest days in May-September, it was lower during heat days than during the remaining ones, i.e., not classified as heat nor non-heat. This result suggests that the inclusion of the meteorological variables contributed, to some extent, to better capturing peaks caused by extreme temperatures, an advantage previously recognized also in other studies (Silva et al., 2023).

While several empirical studies and systematic reviews have reported that AI-based methods outperform classic statistical models for time series forecasting, especially on large datasets and for multiple time horizons, an ongoing debate persists regarding their suitability compared to traditional models for this problem (Kontopoulou et al., 2023; Silva et al., 2023; Vollmer et al., 2021; Martins et al., 2023). Therefore, hybrid models, combining AI and statistical techniques, have been suggested as a possible optimal solution (Kontopoulou et al., 2023; Silva et al., 2023; Martins et al., 2023). In light of recent advancements in XAI, the implementation of ML algorithms offers the advantage of analysing the influence of each feature on predictions, thereby increasing transparency, which is crucial in real-world public health applications (Di Martino and Delmastro, 2023; Loh et al., 2022; Temenos et al., 2022). Nonetheless, XAI techniques are still underutilized in the healthcare sector for time series tasks compared to computer vision tasks (Di Martino and Delmastro, 2023).

Among hospital management problems, as well as in EMS demand prediction, SHAP technique has been widely adopted, usually with tree-based algorithms (Susnjak and Maddigan, 2023; Petsis et al., 2022; Loh et al., 2022). By decomposing the model's output into contributions from individual features, SHAP allows to understand how each input variable influences the model's forecast at single prediction level, providing insights into the importance and direction of each feature for specific instances. Importantly, SHAP also facilitates the aggregation of local predictions to different levels, enabling the examination of feature importance across broader contexts such as heat and non-heat days. This capability allows to detect how the impact of meteorological variables may vary under different environmental conditions, shedding light on the factors driving fluctuations in EMS demand during extreme weather events. Indeed, in our study, while the majority of SHAP values oscillated near a relatively small value for meteorological variables on non-heat days, in the extreme temperatures their contribution became important, as shown in Figure 6.7. This differentiation is not possible using global XAI methods which provide the aggregated influence of each variable. Possibly for this reason, several studies reported low impact of meteorological features on EMS demand forecast using inherent XGBoost and Random Forest feature importance (Hu et al., 2023; Ramgopal et al., 2021), or a unique XAI methodology developed within a specific study (Rivera et al., 2023).

However, despite its utility, SHAP method presents several limitations. One notable constraint is that SHAP values may exhibit sensitivity to the choice of background data used

for reference, potentially leading to variations in interpretation across different datasets or model architectures (Vimbi et al., 2024). Therefore, while SHAP provides valuable insights into the local contributions of individual features, it may not fully capture complex interactions or non-linear relationships among variables, potentially limiting its ability to provide holistic explanations for model behaviour. However, dividing the city of Milan into smaller geographical partitions, more homogenous in terms of various socio-urban variables, could have helped in overcoming this limitation.

6.4.2. Heat and cardiovascular health in urban environment

In Chapter 3, 21 unique combinations of meteorological indicator, mathematical method, and comparison threshold were identified to define heat in studies analysing its impact on CV health. In the majority of cases, heat was defined using either a percentile or an absolute value threshold on temperature distribution, and its impact was further assessed by statistical models such as distributed lag non-linear model or generalized linear models. Nonetheless, ML frameworks have also been proposed to select heat threshold in a broader health context (Boudreault et al., 2023; Masselot et al., 2021) In particular, the analysis proposed in this study can serve as a way to empirically assess the heat threshold in a data-driven framework. Specifically, the dependence plot of a meteorological indicator and its corresponding SHAP values can be used for this task, allowing for the establishment of a threshold value beyond which historical evidence indicates an increase in ambulance calls. In particular, the choice of the 95th percentile of the annual AT distribution as the heat threshold for Milan was validated by the dependence plot (i.e., Figure 6.7), as from the corresponding value onward, the strength of the temperature's impact on prediction, represented by SHAP value, rose considerably. Furthermore, relevant research, overviewed in Chapter 3, has acknowledged that the impact of heat on CV health is immediate and gradually diminishes over the subsequent days. This finding aligns with the results from this chapter, which indicate that while on non-heat days different lag times emerged as the strongest influencers depending on geographical partition, during extreme temperatures the mean daily AT at lag0 exhibited the highest contribution among all meteorological aggregates.

As cities are complex and dynamic environments, recent research emphasizes the need to conduct spatially detailed analysis in urban context, as already argued in Chapter 5. This issue was addressed by performing the EMS demand forecast not only for the whole city of Milan, but also within its two clusters of neighbourhoods, differing by social, urban and demographic features possibly influencing human health. These socio-urban clusters were obtained by k-means clustering, previously applied for similar problems, while other reference spatial partitions in relevant literature on EMS demand forecast were obtained using Gaussian mixture model (Yang et al., 2020) or Hungarian algorithm (Grekousis and Liu, 2019); also, official boundaries of wards or census tracts (Pomeroy-Stevens et al., 2022; Hashtarkhani et al., 2021; Vogel et al., 2022), arbitrarily defined grids (Hermansen and Mengshoel, 2021), or a combination of grid and administrative boundaries (Chen et al., 2015b) were directly used as geographical division.

However, only one recent work compared the algorithm performance in the whole area and in smaller spatial units of the same area, reporting an increased MAPE in higher spatial

resolution (Martin et al., 2021). Similarly, in the case of Milan, increasing spatial resolution led to an increase in MAPE during heat days, from 14.56% in the whole city, to 16.57% in the Central and 22.21% in the Residential clusters, and during non-heat days from 10.89% to 15.92% and 16.68%, respectively. In addition, while the increase in SHAP values in the whole city and in the Residential cluster was observed near the lowest 2017-2022 heat threshold, in the central part of Milan an overall increasing trend in SHAP values was observed. One potential explanation is that in the Central cluster both a relatively high percentage of elderly people reside, whose health conditions are highly susceptible to high temperatures, and the urban heat island phenomenon is observed, meaning that the temperatures are higher than in the Residential cluster. However, further investigation into the interplay between socio-urban characteristics and the independent variables incorporated in our analysis is needed to fully comprehend the observed trends, in particular accounting for the fact that spatial patterns exist in the Central cluster in factors not included in analyses of this thesis, as indicated by the spatial Durbin error model in Chapter 5.

6.4.3. Limitations and conclusions

In addition to the limitations discussed in previous sections, several further constraints of this study need to be considered. Firstly, the time series analysis was conducted on a discontinuous period, omitting data from October to April each year. The inclusion of a complete year, even if no heat days were observed during these months, may yield valuable insights and potentially enhance predictive accuracy. While selecting relevant meteorological variables, we applied methods based on Pearson correlation and mutual information; however, given that two of the three algorithms utilized were tree-based, direct feature selection based on these models might have resulted in the inclusion of more appropriate variables. Furthermore, the evaluation of model performance relied solely on one method, which exhibited minimal and not statistically significant variation across the tested algorithms. Additionally, no confidence intervals were calculated for predictions, and no deepened sensitivity analysis was performed. The errors from XGBoost model were not normally distributed, thus the prediction intervals should not be assessed by relatively simple parametric methods such as quantile regression, but rather by computationally expensive bootstrapping. However, providing them could have offered valuable insights into the uncertainty associated with the forecasts. Finally, the inherent complexity of ML models, even when augmented with XAI methods, may pose challenges to their interpretability for non-technical decision-makers, such as medical professionals, policymakers, or urban planners.

In conclusion, we proposed a spatio-temporal XAI framework for predicting daily demand of CV ambulance dispatches and for assessing the impact of meteorological factors on this forecast. Time series of daily CV emergencies have been first extensively studied using classic statistical approaches, which confirmed the final choice of features for the prediction models. The SHAP values were used to analyse the influence of each feature on final predictions, with the main novelty of this study consisting in performing this analysis separately for heat and non-heat days. Regardless of geographic partition, we found that the mean daily AT at lag0 emerged as the most influential factor during heat, whereas its contribution remained minimal under moderate or low temperatures, increasing beyond the

heat threshold. We have also recognised a trade-off between spatial resolution and predictive accuracy.

Continuous research at a detailed spatial level is necessary to fully capture the factors influencing the predicted daily number of CV emergencies, thereby mitigating the trade-off between geographical resolution and predictive accuracy. In the context of a smart city, where technology and data are leveraged to enhance the quality of urban living, the spatio-temporal prediction of ambulance calls holds significant importance. In particular, as cities grow denser and more complex, and as they are characterized by higher temperatures and air pollution compared to rural areas (Piracha and Chaudhary, 2022), efficient emergency response becomes increasingly crucial for ensuring public safety and well-being.

In particular, there are several paths for future research in the field of spatio-temporal analysis of ambulance dispatch forecasts. One direction could involve exploring the integration of advanced machine learning techniques, particularly XAI, with traditional statistical methods to enhance predictive accuracy and interpretability. Investigating the specific mechanisms through which heat impacts human health and identifying vulnerable populations most at risk could provide valuable insights for public health interventions and policy development. Additionally, as cities continue to evolve into smart urban environments, leveraging data relevant to other meteorological, social and urban factors from internet-of-things sensors, mobile devices, and other sources to develop real-time monitoring systems for heat-related health emergencies could significantly improve emergency response and resilience. Furthermore, collaborative efforts between researchers, policymakers, and healthcare providers are essential for implementing proactive strategies to mitigate the impact of extreme weather events on public health, including targeted outreach programs, urban planning initiatives, and the development of heat-resilient infrastructure. By embracing interdisciplinary approaches and innovative technologies, the understanding of the complex interplay between environmental factors, health outcomes, and urban dynamics can be advanced, ultimately fostering healthier and more resilient communities.

Chapter 7. Conclusions and further research

This thesis rigorously developed novel healthcare-focused urban analytics models and decision making tools designed to mitigate the impact of heat waves on public health, particularly within the context of transitioning toward healthier smart cities. Using both Italy and the city of Milan as specific case studies, this research applied a holistic approach to examine key determinants of heat-health-related risk, i.e., population vulnerability, environmental hazards, and residents' exposure. The flexibility of the developed methodologies, alongside real-world applications, provide a framework not only to deepen academic understanding but also to offer tangible, proactive solutions for addressing the increasing public health challenges posed by rising temperatures.

In line with global imperatives, this research reflects the guidance and calls to action issued by leading international organizations, including the WHO, IPCC, UN (particularly UN-Habitat), WMO, and the Lancet Countdown, with all these bodies highlighting the strong link between climate change and adverse health outcomes. Specifically, some of the most impactful initiatives include:

- European Climate and Health Observatory, managed by the European Commission and the European Environment Agency, with various international organizations in the partnership. It aims to provide actionable insights into past, present, and future impacts of climate change on human health. By engaging public administrations, civil society, and the research community, the observatory disseminates knowledge through reports, work plans, webinars, and interactive tools, such as maps, to facilitate informed decision-making.

- United Nations Development Programme Climate Promise collaborates with governments to integrate health considerations into climate change policies. One of its 15 focal areas is heath, i.e., building climate-resilient health sectors and supporting the incorporation of health-related activities into national climate pledges.

- Alliance for Transformative Action on Climate and Health, as a WHO network, addresses the health-related ambitions set forth at COP26. Its key areas of operation include five following areas - climate resilient health systems, low carbon sustainable health systems, supply chains, financing, climate action and nutrition.

- Global Heat Resilience Service, currently under development by the Group on Earth Observations, a working group of the WMO, leverages advanced technologies, such as AI to evaluate heat risks in urban areas, including those linked to human health. The service will contribute to WMO's Global Early Warning System for All, an initiative supported by the United Nations Secretary-General.

This thesis aligns closely with the objectives of these initiatives, particularly in its contribution to actionable knowledge on public health, heat events and medical emergencies. By situating its approach within these frameworks, the research underscores its relevance and importance in addressing current global challenges related to climate change, public health, and urban resilience.

Additionally, the analytical framework developed in this thesis is particularly aligned with three Sustainable Development Goals (SDGs). First, by prioritizing cardiovascular (CV) health, this work advances SDG3 ("Ensure healthy lives and promote well-being for all at all ages"). Second, the integration of socio-urban features at the neighbourhood level and health determinants at the national municipal level emphasizes SDG11 ("Make cities and human settlements inclusive, safe, resilient, and sustainable"). Finally, by directly addressing the

health impacts of heat events, this thesis also supports SDG13 ("Take urgent action to combat climate change and its impacts"). The interplay between these goals underscores the importance of adopting comprehensive strategies that simultaneously target health, urban sustainability, and climate resilience.

The following sections (i.e., 7.1-7.5) will present detailed responses to the RQs posed in Chapter 1, alongside specific examples of how the methodologies and results from this thesis could benefit end-users, such as emergency medical services (EMS), urban planners, and policymakers. The final section (i.e., 7.6) will address the limitations of the proposed approach and outline directions for future research, emphasizing the potential for further innovation in this critical field.

7.1. Is it possible to construct a national municipality-level SDG3 index and how do Italian municipalities differ from each other?

Chapter 2 addressed this RQ by presenting a novel effort to calculate a municipality-level SDG3 index for all Italian municipalities. This study sheds light on the critical gaps in the availability, temporal accuracy, and spatial resolution of open data that align with official SDG targets. At this halfway point between the adoption of the SDGs and their target date, substantial efforts are still required to enhance the quality and granularity of data.

In spite of these constraints, the SDG3 index was successfully developed and calculated for 7,900 Italian municipalities, providing a unique overview of local disparities in public health performance. The analysis highlighted considerable geographical variation across the performance in 13 official SDG3 targets and in the final aggregated index. Due to insufficient spatial granularity in many of the indicators, clear regional patterns emerged on the map of the final index, with visible regional borders skewing the spatial analysis. Overall, municipalities in central Italy, the far Northeast, and far Northwest exhibited higher SDG3 performance, in contrast to the southern regions, which lagged behind. Furthermore, the absence of official clearly defined numerical benchmarks for SDG3 targets meant that the index reflected relative performance among municipalities rather than concrete progress towards achieving the global goals.

This chapter also laid the foundation for assessing population health vulnerability, in particular CV health vulnerability, critical for the subsequent contents of this thesis. The findings indicated that the median CV mortality rate per 1,000 residents in Italy reached 3.80 in 2019, with Milan's rate at 3.11, placing the city in the top half at national level.

The results of this analysis could offer significant value for local policymakers by providing a national map that allows for comparisons across municipalities, enabling the development of more tailored public health interventions. Moreover, the methodological framework designed to calculate an SDG3 index under conditions of data scarcity represents a notable contribution to the state-of-the-art, particularly in research addressing the practical implementation of globally defined policy targets. This index serves as a tool to inform evidence-based decision-making, providing insights that could help direct resources and efforts toward municipalities most in need of improvements.

7.2. What are currently applied definitions of heat in CV health context, do they influence the results, and how to standardize them?

Chapter 3 presented the findings of a systematic literature review analysing the impact of heat on CV health. Across 54 recent studies, 21 different combinations of criteria, statistical methods, and comparison thresholds were identified. This variety highlights the persistent heterogeneity in heat definitions, even within the same research domain - a challenge previously noted in the literature. Despite this inconsistency, percentile-based thresholds, as opposed to absolute temperature values, emerged as the more commonly used method, however with percentiles varying from the 90th to the 99th.

The studies reviewed exhibited significant variability not only in defining heat but also in medical and meteorological data sources, statistical models, and result reporting. This high level of heterogeneity made it impossible to conduct a comprehensive meta-analysis to determine which specific factors most influence the risk of adverse CV events in relation to heat and by what magnitude. However, limiting the analysis to studies that reported both the heat threshold and the mean temperature for the study period, it revealed a slight increase in relative risk (RR) of adverse CV outcomes with greater deviation of the heat threshold from the mean temperature.

In response to these findings, an attempt was made to standardize the definition of heat in CV health research by combining the most common statistical approaches and proposing a numerical guideline for selecting the final percentile threshold. The distributed lag non-linear model (DLNM), a long-standing gold standard in environmental health research, was applied for selecting the considered time lags. After determining the appropriate lags, Poisson regression, which is less sensitive to hyperparameter selection compared to DLNM, was used to estimate the RR of experiencing an adverse CV outcome on heat days versus non-heat days, with percentile thresholds ranging from the 90th to 99th. Two methods for selecting the final percentile threshold were proposed based on the curvature of the RR plot.

The proposed guideline offers several strengths. It integrates well-established, robust statistical techniques grounded in recent literature and employs a data-driven approach, aligning with the demands of the big data era. Furthermore, this approach is highly flexible, capable of extension to various health data (e.g., ambulance dispatches, hospitalizations, or mortality) and different health outcomes (e.g., CV or respiratory diseases). As such, it advances the state-of-the-art by contributing to the potential standardization of studies on temperature hazards and human health, which is crucial for developing effective heat-warning systems and targeted interventions, encompassing both infrastructural coping mechanisms (e.g., installation of cooling systems) and social measures (e.g., educational campaigns).

7.3. How to quantify the impact of heat on CV events on a certain area by analysing the geolocalized data relevant to CV ambulance dispatches?

Building upon the risk assessment, Chapter 4 tested the proposed heat definition guideline and identified specific characteristics of the data on environmental hazards and population exposure, that must be accounted for in statistical modelling, using Milan as a case study. Time-related factors proved essential and should be incorporated into the models, either as an

independent variable with a smoothing function, such as splines used in the DLNM, or as an offset, represented by proxy variables like traffic data, which reflects changes in population presence within the analysed area, when using Poisson regression. Additionally, the COVID-19 pandemic was found to have significantly influenced ambulance dispatches, affecting both daily demand, patient characteristics and, to some extent, the RR of a CV emergency during heat.

The analysis also examined key patient attributes such as gender, age, and emergency outcomes (e.g., if the patient required transportation to a hospital, the case was fatal or non-severe, and the location where the emergency occurred). For each group, the corresponding RR was calculated, revealing that the highest risk subgroups during heat exposure were those involving fatal emergencies and emergencies occurring on the street.

Chapter 4 thus demonstrated that the impact of heat on CV ambulance dispatches can be effectively assessed using DLNM and Poisson regression. However, accurate estimation of the associated RR requires careful consideration of underlying data characteristics to ensure that the models account for these nuances appropriately.

The insights generated by these results are crucial for the management of the EMS. The specific information on which subgroups are most likely to experience a CV emergency enables better preparedness of medical personnel and optimization of ambulance resources. Furthermore, the proposed methodological approach holds importance for international research, as it provides guidelines on the integration of time- and patient-related characteristics into statistical modelling, thereby enhancing the robustness and applicability of future studies.

7.4. What are the socio-urban characteristics that could influence CV health in presence of heat?

In Chapter 5, the focus returned to the concept of vulnerability, specifically addressing socio-urban vulnerability in the context of CV health. Using a k-means clustering method, the city was grouped into three clusters based on socio-urban characteristics, which exhibited significant geographical cohesion. These clusters were labelled as Central, Residential, and Peripheral. Subsequently, spatial regression models were applied to the entire city and separately to the Central and Residential clusters to estimate both the direct and spillover effects of socio-urban features on CV vulnerability to heat.

For the entire city of Milan, five socio-urban variables were found to have a significant direct effect: mean summer temperature, the density of drinking water fountains, and the percentages of elderly, female, and graduate residents. Additionally, three other socio-urban characteristics were found to be significant within specific clusters (i.e., green roofs in both the Central and Residential clusters, and population density and non-residential buildings' volume in the Central cluster). Indirect effects were identified only for two social features (i.e., percentages of elderly and female residents), and only at the city-wide level, suggesting the lack of significant spatial dependencies at finer geographical granularities.

The identification of socio-urban variables that significantly influence CV vulnerability to heat enabled the calculation of a socio-urban vulnerability index, derived from the regression coefficients. When combined with medical data, this index facilitated the creation of a vulnerability map that identified districts of Milan with low and high vulnerability. This map

highlighted areas and specific characteristics where targeted interventions would be required, thus aligning with the proactive approach to public health, allowing to protect residents from becoming patients.

To address this research question, a comprehensive spatial approach was adopted, integrating traditional statistical methods, such as regression modelling, with advanced unsupervised machine learning algorithms (ML), including k-means and hierarchical density-based clustering of applications with noise (HDBSCAN). Methodological guidelines for future research on the dynamic nature of urban environments were thus provided, along with a final vulnerability map. This map holds potential value for urban planners and policymakers in Milan, offering a tangible metric to inform decision-making. Additionally, it could be utilized by the EMS as it identifies areas where the spatial distribution of CV emergencies shifts during heat events, helping to reduce response times and therefore potentially improve patient outcomes.

7.5. How can artificial intelligence be used to forecast CV emergencies in a big city considering meteorological parameters?

This RQ was directly addressed in Chapter 6 based on the findings from Chapter 5, where artificial intelligence techniques (i.e., k-means and HDBSCAN) had already been applied, as discussed in section 7.4. Specifically, regarding the forecasting dimension, three supervised ML algorithms, two decision tree-based and one neural network were tested for predicting the volume of CV emergencies on the following day. All three algorithms demonstrated strong performance, with error rates approaching the random noise component of the time series of daily CV emergencies.

Although time-series prediction with ML itself is not a novel approach, the main innovation lay in the use of explainable artificial intelligence (XAI) to provide greater transparency into the model's decision-making process, particularly concerning the influence of meteorological variables. While the increased CV risk associated with heat has been extensively documented in the literature, predictive studies have often reported only marginal or no impact of the temperature on forecasts. However, XAI enabled a more nuanced analysis, revealing that while the effect of temperature is minimal on most days, it sharply increases during the hottest days of the year.

This pattern was observed across the entire city and its two socio-urban clusters, although the specific magnitude and trend slightly varied across different geographic aggregations. Additionally, a trade-off between prediction accuracy and spatial resolution was identified, indicating that ML-based solutions may require further optimization to accurately capture the specific dynamics of urban environments.

The observed increase in temperature's contribution to the final prediction on heat days underscores the importance of incorporating meteorological features into the set of independent variables. A more precise forecast, encompassing both the volume and location of CV emergencies during extreme weather conditions, holds the potential to significantly enhance the effectiveness of EMS, which face considerable strain during periods of hot weather.

7.6. Final remarks, limitations and future developments

The EMS are a vital component of the healthcare system; however, they are often overloaded, especially during extreme weather conditions, which emphasizes the urgency for optimization strategies. As timely response is paramount in emergency situations when every minute holds critical importance, ambulance dispatches are the frontline, and their efficiency directly impacts patient outcomes.

The findings of this thesis have important implications for healthcare systems, particularly in urban areas vulnerable to climate change. By providing EMS with data-driven insights, this research offers potential strategies for improving response efficiency during heatwaves and for guiding urban planning and educational interventions in the most at-risk areas. The integration of AI approaches, coupled with advanced statistics, is pivotal in developing smart healthy cities that prioritize resident well-being and safety. As such, continued research is essential for fostering resilient and responsive healthcare systems in the smart cities of the future.

Such approach is especially relevant in the context of ongoing climate change and its associated health risks, as recognized by multiple international organizations. By providing a framework for informed decision-making, this research aims to contribute to the development of resilient urban environments, shifting the focus from reactive treatment to proactive safeguarding of public health. However, as this is an emerging field, there is still a lack of common standards for methodology. Despite efforts to enhance the statistical robustness of the proposed framework, several limitations remain:

- Data limitations: There was no official diagnosis for the medical data used in this research, therefore it is uncertain whether the emergencies recorded in the case studies for Milan were indeed CV in nature. Furthermore, temporal misalignment exists between the various data sources, in particular medical and meteorological data with socio-urban data.

- Relative indices: The indices developed in this research, such as the SDG3 and socio-urban vulnerability indices, are relative measures meant for comparison between areas. They do not represent absolute goals, benchmarks, or distances from official thresholds, as no such standards currently exist.

- Reactive heat threshold: While this thesis emphasizes a proactive approach, the selection of heat thresholds, essential for distinguishing heat days from non-heat days, is inherently reactive, and can only be determined a posteriori, after the end of each year, as it depends on annual temperature distribution.

- Resource restriction: The reliance on open-access publications in the systematic review and the limited inclusion of grey literature, such as reports from international organizations or governmental guidelines, may have narrowed the scope of this dissertation and introduced biases in final conclusions. These omissions could have excluded standardized instructions or critical perspectives that are shaping ongoing research on climate change and human health.

- Exclusion of the Peripheral socio-urban cluster: In many analyses, the Peripheral cluster was excluded, leading to a lack of inclusivity and equity in the urban context examined. The reality of global warming necessitates adaptive responses, which this research seeks to address. By elucidating the mechanisms of heat-related CV events and identifying vulnerable

populations, this study offers valuable insights for the development of targeted interventions and urban planning strategies aimed at mitigating health risks associated with climate change. It is crucial to emphasize that while the proposed framework, tested in Milan, has provided valuable city-specific insights, its full validation and refinement require application across diverse urban and climatic contexts to distinguish generalizable findings from those unique to specific geographical settings.

Future research and policymakers should consider the following paths to address identified limitations, which have already started being explored in recent literature:

- Integrated public health data systems: The development of a comprehensive system that connects EMS records with hospital data would enable more precise disease-specific analyses and improve the accuracy of emergency health responses (Adamu et al., 2020; Ksibi et al., 2023).

- Interdisciplinary collaboration: Establishing interdisciplinary teams involving experts in socio-urban planning, medical science, and data analysis would ensure the correct identification of confounding variables and effect modifiers, allowing for a more accurate understanding of urban dynamics and their health impacts (Buttazzoni et al., 2020; UN-Habitat, 2024).

- Enhanced statistical methodologies: Further attention should be given to the mathematical properties of indices. In some cases, the indices presented in this research clustered around the median, suggesting that further standardization could yield better graphical representations and deeper real-world insights.

- Improved spatial and temporal data resolution: Greater focus on hourly analyses is essential, particularly for ambulance dispatches, in case of which the impact of heat is immediate. Additionally, imagery data offer promise for improving spatial resolution, both in terms of meteorological conditions and urban topography, with possible data sources encompassing satellite data from spatial agencies, e.g., European Space Agency (ESA) and National Aeronautics and Space Administration (NASA), and private services, e.g., Google Earth Engine, as well as other imagery data, such as those from Google Street View (Chen et al., 2024; Scepanovic et al., 2024).

- Accurate spatial granularity and macro-level coherence: The observed trade-off between geographical resolution and predictive accuracy, alongside the diminishing spatial dependencies at finer scales, underscores the critical need for meaningful spatial aggregation. While analyses at the intra-city level are essential for localized insights, it is equally important to maintain methodological consistency at broader macro scales, such as national and international levels. This balance is vital to advancing smart, sustainable urban development globally, and ensuring the scalability of findings across different governance tiers.

By addressing these limitations and guidelines, future research can contribute more effectively to the development of equitable and proactive smart cities, ensuring a resilient public health system that is prepared to promptly respond to health risks posed by ongoing climate change.

Bibliography and Sitography

Abdullah, A. M., Ismail, M., Yuen, F. S., Abdullah, S., & Elhadi, R. E. (2017). The relationship between daily maximum temperature and daily maximum ground level ozone concentration. *Polish Journal of Environmental Studies*, *26*(3).

Abrignani, M. G., Lombardo, A., Braschi, A., Renda, N., & Abrignani, V. (2022). Climatic influences on cardiovascular diseases. *World Journal of Cardiology*, *14*(3), 152.

Achebak, H., Devolder, D., & Ballester, J. (2019). Trends in temperature-related age-specific and sex-specific mortality from cardiovascular diseases in Spain: A national time-series analysis. *The Lancet Planetary Health*, *3*(7), e297-e306.

Adamu, A. A., Wang, D., Salau, A. O., & Ajayi, O. (2020). An integrated IoT system pathway for smart cities. *International Journal on Emerging Technologies*, *11*(1), 1-9.

Adhikari, B., Delgado-Ron, J. A., Van den Bosch, M., Dummer, T., Hong, A., Sandhu, J., ... & Frank, L. D. (2021). Community design and hypertension: Walkability and park access relationships with cardiovascular health. *International Journal of Hygiene and Environmental Health*, *237*, 113820.

Agenzia Regionale Emergenza Urgenza (AREU) (2024). *Chi Siamo*. Retrieved from https://www.areu.lombardia.it/web/home/presentazione-areu on 09/09/2024.

Agenzia regionale per la protezione dell'ambiente (ARPA) (2023a). *Form Richiesta Dati*. Retrieved from https://www.arpalombardia.it/temi-ambientali/meteo-e-clima/form-richiesta-dati/ on 27/10/2023.

Agenzia regionale per la protezione dell'ambiente (ARPA) (2023b). *Chi siamo*. Retrieved from https://www.arpalombardia.it/chi-siamo/ on 09/09/2024.

Alahmad, B., Shakarchi, A. F., Khraishah, H., Alseaidan, M., Gasana, J., Al-Hemoud, A., ... & Fox, M. A. (2020). Extreme temperatures and mortality in Kuwait: Who is vulnerable?. *Science of The Total Environment*, *732*, 139289.

Alcamo, J., Thompson, J., Alexander, A., Antoniades, A., Delabre, I., Dolley, J., ... & Scharlemann, J. P. (2020). Analysing interactions among the sustainable development goals: Findings and emerging issues from local and global studies. *Sustainability Science*, *15*, 1561-1572.

Almeida, C. R. D., Teodoro, A. C., & Gonçalves, A. (2021). Study of the urban heat island (UHI) using remote sensing data/techniques: A systematic review. *Environments*, *8*(10), 105.

Alsaiqali, M., De Troeyer, K., Casas, L., Hamdi, R., Faes, C., & Van Pottelbergh, G. (2022). The effects of heatwaves on human morbidity in primary care settings: A case-crossover study. *International Journal of Environmental Research and Public Health*, *19*(2), 832.

Álvarez-Chaves, H., Muñoz, P., & R-Moreno, M. D. (2023). Machine learning methods for predicting the admissions and hospitalisations in the emergency department of a civil and military hospital. *Journal of Intelligent Information Systems*, *61*(3), 881-900.

Aminipouri, M., Knudby, A., & Ho, H. C. (2016). Using multiple disparate data sources to map heat vulnerability: Vancouver case study. *The Canadian Geographer/Le Géographe canadien*, *60*(3), 356-368.

Andrees, V., Bei der Kellen, R., Augustin, M., Gallinat, J., Harth, V., Hoven, H., ... & Augustin, J. (2024). Spatial characteristics of non-communicable diseases and their associations to social conditions in a large urban cohort in Germany—Results from the Hamburg City Health Study. *PloS ONE*, *19*(4), e0301475.

Angelov, P. P., Soares, E. A., Jiang, R., Arnold, N. I., & Atkinson, P. M. (2021). Explainable artificial intelligence: An analytical review. *Wiley Interdisciplinary Reviews: Data Mining and Knowledge Discovery*, *11*(5), e1424.

Anthopoulos, L. G. (2015). Understanding the smart city domain: A literature review. *Transforming City Governments for Successful Smart Cities*, 9-21.

Arcaya, M. C., Tucker-Seeley, R. D., Kim, R., Schnake-Mahl, A., So, M., & Subramanian, S. V. (2016). Research on neighborhood effects on health in the United States: A systematic review of study characteristics. *Social Science & Medicine*, *168*, 16-29.

Aringhieri, R., Bruni, M. E., Khodaparasti, S., & van Essen, J. T. (2017). Emergency medical services and beyond: Addressing new challenges through a wide literature review. *Computers & Operations Research*, *78*, 349-368.

Arnberger, A., Allex, B., Eder, R., Ebenberger, M., Wanka, A., Kolland, F., ... & Hutter, H. P. (2017). Elderly resident's uses of and preferences for urban green spaces during heat periods. *Urban Forestry & Urban Greening*, *21*, 102-115.

Aromataris, E., & Pearson, A. (2014). The systematic review: An overview. *AJN The American Journal of Nursing*, *114*(3), 53-58.

Auchincloss, A. H., Gebreab, S. Y., Mair, C., & Diez Roux, A. V. (2012). A review of spatial methods in epidemiology, 2000–2010. *Annual Review of Public Health*, *33*(1), 107-122.

Aven, T. (2016). Risk assessment and risk management: Review of recent advances on their foundation. *European Journal of Operational Research*, *253*(1), 1-13.

Azer, S. A., & Guerrero, A. P. (2023). The challenges imposed by artificial intelligence: Are we ready in medical education?. *BMC Medical Education*, *23*(1), 680.

Bai, L., Li, Q., Wang, J., Lavigne, E., Gasparrini, A., Copes, R., ... & Chen, H. (2018). Increased coronary heart disease and stroke hospitalisations from ambient temperatures in Ontario. *Heart*, *104*(8), 673-679.

Bakhtsiyarava, M., Schinasi, L. H., Sánchez, B. N., Dronova, I., Kephart, J. L., Ju, Y., ... & Rodríguez, D. A. (2023). Modification of temperature-related human mortality by area-level socioeconomic and demographic characteristics in Latin American cities. *Social Science & Medicine*, *317*, 115526.

Ballester, J., Quijal-Zamorano, M., Méndez Turrubiates, R. F., Pegenaute, F., Herrmann, F. R., Robine, J. M., ... & Achebak, H. (2023). Heat-related mortality in Europe during the summer of 2022. *Nature medicine*, *29*(7), 1857-1866.

Bansal, M. (2020). Cardiovascular disease and COVID-19. *Diabetes & Metabolic Syndrome: Clinical Research & Reviews*, *14*(3), 247-250.

Bao, J., Li, X., & Yu, C. (2015). The construction and validation of the heat vulnerability index, a review. *International Journal of Environmental Research and Public Health*, *12*(7), 7220-7234.

Baptista, E. A., & Queiroz, B. L. (2019). Spatial analysis of mortality by cardiovascular disease in the adult population: a study for Brazilian micro-regions between 1996 and 2015. *Spatial Demography*, *7*, 83-101.

Basu, R. (2009). High ambient temperature and mortality: A review of epidemiologic studies from 2001 to 2008. *Environmental Health*, *8*, 1-13.

Basu, R., & Samet, J. M. (2002). Relation between elevated ambient temperature and mortality: A review of the epidemiologic evidence. *Epidemiologic Reviews*, *24*(2), 190-202.

Becker, S. (2000). Bioclimatological rating of cities and resorts in South Africa according to the climate index. *International Journal of Climatology: A Journal of the Royal Meteorological Society*, *20*(12), 1403-1414.

Bedriñana, K. G. A., Martín, J. A. R., & Añaños, F. T. (2021). Human rights in the least developed countries of Asia: An index for quantifying Sustainable Development Goal 3 (Good Health and Wellbeing). *International Journal of Environmental Research and Public Health*, *18*(9), 4747.

Bennich, T., Weitz, N., & Carlsen, H. (2020). Deciphering the scientific literature on SDG interactions: A review and reading guide. *Science of the Total Environment*, *728*, 138405.

Betti, M., De Tommaso, C. V., & Maino, F. (2023). Health Inequalities in Italy. Comparing regions among prevention, community health services and hospital assistance. *Social Development Issues*, *45*(1), 61-76.

Bharsakade, R., More, S., Nandeshwar, S., Narnaware, R., & Patil, R. (2022, August). Emergency facility location of ambulances using k-means clustering and minimax. In *Biennial International Conference on Future Learning Aspects of Mechanical Engineering* (pp. 635-644). Singapore: Springer Nature Singapore.

Bhaskaran, K., Armstrong, B., Hajat, S., Haines, A., Wilkinson, P., & Smeeth, L. (2012). Heat and risk of myocardial infarction: hourly level case-crossover analysis of MINAP database. *BMJ*, *345*.

Bhaskaran, K., Hajat, S., Haines, A., Herrett, E., Wilkinson, P., & Smeeth, L. (2009). Effects of ambient temperature on the incidence of myocardial infarction. *Heart*, *95*(21), 1760-1769.

Bi, X., Wu, C., Wang, C., Wang, Y., Wang, X., Song, C., ... & Fu, C. (2022). Impacts of air temperature and its extremes on human mortality in Shanghai, China. *Urban Climate*, *41*, 101072.

Biermann, F., Kanie, N., & Kim, R. E. (2017). Global governance by goal-setting: The novel approach of the UN Sustainable Development Goals. *Current Opinion in Environmental Sustainability*, *26*, 26-31.

Black-Ingersoll, F., de Lange, J., Heidari, L., Negassa, A., Botana, P., Fabian, M. P., & Scammell, M. K. (2022). A literature review of cooling center, misting station, cool pavement, and cool roof intervention evaluations. *Atmosphere*, *13*(7), 1103.

Bland, J. M., & Altman, D. G. (2000). The odds ratio. *BMJ*, *320*(7247), 1468.

Blangiardo, M., Boulieri, A., Diggle, P., Piel, F. B., Shaddick, G., & Elliott, P. (2020). Advances in spatiotemporal models for non-communicable disease surveillance. *International Journal of Epidemiology*, *49*(Supplement_1), i26-i37.

Bolshakova, N., & Azuaje, F. (2003). Cluster validation techniques for genome expression data. *Signal processing*, *83*(4), 825-833.

Boots, B., Sugihara, K., Chiu, S. N., & Okabe, A.: *Spatial tessellations: concepts and applications of Voronoi diagrams*. 2nd edn. Wiley, New York (2009).

Bosa, I., Castelli, A., Castelli, M., Ciani, O., Compagni, A., Galizzi, M. M., ... & Vainieri, M. (2021). Corona-regionalism? Differences in regional responses to COVID-19 in Italy. *Health Policy*, *125*(9), 1179-1187.

Boudreault, J., Campagna, C., & Chebana, F. (2023). Machine and deep learning for modelling heat-health relationships. *Science of The Total Environment*, *892*, 164660.

Boulos, M. K., Roudsari, A. V., & Carson, E. R. (2001). Health geomatics: An enabling suite of technologies in health and healthcare. *Journal of Biomedical Informatics*, *34*(3), 195-219.

Bourdrel, T., Bind, M. A., Béjot, Y., Morel, O., & Argacha, J. F. (2017). Cardiovascular effects of air pollution. *Archives of Cardiovascular Diseases*, *110*(11), 634-642.

Braithwaite, J., Tran, Y., Ellis, L. A., & Westbrook, J. (2020). Inside the black box of comparative national healthcare performance in 35 OECD countries: Issues of culture, systems performance and sustainability. *PloS ONE*, *15*(9), e0239776.

Buis, A. (2020). Milankovitch (orbital) cycles and their role in Earth's climate. *NASA Climate*, *27*, 8.

Burse, R. L. (1979). Sex differences in human thermoregulatory response to heat and cold stress. *Human Factors*, *21*(6), 687-699.

Buttazzoni, A., Veenhof, M., & Minaker, L. (2020). Smart city and high-tech urban interventions targeting human health: An equity-focused systematic review. *International Journal of Environmental Research and Public Health*, *17*(7), 2325.

Cambra, K., Martínez–Rueda, T., Alonso–Fustel, E., Cirarda, F. B., Ibanez, B., Esnaola, S., ... & Montoya, I. (2011). Mortality in small geographical areas and proximity to air polluting industries in the Basque Country (Spain). *Occupational and Environmental Medicine*, *68*(2), 140-147.

Campbell, S. L., Remenyi, T. A., Williamson, G. J., White, C. J., & Johnston, F. H. (2019). The value of local heatwave impact assessment: A case-crossover analysis of hospital emergency department presentations in Tasmania, Australia. *International Journal of Environmental Research and Public Health*, *16*(19), 3715.

Campello, R. J., Moulavi, D., & Sander, J. (2013, April). Density-based clustering based on hierarchical density estimates. In *Pacific-Asia conference on knowledge discovery and data mining* (pp. 160-172). Berlin, Heidelberg: Springer Berlin Heidelberg.

Can, G., Şahin, Ü., Sayılı, U., Dubé, M., Kara, B., Acar, H. C., ... & Gosselin, P. (2019). Excess mortality in Istanbul during extreme heat waves between 2013 and 2017. *International Journal of Environmental Research and Public Health*, *16*(22), 4348.

Cardona, O.D., van Aalst M.K., Birkmann J., Fordham M., McGregor G., Perez R., Pulwarty R.S., Schipper E.L.F., & Sinh B.T. (2012). Determinants of risk: exposure and vulnerability. In: *Managing the Risks of Extreme Events and Disasters to Advance Climate Change Adaptation* [Field, C.B., V. Barros, T.F. Stocker, D. Qin, D.J. Dokken, K.L. Ebi, M.D. Mastrandrea, K.J. Mach, G.-K. Plattner, S.K. Allen, M. Tignor, and P.M. Midgley (eds.)]. A Special Report of Working Groups I and II of the Intergovernmental Panel on Climate Change (IPCC). Cambridge University Press, Cambridge, UK, and New York, NY, USA, pp. 65-108.

Casanueva, A., Burgstall, A., Kotlarski, S., Messeri, A., Morabito, M., Flouris, A. D., ... & Schwierz, C. (2019). Overview of existing heat-health warning systems in Europe. *International Journal of Environmental Research and Public Health*, *16*(15), 2657.

Cavalli, L., Farnia, L., Lizzi, G., Romani, I. G., Alibegovic, M., & Vergalli, S. (2020). *The SDSN Italia SDGs city index two years later: update report*. FEEM Report No. 08-2020.

Cerqueira, V., Torgo, L., & Soares, C. (2019). Machine learning vs statistical methods for time series forecasting: Size matters. arXiv preprint arXiv:1909.13316.

Cesario, E., Lindia, P., & Vinci, A. (2023). Detecting multi-density urban hotspots in a smart city: Approaches, challenges and applications. *Big Data and Cognitive Computing*, *7*(1), 29.

Chen, A. Y., Lu, T. Y., Ma, M. H. M., & Sun, W. Z. (2015b). Demand forecast using data analytics for the preallocation of ambulances. *IEEE Journal of Biomedical and Health Informatics*, *20*(4), 1178-1187.

Chen, J., Cheng, Y. R., Fu, X. Y., Wang, C. Y., Wen, W., Ni, J., ... & Chen, G. F. (2021). Exploring the impact of the COVID-19 epidemic on the medical emergency calls and calls for cardiovascular diseases in Hangzhou, China. *Irish Journal of Medical Science* (1971-), 1-5.

Chen, J., Yang, S. T., Li, H. W., Zhang, B., & Lv, J. R. (2013). Research on geographical environment unit division based on the method of natural breaks (Jenks). *The International Archives of the Photogrammetry, Remote Sensing and Spatial Information Sciences*, *40*, 47-50.

Chen, K., Bi, J., Chen, J., Chen, X., Huang, L., & Zhou, L. (2015a). Influence of heat wave definitions to the added effect of heat waves on daily mortality in Nanjing, China. *Science of the Total Environment*, *506*, 18-25.

Chen, K., Breitner, S., Wolf, K., Hampel, R., Meisinger, C., Heier, M., ... & KORA Study Group Peters A Schulz H Schwettmann L Leidl R Heier M Strauch K. (2019). Temporal variations in the triggering of myocardial infarction by air temperature in Augsburg, Germany, 1987–2014. *European Heart Journal*, *40*(20), 1600-1608.

Chen, K., Dubrow, R., Breitner, S., Wolf, K., Linseisen, J., Schmitz, T., ... & Schneider, A. (2022). Triggering of myocardial infarction by heat exposure is modified by medication intake. *Nature Cardiovascular Research*, *1*(8), 727-731.

Chen, R., Yin, P., Wang, L., Liu, C., Niu, Y., Wang, W., ... & Zhou, M. (2018). Association between ambient temperature and mortality risk and burden: Time series study in 272 main Chinese cities. *BMJ*, *363*.

Chen, T., & Guestrin, C. (2016, August). Xgboost: A scalable tree boosting system. In *Proceedings of the 22nd ACM SIGKDD International Conference on Knowledge Discovery and Data Mining* (pp. 785-794).

Chen, Y. (2013). New approaches for calculating Moran's index of spatial autocorrelation. *PloS ONE*, *8*(7), e68336.

Chen, Z., Dazard, J. E., Khalifa, Y., Motairek, I., Al-Kindi, S., & Rajagopalan, S. (2024). Artificial intelligence–based assessment of built environment from Google Street View and coronary artery disease prevalence. *European Heart Journal*, *45*(17), 1540-1549.

Cheng, J., Xu, Z., Bambrick, H., Prescott, V., Wang, N., Zhang, Y., ... & Hu, W. (2019). Cardiorespiratory effects of heatwaves: A systematic review and meta-analysis of global epidemiological evidence. *Environmental Research*, *177*, 108610.

Cheng, W., Li, D., Liu, Z., & Brown, R. D. (2021). Approaches for identifying heat-vulnerable populations and locations: A systematic review. *Science of The Total Environment*, *799*, 149417.

Chiabai, A., Spadaro, J. V., & Neumann, M. B. (2018). Valuing deaths or years of life lost? Economic benefits of avoided mortality from early heat warning systems. *Mitigation and Adaptation Strategies for Global Change*, *23*, 1159-1176.

Choi, H. M., Lee, W., Roye, D., Heo, S., Urban, A., Entezari, A., ... & Bell, M. L. (2022). Effect modification of greenness on the association between heat and mortality: A multi-city multi-country study. *EBioMedicine*, *84*.

Chollet, F., & others. (2015). Keras. *GitHub*. Retrieved from https://github.com/fchollet/keras on 19/04/2024.

Christensen, E. F., Bendtsen, M. D., Larsen, T. M., Jensen, F. B., Lindskou, T. A., Holdgaard, H. O., ... & Christiansen, C. F. (2017). Trends in diagnostic patterns and mortality in emergency ambulance service patients in 2007− 2014: A population-based cohort study from the North Denmark region. *BMJ Open*, *7*(8), e014508.

Cicci, K. R., Maltby, A., Clemens, K. K., Vicedo-Cabrera, A. M., Gunz, A. C., Lavigne, É., & Wilk, P. (2022). High temperatures and cardiovascular-related morbidity: A scoping review. *International Journal of Environmental Research and Public Health*, *19*(18), 11243.

Clerkin, K. J., Fried, J. A., Raikhelkar, J., Sayer, G., Griffin, J. M., Masoumi, A., ... & Uriel, N. (2020). COVID-19 and cardiovascular disease. *Circulation*, *141*(20), 1648-1655.

Clifton, J., Díaz-Fuentes, D., & Fernández-Gutiérrez, M. (2016). Public infrastructure services in the European Union: Challenges for territorial cohesion. *Regional Studies*, *50*(2), 358-373.

Coles, E., Kruger, E., Anjrini, A. A., & Tennant, M. (2017). The urban dental index: A method for measuring and mapping dental health disparities across urban areas. *Journal of Urban Health*, *94*(2), 211-219.

Comune di Milano (2023a). *Nuclei d'Identità Locale (NIL) VIGENTI - PGT 2030*. Retrieved from https://dati.comune.milano.it/dataset/ds964-nil-vigenti-pgt-2030#:~:text=Vengono%20introdotti%20dal%20PGT%20(Piano,per%20la%20mobilit%C3%A0%2C%20il%20verde on 12/01/2023a.

Comune di Milano (2023b). Retrieved from https://dati.comune.milano.it/ on 12/01/2023b.

Conlon, K. C., Mallen, E., Gronlund, C. J., Berrocal, V. J., Larsen, L., & O'Neill, M. S. (2020). Mapping human vulnerability to extreme heat: A critical assessment of heat vulnerability indices created using principal components analysis. *Environmental Health Perspectives*, *128*(9), 097001.

Copernicus (2024). *Global Climate Highlights 2023*. Retrieved from https://climate.copernicus.eu/global-climate-highlights-2023 on 29/04/2024.

Costa, C., Santana, P., Dimitroulopoulou, S., Burstrom, B., Borrell, C., Schweikart, J., ... & Costa, G. (2019). Population health inequalities across and within European metropolitan areas through the lens of the EURO-HEALTHY Population Health Index. *International Journal of Environmental Research and Public Health*, *16*(5), 836.

Crandall, C. G., & Gonzalez-Alonso, J. (2010). Cardiovascular function in the heat-stressed human. *Acta Physiologica*, *199*(4), 407-423.

Crandall, C. G., & Wilson, T. E. (2015). Human cardiovascular responses to passive heat stress. *Comprehensive Physiology*, *5*(1), 17.

D'Ascenzi, F., Cameli, M., Forni, S., Gemmi, F., Szasz, C., Fabrizio, V. D., ... & Valente, S. (2021). Reduction of emergency calls and hospitalizations for cardiac causes: Effects of Covid-19 pandemic and lockdown in Tuscany region. *Frontiers in Cardiovascular Medicine*, *8*, 625569.

D'Adamo, I., Gastaldi, M., Imbriani, C., & Morone, P. (2021). Assessing regional performance for the Sustainable Development Goals in Italy. *Scientific Reports*, *11*(1), 24117.

D'Adamo, I., Gastaldi, M., Ioppolo, G., & Morone, P. (2022). An analysis of Sustainable Development Goals in Italian cities: Performance measurements and policy implications. *Land Use Policy*, *120*, 106278.

da Silva, E. L. C., Rosa, M. D. O., Fonseca, K. V. O., Luders, R., & Kozievitch, N. P. (2016, November). Combining k-means method and complex network analysis to evaluate city mobility. In *2016 IEEE 19th International Conference on Intelligent Transportation Systems (ITSC)* (pp. 1666-1671). IEEE.

Dang, T. A. T., Wraith, D., Bambrick, H., Dung, N., Truc, T. T., Tong, S., ... & Dunne, M. P. (2019). Short-term effects of temperature on hospital admissions for acute myocardial infarction: A comparison between two neighboring climate zones in Vietnam. *Environmental Research*, *175*, 167-177.

Davies, H. T. O., Crombie, I. K., & Tavakoli, M. (1998). When can odds ratios mislead?. *BMJ*, *316*(7136), 989-991.

de Freitas, C. R., & Grigorieva, E. A. (2015). A comprehensive catalogue and classification of human thermal climate indices. *International Journal of Biometeorology*, *59*, 109-120.

de Moraes, S. L., Almendra, R., & Barrozo, L. V. (2022). Impact of heat waves and cold spells on cause-specific mortality in the city of São Paulo, Brazil. *International Journal of Hygiene and Environmental Health*, *239*, 113861.

Deilami, K., Kamruzzaman, M., & Liu, Y. (2018). Urban heat island effect: A systematic review of spatio-temporal factors, data, methods, and mitigation measures. *International Journal of Applied Earth Observation and Geoinformation*, *67*, 30-42.

Delaney, T., Dominie, W., Dowling, H., Maizlish, N., Chapman, D., Hill, L., ... & Woolf, S. (2018). *Healthy places index*. Public Health Alliance of Southern California, Long Beach, CA.

Delgado, E. J., Cabezas, X., Martin-Barreiro, C., Leiva, V., & Rojas, F. (2022). An equity-based optimization model to solve the location problem for healthcare centers applied to hospital beds and COVID-19 vaccination. *Mathematics*, *10*(11), 1825.

Dello Strologo, A., D'Andrassi, E., Paoloni, N., & Mattei, G. (2021). Italy versus other European countries: Sustainable Development Goals, policies and future hypothetical results. *Sustainability*, *13*(6), 3417.

Delmelle, E. C. (2015). Five decades of neighborhood classifications and their transitions: A comparison of four US cities, 1970–2010. *Applied Geography*, *57*, 1-11.

Demoury, C., Aerts, R., Vandeninden, B., Van Schaeybroeck, B., & De Clercq, E. M. (2022). Impact of short-term exposure to extreme temperatures on mortality: A multi-city study in Belgium. *International Journal of Environmental Research and Public Health*, *19*(7), 3763.

Desai, D. D., Dey, J., Satapathy, S. K., Mishra, S., Mohanty, S. N., Mishra, P., & Panda, S. K. (2023). Optimal ambulance positioning for road accidents with deep embedded clustering. *IEEE Access*, *11*, 59917-59934.

Di Martino, F., & Delmastro, F. (2023). Explainable AI for clinical and remote health applications: A survey on tabular and time series data. *Artificial Intelligence Review*, *56*(6), 5261-5315.

Dong, J., Peng, J., He, X., Corcoran, J., Qiu, S., & Wang, X. (2020). Heatwave-induced human health risk assessment in megacities based on heat stress-social vulnerability-human exposure framework. *Landscape and Urban Planning*, *203*, 103907.

Dong, W., Liu, Z., Liao, H., Tang, Q., & Li, X. E. (2015). New climate and socio-economic scenarios for assessing global human health challenges due to heat risk. *Climatic Change*, *130*, 505-518.

Donkin, A., Goldblatt, P., Allen, J., Nathanson, V., & Marmot, M. (2018). Global action on the social determinants of health. *BMJ Global Health*, *3*(Suppl 1), e000603.

dos Santos, B. S., Steiner, M. T. A., Fenerich, A. T., & Lima, R. H. P. (2019). Data mining and machine learning techniques applied to public health problems: A bibliometric analysis from 2009 to 2018. *Computers & Industrial Engineering*, *138*, 106120.

Dubin, R., Fotheringham, A. S., & Rogerson, P. A. (2009). Spatial weights. *The Sage Handbook of Spatial Analysis*, 125-158.

Düzgün, H., & Kemeç, S. (2008). Spatial and geographically weighted regression. In: Shekhar, S., Xiong, H. (eds) *Encyclopedia of GIS*. Springer, Boston, MA.

Ebi, K. L., & Hess, J. J. (2020). Health risks due to climate change: Inequity in causes and consequences: Study examines health risks due to climate change. *Health Affairs*, *39*(12), 2056-2062.

Ebi, K. L., Capon, A., Berry, P., Broderick, C., de Dear, R., Havenith, G., ... & Jay, O. (2021). Hot weather and heat extremes: Health risks. *The Lancet*, *398*(10301), 698-708.

Edwards, P. N. (2011). History of climate modeling. *Wiley Interdisciplinary Reviews: Climate Change*, *2*(1), 128-139.

Ehrlich, M. V., & Overman, H. G. (2020). Place-based policies and spatial disparities across European cities. *Journal of Economic Perspectives*, *34*(3), 128-149.

Ellena, M., Ballester, J., Mercogliano, P., Ferracin, E., Barbato, G., Costa, G., & Ingole, V. (2020b). Social inequalities in heat-attributable mortality in the city of Turin, northwest of Italy: A time series analysis from 1982 to 2018. *Environmental Health*, *19*(1), 1-14.

Ellena, M., Breil, M., & Soriani, S. (2020a). The heat-health nexus in the urban context: A systematic literature review exploring the socio-economic vulnerabilities and built environment characteristics. *Urban Climate*, *34*, 100676.

European Environment Agency (2024). *European city air quality viewer*. Retrieved from https://www.eea.europa.eu/en/topics/in-depth/air-pollution/european-city-air-quality-viewer on 09/09/2024.

Farnia, L., Cavalli, L., Lizzi, G., & Vergalli, S. (2019). Methodological insights to measure the Agenda 2030 at urban level in Italy. *Sustainability*, *11*(17), 4598.

Fenner, R., & Cernev, T. (2021). The implications of the Covid-19 pandemic for delivering the Sustainable Development Goals. *Futures*, *128*, 102726.

Ferreira, L. D. C. M., Nogueira, M. C., Pereira, R. V. D. B., de Farias, W. C. M., Rodrigues, M. M. D. S., Teixeira, M. T. B., & Carvalho, M. S. (2019). Ambient temperature and mortality due to acute myocardial infarction in Brazil: An ecological study of time-series analyses. *Scientific Reports*, *9*(1), 13790.

Flowerdew, R., Manley, D. J., & Sabel, C. E. (2008). Neighbourhood effects on health: does it matter where you draw the boundaries?. *Social Science & Medicine*, *66*(6), 1241-1255.

Fonseca-Rodríguez, O., Sheridan, S. C., Lundevaller, E. H., & Schumann, B. (2020). Hot and cold weather based on the spatial synoptic classification and cause-specific mortality in Sweden: A time-stratified case-crossover study. *International Journal of Biometeorology*, *64*(9), 1435-1449.

Frome, E. L., & Checkoway, H. (1985). Use of Poisson regression models in estimating incidence rates and ratios. *American Journal of Epidemiology*, *121*(2), 309-323.

Gafni-Pappas, G., & Khan, M. (2023). Predicting daily emergency department visits using machine learning could increase accuracy. *The American Journal of Emergency Medicine*, *65*, 5-11.

Gardner, W., Mulvey, E. P., & Shaw, E. C. (1995). Regression analyses of counts and rates: Poisson, overdispersed Poisson, and negative binomial models. *Psychological Bulletin*, *118*(3), 392.

Gasparrini, A. (2014). Modeling exposure–lag–response associations with distributed lag non-linear models. *Statistics in Medicine*, *33*(5), 881-899.

Gasparrini, A., Armstrong, B., & Kenward, M. G. (2010). Distributed lag non-linear models. *Statistics in Medicine*, *29*(21), 2224-2234.

Ge, E., Su, M., Zhao, R., Huang, Z., Shan, Y., & Wei, X. (2021). Geographical disparities in access to hospital care in Ontario, Canada: A spatial coverage modelling approach. *BMJ Open*, *11*(1), e041474.

Gerlings, J., Jensen, M. S., & Shollo, A. (2022). Explainable AI, but explainable to whom? An exploratory case study of XAI in healthcare. *Handbook of Artificial Intelligence in Healthcare: Vol 2: Practicalities and Prospects*, 169-198.

Gestal Romaní, S., Figueiras, A., & Royé, D. (2023). Effect of temperature on emergency ambulance call-outs for cardiovascular causes: A scoping review. *Environment & Health*, *1*(1), 6-14.

Getis, A., & Aldstadt, J. (2004). Constructing the spatial weights matrix using a local statistic. *Geographical Analysis*, *36*(2), 90-104.

Ghazal, T. M., Hasan, M. K., Alshurideh, M. T., Alzoubi, H. M., Ahmad, M., Akbar, S. S., ... & Akour, I. A. (2021). IoT for smart cities: Machine learning approaches in smart healthcare—A review. *Future Internet*, *13*(8), 218.

Gianquintieri, L., Brovelli, M. A., Pagliosa, A., Bonora, R., Sechi, G. M., & Caiani, E. G. (2021). Geospatial correlation analysis between air pollution indicators and estimated speed of COVID-19 diffusion in the Lombardy region (Italy). *International Journal of Environmental Research and Public Health*, *18*(22), 12154.

Gianquintieri, L., Brovelli, M. A., Pagliosa, A., Dassi, G., Brambilla, P. M., Bonora, R., ... & Caiani, E. G. (2022). Generating high-granularity COVID-19 territorial early alerts using emergency medical services and machine learning. *International Journal of Environmental Research and Public Health*, *19*(15), 9012.

Gianquintieri, L., Oxoli, D., Caiani, E.G., Brovelli, M.A. (2023). Land use influence on ambient PM2.5 and ammonia concentrations: Correlation analyses in the Lombardy region, Italy. *AGILE GIScience Series 4*, 1-7.

Giles-Corti, B., Lowe, M., & Arundel, J. (2020). Achieving the SDGs: Evaluating indicators to be used to benchmark and monitor progress towards creating healthy and sustainable cities. *Health Policy*, *124*(6), 581-590.

Godfrey, R., & Julien, M. (2005). Urbanisation and health. *Clinical Medicine*, *5*(2), 137.

Goldberg, S. A., Cash, R. E., Peters, G., Weiner, S. G., Greenough, P. G., & Seethala, R. (2021). The impact of COVID-19 on statewide EMS use for cardiac emergencies and stroke in Massachusetts. *Journal of the American College of Emergency Physicians Open*, *2*(1), e12351.

Golgher, A. B., & Voss, P. R. (2016). How to interpret the coefficients of spatial models: Spillovers, direct and indirect effects. *Spatial Demography*, *4*(3), 175-205.

González-Alonso, J. (2012). Human thermoregulation and the cardiovascular system. *Experimental Physiology*, *97*(3), 340-346.

Gospodini, A. (2006). Portraying, classifying and understanding the emerging landscapes in the post-industrial city. *Cities*, *23*(5), 311-330.

Green, M. A., Daras, K., Davies, A., Barr, B., & Singleton, A. (2018). Developing an openly accessible multi-dimensional small area index of 'Access to Healthy Assets and Hazards' for Great Britain, 2016. *Health & Place*, *54*, 11-19.

Greenberg, M., & Schneider, D. (2023). Population density: What does it really mean in geographical health studies?. *Health & Place*, *81*, 103001.

Grekousis, G., & Liu, Y. (2019). Where will the next emergency event occur? Predicting ambulance demand in emergency medical services using artificial intelligence. *Computers, Environment and Urban Systems*, *76*, 110-122.

Griggs, D. J., Nilsson, M., Stevance, A., & McCollum, D. (2017). *A guide to SDG interactions: from science to implementation*. International Council for Science, Paris.

Gu, S., Zhang, L., Sun, S., Wang, X., Lu, B., Han, H., ... & Wang, A. (2020). Projections of temperature-related cause-specific mortality under climate change scenarios in a coastal city of China. *Environment International*, *143*, 105889.

Guijarro, F., & Poyatos, J. A. (2018). Designing a sustainable development goal index through a goal programming model: The case of EU-28 countries. *Sustainability*, *10*(9), 3167.

Guo, H., Du, P., Zhang, H., Zhou, Z., Zhao, M., Wang, J., ... & Feng, X. (2022b). Time series study on the effects of daily average temperature on the mortality from respiratory diseases and circulatory diseases: A case study in Mianyang City. *BMC Public Health*, *22*(1), 1001.

Guo, Y. T., Bernard Goggins, W., Chan, E. Y. Y., & Ho, K. F. (2022a). Individual socioeconomic status as a modifier of the association between high ambient temperature and hospital admissions: A time series study in Hong Kong, 2010–2019. *Environmental Science and Pollution Research*, *29*(44), 67353-67361.

Hajat, S., Vardoulakis, S., Heaviside, C., & Eggen, B. (2014). Climate change effects on human health: Projections of temperature-related mortality for the UK during the 2020s, 2050s and 2080s. *J Epidemiol Community Health*, *68*(7), 641-648.

Hák, T., Janoušková, S., & Moldan, B. (2016). Sustainable Development Goals: A need for relevant indicators. *Ecological Indicators*, *60*, 565-573.

Halleck Vega, S., & Elhorst, J. P. (2015). The SLX model. *Journal of Regional Science*, *55*(3), 339-363.

Hamdi, M., Lachiver, G., & Michaud, F. (1999). A new predictive thermal sensation index of human response. *Energy and Buildings*, *29*(2), 167-178.

Han, Z., Zhao, J., Leung, H., Ma, K. F., & Wang, W. (2019). A review of deep learning models for time series prediction. *IEEE Sensors Journal*, *21*(6), 7833-7848.

Hartigan, J. A., & Wong, M. A. (1979). Algorithm AS 136: A k-means clustering algorithm. *Journal of the Royal Statistical Society. Series C (Applied Statistics)*, *28*(1), 100-108.

Hashtarkhani, S., Kiani, B., Mohammadi, A., MohammadEbrahimi, S., Dehghan-Tezerjani, M., Samimi, T., ... & Matthews, S. A. (2021). Spatio-temporal epidemiology of emergency medical requests in a large urban area. A scan-statistic approach. *Geospatial Health*, *16*(2).

Heaviside, C., Macintyre, H., & Vardoulakis, S. (2017). The urban heat island: Implications for health in a changing environment. *Current Environmental Health Reports*, *4*, 296-305.

Helm, J. M., Swiergosz, A. M., Haeberle, H. S., Karnuta, J. M., Schaffer, J. L., Krebs, V. E., ... & Ramkumar, P. N. (2020). Machine learning and artificial intelligence: Definitions, applications, and future directions. *Current Reviews in Musculoskeletal Medicine*, *13*, 69-76.

Heo, S., Chen, C., Kim, H., Sabath, B., Dominici, F., Warren, J. L., ... & Bell, M. L. (2021). Temporal changes in associations between high temperature and hospitalizations by greenspace: Analysis in the Medicare population in 40 US northeast counties. *Environment International*, *156*, 106737.

Hermansen, A. H., & Mengshoel, O. J. (2021, December). Forecasting ambulance demand using machine learning: A case study from Oslo, Norway. In *2021 IEEE Symposium Series on Computational Intelligence (SSCI)* (pp. 01-10). IEEE.

Heymann, M. (2010). The evolution of climate ideas and knowledge. *Wiley Interdisciplinary Reviews: Climate Change*, *1*(4), 581-597.

Ho, H. C., Wong, M. S., Man, H. Y., Shi, Y., & Abbas, S. (2019). Neighborhood-based subjective environmental vulnerability index for community health assessment: Development, validation and evaluation. *Science of the Total Environment*, *654*, 1082-1090.

Hopkins, E. (1986). Working-class housing in Birmingham during the Industrial Revolution. *International Review of Social History*, *31*(1), 80-94.

Hopp, S., Dominici, F., & Bobb, J. F. (2018). Medical diagnoses of heat wave-related hospital admissions in older adults. *Preventive Medicine*, *110*, 81-85.

Houghton, J. (2005). Global warming. *Reports on Progress in Physics*, *68*(6), 1343.

Hu, K., Guo, Y., Hochrainer-Stigler, S., Liu, W., See, L., Yang, X., ... & Qi, J. (2019). Evidence for urban–rural disparity in temperature–mortality relationships in Zhejiang Province, China. *Environmental Health Perspectives*, *127*(3), 037001.

Hu, Y., Cato, K. D., Chan, C. W., Dong, J., Gavin, N., Rossetti, S. C., & Chang, B. P. (2023). Use of real-time information to predict future arrivals in the emergency department. *Annals of Emergency Medicine*, *81*(6), 728-737.

Huang, C., Cheng, J., Phung, D., Tawatsupa, B., Hu, W., & Xu, Z. (2018). Mortality burden attributable to heatwaves in Thailand: A systematic assessment incorporating evidence-based lag structure. *Environment International*, *121*, 41-50.

Huang, W. T. K., Masselot, P., Bou-Zeid, E., Fatichi, S., Paschalis, A., Sun, T., ... & Manoli, G. (2023). Economic valuation of temperature-related mortality attributed to urban heat islands in European cities. *Nature Communications*, *14*(1), 7438.

Huang, Z., Lin, H., Liu, Y., Zhou, M., Liu, T., Xiao, J., ... & Wang, L. (2015). Individual-level and community-level effect modifiers of the temperature–mortality relationship in 66 Chinese communities. *BMJ Open*, *5*(9), e009172.

Huijts, T., Stornes, P., Eikemo, T. A., Bambra, C., & HiNews Consortium. (2017). The social and behavioural determinants of health in Europe: Findings from the European Social Survey (2014) special module on the social determinants of health. *The European Journal of Public Health*, *27*(suppl_1), 55-62.

Hunt, B. G. (2007). A climatology of heat waves from a multimillennial simulation. *Journal of Climate*, *20*(15), 3802-3821.

Ikotun, A. M., Ezugwu, A. E., Abualigah, L., Abuhaija, B., & Heming, J. (2023). K-means clustering algorithms: A comprehensive review, variants analysis, and advances in the era of big data. *Information Sciences*, *622*, 178-210.

Iñiguez, C., Royé, D., & Tobías, A. (2021). Contrasting patterns of temperature related mortality and hospitalization by cardiovascular and respiratory diseases in 52 Spanish cities. *Environmental Research*, *192*, 110191.

International Organization for Standardization (ISO). *ISO/TS 21564:2019 – Health Informatics — Terminology resource map quality measures (MapQual).* Retrieved from https://www.iso.org/standard/71088.html on 14/10/2023.

Intergovernmental Panel on Climate Change (IPCC) (2022). *Climate Change 2022: Impacts, Adaptation and Vulnerability*. Contribution of Working Group II to the Sixth Assessment Report of the Intergovernmental Panel on Climate Change [H.-O. Pörtner, D.C. Roberts, M. Tignor, E.S. Poloczanska, K. Mintenbeck, A. Alegría, M. Craig, S. Langsdorf, S. Löschke, V. Möller, A. Okem, B. Rama (eds.)]. Cambridge University Press. 3056.

Intergovernmental Panel on Climate Change (IPCC) (2023). *Summary for Policymakers*. In: Climate Change 2023: Synthesis Report.Contribution of Working Groups I, II and III to the Sixth Assessment Report of the Intergovernmental Panel on Climate Change [Core Writing Team, H. Lee and J. Romero (eds.)]. IPCC, Geneva, Switzerland, pp. 1-34

Iranpour, S., Khodakarim, S., Shahsavani, A., Khosravi, A., & Etemad, K. (2020). Modification of the effect of ambient air temperature on cardiovascular and respiratory mortality by air pollution in Ahvaz, Iran. *Epidemiology and Health*, *42*.

Istituto Nazionale di Statistica (Istat) (2024). *Banca Dati*. Retrieved from http://dati.istat.it/ on 24/03/2024.

Istituto Nazionale di Statistica (Istat) (2023a). *Popolazione residente al 1° gennaio – Lombardia*. Retrieved from http://dati.istat.it/ on 27/10/2023a.

Istituto Nazionale di Statistica (Istat) (2023b). *Il Rapporto SDGs*. Retrieved from https://www.istat.it/it/benessere-e-sostenibilit%C3%A0/obiettivi-di-sviluppo-sostenibile/il-rapporto-sdgs on 1/082023b.

Jay, O., Capon, A., Berry, P., Broderick, C., de Dear, R., Havenith, G., ... & Ebi, K. L. (2021). Reducing the health effects of hot weather and heat extremes: from personal cooling strategies to green cities. *The Lancet*, *398*(10301), 709-724.

Jia, P., Stein, A., James, P., Brownson, R. C., Wu, T., Xiao, Q., ... & Wang, Y. (2019). Earth observation: Investigating noncommunicable diseases from space. *Annual Review of Public Health*, *40*(1), 85-104.

Jiang, S., Liu, Q., & Ding, B. (2023). A systematic review of the modelling of patient arrivals in emergency departments. *Quantitative Imaging in Medicine and Surgery*, *13*(3), 1957.

Jiang, S., Warren, J. L., Scovronick, N., Moss, S. E., Darrow, L. A., Strickland, M. J., ... & Chang, H. H. (2021). Using logic regression to characterize extreme heat exposures and their health associations: A time-series study of emergency department visits in Atlanta. *BMC Medical Research Methodology*, *21*(1), 87.

Jiang, Y., Hu, J., Peng, L., Li, H., Ji, J. S., Fang, W., ... & Chen, R. (2022). Non-optimum temperature increases risk and burden of acute myocardial infarction onset: A nationwide case-crossover study at hourly level in 324 Chinese cities. *EClinicalMedicine*, *50*.

Jiang, Y., Mao, F., Li, Y., Liu, J., Zhang, Y., Jiang, Y., ... & Zhou, M. (2018). Construction of China cardiovascular health index. *BMC Public Health*, *18*(1), 1-10.

Ju, L., Ringler, T., & Gunzburger, M. (2011). Voronoi tessellations and their application to climate and global modeling. *Numerical Techniques for Global Atmospheric Models*, 313-342.

Kåks, P., & Målqvist, M. (2021). Using an urban child health index to detect intra-urban disparities in Sweden. *Scandinavian Journal of Public Health*, *49*(5), 563-570.

Kaltenthaler, E., Maheswaran, R., & Beverley, C. (2004). Population-based health indexes: A systematic review. *Health Policy*, *68*(2), 245-255.

Kameneva, M. V., Watach, M. J., & Borovetz, H. S. (1999). Gender difference in rheologic properties of blood and risk of cardiovascular diseases. *Clinical Hemorheology and Microcirculation*, *21*(3-4), 357-363.

Kamireddy, C. R., & Keshavamurthy, B. N. (2016, December). Efficient routing of 108 ambulances using clustering techniques. In *2016 IEEE International Conference on Computational Intelligence and Computing Research (ICCIC)* (pp. 1-6). IEEE.

Kang, C., Park, C., Lee, W., Pehlivan, N., Choi, M., Jang, J., & Kim, H. (2020). Heatwave-related mortality risk and the risk-based definition of heat wave in South Korea: A nationwide time-series study for 2011–2017. *International Journal of Environmental Research and Public Health*, *17*(16), 5720.

Karingula, S. R., Ramanan, N., Tahmasbi, R., Amjadi, M., Jung, D., Si, R., ... & Coelho Jr, C. N. (2021, October). Boosted embeddings for time-series forecasting. In *International Conference on Machine Learning, Optimization, and Data Science* (pp. 1-14). Cham: Springer International Publishing.

Katayama, Y., Kanehara, A., Yamashita, Y., & Kitamura, T. (2022). The characteristics and outcomes of patients transported by ambulance due to ambulatory care sensitive condition: A population-based descriptive study in Osaka, Japan. *Frontiers in Public Health*, *10*, 911675.

Kaushik, S., Choudhury, A., Sheron, P. K., Dasgupta, N., Natarajan, S., Pickett, L. A., & Dutt, V. (2020). AI in healthcare: Time-series forecasting using statistical, neural, and ensemble architectures. *Frontiers in Big Data*, *3*, 4.

Kenney, W. L. (1985). A review of comparative responses of men and women to heat stress. *Environmental Research*, *37*(1), 1-11.

Kenny, G. P., Yardley, J., Brown, C., Sigal, R. J., & Jay, O. (2010). Heat stress in older individuals and patients with common chronic diseases. *CMAJ*, *182*(10), 1053-1060.

Khan, Y., Verhaeghe, N., Devleesschauwer, B., Cavillot, L., Gadeyne, S., Pauwels, N. S., ... & De Smedt, D. (2023). Impact of the COVID-19 pandemic on delayed care of cardiovascular diseases in Europe: A systematic review. *The Lancet*, *402*, S61.

Kienbacher, C. L., Kaltenberger, R., Schreiber, W., Tscherny, K., Fuhrmann, V., Roth, D., & Herkner, H. (2021). Extreme weather conditions as a gender-specific risk factor for acute myocardial infarction. *The American Journal of Emergency Medicine*, *43*, 50-53.

Kim, E. J., & Kim, H. (2017). Effect modification of individual-and regional-scale characteristics on heat wave-related mortality rates between 2009 and 2012 in Seoul, South Korea. *Science of The Total Environment*, *595*, 141-148.

Kim, J. H., & Choi, I. (2021). Choosing the level of significance: A decision-theoretic approach. *Abacus*, *57*(1), 27-71.

Kim, K. H., Kabir, E., & Ara Jahan, S. (2014). A review of the consequences of global climate change on human health. *Journal of Environmental Science and Health, Part C*, *32*(3), 299–318.

Kim, S. W., & Brown, R. D. (2021). Urban heat island (UHI) variations within a city boundary: A systematic literature review. *Renewable and Sustainable Energy Reviews*, *148*, 111256.

Kino, S., Hsu, Y. T., Shiba, K., Chien, Y. S., Mita, C., Kawachi, I., & Daoud, A. (2021). A scoping review on the use of machine learning in research on social determinants of health: Trends and research prospects. *SSM-Population Health*, *15*, 100836.

Kirby, R. S., Delmelle, E., & Eberth, J. M. (2017). Advances in spatial epidemiology and geographic information systems. *Annals of Epidemiology*, *27*(1), 1-9.

Kiss, P., Carcel, C., Hockham, C., & Peters, S. A. (2021). The impact of the COVID-19 pandemic on the care and management of patients with acute cardiovascular disease: A systematic review. *European Heart Journal-Quality of Care and Clinical Outcomes*, *7*(1), 18-27.

Knol, M. J., Le Cessie, S., Algra, A., Vandenbroucke, J. P., & Groenwold, R. H. (2012). Overestimation of risk ratios by odds ratios in trials and cohort studies: Alternatives to logistic regression. *CMAJ*, *184*(8), 895-899.

Komac, B., Ciglič, R., Loose, A., Pavšek, M., Čermelj, S., Oštir, K., ... & Topole, M. (2016). Urban heat island in the Ljubljana city. *Counteracting Urban Heat Island Effects in a Global Climate Change Scenario*, 323-344.

Kontopoulou, V. I., Panagopoulos, A. D., Kakkos, I., & Matsopoulos, G. K. (2023). A review of ARIMA vs. machine learning approaches for time series forecasting in data driven networks. *Future Internet*, *15*(8), 255.

Kranc, H., Novack, V., Shtein, A., Sherman, R., & Novack, L. (2021). Extreme temperature and out-of-hospital-cardiac-arrest. Nationwide study in a hot climate country. *Environmental Health*, *20*, 1-13.

Kreatsoulas, C., & Anand, S. S. (2010). The impact of social determinants on cardiovascular disease. *Canadian Journal of Cardiology*, *26*, 8C-13C.

Krellenberg, K., Welz, J., Link, F., & Barth, K. (2017). Urban vulnerability and the contribution of socio-environmental fragmentation: Theoretical and methodological pathways. *Progress in Human Geography*, *41*(4), 408-431.

Ksibi, A., Mhamdi, H., Ayadi, M., Almuqren, L., Alqahtani, M. S., Ansari, M. D., ... & Hedi, S. (2023). Secure and fast emergency road healthcare service based on blockchain technology for smart cities. *Sustainability*, *15*(7), 5748.

Kubiszewski, I., Mulder, K., Jarvis, D., & Costanza, R. (2022). Toward better measurement of sustainable development and wellbeing: A small number of SDG indicators reliably predict life satisfaction. *Sustainable Development*, *30*(1), 139-148.

Kyobutungi, C., Grau, A., Stieglbauer, G., & Becher, H. (2005). Absolute temperature, temperature changes and stroke risk: A case-crossover study. *European Journal of Epidemiology*, *20*, 693-698.

Lafortune, G., Fuller, G., Moreno, J., Schmidt-Traub, G., & Kroll, C. (2018). SDG index and dashboards detailed methodological paper. *Sustainable Development Solutions Network*, *9*, 1-56.

Lam, H. C. Y., Chan, J. C. N., Luk, A. O. Y., Chan, E. Y. Y., & Goggins, W. B. (2018). Short-term association between ambient temperature and acute myocardial infarction hospitalizations for diabetes mellitus patients: A time series study. *PLoS Medicine*, *15*(7), e1002612.

Lamichhane, S., Eğilmez, G., Gedik, R., Bhutta, M. K. S., & Erenay, B. (2021). Benchmarking OECD countries' sustainable development performance: A goal-specific principal component analysis approach. *Journal of Cleaner Production*, *287*, 125040.

Lavados, P. M., Olavarría, V. V., & Hoffmeister, L. (2018). Ambient temperature and stroke risk: Evidence supporting a short-term effect at a population level from acute environmental exposures. *Stroke*, *49*(1), 255-261.

Lawrence, M. G. (2005). The relationship between relative humidity and the dewpoint temperature in moist air: A simple conversion and applications. *Bulletin of the American Meteorological Society*, *86*(2), 225-234.

Layton, J. B., Li, W., Yuan, J., Gilman, J. P., Horton, D. B., & Setoguchi, S. (2020). Heatwaves, medications, and heat-related hospitalization in older Medicare beneficiaries with chronic conditions. *PloS ONE*, *15*(12), e0243665.

Lee, B. J., Kim, B., & Lee, K. (2014). Air pollution exposure and cardiovascular disease. *Toxicological Research*, *30*(2), 71-75.

Leichtmann, B., Humer, C., Hinterreiter, A., Streit, M., & Mara, M. (2023). Effects of Explainable Artificial Intelligence on trust and human behavior in a high-risk decision task. *Computers in Human Behavior*, *139*, 107539.

Leon, D. A. (2008). Cities, urbanization and health. *International Journal of Epidemiology*, *37*(1), 4-8.

Li, F., Yigitcanlar, T., Nepal, M., Thanh, K. N., & Dur, F. (2022). Understanding urban heat vulnerability assessment methods: A PRISMA review. *Energies*, *15*(19), 6998.

Li, M., Shaw, B. A., Zhang, W., Vásquez, E., & Lin, S. (2019b). Impact of extremely hot days on emergency department visits for cardiovascular disease among older adults in New York State. *International Journal of Environmental Research and Public Health*, *16*(12), 2119.

Li, N., Ma, J., Liu, F., Zhang, Y., Ma, P., Jin, Y., & Zheng, Z. J. (2021). Associations of apparent temperature with acute cardiac events and subtypes of acute coronary syndromes in Beijing, China. *Scientific Reports*, *11*(1), 15229.

Li, Y., Akkus, C., Yu, X., Joyner, A., Kmet, J., Sweat, D., & Jia, C. (2019a). Heatwave events and mortality outcomes in Memphis, Tennessee: Testing effect modification by socioeconomic status and urbanicity. *International Journal of Environmental Research and Public Health*, *16*(22), 4568.

Lian, H., Ruan, Y., Liang, R., Liu, X., & Fan, Z. (2015). Short-term effect of ambient temperature and the risk of stroke: A systematic review and meta-analysis. *International Journal of Environmental Research and Public Health*, *12*(8), 9068-9088.

Lim, B., & Zohren, S. (2021). Time-series forecasting with deep learning: A survey. *Philosophical Transactions of the Royal Society A*, *379*(2194), 20200209.

Lim, S. S., Allen, K., Bhutta, Z. A., Dandona, L., Forouzanfar, M. H., Fullman, N., ... & Chang, J. C. (2016). Measuring the health-related Sustainable Development Goals in 188 countries: A baseline analysis from the Global Burden of Disease Study 2015. *The Lancet*, *388*(10053), 1813-1850.

Lima, O. A. C. P. D., Kruger, E., & Tennant, M. (2022). São Paulo urban health index: Measuring and mapping health disparities. *Revista Brasileira de Epidemiologia*, *25*, e220005.

Lin, Y. K., Cheng, C. P., Kim, H., & Wang, Y. C. (2021). Risk of ambulance services associated with ambient temperature, fine particulate and its constituents. *Scientific Reports*, *11*(1), 1651.

Liu, H., Yan, G., Duan, Z., & Chen, C. (2021b). Intelligent modeling strategies for forecasting air quality time series: A review. *Applied Soft Computing*, *102*, 106957.

Liu, J., Varghese, B. M., Hansen, A., Xiang, J., Zhang, Y., Dear, K., ... & Bi, P. (2021a). Is there an association between hot weather and poor mental health outcomes? A systematic review and meta-analysis. *Environment International*, *153*, 106533.

Liu, J., Varghese, B. M., Hansen, A., Zhang, Y., Driscoll, T., Morgan, G., ... & Bi, P. (2022). Heat exposure and cardiovascular health outcomes: A systematic review and meta-analysis. *The Lancet Planetary Health*, *6*(6), e484-e495.

Liu, L., Peng, Z., Wu, H., Jiao, H., Yu, Y., & Zhao, J. (2018b). Fast identification of urban sprawl based on K-means clustering with population density and local spatial entropy. *Sustainability*, *10*(8), 2683.

Liu, S., Chan, E. Y. Y., Goggins, W. B., & Huang, Z. (2020). The mortality risk and socioeconomic vulnerability associated with high and low temperature in Hong Kong. *International Journal of Environmental Research and Public Health*, *17*(19), 7326.

Liu, X., Kong, D., Fu, J., Zhang, Y., Liu, Y., Zhao, Y., ... & Fan, Z. (2018a). Association between extreme temperature and acute myocardial infarction hospital admissions in Beijing, China: 2013–2016. *PloS ONE*, *13*(10), e0204706.

Logullo, P., de Beyer, J. A., Kirtley, S., Schlüssel, M. M., & Collins, G. S. (2024). Open access journal publication in health and medical research and open science: benefits, challenges and limitations. *BMJ Evidence-Based Medicine*, *29*(4), 223-228.

Loh, H. W., Ooi, C. P., Seoni, S., Barua, P. D., Molinari, F., & Acharya, U. R. (2022). Application of explainable artificial intelligence for healthcare: A systematic review of the last decade (2011–2022). *Computer Methods and Programs in Biomedicine*, *226*, 107161.

Lorant, V., Thomas, I., Deliège, D., & Tonglet, R. (2001). Deprivation and mortality: The implications of spatial autocorrelation for health resources allocation. *Social Science & Medicine*, *53*(12), 1711-1719.

Loyola-Gonzalez, O. (2019). Black-box vs. white-box: Understanding their advantages and weaknesses from a practical point of view. *IEEE Access*, *7*, 154096-154113.

Lu, P., Zhao, Q., Xia, G., Xu, R., Hanna, L., Jiang, J., ... & Guo, Y. (2021). Temporal trends of the association between ambient temperature and cardiovascular mortality: A 17-year case-crossover study. *Environmental Research Letters*, *16*(4), 045004.

Lu, Y., Nakicenovic, N., Visbeck, M., & Stevance, A. S. (2015). Policy: Five priorities for the UN Sustainable Development Goals. *Nature*, *520*(7548), 432-433.

Lundberg, S. M., & Lee, S. I. (2017). A unified approach to interpreting model predictions. *Advances in Neural Information Processing Systems*, *30*.

Luo, J., Chan, E. H., Du, J., Feng, L., Jiang, P., & Xu, Y. (2022). Developing a health-spatial indicator system for a healthy city in small and midsized cities. *International Journal of Environmental Research and Public Health*, *19*(6), 3294.

Luqman, M., Rayner, P. J., & Gurney, K. R. (2023). On the impact of urbanisation on CO2 emissions. *NPJ Urban Sustainability*, *3*(1), 6.

Lynn, R. (2010). In Italy, north–south differences in IQ predict differences in income, education, infant mortality, stature, and literacy. *Intelligence*, *38*(1), 93-100.

Ma, Y., Zhou, L., & Chen, K. (2020). Burden of cause-specific mortality attributable to heat and cold: A multicity time-series study in Jiangsu Province, China. *Environment International*, *144*, 105994.

Macintyre, H. L., Heaviside, C., Taylor, J., Picetti, R., Symonds, P., Cai, X. M., & Vardoulakis, S. (2018). Assessing urban population vulnerability and environmental risks across an urban area during heatwaves–Implications for health protection. *Science of the Total Environment*, *610*, 678-690.

Maclagan, L. C., Park, J., Sanmartin, C., Mathur, K. R., Roth, D., Manuel, D. G., ... & Tu, J. V. (2014). The CANHEART health index: A tool for monitoring the cardiovascular health of the Canadian population. *CMAJ*, *186*(3), 180-187.

Maclure, M. (1991). The case-crossover design: A method for studying transient effects on the risk of acute events. *American Journal of Epidemiology*, *133*(2), 144-153.

Madrigano, J., Mittleman, M. A., Baccarelli, A., Goldberg, R., Melly, S., Von Klot, S., & Schwartz, J. (2013). Temperature, myocardial infarction, and mortality: Effect modification by individual-and area-level characteristics. *Epidemiology*, *24*(3), 439-446.

Malambo, P., Kengne, A. P., De Villiers, A., Lambert, E. V., & Puoane, T. (2016). Built environment, selected risk factors and major cardiovascular disease outcomes: A systematic review. *PloS ONE*, *11*(11), e0166846.

Malchaire, J., Piette, A., Kampmann, B., Mehnert, P., Gebhardt, H. J., Havenith, G., ... & Griefahn, B. (2001). Development and validation of the predicted heat strain model. *Annals of Occupational Hygiene*, *45*(2), 123-135.

Mangano, A. (2010). An analysis of the regional differences in health care utilization in Italy. *Health & Place*, *16*(2), 301-308.

Marek, L., Hobbs, M., Wiki, J., Kingham, S., & Campbell, M. (2021). The good, the bad, and the environment: Developing an area-based measure of access to health-promoting and health-constraining environments in New Zealand. *International Journal of Health Geographics*, *20*, 1-20.

Maria Bruno, R., Di Pilla, M., Ancona, C., Sørensen, M., Gesi, M., Taddei, S., ... & Virdis, A. (2017). Environmental factors and hypertension. *Current Pharmaceutical Design*, *23*(22), 3239-3246.

Maria, E., Budiman, E., & Taruk, M. (2020, February). Measure distance locating nearest public facilities using Haversine and Euclidean methods. In *Journal of Physics: Conference Series* (Vol. *1450*, No. 1, p. 012080). IOP Publishing.

Marmot, M., Allen, J., Bell, R., Bloomer, E., & Goldblatt, P. (2012). WHO European review of social determinants of health and the health divide. *The Lancet*, *380*(9846), 1011-1029.

Martin, R. J., Mousavi, R., & Saydam, C. (2021). Predicting emergency medical service call demand: A modern spatiotemporal machine learning approach. *Operations Research for Health Care*, *28*, 100285.

Martins, L. M., Coz, E., Maucort-Boulch, D., & Hacid, M. S. (2023). Machine Learning with environmental predictors to forecast hospital attendances and in-hospital mortality: A systematic review. *Authorea Preprints*.

Masini, R. P., Medeiros, M. C., & Mendes, E. F. (2023). Machine learning advances for time series forecasting. *Journal of Economic Surveys*, *37*(1), 76-111.

Masselot, P., Chebana, F., Campagna, C., Lavigne, É., Ouarda, T. B., & Gosselin, P. (2021). Machine learning approaches to identify thresholds in a heat-health warning system context. *Journal of the Royal Statistical Society Series A: Statistics in Society*, *184*(4), 1326-1346.

Maulik, U., & Bandyopadhyay, S. (2002). Performance evaluation of some clustering algorithms and validity indices. *IEEE Transactions on Pattern Analysis and Machine Intelligence*, *24*(12), 1650-1654.

Maxwell, S. L., Butt, N., Maron, M., McAlpine, C. A., Chapman, S., Ullmann, A., ... & Watson, J. E. (2019). Conservation implications of ecological responses to extreme weather and climate events. *Diversity and Distributions*, *25*(4), 613-625.

Medina-Ramón, M., Zanobetti, A., Cavanagh, D. P., & Schwartz, J. (2006). Extreme temperatures and mortality: Assessing effect modification by personal characteristics and specific cause of death in a multi-city case-only analysis. *Environmental Health Perspectives*, *114*(9), 1331-1336.

Mena, C., Sepúlveda, C., Fuentes, E., Ormazábal, Y., & Palomo, I. (2018). Spatial analysis for the epidemiological study of cardiovascular diseases: A systematic literature search. *Geospatial Health*, *13*(1).

Michetti, M., Gualtieri, M., Anav, A., Adani, M., Benassi, B., Dalmastri, C., ... & Uccelli, R. (2022). Climate change and air pollution: Translating their interplay into present and future mortality risk for Rome and Milan municipalities. *Science of The Total Environment*, *830*, 154680.

Milano Geoportale (2023). Retrieved from https://geoportale.comune.milano.it/sit/open-data/ on 12/01/2023.

Mishra, P., & Singh, G. (2023). Internet of medical things healthcare for sustainable smart cities: Current status and future prospects. *Applied Sciences*, *13*(15), 8869.

Mitchell, J. F. (1989). The “greenhouse” effect and climate change. *Reviews of Geophysics*, *27*(1), 115-139.

Moghadamnia, M. T., Ardalan, A., Mesdaghinia, A., Keshtkar, A., Naddafi, K., & Yekaninejad, M. S. (2017). Ambient temperature and cardiovascular mortality: A systematic review and meta-analysis. *PeerJ*, *5*, e3574.

Moghadamnia, M. T., Ardalan, A., Mesdaghinia, A., Naddafi, K., & Yekaninejad, M. S. (2018). Association between apparent temperature and acute coronary syndrome admission in Rasht, Iran. *Heart Asia*, *10*(2).

Mooney, S. J., & Pejaver, V. (2018). Big data in public health: Terminology, machine learning, and privacy. *Annual Review of Public Health*, *39*(1), 95-112.

Morais, L., Lopes, A., & Nogueira, P. (2021). Human health outcomes at the neighbourhood scale implications: Elderly's heat-related cardiorespiratory mortality and its influencing factors. *Science of the Total Environment*, *760*, 144036.

Moran, D. S., Pandolf, K. B., Shapiro, Y., Heled, Y., Shani, Y., Mathew, W. T., & Gonzalez, R. R. (2001). An environmental stress index (ESI) as a substitute for the wet bulb globe temperature (WBGT). *Journal of Thermal Biology*, *26*(4-5), 427-431.

Morgan, R. L., Whaley, P., Thayer, K. A., & Schünemann, H. J. (2018). Identifying the PECO: A framework for formulating good questions to explore the association of environmental and other exposures with health outcomes. *Environment International*, *121*(Pt 1), 1027.

Münzel, T., Hahad, O., Sørensen, M., Lelieveld, J., Duerr, G. D., Nieuwenhuijsen, M., & Daiber, A. (2022). Environmental risk factors and cardiovascular diseases: A comprehensive expert review. *Cardiovascular Research*, *118*(14), 2880-2902.

Murage, P., Kovats, S., Sarran, C., Taylor, J., McInnes, R., & Hajat, S. (2020). What individual and neighbourhood-level factors increase the risk of heat-related mortality? A case-crossover study of over 185,000 deaths in London using high-resolution climate datasets. *Environment International*, *134*, 105292.

Murtagh, F., & Legendre, P. (2014). Ward's hierarchical agglomerative clustering method: Which algorithms implement Ward's criterion?. *Journal of Classification*, *31*(3), 274-295.

Murtas, R., Tunesi, S., Andreano, A., & Russo, A. G. (2022). Time-series cohort study to forecast emergency department visits in the city of Milan and predict high demand: A 2-day warning system. *BMJ Open*, *12*(4), e056017.

Mustajoki, J., Borchardt, S., Büttner, L., Köhler, B., Lepenies, R., Lyytimäki, J., ... & Richard, D. (2022). Ambitiousness of Sustainable Development Goal (SDG) targets: Classification and implications for policy making. *Discover Sustainability*, *3*(1), 36.

Nagano, K., & Horikoshi, T. (2011). Development of outdoor thermal index indicating universal and separate effects on human thermal comfort. *International Journal of Biometeorology*, *55*, 219-227.

Nairn, J. R., & Fawcett, R. J. (2015). The excess heat factor: A metric for heatwave intensity and its use in classifying heatwave severity. *International Journal of Environmental Research and Public Health*, *12*(1), 227-253.

Nakai, T., Saiki, S., & Nakamura, M. (2021, December). Medium-term prediction for ambulance demand of heat stroke using weekly weather forecast. In *2021 8th International Conference on Internet of Things: Systems, Management and Security (IOTSMS)* (pp. 1-8). IEEE.

National Academies of Sciences, Division on Earth, Life Studies, Board on Atmospheric Sciences, Committee on Extreme Weather Events, & Climate Change Attribution. (2016). Attribution of extreme weather events in the context of climate change. *National Academies Press*.

Nawrot, T. S., Staessen, J. A., Fagard, R. H., Bortel, L. M. V., & Struijker-Boudier, H. A. (2005). Endothelial function and outdoor temperature. *European Journal of Epidemiology*, *20*, 407-410.

Neelin, J. D. (2010). *Climate change and climate modeling*. Cambridge University Press.

Neiderud, C. J. (2015). How urbanization affects the epidemiology of emerging infectious diseases. *Infection Ecology & Epidemiology*, *5*(1), 27060.

Nieuwenhuijsen, M. J. (2018). Influence of urban and transport planning and the city environment on cardiovascular disease. *Nature Reviews Cardiology*, *15*(7), 432-438.

Nikolov, G., & Botseva, D. (2018). European Cities of the future in a response to the urban challenges. *Synthesis of Science and Society in Solving Global Problems*, *58*.

Niu, Y., Li, Z., Gao, Y., Liu, X., Xu, L., Vardoulakis, S., ... & Liu, Q. (2021). A systematic review of the development and validation of the heat vulnerability index: major factors, methods, and spatial units. *Current Climate Change Reports*, *7*(3), 87-97.

North, B. J., & Sinclair, D. A. (2012). The intersection between aging and cardiovascular disease. *Circulation Research*, *110*(8), 1097-1108.

Novaes, A. G., de Cursi, J. S., da Silva, A. C., & Souza, J. C. (2009). Solving continuous location–districting problems with Voronoi diagrams. *Computers & Operations Research*, *36*(1), 40-59.

Nwani, S., & Ujah, J. C. (2023). Achieving infant mortality SDG 3 target in South Asia and Sub-Saharan Africa: Does carbon emission matter?. *Green and Low-Carbon Economy*.

O'Neill, M. S., Zanobetti, A., & Schwartz, J. (2003). Modifiers of the temperature and mortality association in seven US cities. *American Journal of Epidemiology*, *157*(12), 1074-1082.

Obradovich, N., Migliorini, R., Paulus, M. P., & Rahwan, I. (2018). Empirical evidence of mental health risks posed by climate change. *Proceedings of the National Academy of Sciences*, *115*(43), 10953-10958.

OECD| European Commission. (2020). *A new perspective on urbanisation*.

Ogojiaku, C. N., Allen, J. C., Anson-Dwamena, R., Barnett, K. S., Adetona, O., Im, W., & Hood, D. B. (2020). The health opportunity index: Understanding the input to disparate health outcomes in vulnerable and high-risk census tracts. *International Journal of Environmental Research and Public Health*, *17*(16), 5767.

Oliveira, G. M., Vidal, D. G., Ferraz, M. P., Cabeda, J. M., Pontes, M., Maia, R. L., ... & Barreira, E. (2019). Measuring health vulnerability: An interdisciplinary indicator applied to mainland Portugal. *International Journal of Environmental Research and Public Health*, *16*(21), 4121.

Onozuka, D., Gasparrini, A., Sera, F., Hashizume, M., & Honda, Y. (2019). Future projections of temperature-related excess out-of-hospital cardiac arrest under climate change scenarios in Japan. *Science of the Total Environment*, *682*, 333-339.

Ostfeld, R. S., Glass, G. E., & Keesing, F. (2005). Spatial epidemiology: an emerging (or re-emerging) discipline. *Trends in Ecology & Evolution*, *20*(6), 328-336.

Oudin Åström, D., Åström, C., Forsberg, B., Vicedo-Cabrera, A. M., Gasparrini, A., Oudin, A., & Sundquist, K. (2020). Heat wave–related mortality in Sweden: A case-crossover study investigating effect modification by neighbourhood deprivation. *Scandinavian Journal of Public Health*, *48*(4), 428-435.

Page, M. J., McKenzie, J. E., Bossuyt, P. M., Boutron, I., Hoffmann, T. C., Mulrow, C. D., ... & Moher, D. (2021). The PRISMA 2020 statement: an updated guideline for reporting systematic reviews. *BMJ*, *372*.

Paillard, D. (2001). Glacial cycles: toward a new paradigm. *Reviews of Geophysics*, *39*(3), 325-346.

Pampalon, R., Hamel, D., & Gamache, P. (2010). Health inequalities in urban and rural Canada: Comparing inequalities in survival according to an individual and area-based deprivation index. *Health & Place*, *16*(2), 416-420.

Pandit, S., & Gupta, S. (2011). A comparative study on distance measuring approaches for clustering. *International Journal of Research in Computer Science*, *2*(1), 29-31.

Parliari, D., Cheristanidis, S., Giannaros, C., Keppas, S. C., Papadogiannaki, S., de'Donato, F., ... & Melas, D. (2022). Short-term effects of apparent temperature on cause-specific mortality in the Urban Area of Thessaloniki, Greece. *Atmosphere*, *13*(6), 852.

Parmezan, A. R. S., Souza, V. M., & Batista, G. E. (2019). Evaluation of statistical and machine learning models for time series prediction: Identifying the state-of-the-art and the best conditions for the use of each model. *Information Sciences*, *484*, 302-337.

Parry, M., Green, D., Zhang, Y., & Hayen, A. (2019). Does particulate matter modify the short-term association between heat waves and hospital admissions for cardiovascular diseases in greater Sydney, Australia?. *International Journal of Environmental Research and Public Health*, *16*(18), 3270.

Peel, M. C., Finlayson, B. L., & McMahon, T. A. (2007). Updated world map of the Köppen-Geiger climate classification. *Hydrology and Earth System Sciences*, *11*(5), 1633-1644.

Perčič, S., Kukec, A., Cegnar, T., & Hojs, A. (2018). Number of heat wave deaths by diagnosis, sex, age groups, and area, in Slovenia, 2015 vs. 2003. *International Journal of Environmental Research and Public Health*, *15*(1), 173.

Pérez, E., Braën, C., Boyer, G., Mercille, G., Rehany, É., Deslauriers, V., ... & Potvin, L. (2020). Neighbourhood community life and health: A systematic review of reviews. *Health & Place*, *61*, 102238.

Perkins-Kirkpatrick, S. E., & Lewis, S. C. (2020). Increasing trends in regional heatwaves. *Nature Communications*, *11*(1), 3357.

Perkins, S. E., & Alexander, L. V. (2013). On the measurement of heat waves. *Journal of Climate*, *26*(13), 4500-4517.

Petralli, M., Morabito, M., Cecchi, L., Crisci, A., & Orlandini, S. (2012). Urban morbidity in summer: Ambulance dispatch data, periodicity and weather. *Open Medicine*, *7*(6), 775-782.

Petsis, S., Karamanou, A., Kalampokis, E., & Tarabanis, K. (2022). Forecasting and explaining emergency department visits in a public hospital. *Journal of Intelligent Information Systems*, *59*(2), 479-500.

Pfeifer, K., Oudin Åström, D., Martinsone, Ž., Kaļužnaja, D., & Oudin, A. (2020). Evaluating mortality response associated with two different Nordic heat warning systems in Riga, Latvia. *International Journal of Environmental Research and Public Health*, *17*(21), 7719.

Phillips, D. R. (1993). Urbanization and human health. *Parasitology*, *106*(S1), S93-S107.

Piliuk, K., & Tomforde, S. (2023). Artificial Intelligence in emergency medicine. A systematic literature review. *International Journal of Medical Informatics*, *105274*.

Pineo, H., Glonti, K., Rutter, H., Zimmermann, N., Wilkinson, P., & Davies, M. (2018a). Urban health indicator tools of the physical environment: A systematic review. *Journal of Urban Health*, *95*, 613-646.

Pineo, H., Zimmermann, N., Cosgrave, E., Aldridge, R. W., Acuto, M., & Rutter, H. (2018b). Promoting a healthy cities agenda through indicators: Development of a global urban environment and health index. *Cities & Health*, *2*(1), 27-45.

Piracha, A., & Chaudhary, M. T. (2022). Urban air pollution, urban heat island and human health: A review of the literature. *Sustainability*, *14*(15), 9234.

Pizzi, S., Caputo, F., & Venturelli, A. (2020). Accounting to ensure healthy lives: Critical perspective from the Italian National Healthcare System. Corporate Governance: *The International Journal of Business in Society*, *20*(3), 445-460.

Porter, W. C., & Heald, C. L. (2019). The mechanisms and meteorological drivers of the summertime ozone–temperature relationship. *Atmospheric Chemistry and Physics*, *19*(21), 13367-13381.

Pradhan, P., Costa, L., Rybski, D., Lucht, W., & Kropp, J. P. (2017). A systematic study of Sustainable Development Goal (SDG) interactions. *Earth's Future*, *5*(11), 1169-1179.

Pramanik, S., Punia, M., Yu, H., & Chakraborty, S. (2022). Is dense or sprawl growth more prone to heat-related health risks? Spatial regression-based study in Delhi, India. *Sustainable Cities and Society*, *81*, 103808.

Praveen, S., & Joshi, K. (2022). Explainable Artificial Intelligence in health care: How XAI improves user trust in high-risk decisions. In *Explainable Edge AI: A Futuristic Computing Perspective* (pp. 89-99). Cham: Springer International Publishing.

Prokhorenkova, L., Gusev, G., Vorobev, A., Dorogush, A. V., & Gulin, A. (2018). CatBoost: Unbiased boosting with categorical features. *Advances in Neural Information Processing Systems*, *31*.

Puertas, R., & Marti, L. (2023). Regional analysis of the sustainable development of two Mediterranean countries: Spain and Italy. *Sustainable Development*, *31*(2), 797-811.

Qiu, H., Luo, L., Su, Z., Zhou, L., Wang, L., & Chen, Y. (2020). Machine learning approaches to predict peak demand days of cardiovascular admissions considering environmental exposure. *BMC Medical Informatics and Decision Making*, *20*, 1-11.

Rahimi, H. (2022). Assessment of the spatial difference at the level of neighborhoods based on accessibility variables in Yazd city, Iran. *GeoJournal*, 1-18.

Ramgopal, S., Dunnick, J., Owusu-Ansah, S., Siripong, N., Salcido, D. D., & Martin-Gill, C. (2019). Weather and temporal factors associated with use of emergency medical services. *Prehospital Emergency Care*, *23*(6), 802-810.

Ramgopal, S., Westling, T., Siripong, N., Salcido, D. D., & Martin-Gill, C. (2021). Use of a metalearner to predict emergency medical services demand in an urban setting. *Computer Methods and Programs in Biomedicine*, *207*, 106201.

Ramírez-Moreno, M. A., Keshtkar, S., Padilla-Reyes, D. A., Ramos-López, E., García-Martínez, M., Hernández-Luna, M. C., ... & Lozoya-Santos, J. D. J. (2021). Sensors for sustainable smart cities: A review. *Applied Sciences*, *11*(17), 8198.

Ranta, A., Kang, J., Saad, A., Wasay, M., Béjot, Y., Ozturk, S., ... & Douwes, J. (2024). Climate change and stroke: A topical narrative review. *Stroke*, *55*(4), 1118-1128.

Rausand, M. (2013). *Risk assessment: Theory, methods, and applications* (Vol. *115*). John Wiley & Sons.

Regione Lombardia (2022). *CITTA METROPOLITANA MILANO - 2016 Dati traffic*. Retrieved from https://dati.lombardia.it/ on 19/07/2022.

Reiners, P., Sobrino, J., & Kuenzer, C. (2023). Satellite-derived land surface temperature dynamics in the context of global change—A review. *Remote Sensing*, *15*(7), 1857.

Remeseiro, B., & Bolon-Canedo, V. (2019). A review of feature selection methods in medical applications. *Computers in Biology and Medicine*, *112*, 103375.

Remigio, R. V., Jiang, C., Raimann, J., Kotanko, P., Usvyat, L., Maddux, F. W., ... & Sapkota, A. (2019). Association of extreme heat events with hospital admission or mortality among patients with end-stage renal disease. *JAMA Network Open*, *2*(8), e198904-e198904.

Remington, P. L., Catlin, B. B., & Gennuso, K. P. (2015). The county health rankings: Rationale and methods. *Population Health Metrics*, *13*(1), 1-12.

Richiedei, A., & Pezzagno, M. (2022). Territorializing and monitoring of sustainable development goals in italy: An overview. *Sustainability*, *14*(5), 3056.

Rickels, W., Dovern, J., Hoffmann, J., Quaas, M. F., Schmidt, J. O., & Visbeck, M. (2016). Indicators for monitoring Sustainable Development Goals: An application to oceanic development in the European Union. *Earth's Future*, *4*(5), 252-267.

Rivera, A. J., Muñoz, J. C., Pérez-Goody, M. D., de San Pedro, B. S., Charte, F., Elizondo, D., ... & del Jesus, M. J. (2023). XAIRE: An ensemble-based methodology for determining the relative importance of variables in regression tasks. Application to a hospital emergency department. *Artificial Intelligence in Medicine*, *137*, 102494.

Robinson, P. J. (2001). On the definition of a heat wave. *Journal of Applied Meteorology and Climatology*, *40*(4), 762-775.

Rochat, D., & Marty, F. (2018). *Economiesuisse. Santé: quatre facteurs qui pèsent plus dans la balance que les soins et les traitements*. Retrieved from https://www.economiesuisse.ch/fr/articles/sante-quatre-facteurs-qui-pesent-plus-dans-la-balance-que-les-soins-et-les-traitements on 01/08/2024.

Rocque, R. J., Beaudoin, C., Ndjaboue, R., Cameron, L., Poirier-Bergeron, L., Poulin-Rheault, R. A., ... & Witteman, H. O. (2021). Health effects of climate change: An overview of systematic reviews. *BMJ Open*, *11*(6), e046333.

Rodrigues, M., Santana, P., & Rocha, A. (2020). Statistical modelling of temperature-attributable deaths in Portuguese metropolitan areas under climate change: Who is at risk?. *Atmosphere*, *11*(2), 159.

Roldán, E., Gómez, M., Pino, M. R., & Díaz, J. (2015). The impact of extremely high temperatures on mortality and mortality cost. *International Journal of Environmental Health Research*, *25*(3), 277-287.

Romani, S. G., Royé, D., Sánchez Santos, L., & Figueiras, A. (2020). Impact of extreme temperatures on ambulance dispatches due to cardiovascular causes in North-West Spain. *International Journal of Environmental Research and Public Health*, *17*(23), 9001.

Rostami-Tabar, B., & Hyndman, R. J. (2024). Hierarchical time series forecasting in emergency medical services. *Journal of Service Research*, 10946705241232169.

Rothenberg, R., Stauber, C., Weaver, S., Dai, D., Prasad, A., & Kano, M. (2015). Urban health indicators and indices—Current status. *BMC Public Health*, *15*, 1-14.

Rothenberg, R., Weaver, S. R., Dai, D., Stauber, C., Prasad, A., & Kano, M. (2014). A flexible urban health index for small area disparities. *Journal of Urban Health*, *91*, 823-835.

Roux, A. V. D., Mujahid, M. S., Hirsch, J. A., Moore, K., & Moore, L. V. (2016). The impact of neighborhoods on CV risk. *Global Heart*, *11*(3), 353-363.

Royé, D., Codesido, R., Tobías, A., & Taracido, M. (2020). Heat wave intensity and daily mortality in four of the largest cities of Spain. *Environmental Research*, *182*, 109027.

Sachs, J. D., Lafortune, G., Fuller, G., & Drumm, E. (2023). Implementing the SDG stimulus. *Sustainable development report*.

Sadler, R. C., Hippensteel, C., Nelson, V., Greene-Moton, E., & Furr-Holden, C. D. (2019). Community-engaged development of a GIS-based healthfulness index to shape health equity solutions. *Social Science & Medicine*, *227*, 63-75.

Saffary, T., Adegboye, O. A., Gayawan, E., Elfaki, F., Kuddus, M. A., & Saffary, R. (2020). Analysis of COVID-19 cases' spatial dependence in US counties reveals health inequalities. *Frontiers in Public Health*, *8*, 579190.

Sangkharat, K., Fisher, P., Thomas, G. N., Thornes, J., & Pope, F. D. (2019). The impact of air pollutants on ambulance dispatches: A systematic review and meta-analysis of acute effects. *Environmental Pollution*, *254*, 112769.

Sanhueza, A., Carvajal-Vélez, L., Mújica, O. J., Vidaletti, L. P., Victora, C. G., & Barros, A. J. (2021). SDG3-related inequalities in women's, children's and adolescents' health: An SDG monitoring baseline for Latin America and the Caribbean using national cross-sectional surveys. *BMJ Open*, *11*(8), e047779.

Sankoff, J. (2015). Environmental: heat illnesses: A hot topic in the setting of global climate change. *Australian Family Physician*, *44*(1/2), 22-26.

Santana, P., Freitas, Â., Costa, C., Stefanik, I., Santinha, G., Krafft, T., & Pilot, E. (2020). The role of cohesion policy funds in decreasing the health gaps measured by the EURO-HEALTHY population health index. *International Journal of Environmental Research and Public Health*, *17*(5), 1567.

Saranya, A., & Subhashini, R. (2023). A systematic review of Explainable Artificial Intelligence models and applications: Recent developments and future trends. *Decision Analytics Journal*, 100230.

Saucy, A., Ragettli, M. S., Vienneau, D., de Hoogh, K., Tangermann, L., Schäffer, B., ... & Röösli, M. (2021). The role of extreme temperature in cause-specific acute cardiovascular mortality in Switzerland: A case-crossover study. *Science of The Total Environment*, *790*, 147958.

Scepanovic, S., Obadic, I., Joglekar, S., Giustarini, L., Nattero, C., Quercia, D., & Zhu, X. (2024). MedSat: A public health dataset for England featuring medical prescriptions and satellite imagery. *Advances in Neural Information Processing Systems*, *36*.

Scharlemann, J. P., Brock, R. C., Balfour, N., Brown, C., Burgess, N. D., Guth, M. K., ... & Kapos, V. (2020). Towards understanding interactions between Sustainable Development Goals: The role of environment–human linkages. *Sustainability Science*, *15*, 1573-1584.

Schmidt-Traub, G., Kroll, C., Teksoz, K., Durand-Delacre, D., & Sachs, J. D. (2017). National baselines for the Sustainable Development Goals assessed in the SDG index and dashboards. *Nature Geoscience*, *10*(8), 547-555.

Schneider, A., & Breitner, S. (2016). Temperature effects on health—Current findings and future implications. *EBioMedicine*, *6*, 29-30.

Schulte, F., Röösli, M., & Ragettli, M. S. (2021). Heat-related cardiovascular morbidity and mortality in Switzerland: A clinical perspective. *Swiss Med Wkly*, *151*, w30013.

Schuurman, N., Bell, N., Dunn, J. R., & Oliver, L. (2007). Deprivation indices, population health and geography: An evaluation of the spatial effectiveness of indices at multiple scales. *Journal of Urban Health*, *84*, 591-603.

Scovronick, N., Sera, F., Acquaotta, F., Garzena, D., Fratianni, S., Wright, C. Y., & Gasparrini, A. (2018). The association between ambient temperature and mortality in South Africa: A time-series analysis. *Environmental Research*, *161*, 229-235.

Sera, F., Armstrong, B., Tobias, A., Vicedo-Cabrera, A. M., Åström, C., Bell, M. L., ... & Gasparrini, A. (2019). How urban characteristics affect vulnerability to heat and cold: A multi-country analysis. *International Journal of Epidemiology*, *48*(4), 1101-1112.

Shahmohamadi, P., Che-Ani, A. I., Etessam, I., Maulud, K. N. A., & Tawil, N. M. (2011). Healthy environment: The need to mitigate urban heat island effects on human health. *Procedia Engineering*, *20*, 61-70.

Sharifi, A., Pathak, M., Joshi, C., & He, B. J. (2021). A systematic review of the health co-benefits of urban climate change adaptation. *Sustainable Cities and Society*, *74*, 103190.

Sharma, A., Woodruff, S., Budhathoki, M., Hamlet, A. F., Chen, F., & Fernando, H. J. S. (2018). Role of green roofs in reducing heat stress in vulnerable urban communities—A multidisciplinary approach. *Environmental Research Letters*, *13*(9), 094011.

Sharma, S., Malarcher, A. M., Giles, W. H., & Myers, G. (2004). Racial, ethnic and socioeconomic disparities in the clustering of cardiovascular disease risk factors. *Ethnicity & Disease*, *14*(1), 43-48.

Shi, Y., Yang, J., Keith, M., Song, K., Li, Y., & Guan, C. (2022). Spatial accessibility patterns to public hospitals in Shanghai: An improved gravity model. *The Professional Geographer*, *74*(2), 265-289.

Shrestha, R., Flacke, J., Martinez, J., & Van Maarseveen, M. (2016). Environmental health related socio-spatial inequalities: Identifying “hotspots” of environmental burdens and social vulnerability. *International Journal of Environmental Research and Public Health*, *13*(7), 691.

Silva, E., Pereira, M. F., Vieira, J. T., Ferreira-Coimbra, J., Henriques, M., & Rodrigues, N. F. (2023). Predicting hospital emergency department visits accurately: A systematic review. *The International Journal of Health Planning and Management*, *38*(4), 904-917.

Silveira, I. H., Cortes, T. R., Oliveira, B. F. A., & Junger, W. L. (2021). Temperature and cardiovascular mortality in Rio de Janeiro, Brazil: Effect modification by individual-level and neighbourhood-level factors. *J Epidemiol Community Health*, *75*(1), 69-75.

Singh, N., Areal, A. T., Breitner, S., Zhang, S., Agewall, S., Schikowski, T., & Schneider, A. (2024). Heat and cardiovascular mortality: An epidemiological perspective. *Circulation Research*, *134*(9), 1098-1112.

Smith, J. B., Schneider, S. H., Oppenheimer, M., Yohe, G. W., Hare, W., Mastrandrea, M. D., ... & van Ypersele, J. P. (2009). Assessing dangerous climate change through an update of the Intergovernmental Panel on Climate Change (IPCC)“reasons for concern”. *Proceedings of the National Academy of Sciences*, *106*(11), 4133-4137.

Smith, T. T., Zaitchik, B. F., & Gohlke, J. M. (2013). Heat waves in the United States: Definitions, patterns and trends. *Climatic Change*, *118*, 811-825.

Sogno, P., Traidl-Hoffmann, C., & Kuenzer, C. (2020). Earth observation data supporting non-communicable disease research: A review. *Remote Sensing*, *12*(16), 2541.

Son, J. Y., Liu, J. C., & Bell, M. L. (2019). Temperature-related mortality: A systematic review and investigation of effect modifiers. *Environmental Research Letters*, *14*(7).

Song, X., Wang, S., Hu, Y., Yue, M., Zhang, T., Liu, Y., ... & Shang, K. (2017). Impact of ambient temperature on morbidity and mortality: An overview of reviews. *Science of the Total Environment*, *586*, 241-254.

Spensberger, C., Madonna, E., Boettcher, M., Grams, C. M., Papritz, L., Quinting, J. F., ... & Zschenderlein, P. (2020). Dynamics of concurrent and sequential Central European and Scandinavian heatwaves. *Quarterly Journal of the Royal Meteorological Society*, *146*(732), 2998-3013.

Staiger, H., Laschewski, G., & Grätz, A. (2012). The perceived temperature—A versatile index for the assessment of the human thermal environment. Part A: Scientific basics. *International Journal of Biometeorology*, *56*, 165-176.

Stanujkic, D., Popovic, G., Zavadskas, E. K., Karabasevic, D., & Binkyte-Veliene, A. (2020). Assessment of progress towards achieving Sustainable Development Goals of the “Agenda 2030” by using the CoCoSo and the Shannon Entropy methods: The case of the EU countries. *Sustainability*, *12*(14), 5717.

Steffen, W., Hughes, L., & Perkins, S. (2014). Heatwaves: Hotter, longer, more often. *Climate Council of Australia*.

Stephens, G. L., O'Brien, D., Webster, P. J., Pilewski, P., Kato, S., & Li, J. L. (2015). The albedo of Earth. *Reviews of Geophysics*, *53*(1), 141-163.

Stramba-Badiale, M., Fox, K. M., Priori, S. G., Collins, P., Daly, C., Graham, I., ... & Tendera, M. (2006). Cardiovascular diseases in women: A statement from the policy conference of the European Society of Cardiology. *European Heart Journal*, *27*(8), 994-1005.

Sudarshan, V. K., Brabrand, M., Range, T. M., & Wiil, U. K. (2021). Performance evaluation of Emergency Department patient arrivals forecasting models by including meteorological and calendar information: A comparative study. *Computers in Biology and Medicine*, *135*, 104541.

Susnjak, T., & Maddigan, P. (2023). Forecasting patient demand at urgent care clinics using explainable machine learning. *CAAI Transactions on Intelligence Technology*, *8*(3), 712-733.

Sustainable Development Solutions Network (SDSN) (2024). *About Us*. Retrieved from https://www.unsdsn.org/about/ on 13/05/2024.

Swain, R. B., & Ranganathan, S. (2021). Modeling interlinkages between Sustainable Development Goals using network analysis. *World Development*, *138*, 105136.

Syakur, M. A., Khotimah, B. K., Rochman, E. M. S., & Satoto, B. D. (2018, April). Integration k-means clustering method and elbow method for identification of the best customer profile cluster. In *IOP Conference Series: Materials Science and Engineering* (Vol. *336*, No. 1, p. 012017). IOP Publishing.

Szagri, D., Nagy, B., & Szalay, Z. (2023). How can we predict where heatwaves will have an impact?—A literature review on heat vulnerability indexes. *Urban Climate*, *52*, 101711.

Takano, T., & Nakamura, K. (2001). An analysis of health levels and various indicators of urban environments for Healthy Cities projects. *Journal of Epidemiology & Community Health*, *55*(4), 263-270.

Tamura, K., Langerman, S. D., Ceasar, J. N., Andrews, M. R., Agrawal, M., & Powell-Wiley, T. M. (2019). Neighborhood social environment and cardiovascular disease risk. *Current Cardiovascular Risk Reports*, *13*(4), 1-13.

Tan, J., Zheng, Y., Tang, X., Guo, C., Li, L., Song, G., ... & Chen, H. (2010). The urban heat island and its impact on heat waves and human health in Shanghai. *International Journal of Biometeorology*, *54*, 75-84.

Tang, K. J. W., Ang, C. K. E., Constantinides, T., Rajinikanth, V., Acharya, U. R., & Cheong, K. H. (2021). Artificial intelligence and machine learning in emergency medicine. *Biocybernetics and Biomedical Engineering*, *41*(1), 156-172.

Temenos, A., Tzortzis, I. N., Kaselimi, M., Rallis, I., Doulamis, A., & Doulamis, N. (2022). Novel insights in spatial epidemiology utilizing explainable AI (XAI) and remote sensing. *Remote Sensing*, *14*(13), 3074.

Thomas, R., Hsu, A., & Weinfurter, A. (2021). Sustainable and inclusive—Evaluating urban sustainability indicators' suitability for measuring progress towards SDG-11. *Environment and Planning B: Urban Analytics and City Science*, *48*(8), 2346-2362.

Tibshirani, R., Walther, G., & Hastie, T. (2001). Estimating the number of clusters in a data set via the gap statistic. *Journal of the Royal Statistical Society: Series B (Statistical Methodology)*, *63*(2), 411-423.

Toloo, G., FitzGerald, G., Aitken, P., Verrall, K., & Tong, S. (2013). Evaluating the effectiveness of heat warning systems: Systematic review of epidemiological evidence. *International Journal of Public Health*, *58*, 667-681.

Tong, S., & Ebi, K. (2019). Preventing and mitigating health risks of climate change. *Environmental Research*, *174*, 9-13.

Tong, S., FitzGerald, G., Wang, X. Y., Aitken, P., Tippett, V., Chen, D., ... & Guo, Y. (2015). Exploration of the health risk-based definition for heatwave: A multi-city study. *Environmental Research*, *142*, 696-702.

Toth, F. (2014). How health care regionalisation in Italy is widening the North–South gap. *Health Economics, Policy and Law*, *9*(3), 231-249.

Tuoane-Nkhasi, M., & van Eeden, A. (2017). Spatial patterns and correlates of mortality due to selected non-communicable diseases among adults in South Africa, 2011. *GeoJournal*, *82*, 1005-1034.

Turner, L. R., Barnett, A. G., Connell, D., & Tong, S. (2012). Ambient temperature and cardiorespiratory morbidity: A systematic review and meta-analysis. *Epidemiology*, *23*(4), 594-606.

Ummenhofer, C. C., & Meehl, G. A. (2017). Extreme weather and climate events with ecological relevance: A review. *Philosophical Transactions of the Royal Society B: Biological Sciences*, *372*(1723), 20160135.

United Nations Human Settlements Programme (UN-Habitat) (2024). *People Centred-Smart Cities*. Retrieved from https://unhabitat.org/programme/people-centred-smart-cities on 02/10/2024

United Nations (2023). *History of the Sustainable Development Goals*. Retrieved from https://sdgs.un.org/goals#history on 23/08/2023.

United Nations Human Settlements Programme (UN-Habitat) (2022). *Envisaging the future of Cities*. Retrieved from https://unhabitat.org/wcr/ on 01/08/2024.

Vimbi, V., Shaffi, N., & Mahmud, M. (2024). Interpreting artificial intelligence models: A systematic review on the application of LIME and SHAP in Alzheimer's disease detection. *Brain Informatics*, *11*(1), 10.

Vlahov, D., & Galea, S. (2002). Urbanization, urbanicity, and health. *Journal of Urban Health*, *79*, S1-S12.

Vogel, J. A., Burnham, R. I., McVaney, K., Havranek, E. P., Edwards, D., Hulac, S., & Sasson, C. (2022). The importance of neighborhood in 9-1-1 ambulance contacts: A geospatial analysis of medical and trauma emergencies in Denver. *Prehospital Emergency Care*, *26*(2), 233-245.

Vollmer, M. A., Glampson, B., Mellan, T., Mishra, S., Mercuri, L., Costello, C., ... & Bhatt, S. (2021). A unified machine learning approach to time series forecasting applied to demand at emergency departments. *BMC Emergency Medicine*, *21*, 1-14.

Wallgren, U. M., Järnbert-Pettersson, H., Sjölin, J., & Kurland, L. (2022). Association between variables measured in the ambulance and in-hospital mortality among adult patients with and without infection: A prospective cohort study. *BMC Emergency Medicine*, *22*(1), 185.

Wang, J. C., Chien, W. C., Chu, P., Chung, C. H., Lin, C. Y., & Tsai, S. H. (2019). The association between heat stroke and subsequent cardiovascular diseases. *PloS ONE*, *14*(2), e0211386.

Wang, P., Zhang, X., Hashizume, M., Goggins, W. B., & Luo, C. (2021a). A systematic review on lagged associations in climate–health studies. *International Journal of Epidemiology*, *50*(4), 1199-1212.

Wang, Q., He, Y., Hajat, S., Cheng, J., Xu, Z., Hu, W., ... & Huang, C. (2021b). Temperature-sensitive morbidity indicator: Consequence from the increased ambulance dispatches associated with heat and cold exposure. *International Journal of Biometeorology*, *65*(11), 1871-1880.

Wang, Y. C., Lin, Y. K., Chen, Y. J., Hung, S. C., Zafirah, Y., & Sung, F. C. (2020). Ambulance services associated with extreme temperatures and fine particles in a subtropical island. *Scientific Reports*, *10*(1), 2855.

Wargon, M., Guidet, B., Hoang, T. D., & Hejblum, G. (2009). A systematic review of models for forecasting the number of emergency department visits. *Emergency Medicine Journal*, *26*(6), 395-399.

Watts, J. D., & Kalkstein, L. S. (2004). The development of a warm-weather relative stress index for environmental applications. *Journal of Applied Meteorology and Climatology*, *43*(3), 503-513.

Weaver, S., Dai, D., Stauber, C. E., & Luo, R. (2014). *The Urban Health Index: A handbook for its calculation and use*.

Williamson, J. G. (1988). Migrant selectivity, urbanization, and industrial revolutions. *Population and Development Review*, 287-314.

Wong, H. T. (2023). Forecasting daily emergency ambulance service demand using biometeorological indexes. *International Journal of Biometeorology*, *67*(4), 565-572.

Wong, K. V., Paddon, A., & Jimenez, A. (2013). Review of world urban heat islands: Many linked to increased mortality. *Journal of Energy Resources Technology*, *135*(2), 022101.

World Bank Open Data. (2024). *Urban population (% of total population).* Retrieved from https://data.worldbank.org/indicator/SP.URB.TOTL.IN.ZS on 01/08/2024.

World Bank. (2022, October 6). *Urban Development*. Retrieved from https://www.worldbank.org/en/topic/urbandevelopment/overview on 26/01/2023.

World Health Organization (WHO) (2024a). *Heatwaves*. Retrieved from https://www.who.int/health-topics/heatwaves#tab=tab_1 on 29/07/2024.

World Health Organization (WHO) (2024b). *The top 10 causes of death*. Retrieved from https://www.who.int/news-room/fact-sheets/detail/the-top-10-causes-of-death on 29/07/2024.

World Health Organization (2021). *COP26 special report on climate change and health: the health argument for climate action*.

World Meteorological Organization (WMO) (2023). *Past eight years confirmed to be the eight warmest on record*. Retrieved from https://wmo.int/news/media-centre/past-eight-years-confirmed-be-eight-warmest-record on 07/09/2024.

World Meteorological Organization (WMO) (2024). *Climate*. Retrieved from https://wmo.int/topics/climate#:~:text=Main%20themes,to%20determine%20the%20average%20climate. on 28/04/2024.

Wright, R. W., Brand, R. A., Dunn, W., & Spindler, K. P. (2007). How to write a systematic review. *Clinical Orthopaedics and Related Research*, *455*, 23-29.

Wu, P. C., Lin, C. Y., Lung, S. C., Guo, H. R., Chou, C. H., & Su, H. J. (2011). Cardiovascular mortality during heat and cold events: Determinants of regional vulnerability in Taiwan. *Occupational and Environmental Medicine*, *68*(7), 525-530.

Wu, X., Fu, B., Wang, S., Song, S., Li, Y., Xu, Z., ... & Liu, J. (2022a). Decoupling of SDGs followed by re-coupling as sustainable development progresses. *Nature Sustainability*, *5*(5), 452-459.

Wu, Y., Mashhoodi, B., Patuano, A., Lenzholzer, S., Zertuche, L. N., & Acred, A. (2022b). Heat-prone neighbourhood typologies of European cities with temperate climate. *Sustainable Cities and Society*, *87*, 104174.

Xie, Y., Kulpanowski, D., Ong, J., Nikolova, E., & Tran, N. M. (2021). Predicting Covid-19 emergency medical service incidents from daily hospitalisation trends. *International Journal of Clinical Practice*, *75*(12), e14920.

Xie, Y., Xu, E., Bowe, B., & Al-Aly, Z. (2022). Long-term cardiovascular outcomes of COVID-19. *Nature Medicine*, *28*(3), 583-590.

Xu, E., Li, Y., Li, T., & Li, Q. (2022b). Association between ambient temperature and ambulance dispatch: A systematic review and meta-analysis. *Environmental Science and Pollution Research*, *29*(44), 66335-66347.

Xu, R., Shi, C., Wei, J., Lu, W., Li, Y., Liu, T., ... & Liu, Y. (2022a). Cause-specific cardiovascular disease mortality attributable to ambient temperature: A time-stratified case-crossover study in Jiangsu province, China. *Ecotoxicology and Environmental Safety*, *236*, 113498.

Xu, Z., Cheng, J., Hu, W., & Tong, S. (2018). Heatwave and health events: A systematic evaluation of different temperature indicators, heatwave intensities and durations. *Science of the Total Environment*, *630*, 679-689.

Xu, Z., FitzGerald, G., Guo, Y., Jalaludin, B., & Tong, S. (2016). Impact of heatwave on mortality under different heatwave definitions: A systematic review and meta-analysis. *Environment International*, *89*, 193-203.

Xu, Z., Watzek, J. T., Phung, D., Oberai, M., Rutherford, S., & Bach, A. J. (2023). Heat, heatwaves, and ambulance service use: A systematic review and meta-analysis of epidemiological evidence. *International Journal of Biometeorology*, *67*(10), 1523-1542.

Yan, D., Wu, S., Zhou, S., Li, F., & Wang, Y. (2021). Healthy city development for Chinese cities under dramatic imbalance: Evidence from 258 cities. *Sustainable Cities and Society*, *74*, 103157.

Yan, H. B., Li, S., Hui, C., Zhang, J., Li, S. Y., Li, Q. X., ... & Hu, D. Y. (2009). Factors influencing ambulance use in patients with ST-elevation myocardial infarction in Beijing, China. *Chinese Medical Journal*, *122*(3), 272-278.

Yang, J., Ou, C. Q., Ding, Y., Zhou, Y. X., & Chen, P. Y. (2012). Daily temperature and mortality: A study of distributed lag non-linear effect and effect modification in Guangzhou. *Environmental Health*, *11*, 1-9.

Yang, T. C., & Jensen, L. (2017). Climatic conditions and human mortality: Spatial and regional variation in the United States. *Population and Environment*, *38*, 261-285.

Yang, W., Su, Q., Zhou, M., & Qin, X. (2020). Ambulance allocation considering the spatial randomness of demand. *Computers & Industrial Engineering*, *139*, 106202.

Yanuar, F., Ibrahim, K., & Jemain, A. A. (2010). On the application of structural equation modeling for the construction of a health index. *Environmental Health and Preventive Medicine*, *15*, 285-291.

Yatim, A. N. M., Latif, M. T., Sofwan, N. M., Ahamad, F., Khan, M. F., Mahiyuddin, W. R. W., & Sahani, M. (2021). The association between temperature and cause-specific mortality in the Klang Valley, Malaysia. *Environmental Science and Pollution Research*, *28*(42), 60209-60220.

Ye, C., Schröder, P., Yang, D., Chen, M., Cui, C., & Zhuang, L. (2022). Toward healthy and liveable cities: A new framework linking public health to urbanization. *Environmental Research Letters*, *17*(6), 064035.

Yen, I. H., Michael, Y. L., & Perdue, L. (2009). Neighborhood environment in studies of health of older adults: A systematic review. *American Journal of Preventive Medicine*, *37*(5), 455-463.

Yin, P., Chen, R., Wang, L., Liu, C., Niu, Y., Wang, W., ... & Kan, H. (2018). The added effects of heatwaves on cause-specific mortality: A nationwide analysis in 272 Chinese cities. *Environment International*, *121*, 898-905.

You, Q., Jiang, Z., Kong, L., Wu, Z., Bao, Y., Kang, S., & Pepin, N. (2017). A comparison of heat wave climatologies and trends in China based on multiple definitions. *Climate Dynamics*, *48*, 3975-3989.

Yu, X., Xia, L., Xiao, J., Zheng, J., Xu, N., Feng, X., & Wei, X. (2021). Association of daily mean temperature and temperature variability with onset risks of acute aortic dissection. *Journal of the American Heart Association*, *10*(13), e020190.

Yuan, C., & Yang, H. (2019). Research on K-value selection method of K-means clustering algorithm. *J*, *2*(2), 226-235.

Zhai, G., Tian, Y., Zhang, K., Qi, J., & Chai, G. (2022). The effect of apparent temperature on hospital admissions for cardiovascular diseases in rural areas of Pingliang, China. *Annals of Agricultural and Environmental Medicine*, *29*(2).

Zhang, H., Wang, Y., Park, T. W., & Deng, Y. (2017). Quantifying the relationship between extreme air pollution events and extreme weather events. *Atmospheric Research*, *188*, 64-79.

Zhang, J., & Kai, F. Y. (1998). What's the relative risk?: A method of correcting the odds ratio in cohort studies of common outcomes. *Jama*, *280*(19), 1690-1691.

Zhang, W., Du, G., Xiong, L., Liu, T., Zheng, Z., Yuan, Q., ... & Hu, G. (2021). Extreme temperatures and cardiovascular mortality: Assessing effect modification by subgroups in Ganzhou, China. *Global Health Action*, *14*(1), 1965305.

Zhang, X. Q. (2016). The trends, promises and challenges of urbanisation in the world. *Habitat International*, *54*, 241-252.

Zhang, X., Noda, S., Himeno, R., & Liu, H. (2016). Cardiovascular disease-induced thermal responses during passive heat stress: An integrated computational study. *International Journal for Numerical Methods in Biomedical Engineering*, *32*(11), e02768.

Zhang, Z., Zhao, M., Zhang, Y., & Feng, Y. (2023). How does urbanization affect public health? New evidence from 175 countries worldwide. *Frontiers in Public Health*, *10*, 1096964.

Zheng, Y. Y., Ma, Y. T., Zhang, J. Y., & Xie, X. (2020). COVID-19 and the cardiovascular system. *Nature Reviews Cardiology*, *17*(5), 259-260.

Zhou, L., Chen, K., Chen, X., Jing, Y., Ma, Z., Bi, J., & Kinney, P. L. (2017). Heat and mortality for ischemic and hemorrhagic stroke in 12 cities of Jiangsu Province, China. *Science of the Total Environment*, *601*, 271-277.

Zio, E. (2018). The future of risk assessment. *Reliability Engineering & System Safety*, *177*, 176-190.

Zlatanova, S., Yan, J., Wang, Y., Diakité, A., Isikdag, U., Sithole, G., & Barton, J. (2020). Spaces in spatial science and urban applications—State of the art review. *ISPRS International Journal of Geo-Information*, *9*(1), 58.

List of Figures

Figure 1.1. Change in annual average global surface temperature as observed and simulated using human and natural, and only natural factors between 1850 and 2020. Shaded area represents 90% confidence interval for simulated values. 20
Figure 1.2. Global surface air temperature anomaly in 2023 with respect to 1991-2020 average 21
Figure 1.3. World's and European Union's urban population as percentage of total population in 1960-2023 (World Bank, 2024) 24
Figure 1.4. Rook, queen, and bishop contiguity first order neighbours 30
Figure 2.1. Administrative division of Italy on 1st January 2023 37
Figure 2.2. Geographical distribution of classes of municipalities defined by the Italian National Institute of Statistics (Istat) 37
Figure 2.3. Workflow of SDG3 index computation for the Italian municipalities 45
Figure 2.4. ISO/TS 21564:2019 measures of the quality of matching (represented by the colours where 0 is the best and 3 is the worst) of each Italian indicator included in the computation for each of the 28 official SDG3 indicators, here summarized in the 13 SDG3 targets. 47
Figure 2.5. Top panel: Boxplots of the considered 29 Italian indicators after normalization and ranking, as described in section 2.2.3. Bottom panel: Boxplots of the 11 SDG3 targets (i.e., the average of official indicators as described in equation 2.4 in section 2.2.3). 49
Figure 2.6. Final SDG3 index computed for all the 7,900 Italian municipalities 51
Figure 2.7. Boxplots of the SDG3 index in the Italian regions. The width of the boxplot is represented as proportional to the resident population. 52
Figure 2.8. Final SDG3 index and target 3.4. Noncommunicable diseases spatial autocorrelation types (from local Moran's Index as defined in section 2.2.4) 52
Figure 2.9. SDG3 targets' scores for 7,900 Italian municipalities: targets for which northern municipalities scores are high and southern municipalities scores are low 53
Figure 2.10. SDG3 targets' scores for 7,900 Italian municipalities: targets for which northern municipalities scores are low and southern municipalities scores are high 54
Figure 2.11. SDG3 targets' scores for 7,900 Italian municipalities: targets for which no clear geographical trend emerges. For targets 3.6. Road traffic, and 3.9. Environmental health, Jenks natural breaks method was used to optimize the visualization; for 3.9. Environmental health, nine classes instead of 10 were used to optimize the categorization. 54
Figure 2,12. Standard deviation across all targets' scores 55
Figure 2.13. Final SDG3 index computed for all the 7,900 Italian municipalities, with a focus on the Lombardy region 56
Figure 2.14. (a) CV mortality rate (per 1,000 residents) computed for all the 7,900 Italian municipalities, (b) with a focus on the Lombardy region 58
Figure 2.15. (a) LISA clusters for CV mortality rate for all the 7,900 Italian municipalities, (b) with a focus on the Lombardy region 58
Figure 3.1. Schematic of the results of the systematic literature selection process, including open access papers published between 2018 and 2022, written in English language, and resulting from the application of the selected query (see text for details) 71
Figure 3.2. Heat indexes as a function of air temperature as defined in Table 3.2, computed assuming relative humidity=50%, wind speed=1 m/s, water vapor pressure=2.34 kPa and dew point temperature calculated according to Lawrence (2005) 74
Figure 3.3. Summary of articles by the outcome 75
Figure 3.4. Geographical distribution of the studies. Countries with at least three studies are labelled with the corresponding number of articles. 76
Figure 3.5. Summary of selected articles divided by continent of interest for the analysis, stratified by sample size of the examined study group; in 10 (18.5%) studies, the sample size was inferred considering the average incidence and the study period. 76
Figure 3.6. Summary of the influence of heat on all-cause cardiovascular outcomes. The notation e in the last column means that the sample size was inferred as not directly specified in the relevant study. The letters a–l refer to the combination of criteria used to define heat (MMT – minimum mortality temperature): a – air temperature + percentile + MMT or equivalent, b – air temperature + percentile and duration + non-heatwave, c – air temperature +relative humidity+wind speed + percentile + MMT or equivalent, d – air temperature + percentile + non-heatwave, f – air temperature + dew point temperature + percentile + MMT or equivalent, g – air temperature + percentile + another percentile, h – air temperature + absolute value and duration + non-heatwave, i – air temperature + other + another percentile, j – air temperature +relative humidity+wind speed + percentile + another

percentile, k – air temperature + absolute value + MMT or equivalent, l – air temperature +water vapor pressure + absolute value and duration + non-heatwave. References as defined in Table A3.1.....78
Figure 3.7. Relationship between the percentage deviation of the considered heat threshold from the mean annual temperature and associated cardiovascular risk, subdivided as all-cause and cause-specific mortality or morbidity. RR - relative risk; OR - odds ratio; IDR - incidence density ratio. Dot size is proportional to the duration of the observation period expressed as number of years.....82
Figure 4.1. (a) The location of Milan in national and regional geographical context, and (b) borders of the city of Milan 92
Figure 4.2. Population pyramid for Milan on 1st January 2023 (Istat, 2023a) 93
Figure 4.3. Schema of calculation of hourly final value for each meteorological indicator. Absolute values are illustrative and do not represent true values of any of the indicators. NaN – missing value; n – number of stations considered; Station_i – non-missing value of an indicator for station i.....96
Figure 4.4. Schema of calculation of mean, minimum and maximum daily apparent temperature (AT). T – temperature (°C), RH – relative humidity (%), WS – wind speed (m/s); AT_i - value of AT at hour i.....97
Figure 4.5. Contour plot obtained through distributed lag non-linear model for cardiovascular emergencies in Milan, Italy in May-September 2017-2022, (a) with the inclusion of air pollutants, and (b) without the inclusion of air pollutants. RR – relative risk estimated against reference mean daily apparent temperature of 19.6 °C. .100
Figure 4.6. Contour plot obtained through distributed lag non-linear model for cardiovascular emergencies in Milan, Italy in May-September 2017-2022 for (a) female patients, (b) above 65 years old patients, (c) non-severe emergencies, (d) emergencies requiring transportation to hospital, (e) fatal emergencies. RR – relative risk estimated against reference mean daily apparent temperature.....101
Figure 4.7. Relative risk estimated by Poisson regression for heat thresholds set from the 90th to 99th percentile of annual apparent temperature distribution for three lags considered (see text for details). Shaded area represents 95% confidence interval.....102
Figure 4.8. Relative risk of a cardiovascular emergency associated with each percentile of the apparent temperature distribution at lag0 in Milan, Italy. The blue shaded area represents a 95% confidence interval. RR – relative risk, CI – confidence interval.....103
Figure 4.9. Geographical location of ARPA measurement stations for meteorological parameters and air pollutants. T – air temperature, RH – relative humidity, WS – wind speed, CO – carbon monoxide, NO_2 – nitrogen dioxide, SO_2 – sulfur dioxide, O_3 – ozone, PM10 – particulate matters of less than 10 µm in diameter, PM2.5 – particulate matters of less than 2.5 µm in diameter. 104
Figure 4.10. Spearman correlation matrix for mean daily values of meteorological parameters and air pollutants in May-September 2017-2022 in Milan, Italy. AT – apparent temperature, T – air temperature, RH – relative humidity, WS – wind speed, CO – carbon monoxide, NO_2 – nitrogen dioxide, SO_2 – sulfur dioxide, O_3 – ozone, PM10 – particulate matters of less than 10 µm in diameter, PM2.5 – particulate matters of less than 2.5 µm in diameter.....105
Figure 4.11. Apparent temperature, air temperature and relative humidity in May-September 2017-2022 in Milan, Italy 107
Figure 4.12. Daily number of cardiovascular emergencies in May-September 2017-2022 in Milan, Italy and mean daily apparent temperature. Heat days are marked in red. CV – cardiovascular, AT – apparent temperature....108
Figure 4.13. Summary of the distribution of the daily number of cardiovascular emergencies in May-September 2017-2022 in Milan, Italy, stratified by year, month, day of the week and heat days.....109
Figure 4.14. Heatmap of CV emergencies in May-September 2017-2022 in Milan, Italy (a) on non-heat days and (b) on heat days. Radius equal to 1,000 meters.....113
Figure 5.1. The 88 Nuclei of Local Identity (NIL) of Milan 118
Figure 5.2. Geographical distribution of the Central, Residential, and Peripheral socio-urban clusters obtained through k-means clustering of socio-urban features of Milan's 86 Nuclei of Local Identity (NIL) 126
Figure 5.3. Top panel: (a) Map of cardiovascular vulnerability to heat (CV_VtoH) in each Nucleus of Local Identity (NIL), with reference to three socio-urban clusters, and (b) LISA clusters derived from local Moran's Index. HH – high-high, LL – low-low, HL – high-low, LH – low-high, gMI – global Moran's Index. Bottom panel: Boxplots of the CV_VtoH in each of three socio-urban clusters. The width of the boxplots is proportional to the logarithm of the number of residents. Dashed lines within boxplots represent standard deviation.....128
Figure 5.4. (a) Geographical distribution of the socio-urban vulnerability to heat (SU_VtoH) in the whole city of Milan, and (b) the corresponding LISA clusters. HH – high-high, LL – low-low, HL – high-low, LH – low-high, gMI – global Moran's Index. 133
Figure 5.5. Relationship between cardiovascular vulnerability to heat (CV_VtoH) and socio-urban vulnerability to heat (SU_VtoH). Dot size is proportional to the logarithm of the number of residents. Dashed lines represent the ordinary least squares regression line in the whole city and in the three socio-urban clusters.....133
Figure 5.6. Geographical distribution of the Nuclei of Local Identity (NIL) with both cardiovascular vulnerability to heat (CV_VtoH) and socio-urban vulnerability to heat (SU_VtoH) above the 60th percentile of their distribution

(red tones; highly vulnerable NIL), or below the 40th percentile of their distribution (green tones; low vulnerable NIL).....134
Figure 5.7. Emergencies forming non-noise HDBSCAN clusters during heat and non-heat days. Zone A - zone where HDBSCAN clusters exist during non-heat days but not during heat days; zone B - zone where HDBSCAN clusters exist in both meteorological conditions, but with a considerable spatial shift in point concentration; zone C - zones where HDBSCAN clusters experience a considerable increase in spatial coverage during heat days compared to non-heat days. CV_VtoH – cardiovascular vulnerability to heat, SU_VtoH – socio-urban vulnerability to heat.....135
Figure 6.1. Time series of daily cardiovascular (CV) emergencies in Milan in May-September 2017-2023, decomposed into trend, seasonal component and residual. Red dots indicate heat days based on the applied criterion (see text for further detail). Mean daily apparent temperature (AT) is also shown overimposed to the daily emergencies.....152
Figure 6.2. Summary of the distribution of the daily number of cardiovascular (CV) emergencies in May-September 2017-2023 for each of the three socio-urban clusters of Milan (i.e., Central, Residential, Peripheral), stratified by year, month, day of the week and heat days 154
Figure 6.3. Autocorrelation plots for daily cardiovascular emergencies in May-September 2017-2023 in the whole city and for its three socio-urban clusters (i.e., Central, Residential, Peripheral). Results outside the shaded area are significant at alpha=0.05. 156
Figure 6.4. True and predicted values of daily cardiovascular (CV) emergencies in May-September 2023 in the whole city, the Central cluster and the Residential cluster. Red dots indicate heat days on the true values curve, orange dots – on predicted values curve. Violet dots indicate non-heat days on the true values curve, blue dots – on predicted values curve.....161
Figure 6.5. Density plot and rug plot of absolute percentage errors on test set (i.e., May-September 2023) in the whole city, the Central cluster and the Residential cluster 162
Figure 6.6. Summary plot of SHAP values for XGBoost algorithm on the training set (i.e., May-September 2017-2022) in the whole city, the Central cluster and the Residential cluster during heat and non-heat days.....163
Figure 6.7. Relationship between the mean daily apparent temperature (AT) and the SHAP values on the training set (i.e., May-September 2017-2022) in the whole city, the Central cluster and the Residential cluster, and the ordinary least squares regression line fitted to heat days.....165
Figure A2.1. Final SDG3 index by region 226
Figure A4.1. Polygons resulting from Voronoi diagrams for air temperature, relative humidity and wind speed for the Lombardy region in Italy, with focus on the city of Milan……227
Figure A5.1. Regression models diagnostics for the whole city of Milan. Green box indicates the best model. From the top: tests for regression assumptions and VIF; coefficients/impacts, standard errors, p-values for each model. AIC – Akaike information criterion, RESET – Ramsey Regression Equation Specification Error Test, VIF – variance inflation factor, m1 – ordinary least squares linear regression, m2 – spatially lagged X model, m3 – spatial autoregressive model, m4 – spatial error model, m5 – spatial Durbin error model, m6 – spatial Durbin model, m7 – Kelejian-Prucha model……228
Figure A5.2. Regression models diagnostics for the Central socio-urban cluster. Green box indicates the best model. From the top: tests for regression assumptions and VIF; coefficients/impacts, standard errors, p-values for each model. AIC – Akaike information criterion, RESET – Ramsey Regression Equation Specification Error Test, VIF – variance inflation factor, m1 – ordinary least squares linear regression, m2 – spatially lagged X model, m3 – spatial autoregressive model, m4 – spatial error model, m5 – spatial Durbin error model, m6 – spatial Durbin model, m7 – Kelejian-Prucha model.....229
Figure A5.3. Regression models diagnostics for the Residential socio-urban cluster. Green box indicates the best model. From the top: tests for regression assumptions and VIF; coefficients/impacts, standard errors, p-values for each model. AIC – Akaike information criterion, RESET – Ramsey Regression Equation Specification Error Test, VIF – variance inflation factor, m1 – ordinary least squares linear regression, m2 – spatially lagged X model, m3 – spatial autoregressive model, m4 – spatial error model, m5 – spatial Durbin error model, m6 – spatial Durbin model, m7 – Kelejian-Prucha model.....231

List of Tables

Table 2.1. The largest municipalities and provinces of metropolitan areas in terms of population, area covered and number of municipalities 38
Table 2.2. SDG3 targets and indicators, together with the details of corresponding Italian indicators, when available. ICD - International Classification of Diseases; Istat - Italian National Institute of Statistics, ISS - Italian National Institute of Health. Regional data refer to 19 regions and two autonomous provinces of Bolzano and Trento. 39
Table 2.3. Median (25th – 75th percentile) of raw values (i.e., values assigned to each municipality, as described in the first black box in Figure 2.3) of selected Italian indicators 49
Table 2.4. Mortality rate attributed to cardiovascular diseases (International Classification of Diseases code: I00-I99) per 1,000 residents 57
Table 3.1. Summary of indicators used to define heat. MMT - minimum mortality temperature; EHF - Excess Heat Factor. The total amounts to 57 articles, as three of 54 studies applied more than one combination of different criteria. References as defined in Table A3.1. 72
Table 3.2. Calculation formulas for complex heat indices. References as defined in Table A3.1. 73
Table 3.3. National definitions of heat. Country column refers to the country in which the definition is used at national level. EHF - Excess Heat Factor as defined in Nairn and Fawcett (2015). References as defined in Table A3.1. 73
Table 3.4. Summary of the influence of heat on cause-specific cardiovascular outcomes. The notation e in the "Sample size" column means that it was inferred as not directly specified in the relevant study. MMT – minimum mortality temperature. References as defined in Table A3.1. 79
Table 4.1. Descriptive statistics of mean daily values of meteorological parameters and air pollutants in May-September 2017-2022 in Milan, Italy. CO – carbon monoxide, NO_2 – nitrogen dioxide, SO_2 – sulfur dioxide, O_3 – ozone, PM10 – particulate matters of less than 10 µm in diameter, PM2.5 – particulate matters of less than 2.5 µm in diameter. 104
Table 4.2. Descriptive statistics of the mean daily apparent temperature in May-September 2017-2022 in Milan, Italy. Heat threshold defined as the 95th percentile of annual daily mean apparent temperature distribution. 106
Table 4.3. Summary of characteristics of cardiovascular emergencies during heat (as defined in section 4.2.1) and non-heat days of May-September 2017-2022 in Milan, Italy, and the corresponding relative risk of having a CV emergency in heat days in respect to non-heat days. RR – relative risk, CI – confidence interval. 111
Table 4.4. Characteristic of cardiovascular emergencies in pre-COVID-19 (reference period), COVID-19, and post- COVID-19 periods. RR – relative risk, CI– confidence interval. 112
Table 5.1. Description of the socio-urban features computed for each Nucleus of Local Identity (NIL), with the relevant formula and the reference year(s) for which the data were available 119
Table 5.2. Descriptive statistics of the distribution of values among the 86 Nuclei of Local Identity (NIL) in the city of Milan for each selected socio-urban feature and the cardiovascular vulnerability to heat (CV_VtoH) 125
Table 5.3. Median (25th-75th percentile) of the distribution of the socio-urban features and the cardiovascular vulnerability to heat (CV_VtoH) for the Nuclei of Local Identity (NIL) composing each socio-urban cluster 127
Table 5.4. Results of the regression analysis considering coefficient, direct, indirect and total effects in all districts, and in districts grouped in Central and Residential socio-urban clusters. SLX – spatially lagged X model, SDEM – spatial Durbin error model, OLS – ordinary least squares. 130
Table 5.5. Global Moran's Index (gMI) and significant LISA clusters numerosity for cardiovascular vulnerability to heat (CV_VtoH) and each significant independent variable in the Central and the Residential socio-urban clusters. HH – high-high, LH – low-high, HL – high-low, LL – low-low, n/a – not applicable. 132
Table 5.6. Fraction of elderly patients, female patients, and fatal emergencies in heat days with respect to non-heat days in zones B5, C6-C8 137
Table 6.1. Range of values considered in setting the hyperparameters for each tested prediction model 149
Table 6.2. Apparent temperature aggregates returned by the feature selection methods in the whole city, the Central cluster and the Residential cluster 156
Table 6.3. Final independent variables included in the prediction models for the whole city, the Central cluster and the Residential cluster. AT – apparent temperature, CV – cardiovascular. 157
Table 6.4. Descriptive statistics of the mean daily apparent temperature during heat and non-heat days (as defined in section 6.2) in Milan, Italy. 158
Table 6.5. The optimal hyperparameters for XGBoost, CatBoost and LSTM trained on train set (i.e., May-September 2017-2022), and the corresponding Mean Absolute Error (MAE) on the test set (i.e., May-September 2023) 159
Table 6.6. The Mean Absolute Error (MAE) on the test set (i.e., May-September 2023) for five simpler models. For details see section 6.2.3. 160

Table A2.1. Descriptive statistics of Italian indicators mapped to SDG3 targets 213
Table A3.1. References for 54 articles which were systematically reviewed in Chapter 3……..……...216
Table A5.1. Official names of 88 Nuclei of Local Identity of Milan, Italy……219
Table A5.2. Pearson correlation coefficient between 11 socio-urban variables in the whole city of Milan, and in the three socio-urban clusters (i.e., Central, Residential, Peripheral) 221
Table A6.1. Sensitivity analysis: optimal hyperparameters (randomized search) and Mean Absolute Error (MAE) on test set for XGBoost performed with meteorological variables in the whole city……...224
Table A6.2. Sensitivity analysis: optimal hyperparameters (randomized search) and Mean Absolute Error (MAE) on test set for XGBoost performed with meteorological variables in the Central cluster……....224
Table A6.3. Sensitivity analysis: optimal hyperparameters (randomized search) and Mean Absolute Error (MAE) on test set for XGBoost performed with meteorological variables in the Residential cluster 225

Appendix

Table A2.1. Descriptive statistics of Italian indicators mapped to SDG3 targets and their contribution to final SDG3 index for Italy

Official target [contribution to SDG3 index]	3.2. Neonatal and child mortality [9.09%]		3.3. Infectious diseases [9.09%]			3.4. Noncommunicable diseases [9.09%]					3.5. Substance abuse [9.09%]
Official indicator [contribution to SDG3 index]	3.2.1 [4.55%]	3.2.2 [4.55%]	3.3.1 [3.03%]	3.3.2 [3.03%]	3.3.4 [3.03%]	3.4.1 [4.55%]				3.4.2 [4.55%]	3.5.2 [9.09%]
Italian indicator [contribution to SDG3 index]	Mortality rate 0-4 years old (per 1,000 births) [4.55%]	Neonatal mortality rate (per 10,000 live births) [4.55%]	HIV infections (per 1,000 residents) [3.03%]	Tuberculosis incidence rate (per 100,000 residents) [3.03%]	Hepatitis B incidence rate (per 100,000 residents) [3.03%]	Mortality rate: cardiovascular diseases (per 1,000 residents) [1.14%]	Mortality rate: malignant neoplasms (per 1,000 residents) [1.14%]	Mortality rate: diabetes mellitus (per 1,000 residents) [1.14%]	Mortality rate: respiratory diseases (per 1,000 residents) [1.14%]	Suicide mortality rate (per 1,000 residents) [4.55%]	Residents who consume alcohol between meals (%) [9.09%]
Mean	3,42	12,84	0,044	7,78	0,175	4,26	2,82	0,387	0,959	0,057	31,69
Standard deviation	28,43	5,39	0,018	3,91	0,160	2,92	1,82	0,623	1,035	0,204	5,48
Min	0,00	5,28	0,002	1,30	0,000	0,00	0,00	0,000	0,000	0,000	21,10
25%	0,00	7,87	0,032	2,60	0,079	2,59	1,89	0,000	0,277	0,000	28,46
50%	0,00	11,49	0,039	10,80	0,189	3,80	2,70	0,205	0,785	0,000	32,24
75%	0,00	15,66	0,064	10,80	0,191	5,37	3,58	0,533	1,286	0,000	35,56
Max	1000,00	23,06	0,083	10,80	0,922	36,53	25,67	10,58	17,241	5,952	48,52

Official target [contribution to SDG3 index]	3.6. Road traffic [9.09%]	3.7. Sexual and reproductive health [9.09%]		3.8. Universal health coverage [9.09%]					3.9. Environmental health [9.09%]	3.a. Tobacco control [9.09%]
Official indicator [contribution to SDG3 index]	3.6.1 [9.09%]	3.7.2 [9.09%]		3.8.1 [4.55%]				3.8.2 [4.55%]	3.9.3 [9.09%]	3.a.1 [9.09%]
Italian indicator [contribution to SDG3 index]	Mortality rate in road accidents (per 10,000 residents) [9.09%]	Fertility rate per women 10-14 years old (%) [4.55%]	Fertility rate per women 15-19 years old (%) [4.55%]	Beds in public hospitalisation facilities (per 1,000 residents) [1.14%]	Pharmacies (per 10,000 residents) [1.14%]	Places in residential social-welfare and social-health facilities (per 100,000 residents) [1.14%]	Anti-influenza vaccination coverage (%) [1.14%]	Households who do not have enough money for health care (%) [4.55%]	Mortality rate attributed to unintentional poisoning (per 1,000 residents) [9.09%]	People who smoke cigarettes (%) [9.09%]
Mean	0,68	0,018	2,54	2,39	7,06	773,64	19,59	4,26	0,005	19,18
Standard deviation	4,76	0,029	1,41	0,98	9,36	319,38	2,18	2,46	0,082	1,93
Min	0,00	0,000	1,62	0,00	0,00	188,40	10,90	1,31	0,000	15,22
25%	0,00	0,000	1,87	1,61	2,80	501,50	18,80	2,32	0,000	18,12
50%	0,00	0,000	1,95	2,43	4,16	847,60	19,50	3,62	0,000	19,04
75%	0,00	0,025	2,62	3,05	8,14	1097,60	20,70	5,51	0,000	20,63
Max	312,50	0,115	7,73	5,65	144,93	1469,70	23,60	11,00	4,032	25,27

Official target [contribution to SDG3 index]	3.b. Medicines and vaccines [9.09%]		3.c. Health financing and workforce [9.09%]					
Official indicator [contribution to SDG3 index]	3.b.1 [4.55%]	3.b.2 [4.55%]	3.c.1 [9.09%]					
Italian indicator [contribution to SDG3 index]	Children obligatory vaccination coverage (%) [4.55%]	Municipality expenditure for health services (per resident) (EUR) [4.55%]	Specialist practitioners per (10,000 residents) [1.52%]	General practitioners (per 10,000 residents) [1.52%]	Dentists (per 10,000 residents) [1.52%]	Doctors in public hospitalization facilities (per 10,000 residents) [1.52%]	Nurses in public hospitalization facilities (per 10,000 residents) [1.52%]	Pharmacists (per 10,000 residents) [1.52%]
Mean	92,20	18,37	31,96	8,15	8,45	16,14	22,31	13,49
Standard deviation	4,56	30,53	3,64	1,07	0,96	5,02	13,59	2,57
Min	73,04	0,00	24,17	6,07	5,71	1,21	0,03	6,00
25%	92,97	5,32	29,32	7,51	8,25	12,70	10,83	12,46
50%	93,72	11,70	31,27	8,01	8,35	16,04	23,24	13,05
75%	94,16	21,48	34,81	8,63	8,73	18,64	31,47	15,85
Max	96,25	580,92	39,69	11,08	11,57	32,80	53,59	17,19

Table A3.1. References for 54 articles which were systematically reviewed in Chapter 3

Reference number	Reference
1	Alsaiqali, M., De Troeyer, K., Casas, L., Hamdi, R., Faes, C., & Van Pottelbergh, G. (2022). The effects of heatwaves on human morbidity in primary care settings: A case-crossover study. *International Journal of Environmental Research and Public Health*, *19*(2), 832.
2	Saucy, A., Ragettli, M. S., Vienneau, D., de Hoogh, K., Tangermann, L., Schäffer, B., ... & Röösli, M. (2021). The role of extreme temperature in cause-specific acute cardiovascular mortality in Switzerland: A case-crossover study. *Science of The Total Environment*, *790*, 147958.
3	Yin, P., Chen, R., Wang, L., Liu, C., Niu, Y., Wang, W., ... & Kan, H. (2018). The added effects of heatwaves on cause-specific mortality: A nationwide analysis in 272 Chinese cities. *Environment International*, *121*, 898-905.
4	Li, Y., Akkus, C., Yu, X., Joyner, A., Kmet, J., Sweat, D., & Jia, C. (2019a). Heatwave events and mortality outcomes in Memphis, Tennessee: Testing effect modification by socioeconomic status and urbanicity. *International Journal of Environmental Research and Public Health*, *16*(22), 4568.
5	Kienbacher, C. L., Kaltenberger, R., Schreiber, W., Tscherny, K., Fuhrmann, V., Roth, D., & Herkner, H. (2021). Extreme weather conditions as a gender-specific risk factor for acute myocardial infarction. *The American Journal of Emergency Medicine*, *43*, 50-53.
6	Huang, C., Cheng, J., Phung, D., Tawatsupa, B., Hu, W., & Xu, Z. (2018). Mortality burden attributable to heatwaves in Thailand: A systematic assessment incorporating evidence-based lag structure. *Environment International*, *121*, 41-50.
7	Campbell, S. L., Remenyi, T. A., Williamson, G. J., White, C. J., & Johnston, F. H. (2019). The value of local heatwave impact assessment: A case-crossover analysis of hospital emergency department presentations in Tasmania, Australia. *International Journal of Environmental Research and Public Health*, *16*(19), 3715.
8	Liu, X., Kong, D., Fu, J., Zhang, Y., Liu, Y., Zhao, Y., ... & Fan, Z. (2018a). Association between extreme temperature and acute myocardial infarction hospital admissions in Beijing, China: 2013–2016. *PloS ONE*, *13*(10), e0204706.
9	Dang, T. A. T., Wraith, D., Bambrick, H., Dung, N., Truc, T. T., Tong, S., ... & Dunne, M. P. (2019). Short-term effects of temperature on hospital admissions for acute myocardial infarction: A comparison between two neighboring climate zones in Vietnam. *Environmental Research*, *175*, 167-177.
10	Bai, L., Li, Q., Wang, J., Lavigne, E., Gasparrini, A., Copes, R., ... & Chen, H. (2018). Increased coronary heart disease and stroke hospitalisations from ambient temperatures in Ontario. *Heart*, *104*(8), 673-679.
11	Parry, M., Green, D., Zhang, Y., & Hayen, A. (2019). Does particulate matter modify the short-term association between heat waves and hospital admissions for cardiovascular diseases in greater Sydney, Australia?. *International Journal of Environmental Research and Public Health*, *16*(18), 3270.
12	Ma, Y., Zhou, L., & Chen, K. (2020). Burden of cause-specific mortality attributable to heat and cold: A multicity time-series study in Jiangsu Province, China. *Environment International*, *144*, 105994.
13	Chen, R., Yin, P., Wang, L., Liu, C., Niu, Y., Wang, W., ... & Zhou, M. (2018). Association between ambient temperature and mortality risk and burden: Time series study in 272 main Chinese cities. *BMJ*, *363*.
14	Xu, R., Shi, C., Wei, J., Lu, W., Li, Y., Liu, T., ... & Liu, Y. (2022a). Cause-specific cardiovascular disease mortality attributable to ambient temperature: A time-stratified case-crossover study in Jiangsu province, China. *Ecotoxicology and Environmental Safety*, *236*, 113498.
15	Ferreira, L. D. C. M., Nogueira, M. C., Pereira, R. V. D. B., de Farias, W. C. M., Rodrigues, M. M. D. S., Teixeira, M. T. B., & Carvalho, M. S. (2019). Ambient temperature and mortality due to acute myocardial infarction in Brazil: An ecological study of time-series analyses. *Scientific Reports*, *9*(1), 13790.
16	Romani, S. G., Royé, D., Sánchez Santos, L., & Figueiras, A. (2020). Impact of extreme temperatures on ambulance dispatches due to cardiovascular causes in North-West Spain. *International Journal of Environmental Research and Public Health*, *17*(23), 9001.

17	Lam, H. C. Y., Chan, J. C. N., Luk, A. O. Y., Chan, E. Y. Y., & Goggins, W. B. (2018). Short-term association between ambient temperature and acute myocardial infarction hospitalizations for diabetes mellitus patients: A time series study. *PloS Medicine*, *15*(7), e1002612.
18	Zhang, W., Du, G., Xiong, L., Liu, T., Zheng, Z., Yuan, Q., ... & Hu, G. (2021). Extreme temperatures and cardiovascular mortality: Assessing effect modification by subgroups in Ganzhou, China. *Global Health Action*, *14*(1), 1965305.
19	Li, N., Ma, J., Liu, F., Zhang, Y., Ma, P., Jin, Y., & Zheng, Z. J. (2021). Associations of apparent temperature with acute cardiac events and subtypes of acute coronary syndromes in Beijing, China. *Scientific Reports*, *11*(1), 15229.
20	de Moraes, S. L., Almendra, R., & Barrozo, L. V. (2022). Impact of heat waves and cold spells on cause-specific mortality in the city of São Paulo, Brazil. *International Journal of Hygiene and Environmental Health*, *239*, 113861.
21	Lu, P., Zhao, Q., Xia, G., Xu, R., Hanna, L., Jiang, J., ... & Guo, Y. (2021). Temporal trends of the association between ambient temperature and cardiovascular mortality: A 17-year case-crossover study. *Environmental Research Letters*, *16*(4), 045004.
22	Kranc, H., Novack, V., Shtein, A., Sherman, R., & Novack, L. (2021). Extreme temperature and out-of-hospital-cardiac-arrest. Nationwide study in a hot climate country. *Environmental Health*, *20*, 1-13.
23	Chen, K., Breitner, S., Wolf, K., Hampel, R., Meisinger, C., Heier, M., ... & KORA Study Group Peters A Schulz H Schwettmann L Leidl R Heier M Strauch K. (2019). Temporal variations in the triggering of myocardial infarction by air temperature in Augsburg, Germany, 1987–2014. *European Heart Journal*, *40*(20), 1600-1608.
24	Li, M., Shaw, B. A., Zhang, W., Vásquez, E., & Lin, S. (2019b). Impact of extremely hot days on emergency department visits for cardiovascular disease among older adults in New York State. *International Journal of Environmental Research and Public Health*, *16*(12), 2119.
25	Guo, Y. T., Bernard Goggins, W., Chan, E. Y. Y., & Ho, K. F. (2022a). Individual socioeconomic status as a modifier of the association between high ambient temperature and hospital admissions: A time series study in Hong Kong, 2010–2019. *Environmental Science and Pollution Research*, *29*(44), 67353-67361.
26	Parliari, D., Cheristanidis, S., Giannaros, C., Keppas, S. C., Papadogiannaki, S., de'Donato, F., ... & Melas, D. (2022). Short-term effects of apparent temperature on cause-specific mortality in the Urban Area of Thessaloniki, Greece. *Atmosphere*, *13*(6), 852.
27	Heo, S., Chen, C., Kim, H., Sabath, B., Dominici, F., Warren, J. L., ... & Bell, M. L. (2021). Temporal changes in associations between high temperature and hospitalizations by greenspace: Analysis in the Medicare population in 40 US northeast counties. *Environment International*, *156*, 106737.
28	Demoury, C., Aerts, R., Vandeninden, B., Van Schaeybroeck, B., & De Clercq, E. M. (2022). Impact of short-term exposure to extreme temperatures on mortality: A multi-city study in Belgium. *International Journal of Environmental Research and Public Health*, *19*(7), 3763.
29	Hopp, S., Dominici, F., & Bobb, J. F. (2018). Medical diagnoses of heat wave-related hospital admissions in older adults. *Preventive Medicine*, *110*, 81-85.
30	Iranpour, S., Khodakarim, S., Shahsavani, A., Khosravi, A., & Etemad, K. (2020). Modification of the effect of ambient air temperature on cardiovascular and respiratory mortality by air pollution in Ahvaz, Iran. *Epidemiology and Health*, *42*.
31	Bi, X., Wu, C., Wang, C., Wang, Y., Wang, X., Song, C., ... & Fu, C. (2022). Impacts of air temperature and its extremes on human mortality in Shanghai, China. *Urban Climate*, *41*, 101072.
32	Liu, S., Chan, E. Y. Y., Goggins, W. B., & Huang, Z. (2020). The mortality risk and socioeconomic vulnerability associated with high and low temperature in Hong Kong. *International Journal of Environmental Research and Public Health*, *17*(19), 7326.
33	Yatim, A. N. M., Latif, M. T., Sofwan, N. M., Ahamad, F., Khan, M. F., Mahiyuddin, W. R. W., & Sahani, M. (2021). The association between temperature and cause-specific mortality in the Klang Valley, Malaysia. *Environmental Science and Pollution Research*, *28*(42), 60209-60220.
34	Hu, K., Guo, Y., Hochrainer-Stigler, S., Liu, W., See, L., Yang, X., ... & Qi, J. (2019). Evidence for urban–rural disparity in temperature–mortality relationships in Zhejiang Province, China. *Environmental Health Perspectives*, *127*(3), 037001.
35	Royé, D., Codesido, R., Tobías, A., & Taracido, M. (2020). Heat wave intensity and daily mortality in four of the largest cities of Spain. *Environmental Research*, *182*, 109027.

36	Iñiguez, C., Royé, D., & Tobías, A. (2021). Contrasting patterns of temperature related mortality and hospitalization by cardiovascular and respiratory diseases in 52 Spanish cities. *Environmental Research*, *192*, 110191.
37	Moghadamnia, M. T., Ardalan, A., Mesdaghinia, A., Naddafi, K., & Yekaninejad, M. S. (2018). Association between apparent temperature and acute coronary syndrome admission in Rasht, Iran. *Heart Asia*, *10*(2).
38	Can, G., Şahin, Ü., Sayılı, U., Dubé, M., Kara, B., Acar, H. C., ... & Gosselin, P. (2019). Excess mortality in Istanbul during extreme heat waves between 2013 and 2017. *International Journal of Environmental Research and Public Health*, *16*(22), 4348.
39	Alahmad, B., Shakarchi, A. F., Khraishah, H., Alseaidan, M., Gasana, J., Al-Hemoud, A., ... & Fox, M. A. (2020). Extreme temperatures and mortality in Kuwait: Who is vulnerable?. *Science of The Total Environment*, *732*, 139289.
40	Fonseca-Rodríguez, O., Sheridan, S. C., Lundevaller, E. H., & Schumann, B. (2020). Hot and cold weather based on the spatial synoptic classification and cause-specific mortality in Sweden: A time-stratified case-crossover study. *International Journal of Biometeorology*, *64*(9), 1435-1449.
41	Yu, X., Xia, L., Xiao, J., Zheng, J., Xu, N., Feng, X., & Wei, X. (2021). Association of daily mean temperature and temperature variability with onset risks of acute aortic dissection. *Journal of the American Heart Association*, *10*(13), e020190.
42	Jiang, S., Warren, J. L., Scovronick, N., Moss, S. E., Darrow, L. A., Strickland, M. J., ... & Chang, H. H. (2021). Using logic regression to characterize extreme heat exposures and their health associations: A time-series study of emergency department visits in Atlanta. *BMC Medical Research Methodology*, *21*(1), 87.
43	Pfeifer, K., Oudin Åström, D., Martinsone, Ž., Kaļužnaja, D., & Oudin, A. (2020). Evaluating mortality response associated with two different Nordic heat warning systems in Riga, Latvia. *International Journal of Environmental Research and Public Health*, *17*(21), 7719.
44	Lin, Y. K., Cheng, C. P., Kim, H., & Wang, Y. C. (2021). Risk of ambulance services associated with ambient temperature, fine particulate and its constituents. *Scientific Reports*, *11*(1), 1651.
45	Schulte, F., Röösli, M., & Ragettli, M. S. (2021). Heat-related cardiovascular morbidity and mortality in Switzerland: A clinical perspective. *Swiss Med Wkly*, *151*, w30013.
46	Wang, Y. C., Lin, Y. K., Chen, Y. J., Hung, S. C., Zafirah, Y., & Sung, F. C. (2020). Ambulance services associated with extreme temperatures and fine particles in a subtropical island. *Scientific Reports*, *10*(1), 2855.
47	Oudin Åström, D., Åström, C., Forsberg, B., Vicedo-Cabrera, A. M., Gasparrini, A., Oudin, A., & Sundquist, K. (2020). Heat wave–related mortality in Sweden: A case-crossover study investigating effect modification by neighbourhood deprivation. *Scandinavian Journal of Public Health*, *48*(4), 428-435.
48	Layton, J. B., Li, W., Yuan, J., Gilman, J. P., Horton, D. B., & Setoguchi, S. (2020). Heatwaves, medications, and heat-related hospitalization in older Medicare beneficiaries with chronic conditions. *PloS ONE*, *15*(12), e0243665.
49	Zhai, G., Tian, Y., Zhang, K., Qi, J., & Chai, G. (2022). The effect of apparent temperature on hospital admissions for cardiovascular diseases in rural areas of Pingliang, China. *Annals of Agricultural and Environmental Medicine*, *29*(2).
50	Scovronick, N., Sera, F., Acquaotta, F., Garzena, D., Fratianni, S., Wright, C. Y., & Gasparrini, A. (2018). The association between ambient temperature and mortality in South Africa: A time-series analysis. *Environmental Research*, *161*, 229-235.
51	Remigio, R. V., Jiang, C., Raimann, J., Kotanko, P., Usvyat, L., Maddux, F. W., ... & Sapkota, A. (2019). Association of extreme heat events with hospital admission or mortality among patients with end-stage renal disease. *JAMA Network Open*, *2*(8), e198904-e198904.
52	Jiang, Y., Hu, J., Peng, L., Li, H., Ji, J. S., Fang, W., ... & Chen, R. (2022). Non-optimum temperature increases risk and burden of acute myocardial infarction onset: A nationwide case-crossover study at hourly level in 324 Chinese cities. *EClinicalMedicine*, *50*.
53	Guo, H., Du, P., Zhang, H., Zhou, Z., Zhao, M., Wang, J., ... & Feng, X. (2022b). Time series study on the effects of daily average temperature on the mortality from respiratory diseases and circulatory diseases: A case study in Mianyang City. *BMC Public Health*, *22*(1), 1001.
54	Perčič, S., Kukec, A., Cegnar, T., & Hojs, A. (2018). Number of heat wave deaths by diagnosis, sex, age groups, and area, in Slovenia, 2015 vs. 2003. *International Journal of Environmental Research and Public Health*, *15*(1), 173.

Table A5.1. Official names of 88 Nuclei of Local Identity of Milan, Italy

NIL identification number	Name
1	DUOMO
2	BRERA
3	GIARDINI P.TA VENEZIA
4	GUASTALLA
5	PORTA VIGENTINA - PORTA LODOVICA
6	PORTA TICINESE - CONCA DEL NAVIGLIO
7	MAGENTA - S. VITTORE
8	PARCO SEMPIONE
9	PORTA GARIBALDI - PORTA NUOVA
10	STAZIONE CENTRALE - PONTE SEVESO
11	ISOLA
12	MACIACHINI - MAGGIOLINA
13	GRECO - SEGNANO
14	NIGUARDA - CA' GRANDA - PRATO CENTENARO - Q.RE FULVIO TESTI
15	BICOCCA
16	GORLA - PRECOTTO
17	ADRIANO
18	CIMIANO - ROTTOLE - Q.RE FELTRE
19	PADOVA - TURRO - CRESCENZAGO
20	LORETO - CASORETTO - NOLO
21	BUENOS AIRES - PORTA VENEZIA - PORTA MONFORTE
22	CITTA' STUDI
23	LAMBRATE - ORTICA
24	PARCO FORLANINI - CAVRIANO
25	CORSICA
26	XXII MARZO
27	PTA ROMANA
28	UMBRIA - MOLISE - CALVAIRATE
29	ORTOMERCATO
30	TALIEDO - MORSENCHIO - Q.RE FORLANINI
31	MONLUE' - PONTE LAMBRO
32	TRIULZO SUPERIORE
33	ROGOREDO - SANTA GIULIA
34	CHIARAVALLE
35	LODI - CORVETTO
36	SCALO ROMANA
37	MORIVIONE
38	VIGENTINO - Q.RE FATIMA
39	QUINTOSOLE
40	RONCHETTO DELLE RANE
41	GRATOSOGLIO - Q.RE MISSAGLIA - Q.RE TERRAZZE
42	STADERA - CHIESA ROSSA - Q.RE TORRETTA - CONCA FALLATA
43	TIBALDI
44	PORTA TICINESE - CONCHETTA
45	MONCUCCO - SAN CRISTOFORO
46	BARONA
47	CANTALUPA
48	RONCHETTO SUL NAVIGLIO - Q.RE LODOVICO IL MORO
49	GIAMBELLINO
50	PORTA GENOVA
51	PORTA MAGENTA
52	BANDE NERE
53	LORENTEGGIO
54	MUGGIANO
55	BAGGIO - Q.RE DEGLI OLMI - Q.RE VALSESIA
56	FORZE ARMATE

57	SAN SIRO
58	DE ANGELI - MONTE ROSA
59	TRE TORRI
60	STADIO - IPPODROMI
61	QUARTO CAGNINO
62	QUINTO ROMANO
63	FIGINO
64	TRENNO
65	Q.RE GALLARATESE - Q.RE SAN LEONARDO - LAMPUGNANO
66	QT 8
67	PORTELLO
68	PAGANO
69	SARPI
70	GHISOLFA
71	VILLAPIZZONE - CAGNOLA - BOLDINASCO
72	MAGGIORE - MUSOCCO - CERTOSA
73	CASCINA MERLATA
74	ROSERIO
75	STEPHENSON
76	QUARTO OGGIARO - VIALBA - MUSOCCO
77	BOVISA
78	FARINI
79	DERGANO
80	AFFORI
81	BOVISASCA
82	COMASINA
83	BRUZZANO
84	PARCO NORD
85	PARCO DELLE ABBAZIE
86	PARCO DEI NAVIGLI
87	ASSIANO
88	PARCO BOSCO IN CITTA'

Table A5.2. Pearson correlation coefficient between 11 socio-urban variables in the whole city of Milan, and in the three socio-urban clusters (i.e., Central, Residential, Peripheral)

Whole city

Socio-urban variable	Built-up area (%)	Non-residential buildings' volume (m3/m2)	Green roofs (%)	Population density (people/km2)	Vegetation index	Mean summer LST (°C)	Density drinking water fountains (n/ km2)	Cycle paths (km/km2)	Residents >=65 (%)	Female residents (%)	Graduate residents (%)
Built-up area (%)	1.00	-0.45	0.27	0.76	-0.25	0.69	0.51	0.45	0.24	0.37	0.71
Non-residential buildings' volume (m3/m2)	-0.45	1.00	-0.06	-0.51	-0.15	-0.26	-0.42	-0.13	-0.49	-0.35	-0.29
Green roofs (%)	0.27	-0.06	1.00	0.23	0.27	0.07	0.18	0.40	0.25	0.34	0.35
Population density (people/km2)	0.76	-0.51	0.23	1.00	0.02	0.53	0.53	0.30	0.33	0.42	0.48
Vegetation index	-0.25	-0.15	0.27	0.02	1.00	-0.07	0.02	-0.10	0.42	0.24	-0.21
Mean summer LST (°C)	0.69	-0.26	0.07	0.53	-0.07	1.00	0.28	0.28	0.10	0.15	0.22
Density drinking water fountains (n/ km2)	0.51	-0.42	0.18	0.53	0.02	0.28	1.00	0.26	0.31	0.39	0.42
Cycle paths (km/km2)	0.45	-0.13	0.40	0.30	-0.10	0.28	0.26	1.00	0.04	0.19	0.38
Residents >=65 (%)	0.24	-0.49	0.25	0.33	0.42	0.10	0.31	0.04	1.00	0.61	0.27
Female residents (%)	0.37	-0.35	0.34	0.42	0.24	0.15	0.39	0.19	0.61	1.00	0.30
Graduate residents (%)	0.71	-0.29	0.35	0.48	-0.21	0.22	0.42	0.38	0.27	0.30	1.00

Central socio-urban cluster

Socio-urban variable	Built-up area (%)	Non-residential buildings' volume (m3/m2)	Green roofs (%)	Population density (people/km2)	Vegetation index	Mean summer LST (°C)	Density drinking water fountains (n/ km2)	Cycle paths (km/km2)	Residents >=65 (%)	Female residents (%)	Graduate residents (%)
Built-up area (%)	1.00	-0.40	0.25	0.05	-0.46	0.46	-0.31	0.07	0.07	0.03	0.56

Non-residential buildings' volume (m3/m2)	-0.40	1.00	-0.06	-0.68	-0.17	-0.32	0.29	0.28	-0.29	-0.08	-0.08
Green roofs (%)	0.25	-0.06	1.00	-0.27	-0.23	-0.01	-0.08	0.43	0.37	0.21	0.37
Population density (people/km2)	0.05	-0.68	-0.27	1.00	0.37	0.37	-0.12	-0.30	-0.01	-0.18	-0.39
Vegetation index	-0.46	-0.17	-0.23	0.37	1.00	-0.28	0.09	-0.41	0.46	0.18	-0.23
Mean summer LST (°C)	0.46	-0.32	-0.01	0.37	-0.28	1.00	-0.39	0.01	-0.45	-0.61	-0.32
Density drinking water fountains (n/ km2)	-0.31	0.29	-0.08	-0.12	0.09	-0.39	1.00	-0.23	-0.03	0.01	-0.08
Cycle paths (km/km2)	0.07	0.28	0.43	-0.30	-0.41	0.01	-0.23	1.00	-0.11	-0.03	0.03
Residents >=65 (%)	0.07	-0.29	0.37	-0.01	0.46	-0.45	-0.03	-0.11	1.00	0.69	0.48
Female residents (%)	0.03	-0.08	0.21	-0.18	0.18	-0.61	0.01	-0.03	0.69	1.00	0.60
Graduate residents (%)	0.56	-0.08	0.37	-0.39	-0.23	-0.32	-0.08	0.03	0.48	0.60	1.00

Residential socio-urban cluster

Socio-urban variable	Built-up area (%)	Non-residential buildings' volume (m3/m2)	Green roofs (%)	Population density (people/km2)	Vegetation index	Mean summer LST (°C)	Density drinking water fountains (n/ km2)	Cycle paths (km/km2)	Residents >=65 (%)	Female residents (%)	Graduate residents (%)
Built-up area (%)	1.00	-0.15	-0.29	0.47	-0.40	0.73	0.09	0.05	-0.22	-0.22	0.10
Non-residential buildings' volume (m3/m2)	-0.15	1.00	0.49	-0.41	0.19	0.05	-0.41	0.39	-0.22	0.15	0.29
Green roofs (%)	-0.29	0.49	1.00	-0.10	0.42	-0.33	-0.18	0.26	-0.00	0.24	0.21
Population density (people/km2)	0.47	-0.41	-0.10	1.00	0.09	0.25	0.27	0.04	0.19	0.39	0.13
Vegetation index	-0.40	0.19	0.42	0.09	1.00	-0.34	-0.04	0.19	0.42	0.53	0.17
Mean summer LST (°C)	0.73	0.05	-0.33	0.25	-0.34	1.00	-0.14	0.11	-0.22	-0.21	-0.04
Density drinking water fountains (n/ km2)	0.09	-0.41	-0.18	0.27	-0.04	-0.14	1.00	0.15	0.11	-0.02	0.17
Cycle paths (km/km2)	0.05	0.39	0.26	0.04	0.19	0.11	0.15	1.00	-0.28	0.05	-0.10

Residents >=65 (%)	-0.22	-0.22	-0.00	0.19	0.42	-0.22	0.11	-0.28	1.00	0.58	0.15
Female residents (%)	-0.22	0.15	0.24	0.39	0.53	-0.21	-0.02	0.05	0.58	1.00	0.40
Graduate residents (%)	0.10	0.29	0.21	0.13	0.17	-0.04	0.17	-0.10	0.15	0.40	1.00

Peripheral socio-urban cluster

Socio-urban variable	Built-up area (%)	Non-residential buildings' volume (m3/m2)	Green roofs (%)	Population density (people/km2)	Vegetation index	Mean summer LST (°C)	Density drinking water fountains (n/ km2)	Cycle paths (km/km2)	Residents >=65 (%)	Female residents (%)	Graduate residents (%)
Built-up area (%)	1.00	-0.24	0.37	0.71	0.61	0.70	0.15	0.29	-0.55	-0.87	-0.10
Non-residential buildings' volume (m3/m2)	-0.24	1.00	-0.10	-0.65	-0.28	0.28	-0.08	-0.55	-0.27	0.13	-0.72
Green roofs (%)	0.37	-0.10	1.00	0.14	0.85	0.13	0.79	0.35	-0.43	-0.03	-0.33
Population density (people/km2)	0.71	-0.65	0.14	1.00	0.60	0.54	0.29	0.29	-0.24	-0.49	0.21
Vegetation index	0.61	-0.28	0.85	0.60	1.00	0.47	0.85	0.32	-0.53	-0.22	-0.28
Mean summer LST (°C)	0.70	0.28	0.13	0.54	0.47	1.00	0.28	-0.16	-0.59	-0.56	-0.51
Density drinking water fountains (n/ km2)	0.15	-0.08	0.79	0.29	0.85	0.28	1.00	0.12	-0.38	0.21	-0.35
Cycle paths (km/km2)	0.29	-0.55	0.35	0.29	0.32	-0.16	0.12	1.00	0.28	-0.28	0.61
Residents >=65 (%)	-0.55	-0.27	-0.43	-0.24	-0.53	-0.59	-0.38	0.28	1.00	0.40	0.60
Female residents (%)	-0.87	0.13	-0.03	-0.49	-0.22	-0.56	0.21	-0.28	0.40	1.00	-0.13
Graduate residents (%)	-0.10	-0.72	-0.33	0.21	-0.28	-0.51	-0.35	0.61	0.60	-0.13	1.00

Table A6.1. Sensitivity analysis: optimal hyperparameters (randomized search) and Mean Absolute Error (MAE) on test set for XGBoost performed with meteorological variables in the whole city

Training years	Test year	Optimal hyperparameters	MAE on test set
2017	2018	subsample = 0.9, n_estimators = 500, max_depth = 3, learning_rate = 0.2, colsample_bytree = 0.8	11.64
2017-2018	2019	subsample = 0.9, n_estimators = 1000, max_depth = 5, learning_rate = 0.2, colsample_bytree = 1.0	10.99
2017-2019	2020	subsample = 0.8, n_estimators = 500, max_depth = 5, learning_rate = 0.01, colsample_bytree = 1.0	8.52
2017-2020	2021	subsample = 0.8, n_estimators = 1500, max_depth = 3, learning_rate = 0.01, colsample_bytree = 0.8	9.71
2017-2021	2022	subsample = 0.9, n_estimators' = 2000, max_depth = 7, learning_rate = 0.2, colsample_bytree = 0.9	9.56

Table A6.2. Sensitivity analysis: optimal hyperparameters (randomized search) and Mean Absolute Error (MAE) on test set for XGBoost performed with meteorological variables in the Central cluster

Training years	Test year	Optimal hyperparameters	MAE on test set
2017	2018	subsample = 0.8, n_estimators =2000 , max_depth = 3, learning_rate = 0.3, colsample_bytree = 0.8	7.34
2017-2018	2019	subsample = 0.8, n_estimators = 2000, max_depth = 7, learning_rate = 0.01, colsample_bytree = 0.9	6.91
2017-2019	2020	subsample = 0.9, n_estimators = 300, max_depth = 5, learning_rate = 0.1, colsample_bytree = 0.8	6.42
2017-2020	2021	subsample = 0.9, n_estimators = 500, max_depth = 3, learning_rate = 0.01, colsample_bytree = 1.0	6.60
2017-2021	2022	subsample = 0.8,	5.83

		n_estimators' = 300, max_depth = 3, learning_rate = 0.01, colsample_bytree = 1.0	

Table A6.3. Sensitivity analysis: optimal hyperparameters (randomized search) and Mean Absolute Error (MAE) on test set for XGBoost performed with meteorological variables in the Residential cluster

Training years	Test year	Optimal hyperparameters	MAE on test set
2017	2018	subsample = 1.0, n_estimators = 2000, max_depth = 7, learning_rate = 0.2, colsample_bytree = 0.9	6.89
2017-2018	2019	subsample = 0.9, n_estimators = 1500, max_depth = 7, learning_rate = 0.2, colsample_bytree = 0.8	6.33
2017-2019	2020	subsample = 0.9, n_estimators = 300, max_depth = 3, learning_rate = 0.01, colsample_bytree = 1.0	5.66
2017-2020	2021	subsample = 1.0, n_estimators = 300, max_depth = 3, learning_rate = 0.01, colsample_bytree = 0.9	5.71
2017-2021	2022	subsample = 0.8, n_estimators' = 300, max_depth = 3, learning_rate = 0.01, colsample_bytree = 0.9	5.92

Figure A2.1. Final SDG3 index by region

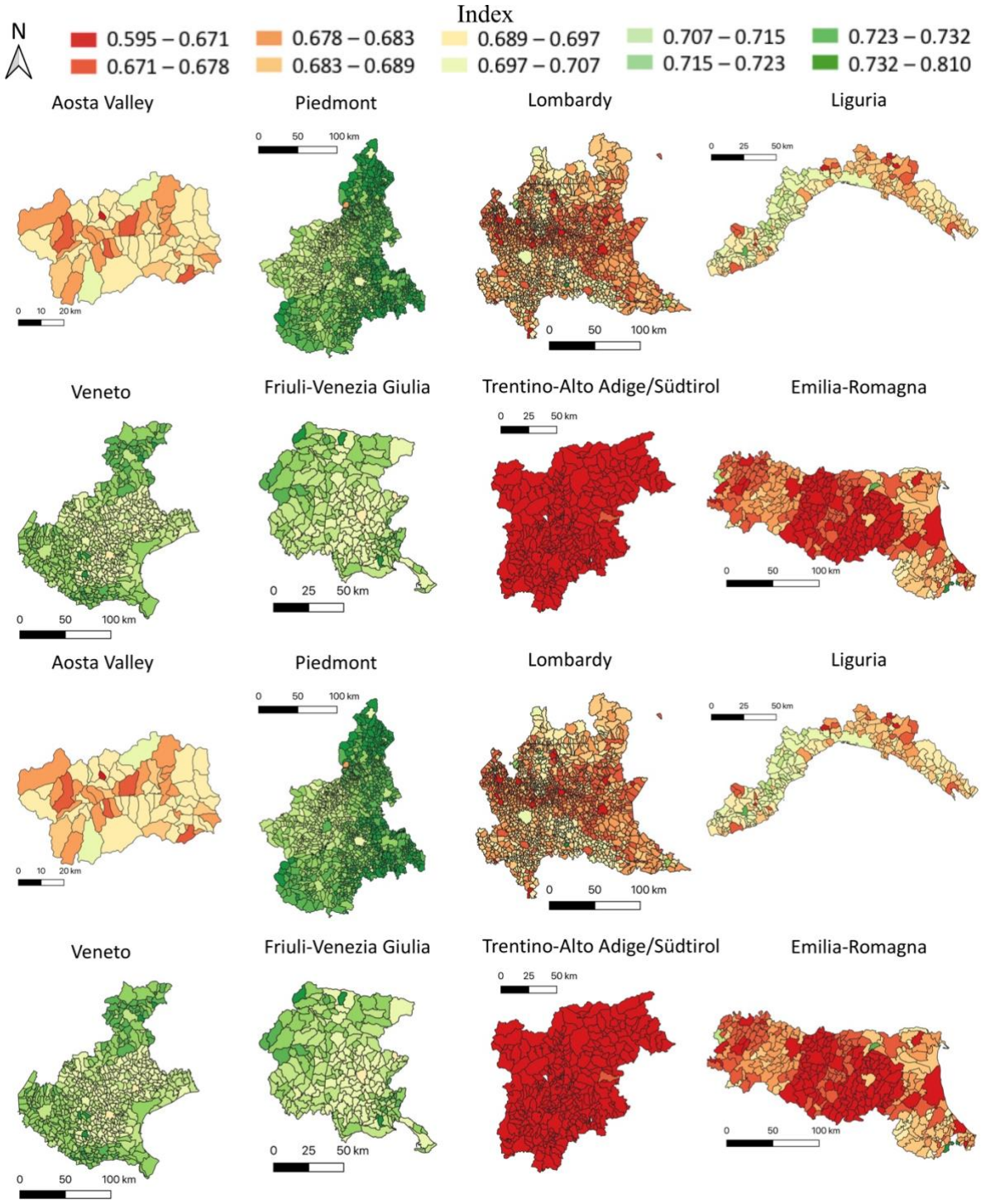

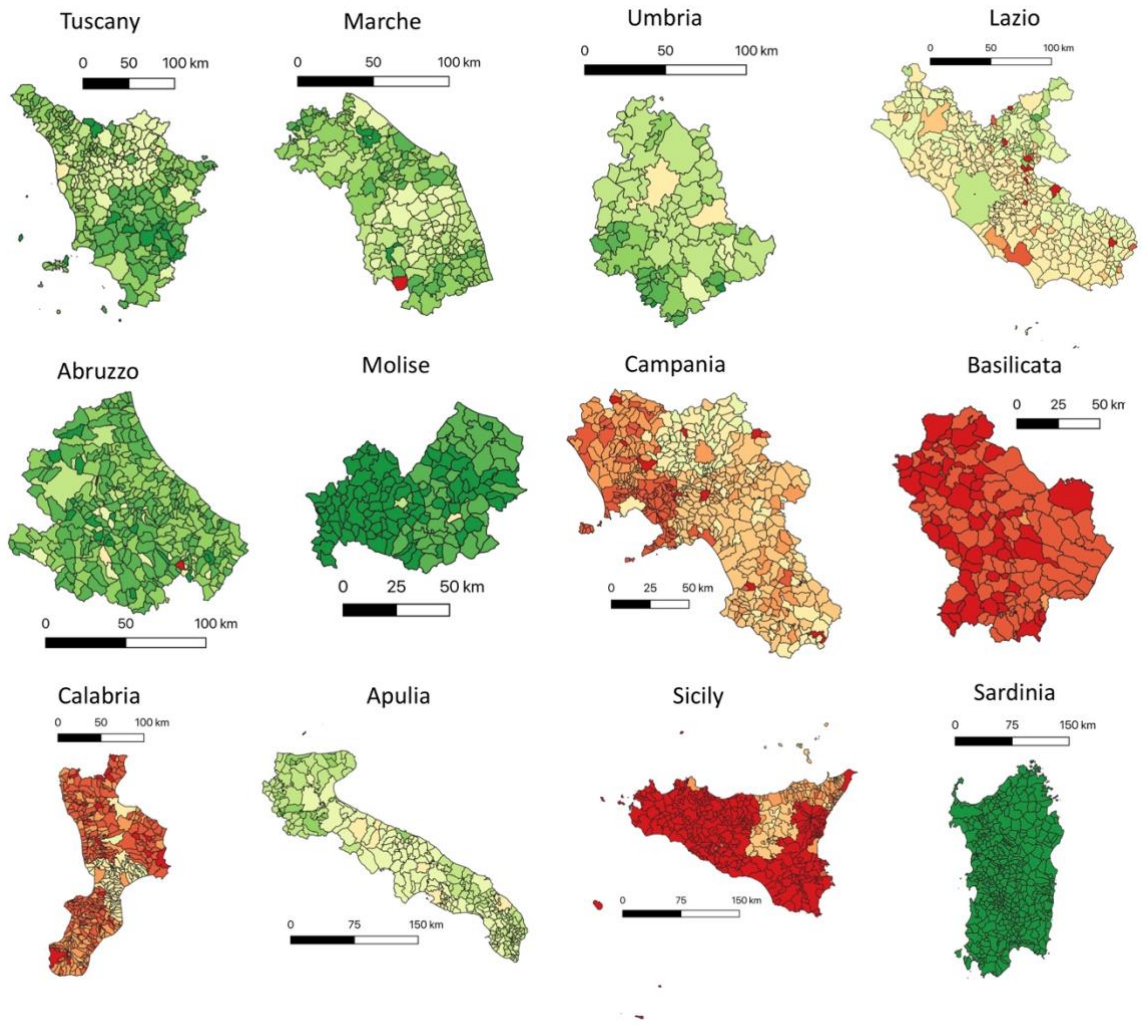

Figure A4.1. Polygons resulting from Voronoi diagrams for air temperature, relative humidity and wind speed for the Lombardy region in Italy, with focus on the city of Milan

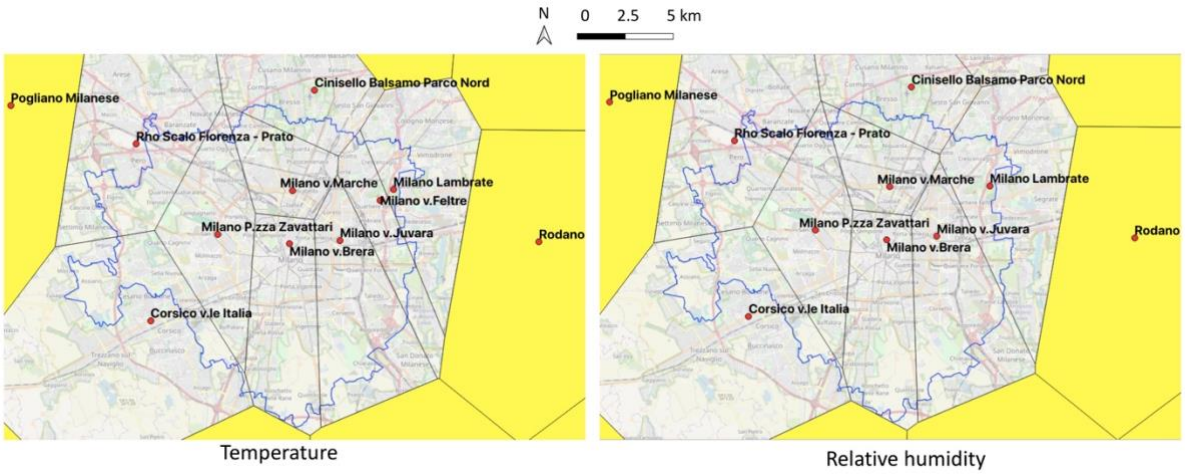

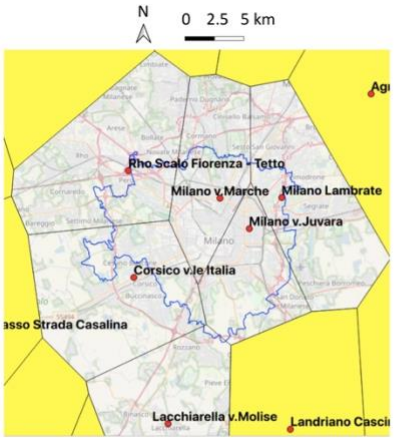

Figure A5.1. Regression models diagnostics for the whole city of Milan. Green box indicates the best model. From the top: tests for regression assumptions and VIF; coefficients/impacts, standard errors, p-values for each model. AIC – Akaike information criterion, RESET – Ramsey Regression Equation Specification Error Test, VIF – variance inflation factor, m1 – ordinary least squares linear regression, m2 – spatially lagged X model, m3 – spatial autoregressive model, m4 – spatial error model, m5 – spatial Durbin error model, m6 – spatial Durbin model, m7 – Kelejian-Prucha model.

m1 (AIC = 208,64)						VIF	
					Built-up area (%)	9,72	
					Non-residential buildings' volume (m3/m2)	1,82	
	Test	Statistic	p-value		Green roofs (%)	1,65	
	RESET test	6,87	<0,01		Population density (people/km2)	2,96	
	Shapiro-Wilk test	0,98	0,11		Vegetation index	1,97	
	Breusch-Pagan test	0,02	0,90		Mean summer LST (°C)	3,07	
	Durbin-Watson test	1,91	0,49		Density drinking water fountains (n/ km2)	1,58	
					Cycle paths (km/km2)	1,45	
					Residents >=65 (%)	2,27	
					Female residents (%)	1,93	
					Graduate residents (%)	3,17	
m2 (AIC = 205,73)						VIF	VIF on spatially lagged version of the variable
					Built-up area (%)	14,70	55,26
					Non-residential buildings' volume (m3/m2)	3,46	7,28
	Test	Statistic	p-value		Green roofs (%)	2,71	5,52
	RESET test	4,18	0,02		Population density (people/km2)	4,10	9,00
	Shapiro-Wilk test	0,97	0,08		Vegetation index	3,47	4,15
	Breusch-Pagan test	0,74	0,39		Mean summer LST (°C)	5,74	14,38
	Durbin-Watson test	1,91	0,27		Density drinking water fountains (n/ km2)	2,04	5,22
					Cycle paths (km/km2)	1,86	4,67
					Residents >=65 (%)	2,64	3,76
					Female residents (%)	2,86	4,15
					Graduate residents (%)	5,86	15,91

m1 (AIC = 208,64)

	Coefficient	Standard error	p-value
Intercept	0,00	0,08	1,00
Built-up area (%)	-0,42	0,25	0,10
Non-residential buildings' volume (m3/m2)	0,10	0,11	0,36
Green roofs (%)	-0,18	0,10	0,10
Population density (people/km2)	0,17	0,14	0,24
Vegetation index	-0,20	0,11	0,08
Mean summer LST (°C)	0,63	0,14	<0,01
Density drinking water fountains (n/ km2)	-0,30	0,10	0,01
Cycle paths (km/km2)	-0,11	0,10	0,25
Residents >=65 (%)	0,43	0,12	<0,01
Female residents (%)	-0,35	0,11	<0,01
Graduate residents (%)	0,09	0,14	0,55

m2 (AIC = 205,73)

Impact measures	Direct	Indirect	Total
Built-up area (%)	-0,28	0,06	-0,21
Non-residential buildings' volume (m3/m2)	0,16	-0,10	0,06
Green roofs (%)	-0,18	-0,11	-0,29
Population density (people/km2)	0,26	-0,44	-0,18
Vegetation index	-0,13	0,06	-0,07
Mean summer LST (°C)	0,71	-0,16	0,55
Density drinking water fountains (n/ km2)	-0,24	-0,52	-0,76
Cycle paths (km/km2)	-0,10	0,27	0,17
Residents >=65 (%)	0,37	0,64	1,01
Female residents (%)	-0,29	-0,82	-1,11
Graduate residents (%)	0,46	-0,20	0,26

Standard errors	Direct	Indirect	Total
Built-up area (%)	0,29	0,70	0,70
Non-residential buildings' volume (m3/m2)	0,14	0,28	0,36
Green roofs (%)	0,13	0,31	0,37
Population density (people/km2)	0,15	0,35	0,35
Vegetation index	0,14	0,26	0,27
Mean summer LST (°C)	0,18	0,40	0,40
Density drinking water fountains (n/ km2)	0,11	0,30	0,32
Cycle paths (km/km2)	0,10	0,28	0,28
Residents >=65 (%)	0,12	0,26	0,29
Female residents (%)	0,13	0,35	0,40
Graduate residents (%)	0,18	0,38	0,38

p-values	Direct	Indirect	Total
Built-up area (%)	0,35	0,93	0,76
Non-residential buildings' volume (m3/m2)	0,26	0,72	0,88
Green roofs (%)	0,15	0,71	0,43
Population density (people/km2)	0,09	0,21	0,61
Vegetation index	0,35	0,80	0,80
Mean summer LST (°C)	<0,01	0,69	0,16
Density drinking water fountains (n/ km2)	0,03	0,08	0,02
Cycle paths (km/km2)	0,35	0,34	0,53
Residents >=65 (%)	<0,01	0,01	<0,01
Female residents (%)	0,02	0,02	<0,01
Graduate residents (%)	0,01	0,59	0,50

m3 (AIC = 208,88)

Impact measures	Direct	Indirect	Total
Built-up area (%)	-0,42	-0,08	-0,50
Non-residential buildings' volume (m3/m2)	0,07	0,01	0,09
Green roofs (%)	-0,17	-0,03	-0,21
Population density (people/km2)	0,18	0,04	0,21
Vegetation index	-0,21	-0,04	-0,25
Mean summer LST (°C)	0,59	0,12	0,71
Density drinking water fountains (n/ km2)	-0,28	-0,06	-0,34
Cycle paths (km/km2)	-0,10	-0,02	-0,12
Residents >=65 (%)	0,42	0,08	0,51
Female residents (%)	-0,36	-0,07	-0,43
Graduate residents (%)	0,11	0,02	0,14

Simulated standard errors	Direct	Indirect	Total
Built-up area (%)	0,24	0,10	0,30
Non-residential buildings' volume (m3/m2)	0,10	0,03	0,13
Green roofs (%)	0,10	0,04	0,12
Population density (people/km2)	0,13	0,05	0,17
Vegetation index	0,11	0,05	0,14
Mean summer LST (°C)	0,13	0,11	0,19
Density drinking water fountains (n/ km2)	0,10	0,06	0,13
Cycle paths (km/km2)	0,09	0,03	0,11
Residents >=65 (%)	0,11	0,09	0,17
Female residents (%)	0,11	0,08	0,15
Graduate residents (%)	0,14	0,05	0,17

Simulated p-values	Direct	Indirect	Total
Built-up area (%)	0,08	0,38	0,09
Non-residential buildings' volume (m3/m2)	0,48	0,64	0,49
Green roofs (%)	0,08	0,38	0,09
Population density (people/km2)	0,17	0,44	0,19
Vegetation index	0,05	0,35	0,06
Mean summer LST (°C)	<0,01	0,26	<0,01
Density drinking water fountains (n/ km2)	<0,01	0,30	0,01
Cycle paths (km/km2)	0,24	0,49	0,26
Residents >=65 (%)	<0,01	0,28	<0,01
Female residents (%)	<0,01	0,30	<0,01
Graduate residents (%)	0,40	0,56	0,41

m4 (AIC = 210,63)

	Coefficient	Standard error	p-value
Intercept	0,00	0,07	0,99
Built-up area (%)	-0,42	0,23	0,08
Non-residential buildings' volume (m3/m2)	0,10	0,10	0,31
Green roofs (%)	-0,18	0,10	0,07
Population density (people/km2)	0,16	0,13	0,21
Vegetation index	-0,20	0,11	0,05
Mean summer LST (°C)	0,64	0,13	<0,01
Density drinking water fountains (n/ km2)	-0,30	0,09	<0,01
Cycle paths (km/km2)	-0,11	0,09	0,21
Residents >=65 (%)	0,44	0,11	<0,01
Female residents (%)	-0,35	0,11	<0,01
Graduate residents (%)	0,09	0,13	0,52

m5 (AIC = 205,90)

Impact measures	Direct	Indirect	Total
Built-up area (%)	-0,32	0,13	-0,19
Non-residential buildings' volume (m3/m2)	0,12	-0,11	0,01
Green roofs (%)	-0,17	-0,06	-0,22
Population density (people/km2)	0,27	-0,58	-0,31
Vegetation index	-0,17	0,11	-0,06
Mean summer LST (°C)	0,70	-0,09	0,61
Density drinking water fountains (n/ km2)	-0,24	-0,47	-0,71
Cycle paths (km/km2)	-0,12	0,29	0,17
Residents >=65 (%)	0,38	0,76	1,14
Female residents (%)	-0,29	-0,79	-1,08
Graduate residents (%)	0,46	-0,27	0,20

Standard errors	Direct	Indirect	Total
Built-up area (%)	0,25	0,55	0,52
Non-residential buildings' volume (m3/m2)	0,12	0,22	0,27
Green roofs (%)	0,10	0,24	0,28
Population density (people/km2)	0,13	0,28	0,26
Vegetation index	0,12	0,22	0,20
Mean summer LST (°C)	0,16	0,31	0,29
Density drinking water fountains (n/ km2)	0,09	0,24	0,24
Cycle paths (km/km2)	0,09	0,23	0,21
Residents >=65 (%)	0,11	0,21	0,21
Female residents (%)	0,11	0,28	0,30
Graduate residents (%)	0,16	0,30	0,28

p-values	Direct	Indirect	Total
Built-up area (%)	0,20	0,81	0,71
Non-residential buildings' volume (m3/m2)	0,29	0,62	0,96
Green roofs (%)	0,10	0,82	0,43
Population density (people/km2)	0,04	0,04	0,23
Vegetation index	0,15	0,61	0,75
Mean summer LST (°C)	<0,01	0,77	0,04
Density drinking water fountains (n/ km2)	0,01	0,05	<0,01
Cycle paths (km/km2)	0,17	0,20	0,41
Residents >=65 (%)	<0,01	<0,01	<0,01
Female residents (%)	0,01	<0,01	<0,01
Graduate residents (%)	<0,01	0,37	0,48

m6 (AIC = 206,74)

Impact measures	Direct	Indirect	Total
Built-up area (%)	-0,29	0,07	-0,23
Non-residential buildings' volume (m3/m2)	0,16	-0,09	0,08
Green roofs (%)	-0,17	-0,10	-0,27
Population density (people/km2)	0,28	-0,45	-0,18
Vegetation index	-0,15	0,06	-0,09
Mean summer LST (°C)	0,71	-0,12	0,60
Density drinking water fountains (n/ km2)	-0,24	-0,46	-0,69
Cycle paths (km/km2)	-0,12	0,26	0,14
Residents >=65 (%)	0,37	0,63	1,01
Female residents (%)	-0,27	-0,74	-1,02
Graduate residents (%)	0,45	-0,23	0,22

Simulated standard errors	Direct	Indirect	Total
Built-up area (%)	0,25	0,58	0,55
Non-residential buildings' volume (m3/m2)	0,12	0,23	0,30
Green roofs (%)	0,11	0,23	0,27
Population density (people/km2)	0,13	0,28	0,27
Vegetation index	0,12	0,21	0,20
Mean summer LST (°C)	0,16	0,33	0,30
Density drinking water fountains (n/ km2)	0,10	0,24	0,25
Cycle paths (km/km2)	0,09	0,22	0,20
Residents >=65 (%)	0,11	0,20	0,21
Female residents (%)	0,11	0,27	0,30
Graduate residents (%)	0,17	0,32	0,30

Simulated p-values	Direct	Indirect	Total
Built-up area (%)	0,25	0,90	0,70
Non-residential buildings' volume (m3/m2)	0,20	0,66	0,85
Green roofs (%)	0,09	0,61	0,27
Population density (people/km2)	0,04	0,10	0,51
Vegetation index	0,22	0,71	0,73
Mean summer LST (°C)	<0,01	0,72	0,05
Density drinking water fountains (n/ km2)	0,02	0,05	<0,01
Cycle paths (km/km2)	0,20	0,21	0,45
Residents >=65 (%)	<0,01	<0,01	<0,01
Female residents (%)	0,01	<0,01	<0,01
Graduate residents (%)	0,01	0,50	0,46

m7 (AIC = 206,54)

Impact measures	Direct	Indirect	Total
Built-up area (%)	-0,37	-0,26	-0,63
Non-residential buildings' volume (m3/m2)	0,11	0,08	0,19
Green roofs (%)	-0,17	-0,12	-0,29
Population density (people/km2)	0,16	0,11	0,27
Vegetation index	-0,21	-0,14	-0,35
Mean summer LST (°C)	0,57	0,39	0,96
Density drinking water fountains (n/ km2)	-0,31	-0,21	-0,52
Cycle paths (km/km2)	-0,08	-0,06	-0,14
Residents >=65 (%)	0,47	0,33	0,80
Female residents (%)	-0,37	-0,26	-0,63
Graduate residents (%)	0,12	0,08	0,20

Simulated standard errors	Direct	Indirect	Total
Built-up area (%)	0,22	0,46	0,60
Non-residential buildings' volume (m3/m2)	0,12	0,20	0,28
Green roofs (%)	0,10	0,18	0,24
Population density (people/km2)	0,12	0,28	0,37
Vegetation index	0,10	0,22	0,27
Mean summer LST (°C)	0,13	0,48	0,52
Density drinking water fountains (n/ km2)	0,10	0,33	0,38
Cycle paths (km/km2)	0,08	0,10	0,16
Residents >=65 (%)	0,12	0,41	0,46
Female residents (%)	0,11	0,38	0,43
Graduate residents (%)	0,13	0,27	0,36

Simulated p-values	Direct	Indirect	Total
Built-up area (%)	0,09	0,48	0,25
Non-residential buildings' volume (m3/m2)	0,32	0,62	0,45
Green roofs (%)	0,07	0,42	0,18
Population density (people/km2)	0,18	0,58	0,39
Vegetation index	0,04	0,42	0,17
Mean summer LST (°C)	<0,01	0,33	0,05
Density drinking water fountains (n/ km2)	<0,01	0,40	0,12
Cycle paths (km/km2)	0,32	0,53	0,39
Residents >=65 (%)	<0,01	0,32	0,06
Female residents (%)	<0,01	0,39	0,10
Graduate residents (%)	0,36	0,66	0,51

Figure A5.2. Regression models diagnostics for the Central socio-urban cluster. Green box indicates the best model. From the top: tests for regression assumptions and VIF; coefficients/impacts, standard errors, p-values for each model. AIC – Akaike information criterion, RESET – Ramsey Regression Equation Specification Error Test, VIF – variance inflation factor, m1 – ordinary least squares linear regression, m2 – spatially lagged X model,

m3 – spatial autoregressive model, m4 – spatial error model, m5 – spatial Durbin error model, m6 – spatial Durbin model, m7 – Kelejian-Prucha model.

					VIF
				Built-up area (%)	5,50
				Non-residential buildings' volume (m3/m2)	3,51
	Test	Statistic	p-value	Green roofs (%)	2,22
	RESET test	8,56	<0,01	Population density (people/km2)	3,78
m1 (AIC = 32,88)	Shapiro-Wilk test	0,98	0,82	Vegetation index	3,44
	Breusch-Pagan test	2,75	0,10	Mean summer LST (°C)	4,92
	Durbin-Watson test			Density drinking water fountains (n/ km2)	1,67
				Cycle paths (km/km2)	2,05
				Residents >=65 (%)	4,53
				Female residents (%)	3,19
				Graduate residents (%)	5,68

					VIF	VIF on spatially lagged version of the variable
				Built-up area (%)	9,36	29,02
				Non-residential buildings' volume (m3/m2)	10,71	38,91
	Test	Statistic	p-value	Green roofs (%)	6,22	10,33
	RESET test	1,29	0,33	Population density (people/km2)	18,92	34,95
m2 (AIC = 30,76)	Shapiro-Wilk test	0,97	0,37	Vegetation index	17,44	26,46
	Breusch-Pagan test	4,15	0,04	Mean summer LST (°C)	24,14	64,42
	Durbin-Watson test	2,23	0,60	Density drinking water fountains (n/ km2)	26,73	25,14
				Cycle paths (km/km2)	5,42	16,89
				Residents >=65 (%)	20,83	56,14
				Female residents (%)	19,66	90,23
				Graduate residents (%)	9,70	42,26

		Coefficient	Standard error	p-value
m1 (AIC = 32,88)	Intercept	-0,31	0,30	0,31
	Built-up area (%)	0,14	0,26	0,60
	Non-residential buildings' volume (m3/m2)	-0,69	0,35	0,06
	Green roofs (%)	-0,07	0,16	0,67
	Population density (people/km2)	-0,11	0,15	0,48
	Vegetation index	0,28	0,17	0,11
	Mean summer LST (°C)	0,24	0,36	0,52
	Density drinking water fountains (n/ km2)	0,00	0,09	0,98
	Cycle paths (km/km2)	0,02	0,08	0,75
	Residents >=65 (%)	-0,19	0,29	0,52
	Female residents (%)	-0,01	0,40	0,98
	Graduate residents (%)	-0,14	0,18	0,44

	Impact measures				Standard errors				p-values			
		Direct	Indirect	Total		Direct	Indirect	Total		Direct	Indirect	Total
m2 (AIC = 30,76)	Built-up area (%)	0,10	-0,43	-0,33	Built-up area (%)	0,34	1,26	1,44	Built-up area (%)	0,78	0,73	0,82
	Non-residential buildings' volume (m3/m2)	-0,31	3,66	3,35	Non-residential buildings' volume (m3/m2)	0,63	2,62	2,92	Non-residential buildings' volume (m3/m2)	0,62	0,16	0,25
	Green roofs (%)	0,01	0,45	0,46	Green roofs (%)	0,27	0,77	0,81	Green roofs (%)	0,98	0,56	0,57
	Population density (people/km2)	-0,14	1,38	1,24	Population density (people/km2)	0,35	0,92	0,97	Population density (people/km2)	0,69	0,13	0,20
	Vegetation index	-0,54	0,11	-0,43	Vegetation index	0,39	0,92	0,91	Vegetation index	0,16	0,90	0,64
	Mean summer LST (°C)	1,63	4,50	6,14	Mean summer LST (°C)	0,81	2,09	2,73	Mean summer LST (°C)	0,04	0,03	0,02
	Density drinking water fountains (n/ km2)	0,64	1,97	2,60	Density drinking water fountains (n/ km2)	0,35	1,01	1,33	Density drinking water fountains (n/ km2)	0,07	0,05	0,05
	Cycle paths (km/km2)	-0,10	-0,27	-0,37	Cycle paths (km/km2)	0,13	0,45	0,52	Cycle paths (km/km2)	0,42	0,55	0,47
	Residents >=65 (%)	-0,26	-0,83	-1,09	Residents >=65 (%)	0,65	1,91	2,41	Residents >=65 (%)	0,69	0,66	0,65
	Female residents (%)	1,58	3,85	5,43	Female residents (%)	1,01	2,75	3,63	Female residents (%)	0,12	0,16	0,13
	Graduate residents (%)	0,01	-0,18	-0,17	Graduate residents (%)	0,24	1,04	1,12	Graduate residents (%)	0,98	0,86	0,88

	Impact measures				Simulated standard errors				Simulated p-values			
		Direct	Indirect	Total		Direct	Indirect	Total		Direct	Indirect	Total
m3 (AIC = 33,44)	Built-up area (%)	0,10	-0,02	0,07	Built-up area (%)	0,20	0,06	0,17	Built-up area (%)	0,64	0,78	0,64
	Non-residential buildings' volume (m3/m2)	-0,72	0,17	-0,54	Non-residential buildings' volume (m3/m2)	0,28	0,16	0,25	Non-residential buildings' volume (m3/m2)	0,01	0,33	0,02
	Green roofs (%)	-0,10	0,02	-0,07	Green roofs (%)	0,12	0,04	0,10	Green roofs (%)	0,42	0,59	0,44
	Population density (people/km2)	-0,11	0,03	-0,08	Population density (people/km2)	0,12	0,04	0,10	Population density (people/km2)	0,37	0,57	0,39
	Vegetation index	0,30	-0,07	0,22	Vegetation index	0,13	0,07	0,12	Vegetation index	0,03	0,35	0,05
	Mean summer LST (°C)	0,35	-0,09	0,27	Mean summer LST (°C)	0,29	0,11	0,23	Mean summer LST (°C)	0,21	0,44	0,23
	Density drinking water fountains (n/ km2)	0,02	-0,01	0,02	Density drinking water fountains (n/ km2)	0,07	0,02	0,05	Density drinking water fountains (n/ km2)	0,74	0,77	0,76
	Cycle paths (km/km2)	0,05	-0,01	0,04	Cycle paths (km/km2)	0,06	0,02	0,05	Cycle paths (km/km2)	0,41	0,57	0,43
	Residents >=65 (%)	-0,16	0,04	-0,12	Residents >=65 (%)	0,23	0,07	0,19	Residents >=65 (%)	0,50	0,67	0,50
	Female residents (%)	-0,03	0,01	-0,03	Female residents (%)	0,32	0,09	0,25	Female residents (%)	0,92	0,90	0,94
	Graduate residents (%)	-0,14	0,03	-0,11	Graduate residents (%)	0,14	0,05	0,12	Graduate residents (%)	0,31	0,53	0,33

		Coefficient	Standard error	p-value
m4 (AIC = 25,32)	Intercept	-0,67	0,21	<0,01
	Built-up area (%)	-0,02	0,16	0,89
	Non-residential buildings' volume (m3/m2)	-0,51	0,20	0,01
	Green roofs (%)	-0,30	0,08	<0,01
	Population density (people/km2)	-0,06	0,08	0,43
	Vegetation index	0,28	0,09	<0,01
	Mean summer LST (°C)	0,76	0,25	<0,01
	Density drinking water fountains (n/ km2)	0,08	0,07	0,24
	Cycle paths (km/km2)	0,18	0,05	<0,01
	Residents >=65 (%)	0,14	0,20	0,49
	Female residents (%)	0,06	0,23	0,79
	Graduate residents (%)	-0,04	0,11	0,74

m5 (AIC = 13,08)

Impact measures	Direct	Indirect	Total
Built-up area (%)	0,07	-0,07	0.0
Non-residential buildings' volume (m3/m2)	-1,27	2,4	1.13
Green roofs (%)	-0,29	-0,14	-0.44
Population density (people/km2)	-0,5	0,74	0.24
Vegetation index	0,08	-0,16	-0.08
Mean summer LST (°C)	1,11	0,65	1.76
Density drinking water fountains (n/ km2)	0,29	0,35	0.63
Cycle paths (km/km2)	0,10	0,11	0.21
Residents >=65 (%)	0,23	1,5	1.72
Female residents (%)	-0,07	0,13	0.07
Graduate residents (%)	-0,12	-0,14	-0.26

Standard errors	Direct	Indirect	Total
Built-up area (%)	0,15	0,81	0,80
Non-residential buildings' volume (m3/m2)	0,29	1,66	1,74
Green roofs (%)	0,15	0,55	0,49
Population density (people/km2)	0,22	0,55	0,50
Vegetation index	0,17	0,42	0,41
Mean summer LST (°C)	0,36	1,01	1,18
Density drinking water fountains (n/ km2)	0,17	0,41	0,52
Cycle paths (km/km2)	0,06	0,38	0,39
Residents >=65 (%)	0,37	0,83	1,10
Female residents (%)	0,60	1,66	2,13
Graduate residents (%)	0,10	0,63	0,60

p-values	Direct	Indirect	Total
Built-up area (%)	0,64	0,93	1
Non-residential buildings' volume (m3/m2)	<0,01	0,15	0,52
Green roofs (%)	0,04	0,8	0,37
Population density (people/km2)	0,02	0,18	0,63
Vegetation index	0,64	0,71	0,85
Mean summer LST (°C)	<0,01	0,52	0,13
Density drinking water fountains (n/ km2)	0,08	0,4	0,22
Cycle paths (km/km2)	0,12	0,76	0,59
Residents >=65 (%)	0,54	0,07	0,12
Female residents (%)	0,91	0,94	0,98
Graduate residents (%)	0,25	0,83	0,67

m6 (AIC = 19,09)

Impact measures	Direct	Indirect	Total
Built-up area (%)	-0,04	-0,14	-0,18
Non-residential buildings' volume (m3/m2)	-1,52	2,37	0,85
Green roofs (%)	-0,42	0,27	-0,16
Population density (people/km2)	-0,51	0,85	0,34
Vegetation index	-0,44	0,49	0,05
Mean summer LST (°C)	1,02	1,42	2,44
Density drinking water fountains (n/ km2)	0,27	0,51	0,79
Cycle paths (km/km2)	0,08	0,01	0,08
Residents >=65 (%)	0,27	0,01	0,28
Female residents (%)	0,52	0,70	1,22
Graduate residents (%)	0,04	-0,01	0,03

Simulated standard errors	Direct	Indirect	Total
Built-up area (%)	0,19	0,34	0,25
Non-residential buildings' volume (m3/m2)	0,52	0,75	0,51
Green roofs (%)	0,20	0,26	0,14
Population density (people/km2)	0,26	0,33	0,17
Vegetation index	0,28	0,35	0,15
Mean summer LST (°C)	0,33	0,48	0,51
Density drinking water fountains (n/ km2)	0,11	0,20	0,25
Cycle paths (km/km2)	0,07	0,12	0,10
Residents >=65 (%)	0,26	0,44	0,42
Female residents (%)	0,32	0,57	0,66
Graduate residents (%)	0,16	0,29	0,19

Simulated p-values	Direct	Indirect	Total
Built-up area (%)	0,78	0,71	0,48
Non-residential buildings' volume (m3/m2)	<0,01	<0,01	0,10
Green roofs (%)	0,02	0,26	0,30
Population density (people/km2)	0,05	0,01	0,05
Vegetation index	0,09	0,14	0,74
Mean summer LST (°C)	<0,01	<0,01	<0,01
Density drinking water fountains (n/ km2)	0,02	0,01	<0,01
Cycle paths (km/km2)	0,28	0,98	0,42
Residents >=65 (%)	0,27	0,95	0,55
Female residents (%)	0,11	0,20	0,06
Graduate residents (%)	0,80	0,98	0,86

m7 (AIC = 26,92)

Impact measures	Direct	Indirect	Total
Built-up area (%)	-0,02	0,00	-0,02
Non-residential buildings' volume (m3/m2)	-0,52	-0,07	-0,59
Green roofs (%)	-0,26	-0,04	-0,30
Population density (people/km2)	-0,07	-0,01	-0,08
Vegetation index	0,27	0,04	0,31
Mean summer LST (°C)	0,69	0,10	0,79
Density drinking water fountains (n/ km2)	0,07	0,01	0,08
Cycle paths (km/km2)	0,16	0,02	0,18
Residents >=65 (%)	0,07	0,01	0,08
Female residents (%)	0,09	0,01	0,11
Graduate residents (%)	-0,04	-0,01	-0,05

Simulated standard errors	Direct	Indirect	Total
Built-up area (%)	0,17	0,11	0,25
Non-residential buildings' volume (m3/m2)	0,21	0,22	0,33
Green roofs (%)	0,10	0,07	0,11
Population density (people/km2)	0,07	0,04	0,10
Vegetation index	0,09	0,10	0,14
Mean summer LST (°C)	0,27	0,30	0,41
Density drinking water fountains (n/ km2)	0,07	0,04	0,10
Cycle paths (km/km2)	0,06	0,04	0,06
Residents >=65 (%)	0,22	0,11	0,29
Female residents (%)	0,24	0,16	0,35
Graduate residents (%)	0,11	0,06	0,15

Simulated p-values	Direct	Indirect	Total
Built-up area (%)	0,91	0,92	0,90
Non-residential buildings' volume (m3/m2)	0,01	0,58	0,06
Green roofs (%)	0,01	0,59	<0,01
Population density (people/km2)	0,36	0,68	0,40
Vegetation index	<0,01	0,53	0,02
Mean summer LST (°C)	0,01	0,63	0,04
Density drinking water fountains (n/ km2)	0,33	0,78	0,39
Cycle paths (km/km2)	0,01	0,59	0,01
Residents >=65 (%)	0,80	0,85	0,91
Female residents (%)	0,64	0,75	0,65
Graduate residents (%)	0,70	0,90	0,74

Figure A5.3. Regression models diagnostics for the Residential socio-urban cluster. Green box indicates the best model. From the top: tests for regression assumptions and VIF; coefficients/impacts, standard errors, p-values for each model. AIC – Akaike information criterion, RESET – Ramsey Regression Equation Specification Error Test, VIF – variance inflation factor, m1 – ordinary least squares linear regression, m2 – spatially lagged X model, m3 – spatial autoregressive model, m4 – spatial error model, m5 – spatial Durbin error model, m6 – spatial Durbin model, m7 – Kelejian-Prucha model.

m1 (AIC = 108,48)

Test	Statistic	p-value
RESET test	7,96	<0,01
Shapiro-Wilk test	0,96	0,17
Breusch-Pagan test	1,45	0,23
Durbin-Watson test	1,99	0,85

	VIF
Built-up area (%)	3,77
Non-residential buildings' volume (m3/m2)	3,87
Green roofs (%)	1,86
Population density (people/km2)	3,49
Vegetation index	2,00
Mean summer LST (°C)	2,87
Density drinking water fountains (n/ km2)	2,08
Cycle paths (km/km2)	2,23
Residents >=65 (%)	2,35
Female residents (%)	3,81
Graduate residents (%)	2,13

m2 (AIC = 114,29)

Test	Statistic	p-value
RESET test	4,41	0,03
Shapiro-Wilk test	0,95	0,05
Breusch-Pagan test	3,72	0,05
Durbin-Watson test	2,08	0,94

	VIF	VIF on spatially lagged version of the variable
Built-up area (%)	6,89	11,10
Non-residential buildings' volume (m3/m2)	5,84	6,62
Green roofs (%)	5,83	6,26
Population density (people/km2)	6,66	11,53
Vegetation index	5,77	5,81
Mean summer LST (°C)	5,86	6,54
Density drinking water fountains (n/ km2)	4,30	4,19
Cycle paths (km/km2)	5,06	4,92
Residents >=65 (%)	2,97	7,88
Female residents (%)	6,19	16,64
Graduate residents (%)	3,66	4,30

m1 (AIC = 108,48)

	Coefficient	Standard error	p-value
Intercept	0,04	0,25	0,87
Built-up area (%)	-0,53	0,39	0,18
Non-residential buildings' volume (m3/m2)	0,17	0,30	0,58
Green roofs (%)	-0,32	0,13	0,02
Population density (people/km2)	0,52	0,36	0,16
Vegetation index	-0,1	0,15	0,52
Mean summer LST (°C)	0,38	0,20	0,07
Density drinking water fountains (n/ km2)	-0,73	0,21	<0,01
Cycle paths (km/km2)	-0,1	0,22	0,66
Residents >=65 (%)	0,39	0,17	0,02
Female residents (%)	-1,16	0,56	0,05
Graduate residents (%)	0,17	0,31	0,58

m2 (AIC = 114,29)

Impact measures	Direct	Indirect	Total
Built-up area (%)	-0,37	0,47	0,11
Non-residential buildings' volume (m3/m2)	0,43	-0,34	0,09
Green roofs (%)	-0,48	-0,35	-0,83
Population density (people/km2)	0,63	-0,09	0,54
Vegetation index	0,13	0,04	0,17
Mean summer LST (°C)	0,37	-0,62	-0,25
Density drinking water fountains (n/ km2)	-0,61	-1,15	-1,76
Cycle paths (km/km2)	-0,13	0,41	0,28
Residents >=65 (%)	0,41	0,12	0,52
Female residents (%)	-1,67	-0,36	-2,03
Graduate residents (%)	0,16	-0,04	0,12

Standard errors	Direct	Indirect	Total
Built-up area (%)	0,54	1,18	1,42
Non-residential buildings' volume (m3/m2)	0,38	0,88	0,94
Green roofs (%)	0,23	0,43	0,59
Population density (people/km2)	0,51	1,26	1,60
Vegetation index	0,26	0,41	0,44
Mean summer LST (°C)	0,29	0,68	0,74
Density drinking water fountains (n/ km2)	0,31	0,64	0,73
Cycle paths (km/km2)	0,34	0,55	0,67
Residents >=65 (%)	0,19	0,50	0,49
Female residents (%)	0,74	2,18	2,43
Graduate residents (%)	0,41	0,74	0,88

p-values	Direct	Indirect	Total
Built-up area (%)	0,50	0,69	0,94
Non-residential buildings' volume (m3/m2)	0,26	0,70	0,93
Green roofs (%)	0,03	0,42	0,16
Population density (people/km2)	0,22	0,94	0,73
Vegetation index	0,61	0,93	0,69
Mean summer LST (°C)	0,20	0,37	0,74
Density drinking water fountains (n/ km2)	0,05	0,07	0,02
Cycle paths (km/km2)	0,70	0,46	0,68
Residents >=65 (%)	0,03	0,81	0,29
Female residents (%)	0,02	0,87	0,40
Graduate residents (%)	0,69	0,96	0,89

m3 (AIC = 109,41)

Impact measures	Direct	Indirect	Total
Built-up area (%)	-0,50	-0,10	-0,61
Non-residential buildings' volume (m3/m2)	0,17	0,04	0,21
Green roofs (%)	-0,31	-0,06	-0,38
Population density (people/km2)	0,54	0,11	0,65
Vegetation index	-0,08	-0,02	-0,10
Mean summer LST (°C)	0,38	0,08	0,46
Density drinking water fountains (n/ km2)	-0,71	-0,15	-0,85
Cycle paths (km/km2)	-0,10	-0,02	-0,12
Residents >=65 (%)	0,39	0,08	0,48
Female residents (%)	-1,17	-0,24	-1,41
Graduate residents (%)	0,17	0,04	0,21

Simulated standard errors	Direct	Indirect	Total
Built-up area (%)	0,34	0,15	0,43
Non-residential buildings' volume (m3/m2)	0,27	0,09	0,34
Green roofs (%)	0,11	0,08	0,15
Population density (people/km2)	0,31	0,16	0,42
Vegetation index	0,13	0,04	0,16
Mean summer LST (°C)	0,17	0,10	0,23
Density drinking water fountains (n/ km2)	0,18	0,16	0,29
Cycle paths (km/km2)	0,20	0,06	0,24
Residents >=65 (%)	0,14	0,10	0,21
Female residents (%)	0,48	0,31	0,68
Graduate residents (%)	0,26	0,09	0,33

Simulated p-values	Direct	Indirect	Total
Built-up area (%)	0,13	0,45	0,15
Non-residential buildings' volume (m3/m2)	0,51	0,63	0,52
Green roofs (%)	0,00	0,33	0,01
Population density (people/km2)	0,08	0,41	0,11
Vegetation index	0,55	0,70	0,56
Mean summer LST (°C)	0,03	0,36	0,04
Density drinking water fountains (n/ km2)	0,00	0,30	<0,01
Cycle paths (km/km2)	0,60	0,77	0,62
Residents >=65 (%)	<0,01	0,34	0,02
Female residents (%)	0,01	0,36	0,03
Graduate residents (%)	0,51	0,66	0,52

m4 (AIC = 110,29)

	Coefficient	Standard error	p-value
Intercept	0,05	0,21	0,81
Built-up area (%)	-0,53	0,33	0,11
Non-residential buildings' volume (m3/m2)	0,17	0,26	0,52
Green roofs (%)	-0,33	0,11	<0,01
Population density (people/km2)	0,52	0,31	0,10
Vegetation index	-0,10	0,12	0,41
Mean summer LST (°C)	0,36	0,17	0,03
Density drinking water fountains (n/ km2)	-0,79	0,18	<0,01
Cycle paths (km/km2)	-0,05	0,19	0,79
Residents >=65 (%)	0,42	0,14	<0,01
Female residents (%)	-1,22	0,48	0,01
Graduate residents (%)	0,19	0,26	0,47

m5 (AIC = 115,27)

Impact measures	Direct	Indirect	Total
Built-up area (%)	-0,47	0,68	0,21
Non-residential buildings' volume (m3/m2)	0,51	-0,65	-0,14
Green roofs (%)	-0,52	-0,22	-0,74
Population density (people/km2)	0,65	-0,46	0,20
Vegetation index	0,17	-0,09	0,08
Mean summer LST (°C)	0,44	-0,70	-0,26
Density drinking water fountains (n/ km2)	-0,53	-1,00	-1,53
Cycle paths (km/km2)	-0,21	0,66	0,45
Residents >=65 (%)	0,38	0,24	0,62
Female residents (%)	-1,72	0,02	-1,72
Graduate residents (%)	0,14	-0,15	-0,01

Standard errors	Direct	Indirect	Total
Built-up area (%)	0,36	0,84	0,94
Non-residential buildings' volume (m3/m2)	0,27	0,58	0,57
Green roofs (%)	0,15	0,29	0,38
Population density (people/km2)	0,34	0,87	1,05
Vegetation index	0,19	0,31	0,30
Mean summer LST (°C)	0,20	0,48	0,49
Density drinking water fountains (n/ km2)	0,23	0,42	0,46
Cycle paths (km/km2)	0,25	0,40	0,44
Residents >=65 (%)	0,14	0,35	0,31
Female residents (%)	0,50	1,56	1,63
Graduate residents (%)	0,30	0,50	0,57

p-values	Direct	Indirect	Total
Built-up area (%)	0,19	0,42	0,82
Non-residential buildings' volume (m3/m2)	0,06	0,27	0,81
Green roofs (%)	0,00	0,44	0,05
Population density (people/km2)	0,06	0,60	0,85
Vegetation index	0,35	0,76	0,79
Mean summer LST (°C)	0,03	0,15	0,60
Density drinking water fountains (n/ km2)	0,02	0,02	<0,01
Cycle paths (km/km2)	0,41	0,10	0,30
Residents >=65 (%)	0,01	0,48	0,04
Female residents (%)	<0,01	0,99	0,29
Graduate residents (%)	0,64	0,76	0,98

m6 (AIC = 115,80)

Impact measures	Direct	Indirect	Total
Built-up area (%)	-0,42	0,45	0,03
Non-residential buildings' volume (m3/m2)	0,46	-0,40	0,06
Green roofs (%)	-0,49	-0,28	-0,76
Population density (people/km2)	0,66	-0,13	0,53
Vegetation index	0,13	0,00	0,13
Mean summer LST (°C)	0,40	-0,58	-0,18
Density drinking water fountains (n/ km2)	-0,59	-1,05	-1,64
Cycle paths (km/km2)	-0,13	0,42	0,29
Residents >=65 (%)	0,41	0,15	0,56
Female residents (%)	-1,68	-0,38	-2,06
Graduate residents (%)	0,18	-0,03	0,15

Simulated standard errors	Direct	Indirect	Total
Built-up area (%)	0,39	0,73	0,87
Non-residential buildings' volume (m3/m2)	0,29	0,58	0,57
Green roofs (%)	0,17	0,28	0,39
Population density (people/km2)	0,37	0,81	1,06
Vegetation index	0,19	0,28	0,27
Mean summer LST (°C)	0,21	0,46	0,46
Density drinking water fountains (n/ km2)	0,23	0,43	0,46
Cycle paths (km/km2)	0,25	0,37	0,43
Residents >=65 (%)	0,15	0,32	0,30
Female residents (%)	0,54	1,37	1,50
Graduate residents (%)	0,29	0,50	0,55

Simulated p-values	Direct	Indirect	Total
Built-up area (%)	0,25	0,52	0,97
Non-residential buildings' volume (m3/m2)	0,11	0,47	0,94
Green roofs (%)	0,00	0,33	0,05
Population density (people/km2)	0,08	0,90	0,59
Vegetation index	0,48	0,98	0,61
Mean summer LST (°C)	0,05	0,18	0,65
Density drinking water fountains (n/ km2)	0,01	0,01	<0,01
Cycle paths (km/km2)	0,58	0,26	0,52
Residents >=65 (%)	0,01	0,61	0,06
Female residents (%)	0,00	0,72	0,15
Graduate residents (%)	0,48	0,98	0,72

m7 (AIC = 110,05)

Impact measures	Direct	Indirect	Total
Built-up area (%)	-0,45	-0,16	-0,62
Non-residential buildings' volume (m3/m2)	0,19	0,07	0,26
Green roofs (%)	-0,36	-0,13	-0,49
Population density (people/km2)	0,58	0,21	0,78
Vegetation index	-0,06	-0,02	-0,08
Mean summer LST (°C)	0,32	0,11	0,43
Density drinking water fountains (n/ km2)	-0,84	-0,30	-1,14
Cycle paths (km/km2)	0,02	0,01	0,03
Residents >=65 (%)	0,45	0,16	0,62
Female residents (%)	-1,33	-0,48	-1,81
Graduate residents (%)	0,20	0,07	0,27

Simulated standard errors	Direct	Indirect	Total
Built-up area (%)	0,35	0,30	0,56
Non-residential buildings' volume (m3/m2)	0,26	0,24	0,45
Green roofs (%)	0,12	0,20	0,27
Population density (people/km2)	0,34	0,52	0,76
Vegetation index	0,12	0,09	0,19
Mean summer LST (°C)	0,18	0,20	0,32
Density drinking water fountains (n/ km2)	0,19	0,51	0,61
Cycle paths (km/km2)	0,19	0,14	0,30
Residents >=65 (%)	0,14	0,28	0,36
Female residents (%)	0,50	0,90	1,22
Graduate residents (%)	0,26	0,21	0,42

Simulated p-values	Direct	Indirect	Total
Built-up area (%)	0,18	0,54	0,24
Non-residential buildings' volume (m3/m2)	0,46	0,62	0,49
Green roofs (%)	0,00	0,40	0,04
Population density (people/km2)	0,07	0,54	0,22
Vegetation index	0,62	0,86	0,70
Mean summer LST (°C)	0,07	0,50	0,15
Density drinking water fountains (n/ km2)	<0,01	0,43	0,04
Cycle paths (km/km2)	0,90	0,91	0,90
Residents >=65 (%)	<0,01	0,43	0,06
Female residents (%)	0,01	0,47	0,10
Graduate residents (%)	0,42	0,66	0,48